reverse electro-dialysis

design and optimization
by
modeling and experimentation

Joost Veerman

Reverse Electrodialysis

design and optimization
by
modeling and experimentation

Joost Veerman

ISBN: 978-90-367-4463-8 (print)
ISBN: 978-90-367-4464-5 (online)

Cover design : Peter van der Sijde, Groningen

Cover painting : Yolanda Wijnsma, Burdaard

Lay-out: Peter van der Sijde, Groningen

Printed by: drukkerij van Denderen, Groningen

RIJKSUNIVERSITEIT GRONINGEN

Reverse Electrodialysis

design and optimization
by
modeling and experimentation

Proefschrift

ter verkrijging van het doctoraat in de
Wiskunde en Natuurwetenschappen
aan de Rijksuniversiteit Groningen
op gezag van de
Rector Magnificus, dr. F. Zwarts,
in het openbaar te verdedigen op
vrijdag 1 oktober 2010
om 14:45 uur

door

Joost Veerman

geboren op 11 december 1945
te Zwolle

Promotor:	Prof. ir. G.J. Harmsen
Copromotor:	Dr. S.J. Metz
Beoordelingscommissie:	Prof. ir. M.W.M. Boesten Prof. ir. G.J. Harmsen Prof. dr. F. Kapteijn Prof. dr. -Ing. M. Wessling

de zee en de rivieren

niemand die dit had verwacht
wat nu gebeurt was eens een droom
de zee die glinstert in haar pracht

de hardste rots wijkt, week en zacht
ontworteld meegesleurd, een boom
rivieren met hun stille kracht

de wind drijft ginds een haastig jacht
een bark vaart stampend onder stoom
de zee die glinstert in haar pracht

de maan, die in het water lacht
de nacht maakt alles monochroom
rivieren met hun stille kracht

het zout dat ons het leven bracht
broedplaats van het oeratoom
de zee die glinstert in haar pracht

bij windstilte en in de nacht
steeds is daar die blauwe stroom
rivieren met hun stille kracht
de zee die glinstert in haar pracht

Joost Veerman
april 2009

Contents

Chapter 1

Introduction

1.1. History

In 1972, the Club of Rome published *Limits to Growth*[1] that created a public shock. The report predicted that economic growth is limited by an finite amount of ores and fossil fuel. Shortly after the publication, the oil crisis broke out and increased the public concern about the scarcity of natural resources. In 1985 a conference on the "Assessment of the Role of Carbon Dioxide and Other Greenhouse Gases in Climate Variations and Associated Impacts" was organized in Villach, Austria by UNEP/WMO/ICSU. The conclusion was that greenhouse gases "are expected" to cause significant warming in the next century and that some warming is inevitable[2]. In June 1988, James E. Hansen stated that human actions had already measurably affects on the global climate[3]. The next milestone was the *Kyoto Protocol***,** adopted in 1997 and entered in force in 2005. The target of the protocol was the reduction of the emission of four greenhouse gases (CO_2, CH_4, N_2O, SF_6) and two groups of ozone attacking gases (hydrofluorocarbons and perfluorocarbons).

New renewable forms of energy are needed without thermal pollution, without emission of environmental unwanted substances and without net emission of greenhouse gasses. Wind power, hydropower, biofuel, solar power, geothermal power and ocean power are contributors to an economy of renewable energy. A relatively young member of this group is salinity gradient power (SGP), the energy that can be generated from reversible mixing of two kinds of water with different salt contents. This technique is proposed by Pattle in 1954[4,5]. In 1954 Pattle wrote[4]: *The osmotic pressure of sea-water is about 20 atmospheres, so that when a river mixes with the sea, free energy equal to that obtainable from a waterfall 680 ft. high is lost. There thus exists an untapped source of power which has (so far as I know) been unmentioned in the literature.*

The potential of salinity gradient power (SGP) is the product of the exergy density of river water times the flow rate of the river water:

$$Potential\ \ power\ =\ Exergy\ \ density\ \ *\ \ Flow\ \ rate$$

The average value of the exergy content of river water can be used for an estimation of the global power. This exergy content is about $2.5 \cdot 10^6$ J/m^3, supposing that a large excess of sea water is used. The total discharge of all rivers in the world is estimated to be $1.13 \cdot 10^6$ m^3/s [6]. Therefore, the global potential power is 2.8·TW, a value near to the 2.6 TW as estimated in 1977 by Wick and Schmitt[7].

In 2008, the average world energy consumption was about 15 TW; 5 TW of his amount was

used to generate 2 TW of electrical energy in most low efficient coal fired power plants[8]. Thus the potential of SGP is more than the current global electricity consumption.

The advantages of SGP are: limitless supply (if river and seawater are used), no production of pollutants like NO_x, no CO_2-exhaust, no thermal pollution, no radioactive waste and no daily fluctuations in production due to variations in wind speed or sunshine. However, relative to other fuels, the salinity gradient energy content of river water is rather poor (*Table 1.1*). Consequently, investment costs for a SGP plant may be rather high and transportation costs of feed water to the plant and inside the plant is substantial.

Table 1.1. Energy per kg of some energy carriers ('fuels').

fuel	process	energy (MJ/1000 kg)
sea and river water	salt gradient energy	1.7
sewage water	methane production	~1
gasoline	burning	40 000
coal	burning	30 000
sea water	deuterium fusion	10 000 000

1.2. Efficiency of salinity gradient power; objectives of the research

Salinity gradient power is an enormous source of clean and renewable energy. The energy density of this 'fuel' is low compared to fossil fuels but the quantities involved are large and the total power – the product of energy density and quantity – is considerable. There are two main challenges: to find suitable locations for SGP and to develop a suitable technique for the conversion of SGP into usable energy. The objective of our research is the second one.

The real generated power is lower than the potential power and is dependent on the availability of the river water (defined by the availability fraction f_{water}), the external efficiency ($\eta_{external}$) and the internal efficiency ($\eta_{internal}$).

$$Real\ power = f_{water} * \eta_{external} * \eta_{internal} * Potential\ power$$

The availability of the river water (f_{water}) is dependent on the local infrastructure; one important limiting factor may be the need for unhindered shipping. However, recent studies have shown that this may not be a limitation[9]. The external efficiency ($\eta_{external}$) is related to the power as needed for transportation of sea and river water to the SGP plant and to the power demand of the prefiltration process.

The internal efficiency ($\eta_{internal}$) is related to all processes within the SGP generator. Our research was restricted to the SGP generator; availability of the river water, prefiltration and transport of feed water to the generator were not included in or project; fouling of the generator was also excluded as research object.

Our goal was the design of a generator, capable to convert salinity gradient power into electricity. Special points of attention are:

- the power density (expressed in Watts per square meter membrane area)
- the total produced power (Watt)
- the internal efficiency of the process

1.3. Definition of the research questions

When we started the project in 2005, the literature revealed two serious candidates: *reverse electrodialysis* (RED) and *pressure-retarded osmosis* (PRO). At that moment only six scientific articles describing real experiments on RED have been published and for PRO there was about the same amount of literature. All described experiments concerned small laboratory generators with a power output of less than 1 Watt. An exception was the work of V. Kniajev of the *Institute of Marine Technology Problems FEB RAS* in Vladivostok (Russia) who constructed a RED generator and tested this using field conditions; regretfully, results were never published in scientific literature[10].

RED compared to PRO

From the two candidate techniques, RED seemed to be more attractive experimentally because by using this method the conversion is rather simple, without the requirement of high pressure set-ups, pressure exchangers and turbines. Therefore, the first research question was (and discussed in *Chapter 2*):

Is RED better than PRO for generating energy from sea and river water?

The techniques should be compared on different aspects; the main are internal efficiency and power density. Efficiency is important to obtain a maximal amount of energy from a given quantity of river water; power density can be defined as the generated power per unit of investment (W/€), power per cubic meter installation (W/m^3) etc. We decided to use the generated power per square meter membrane (W/m^2) because some proper data were available both for RED and for PRO in W/m^2.

Managing parasitic currents

Parasitic currents may be present in a RED stack and decrease the overall efficiency of this process. In principle, there may be an energy loss due to three short circuits: the sea water feed channels, the river water channels and the electrode rinse solution. In principle parasitic currents can be prevented by the use of mechanical valves or air bubble injection, but it would be more practical to design a RED stack with inherently low losses. Therefore, the next research question was (and answered in *Chapter 3*):

Is it possible to manage power losses by ionic short-circuit through a proper stack design?

Electrode systems

In the literature on RED, different electrode systems are described. Some of these systems require a reversal of the electrical current (which is only possible with symmetric stacks), some make use of gas evolving reactions (which may be dangerous) and other apply platinum electrodes in their system (which is expensive). Therefore, we discussed in *Chapter 4*:

What are useful electrode systems for RED?

Used aspects for a comparison should include safety, health, environment, technical feasibility and economics.

Stack properties

The produced net power by a RED stack is the generated electrical power minus the hydrodynamic power losses. The spacers play a crucial role in the power production: thick spacers (with large openings) have a small lateral hydrodynamic resistance but induce, when filled with feed water, a high electrical resistance perpendicular on the membranes and vise versa. High flow rates lead to a large produced power but to a low efficiency and vise versa. Besides the produced net power, also net power density and net efficiency are affected by hydrodynamic losses. A stack of 10x10 cm^2 with 50 cells seems large enough to serve as a prototype of larger stacks and can be used to study the complicated properties of the RED process. Therefore, the next research question was (and is the subject of *Chapter 5*):

What is the performance of a 10x10 cm^2 stack with 50 cells?

Membranes

The central theme will be describing the power density and efficiency in terms of

membrane and spacer properties, stack and cell dimensions and fluid velocities. The performance of a stack is affected by two kinds of losses: hydrodynamic and electrical. The first are located in the manifolds and in the spacers, the second in the feed water supply and in the membranes. Membranes are of particular interest, because they include three sources of losses: osmosis, co-ion transport and membrane resistance. Therefore, we take a closer look at the properties of the membranes in *Chapter 6*:

What is the effect of osmosis, co-ion transport and membrane resistance on the generated power and efficiency of different membranes?

Scale-up

Besides power density and efficiency, especially power is an important response parameter. To obtain more power, the dimensions of the cells should be increased and therewith the length of the flow channels. An important process variable to be studied is the flow rate of the feed, or the residence time. In such an up-scaled stack, the effect of flow direction (co-current or counter-current) should be investigated. Because the salt concentration in the river water compartment increases during the passage through the cells, the area stack resistance decreases locally (the effect of the decreasing concentration in the sea water compartment is less). Therefore, it is expected that segmentation of the electrodes is profitable. Therefore, the research question was (as discussed in *Chapter 7*):

What is the effect of flow channel length, residence time, flow direction and of electrode segmentation on power density and efficiency of a RED stack?

Modeling

There are two types of mass transport in a RED cell: the lateral transport of sea and river water through the spacer filled compartments and perpendicular to the membranes, the transport of ions (co- and counter-ion transport) and water (osmosis). Feed water transport is described by hydrodynamics; the driving forces are the applied hydrostatic pressures. Transport of ions and water is described by the theory of membrane transport and of transport in free solutions; the driving forces are the electrical and chemical potentials.

On the basis of these theoretical considerations, it should be possible to construct a model. This model can be validated by formerly performed experimental data. Our goal is an optimal RED stack design with optimal operation parameters for further upscaling. In short, two research questions can be formulated (and are answered in *Chapter 8*):

How to model the RED process and how to optimize the design with this model?

1.4. The Wetsus Blue Energy project

The idea of Wetsus, centre of excellence for sustainable water technology[11], is combining scientific excellence with commercial relevance. In the Wetsus themes, technical universities work together with participants, companies interested in the different subjects. In January 2005 Wetsus started, the *Blue Energy* theme, the development of salinity gradient energy on economical scale. It was decided to focus on reverse electrodialysis, a technique from with only four experiments were described in scientific literature in the period 1955 to 1986[4, 5,12-15]. The Blue Energy theme is coordinated by Dr. Ir. M. Saakes from the Wetsus institute. Within the Blue Energy project, three aspects were formulated: membrane development, fouling prevention and stack design.

1.4.1. Membrane development

This work was performed by P. Długołęcki under the responsibility of Prof. Dr. –Ing. M. Wessling and Dr. Ir. D.C. Nijmeijer of the University of Twente (The Netherlands) and resulted in five scientific publications[16-20] and a thesis[21]. In short terms, we shall discuss the most important findings.

- It was indicated that the development of special membranes for RED is necessary. The first step was to determine the requirements for these membranes and to investigate the possibility of using commercial membranes for RED to bridge over the time that the new membranes are in development. Długołęcki et al. found that the membrane resistance should be as low as possible, while the membrane selectivity is of minor importance. According to the membrane model calculations, power densities higher than 6 W/m^2 could be obtained by using thin spacers and especially for reverse electrodialysis designed membranes[16].
- With direct current and alternating current experimental stack characterization methods, it is possible to quantify the contribution of the concentration polarization, spacer shadow effects and stack resistance in RED on the power output of a RED stack[17].
- Because the resistance of ion exchange membranes is the key parameter in a RED stack, the effect of the solution concentration was investigated. It proved that at low concentrations the membrane resistance increases very strong. This has large implications for the RED process[18].
- Next to concentration polarization phenomena, especially the spacer shadow effect, has a high impact on the net power output. Normal, non-conductive spacers block the ionic transport in the stack, thus reducing the area effectively available for ionic transport. The authors developed and applied ion conductive spacers for RED, which eliminate the spacer shadow effect and obviously improves the overall process performance[19].

- Because direct current methods do not allow discriminating between these individual resistances, electrochemical impedance spectroscopy (EIS) was applied, which uses an alternating current, to analyze resistance phenomena in ion exchange membranes. The authors found that the increase in membrane resistance with decreasing concentration is the consequence of the strong increase in resistance of the diffusion boundary layer. This also explains the strong effect of the flow rate on the resistance[20].

1.4.2. Fouling prevention

This work was performed by J.W. Post under the supervision of Prof. Dr. Ir. C.J.N. Buisman and Dr. Ir. H.V.M. Hamelers of the Wageningen University (The Netherlands) and resulted in four scientific publications[22-25] and a thesis[26]. Again the main points of this research are summarized:

- The central aspect of this research was the expected fouling on membranes and spacers within a RED stack. However, Post et al. started with a comparison of the two most promising energy conversion techniques: PRO (pressure-retarded osmosis) and RED (reverse electrodialysis). It proved that each technique has its own field of application. PRO seems to be more attractive for power generation using concentrated saline brines and RED seems to be more attractive using seawater and river water. Another conclusion was that for improvements of PRO, membrane characteristics are the most important and for the development of RED, one must focus on system characteristics, i.e. optimization of the internal resistance, which is mainly determined by the width of the spacers[22].
- RED has been investigated generally with a focus on obtained power, without taking care of the energy recovery. However, optimizing the technology to power output only, would generally result in a low energetic efficiency. Therefore, Post et al. studied the aspect of energy recovery. They concluded that under special conditions an energy recovery of >80% can be achieved. This number was obtained with recirculating the feed waters and pump losses were ignored[23].
- In most publications on RED pure sodium chloride solutions were used. In practice, however, also other ions are present in both feed solutions. Therefore, the effect of multivalent ions on the performance of a RED stack was investigated. Results show that, especially the presence of multivalent ions in the dilute solution has a lowering effect on the stack voltage. In order to prevent or hamper this transport against the activity gradient, monovalent-selective membranes can be used[24].
- For pre-treatment, a capital-inexpensive microscreen filter with 50 mm pores was selected and tested. Such a straightforward pre-treatment is only sufficient given the fact that the reverse electrodialysis stack was redesigned towards a more robust

spacer-less system[25].

- For the economic feasibility, a 200 kW repetitive unit was designed. Post et al. estimated a cost price of less than 0.08 €/kWh (excl. any subsidy or compensation), comparable with that of wind energy[25].

1.4.3. Stack design

This work was performed by J. Veerman under responsibility of Prof. Ir. G.J. Harmsen of the University of Groningen (The Netherlands) and Dr. Ir. S.J. Metz of the Wetsus Institute and resulted in four published and two submitted scientific publications[27-32] and this thesis[33]. The structure of this research was discussed in *Chapter 1.3*.

References Chapter 1

1 D.H. Meadows, D.L. Meadows, J. Randers, W.W. Behrens III (1972). *The Limits to Growth*. New York: Universe Books

2 World Meteorological Organization (WMO) (1986). *Report of the International Conference on the assessment of the role of carbon dioxide and of other greenhouse gases in climate variations and associated impacts.* Villach, Austria

3 J. Hansen, *Statement presented to United States senate , Committee on Energy and Natural Resources* (1988)

4 R.E. Pattle, *Production of electric power by mixing fresh and salt water in the hydroelectric pile.* Nature 174 (1954) 660

5 R.E. Pattle, *Electricity from fresh and salt water - without fuel.* Chem. Proc. Eng. 35 (1955) 351–354

6 J.T. Kuleszo, *The global and regional potential of salinity-gradient power.* Dept. Environmental Sciences, Environmental Systems Analysis Group, Wageningen University and Research centre (2008)

7 G.L. Wick, W.R. Schmitt, *Prospects for renewable energy from sea.* Mar. Technol. Soc. J. 11 (1977) 16-21

8 Energy Information Administration, http://www.eia.doe.gov/

9 R. Quak, *Feasibility of a power plant, Blue Energy in Dutch Delta.* Faculty of Civil Engineering and Geosciences, Department of Hydraulic Engineering. Delft University of Technology (2009)

10 V. Kniajev, *Energy of salinity gradient - new source of energy with minimal environmental impact.* Abstracts from the International Workshop "Result of Fundamental Research for Investments" (IWRFRI'2001'), St. Petersburg. Russia (2001)

11 http://www.wetsus.nl

12 J.N. Weinstein, F.B. Leitz, *Electric power from differences in salinity: the dialytic battery.* Science 191 (1976) 557–559

13 R. Audinos, *Electrodialyse inverse. Etude de l'energie electrique obtenue a partir de deux solutions de salinites differentes.* J. Power Sources 10 (1983) 203–217

14 R. Audinos, *Electric power produced from two solutions of unequal salinity by reverse electrodialysis.* Ind. J. Chem. 31A. (1992) 348–354

15 J. Jagur-Grodzinski, R. Kramer, *Novel process for direct conversion of free energy of mixing into electric power.* Ind. Eng. Chem. Process Des. Dev. 25 (1986) 443–449

16 P. Długołęcki, K. Nymeijer, S. Metz, M. Wessling, *Current status of ion exchange membranes for power generation from salinity* gradients J. Membr. Sci. 319 (2008) 214-222

17 P. Długołęcki, A. Gambier A, K. Nijmeijer, M. Wessling, *Practical potential of reverse electrodialysis as process for sustainable energy generation. Environ. S*

18 P. Długołęcki, B. Anet, S.J. Metz, K. Nijmeijer, M. Wessling, *Transport limitations in ion exchange membranes at low salt concentrations.* J. Membr. Sci. 346 (2010) 163-171

19 P. Długołęcki, P. Ogonowski, S.J. Metz, K. Nijmeijer, M. Wessling, *On the resistances of membrane, diffusion boundary layer and double layer in ion exchange membrane transport.* J. Membr. Sci. 349 (2010) 369-379

20 P. Długołęcki, J. Dabrowska, K. Nijmeijer, M. Wessling, *Ion conductive spacers for increased power generation in reverse electrodialysis.* J. Membr. Sci. 347 (2010) 101-107

21 P.E. Długołęcki, *Mass transport in reverse electrodialysis for sustainable energy generation.* Thesis, University of Twente, The Netherlands (2009). ISBN 978-90-365-2928-0

22 J.W. Post, J. Veerman, H.V.M. Hamelers, G.J.W. Euverink, S.J. Mets, K. Nymijer, C.J.N. Buisman, *Salinity-gradient power: Evaluation of pressure-retarded osmosis and reverse electrodialysis.* J. Membr. Sci. 288 (2007) 218-230

23 J.W. Post, H.V.M. Hamelers, C.J.N. Buisman, *Energy recovery from controlled mixing salt and fresh water with a reverse electrodialysis system.* Environ. Sci. Technol. 42 (2008) 5785-5790

24 J.W. Post, H.V.M. Hamelers, C.J.N. Buisman, *Influence of multivalent ions on power production from mixing salt and fresh water with a reverse electrodialysis system.* J. Membr. Sci. 330 (2009) 65-72

25 J.W. Post, C.H. Goeting, J. Valk, S. Goinga, J. Veerman, H.V.M. Hamelers, P.J.F.M. Hack, *Towards implementation of reverse electrodialysis for power generation from salinity gradients.* Desalination and Water Treatment 16 (2010) 182-193

26 J.W. Post, *Blue Energy: electricity production from salinity gradients by reverse electrodialysis.* Thesis, Wageningen University, Wageningen The Netherlands (2009). ISBN 978-90-8585-510-1

27 J. Veerman, J. W. Post, S.J. Metz, M. Saakes, G.J. Harmsen, *Reducing power losses caused by ionic shortcut currents in reverse electrodialysis stacks by a validated model.*J. Membr. Sci. 310 (2008) 418-430

28 J. Veerman, S.J. Metz, M. Saakes, G.J. Harmsen, *Reverse electrodialysis: performance of a stack with 50 cells on the mixing of sea and river water.*J. Membr. Sci. 327 (2009) 136-144

29 J. Veerman, R.M. de Jong, M. Saakes, S.J. Metz, G.J. Harmsen, *Reverse electrodialysis: Comparison of six commercial membrane pairs on the thermodynamic efficiency and power density.*J. Membr. Sci. 343 (2009) 7–15

30 J. Veerman, M. Saakes, S.J. Metz, G.J. Harmsen, Reverse *electrodialysis: evaluation of suitable electrode systems.* J. Appl. Electrochem. *DOI 10.1007/s10800-010-0124-8*

31 J. Veerman, M. Saakes, S.J. Metz, G.J. Harmsen, *Electrical power from sea and river water by reverse electrodialysis: a first step from the laboratory to a real power plant.* Submitted to Environmental Science & Technology.

32 J. Veerman, M. Saakes, S.J. Metz, G.J. Harmsen, *Reverse electrodialysis: a validated process model for design and optimization.* Submitted to the Chemical Engineering Journal.

33 J. Veerman, Reverse *electrodialysis, design and optimization by modeling and experimentation.* Thesis, University of Groningen, The Netherlands (2010). ISBN: 978-90-367-4463-8 (Print), 978-90-367-4464-5 (Online)

Chapter 2

Comparison of different techniques for salinity gradient power

Abstract

Salinity gradient power (SGP) is the energy that can be obtained from the mixing entropy of two solutions with a different salt concentration. It is a potentially huge source of sustainable energy when sea water and river water are used. Literature describes five techniques to convert this energy into electricity. However only *reverse electrodialysis* (RED) and *pressure-retarded osmosis* (PRO) seemed to be realistic when we started the project. In theory both techniques generate the same amount of energy from given volumes of sea and river water with specified salinity; in practice the RED technique seems to be more attractive for power generation using sea water and river water.

2.1. Techniques for energy generation using salinity gradient power (SGP)

There are different processes that can convert the potential energy from SGP into electricity. Most of these methods are the reversal of formerly developed desalination techniques.

(a*) Reverse electrodialysis* (*RED*), the inverse of electrodialysis (ED). The ED technique was founded by Maigrot and Sabates in 1890[1,2]. Manecke proposed to store energy with the ED process in 1952[3]. He demonstrated that it is possible to reuse this electrical energy by the reversal operation of his 'Membranakkumulator'. Pattle was the first who remarked that the combination of river water with seawater can be used as a power source in a 'hydroelectric pile'[4,5].

In principle, the set-up for RED and ED are similar. *Figure 2.1* shows a simple apparatus in the RED mode. Two kinds of membranes are used in this process: one permeable for positive ions (the cation exchanging membrane, CEM) and another only permeable for negative ions (the anion exchanging membrane, AEM). By diffusion of ions, an ionic current is generated. This ionic current is converted in an electron current at the electrodes by proper redox reactions.

There are three ways of using the potential power with a RED technique:

- Conversion into electricity. As stated above, Pattle was the first who performed RED experiments[4,5].
- For desalination. Murphy and Matthews described a process where the SGP was used for demineralization[6,7]. Unaware of their work, Veerman made a new approach of this technique with a four cell device[8].
- Conversion into chemical energy. If the electrode rinse solution does not contain a reversible redox couple, H_2 is evolved at the cathode and O_2 and/or Cl_2 at the anode. Especially H_2 is valuable as energy carrier. The possibility of hydrogen generation with RED was remarked by Weinstein and Leitz in 1976. They stated: *Electrode reactions could be chosen to yield useful products, but the first law of thermodynamics dictates that any energy so used would represent an inefficiency in power generation*[9]. Nevertheless, J.B. Seale obtained a patent on the generation of H_2 with RED in 2006[10]. A specialized RED stack for hydrogen production contains special electrodes with a low overvoltage for gas evolution and a limited amount of cells (~50) in the stack.

(b) *Pressure-retarded osmosis* (*PRO*), the reversal of reverse osmosis (RO). A semi permeable membrane is used: only water can pass but not ions like Na^+ and Cl^-. Loeb and

cooperators are the pioneers of this technique[11].

(c) Vapor pressure difference utilization process (VPDU), the reversal of vacuum distillation. The vapor pressure of water decreases with the salt content. If an amount of water is separated through a copper plate from an amount salt water and the vapor phase of both waters are in contact, there would be water vapor flow from the river to the sea compartment. The formed heat of condensation is directed backward through the copper plate to the evaporating vessel. A demonstration model was built by Olsson et al.[12]. On economical scale, the technique seems to be very difficult: a large area of evaporation surface is needed for the phase transfer and the maintenance of the vacuum in a continuous process will require much effort. Moreover, special turbines would have to be designed for large quantities of vapor with very low pressure differences, typically about 50 Pa.

(d) The 'mechanochemical turbine' (MT). The biophysicist Katchalsky has remarked the contraction of collagen fiber in a salt solution and the expansion is immersed in fresh water. A working machine based on this effect was described by Sussman and Katchalsky[13]. Despite the genius of the concept, a megawatt MT plant seems to be very impractical.

(e) *The reversal of the capacitive deionization (RCD).* Brogioli succeeded to invert capacitive deionization[14]. The capacitor in the setup is formed by two activated carbon electrodes, immersed in the feed solution, alternately salt and fresh water. It is charged when filled with salt water, and discharged when filled with fresh water. Charging and discharging are promoted by the diffusion of ions and consequently there is a net energy gain. Because no membranes are involved, this technique appears to be promising at first sight. However, now the electrodes play the central role in the process and the problem of membrane fouling is now moved to the electrodes.

The number of articles describing real experiments on RED are restricted to about 12; the same holds for PRO. For up-to-date references on RED and PRO, we refer to the review article from Nijmeijer and Metz[15].

2.2. Choice for the RED technique

As the methods of Olsson (VDPU) and Sussman / Katchalsky (MT) looked impractical and the method of Brogioli (RCD) was yet unknown when we started the project in 2005, we concentrated on the two remaining techniques: PRO and RED.

The theoretical amount of energy obtainable with the RED technique and the PRO technique are equal. This is proven in the appendices A, B and C of this chapter. In *Chapter 2- Appendix A*, the energy is calculated from the concept of the mixing entropy, in *Chapter 2- Appendix B* from the RED process as based on the Nernst equation and in *Chapter 2- Appendix C* from the PRO process as based on the Van 't Hoff equation.

A comparison between the two techniques was made by Post et al.[16]. All published data on RED and PRO were analyzed; however, reported performances were incomplete and the measurement conditions were not comparable. A theoretical method was developed which allows a comparison of both techniques under equal conditions, both with respect to power density and energy. The conclusions of Post et al. were:

- RED is more attractive for power generation using river and sea water and PRO is more attractive using concentrated saline brines.
- The installed costs are in the same order of magnitude.
- The costs for ED membranes is about 2-3 times higher than for RO membranes. However, the market for ED is small and a large reduction of the price is expected if the RED will have a breakthrough.

Our goal was to use the large energy potential from river water and sea water and therefore, we decided to choose for the RED technique.

2.3. Conclusions

Several different technologies are described to convert SGP into useful power; the most practical are RED and PRO. PRO and RED can theoretical produce the same amount of energy from SGP. If river water with seawater is used, the RED technique seems to be more attractive for power generation.

References Chapter 2

1 E. Maigrot, J. Sabates, *Apparat zur Läuterung von Zuckersäften mittels Elektriztät*. Germ. Pat. Nr. 50443 (1890)

2 V.A. Shaposhnik, K. Kesore K, *An early history of electrodialysis with permselective membranes.* J. Membr. Sci. 136 (1997) 35-39

3 G. Manecke, *Membranakkumulator*. Zeitschrift für Physikalische Chemie 201 (1952) 1-15

4 R.E. Pattle, *Production of electric power by mixing fresh and salt water in the hydroelectric pile.* Nature 174 (1954) 660

5 R.E. Pattle, *Electricity from fresh and salt water - without fuel.* Chem. Proc. Eng. 35 (1955) 351–354

6 G.W. Murphy, *Osmionic demineralization*. Ind. Eng. Chem. 50 (1958) 1181-1188

7 G.W. Murphy, R.R. Matthews, *Migration in transference cells with and without membranes -application to osmionic demineralization.* Electrochim. Acta 12 (1967) 983-998

8 J. Veerman, *Rijnwater ontzouten hoeft geen energie te kosten.* Polytechnisch Tijdschrift September 1994, 52-55

9 J.N. Weinstein, F.B. Leitz, *Electric power from differences in salinity: The dialytic battery.* Science 191 (1976) 557-559

10 J.B. Seale, *Reverse dialysis for generation of hydrogen*. Patent US20060263646 (2006)

11 S. Loeb, F. van Hessen, D. Shahaf, *Production of energy from concentrated brines by pressure- retarded osmosis II. Experimental results and projected energy costs.* J. Membr. Sci.1 (1976) 249-269

12 M. Olsson, G.L. Wick, J.D. Isaacs, *Salinity gradient power - utilizing vapor-pressure differences.* Science 206 (1979) 452–454

13 M.V. Sussman, A. Katchalsky, *Mechanochemical turbine: a new power cycle*. Science 167 (1970) 45–47

14 D. Brogioli, *Extracting Renewable Energy from a Salinity Difference Using a capacitor.* Phys. Rev. Lett. 103, (2009) 058501 1-5

15 K. Nijmeijer, S.J. Metz, *Salinity Gradient Energy,* Chapter 5 from Sustainability Science and Engineering Volume 2 Sustainable Water for the Future: Water Recycling versus Desalination (Editors I.C. Escobar and A.I. Schäfer)

16 J.W. Post, J. Veerman, H.V.M. Hamelers, G.J.W. Euverink, S.J. Metz, D.C. Nymeijer, C.J.N. Buisman, *Salinity-gradient power: Evaluation of pressure-retarded osmosis and reverse electrodialysis*. J. Membr. Sci. 288 (2007) 218–230

17 C. Forgacs, R.N. O'Brien, *Utilization of membrane processes in the development of non-conventional renewable energy sources.* Chem. Can. 31 (1979) 19-21

18 J.N. Weinstein, F.B. Leitz, *Electric power from differences in salinity: The dialytic battery.* Science 191 (1976) 557-559

19 B.H. Clampitt, F.E. Kiviat, *Energy recovery from saline water by means of electrochemical cells.* Science 194 (1976) 719-720

20 J. Jagur-Grodzinski, R. Kramer, *Novel Process for direct conversion of free energy of mixing into electric power*. Ind. Eng. Chem. Process Des. Dev. 25 (1986) 443-449

Appendix A

Theoretical amount of energy from the mixing entropy of seawater and river water

When two NaCl solutions with different concentrations are mixed, the entropy *S* increases; the volume change is negligible. If the solutions are ideal, there is no thermal effect on irreversible mixing (adding together fresh and salt water and stirring). The electrolyte simulation program OLI (OLI Systems Inc. Morris Plains, NJ, USA) predicts a temperature rise of 0.013 K on mixing of equal volumes of pure water and a 0.5 M NaCl solution (about the total salt concentration of sea water). This implies that, if the process is performed reversible and energy is extracted, there must be added heat to the system (if operated isothermal) or the system should cool down slightly (if the process is adiabatic). The latter is the normal way and it will be proven that the temperature effect is not more than about −0.2 degrees if sea water with river water is used. Consequently, for entropy calculation the mixing process (reversible or irreversible) can be regarded to be isothermal.

We assume the total number of moles (m) in a cubic meter of salt solution at 298 K to be independent of the salt content, thereby regarding the particles H_2O, Na^+ and Cl^- as independent molecules. Then m=55555 mol/m^3 in pure water and in NaCl solutions. The fractions used are *x* for the ions and *y* for water, and the indices used are *S* for the concentrated solution (or seawater), *R* for the diluted solution (or river water) and *M* for the mixture of sea and river water. The seawater contains C_S NaCl/m^3 and the river water C_R mol NaCl/m^3. *Table 2.1* shows the relation of the mol fractions of ions (*x*) and water (*y*) in the sea water, the river water and the mixture.

Table 2.1. Mol fractions as function of volume and salt content

	volume	salt conc.	moles		mol fractions	
	m^3	mol/m^3	ions	water	ions	water
sea	V_S	C_S	$n_{x,S} = 2V_S.C_S$	$n_{y,S} = V_S.m - n_{X,S}$	$x_S = n_{X,S}/(n_{X,S} + n_{Y,S})$	$y_S = 1 - x_S$
river	V_R	C_R	$n_{x,R} = 2V_R.C_R$	$n_{y,R} = V_R.m - n_{X,R}$	$x_R = n_{X,R}/(n_{X,R} + n_{Y,R})$	$y_R = 1 - x_R$
mixture	$V_M=V_S+V_R$	C_M *)	$n_{x,M} = n_{x,S}+n_{X,R}$	$n_{y,M} = n_{Y,S} + n_{Y,R}$	$x_M = n_{X,M}/(n_{X,M} + n_{Y,M})$	$y_M = 1 - x_M$

*) $C_M=(C_SV_S+C_RV_R)/(V_S+V_R)$

First the entropy increase of the river and sea water is calculated if these were composed from pure water and solid salt, using:

$$S = -nR\left[x\,ln(x) + y\,ln(y)\right] \tag{1}$$

where *n* is the number of moles and *R* the gas constant.
Using NaCl concentrations C_R=17.1 mol/m^3 (1 g/L) and C_S=513.3 mol/m^3 (30 g/L) and volumes V_S=V_R = 1m^3, the next entropies are achieved for the sea water (S_S), the river water (S_R) and the mixture (S_M):

$$S_S = -V_S mR\left[x_S\,ln(x_S) + y_S\,ln(y_S)\right] = 42.53 \cdot 10^3\ JK^{-1} \tag{2}$$

$$S_R = -V_R mR\left[x_R\,ln(x_R) + y_R\,ln(y_R)\right] = 2.39 \cdot 10^3\ JK^{-1} \tag{3}$$

$$S_M = -V_M mR\left[x_M\,ln(x_M) + y_M\,ln(y_M)\right] = 49.81 \cdot 10^3\ JK^{-1} \tag{4}$$

The increase of entropy (ΔS_{total}) on mixing is:

$$\Delta S_{total} = S_M - S_S - S_R = 4.89 \cdot 10^3\ JK^{-1} \tag{5}$$

Ignoring the contribution of water to the entropy, the result is:

$$\Delta S = -mR\left[V_M x_M\,ln(x_M) - V_S x_S\,ln(x_S) - V_R x_R\,ln(x_R)\right] = 4.86 \cdot 10^3\ JK^{-1} \tag{6}$$

Eq. (6) can be rewritten to:

$$\Delta S = -mR\left[V_S x_S\,ln\left(\frac{x_S}{x_M}\right) + V_R x_R\,ln\left(\frac{x_R}{x_M}\right)\right] = -2R\left[V_S C_S\,ln\left(\frac{C_S}{C_M}\right) + V_R C_R\,ln\left(\frac{C_R}{C_M}\right)\right] \tag{7}$$

with

$$C_M = \frac{C_S V_S + C_R V_R}{V_S + V_R} \tag{8}$$

The simplification as used in *Eq. (6)* is only 0.8% less than the more correct value from *Eq. (5)* and consequently we will use the derived equation - *Eq. (7)* - in the future. This equation was first derived by Forgacs[17].

In the case of a reversible isothermal process, the change of the free enthalpy can be calculated. If the solutions are ideal, the enthalpy change is zero and the reversible work (from the entropy increase) *W* is equal to the free enthalpy change.

$$W = \Delta G = \Delta H - T \cdot \Delta S = 0 - 298 \cdot 4.857 \cdot 10^4 = -1.45 \cdot 10^6\ J \tag{9}$$

(This numerical result is based on C_R=1 g/L, C_S=30 g/L and V_S=V_R = 1m^3)
If there is no heat-flow from outside, the water must cool down somewhat.

$$\Delta T = \frac{W}{V_M \, \rho_{H2O} \, C_w} = -0.17 \, K \tag{10}$$

Here V_M stands for the total volume (V_M=V_S+V_R), ρ_{H2O} for the density of water (1000 kg/m^3) and C_w for the specific heat of water (4187 J.kg^{-1}.K^{-1}). Because the temperature drop is very small, the approximation of an isothermal process is acceptable.

Appendix B

Theoretical amount of energy from the RED process

In the Reverse ElectroDialysis (RED) process, Na^+-ions can diffuse from the sea water compartments through the cation exchange membranes (CEM) to the river water compartments; Cl^--ions can diffuse through the anion exchange membranes (AEM) from sea to river water in the opposite direction (*Figure 2.1*). Inside the stack there is an ionic current which is converted into an electron current at the electrodes by proper redox reactions. In C*hapter 4* of this thesis the different possibilities for electrode systems are compared.

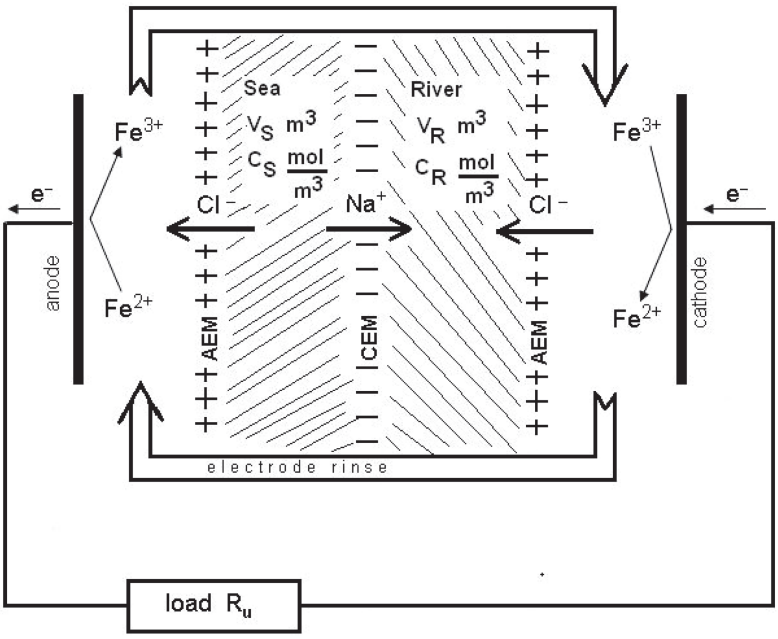

Figure 2.1. A RED stack with one cell.

In the following calculations, we assume a batch process: the compartments are filled with V_S m³ sea water and V_R m³ river water with initial salt concentrations C_S and C_R mol/m³. These solutions are not refreshed in the next consideration.

The generated potential over each membrane is given by the Nernst-equation[18,19,20]. Assuming ideal circumstances, the activities can be replaced by concentrations. Further, for univalent ions, the value of *z* (the valency) is unity. If the poles of a RED stack are connected by a load an electrical current goes through this external resistance R_u and through the internal resistance R_i of the stack the Nernst voltage φ is time dependent en given by the equation:

$$\varphi(t) = \alpha \frac{RT}{zF} ln\left(\frac{a_S(t)}{a_R(t)}\right) \approx \frac{RT}{F} ln\left(\frac{C_S(t)}{C_R(t)}\right) \tag{11}$$

F stands for the Faraday constant (*F* = 96485 C/mol) and a_S and a_R for the mean activity of the ions. Assumed is a permselectivity α =1 for the membranes.

The energy delivered to both resistances is the integral $-\int \Phi(t) dQ$ where *Q* is the transported charge. This generated energy has a minus sign because streams to the system are positive as usual in thermodynamics. This current is proportional to the amount of transported ions n: anions through the AEMs and cations through the CEMs from the sea to the river water compartments.

$$dQ = d(F \cdot n) = d(F \cdot C \cdot V) = F \cdot V \cdot dC \tag{12}$$

$$W_{RED} = -\int \varphi \, dQ = -\frac{RT}{F} FV \int ln\left(\frac{C_S(t)}{C_R(t)}\right) dC \tag{13}$$

The process stops if both concentrations are equal. This equilibrium concentration is the formerly C_M as defined in *Eq. (8)*. The amount of transported ions *d* (mol) at the end is:

$$d = V_S(C_S - C_M) \tag{14}$$

$$W_{RED} = -2RT \int_0^d ln\left(\frac{C_S - \frac{Q}{V_S}}{C_R + \frac{Q}{V_R}}\right) dQ = -1.45 \cdot 10^6 \ J \tag{15}$$

(Again, this numerical result is based on C_R=1 g/L, C_S=30 g/L and V_S=V_R = 1m³)

The result from *Eq. (15)* as calculated with *Mathcad 11.0* (Mathsoft Engineering & Education,

Inc) is the same as the calculated value from the entropy increase W_E in *Eq (9)*. This is not surprising because same physical principles are used in theory of entropy and of the RED process.

Appendix C

Theoretical amount of energy from the PRO process

The Pressure-Retarded Osmosis (PRO) process uses the osmotic pressure from the salt solution. We can imagine a batch-process with a piston made of a semipermeable material between two compartments (*Figure 2.2*).

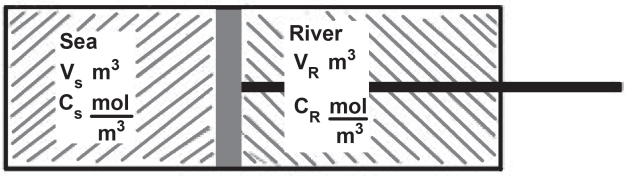

Figure 2.2. A PRO cell. The compartments are separated by a semipermeable piston.

Water diffuses through the piston from the river water to the sea water. The expansion of the seawater compartment produces energy (also thermodynamical written with a minus sign). To derive an expression of this energy, we will start with the classic equation for the osmotic pressure, the Van 't Hoff equation:

$$\Pi V = nRT \quad or \quad \Pi = CRT \tag{16}$$

Where Π is the osmotic pressure (Pa), V the volume (m^3) and n the number of moles.

$$W_{PRO} = -\int \Pi_{left} \cdot dV - \int \Pi_{right} \cdot dV \tag{17}$$

The process stops if the concentrations on each side of the semipermeable piston are equal to C_M as defined in *Eq. (8)*. Due to mass balance, the end volumes of the sea water compartment (V_{SE}) and the river water compartment (V_{RE}) can be achieved:

$$V_{SE} = \frac{C_S V_S}{C_M} \quad ; \; V_{RE} = \frac{C_R V_R}{C_M} \tag{18}$$

$$W_{PRO} = -2RT\left(C_S V_S \int_{V_S}^{V_{SE}} \frac{1}{V} dV + C_R V_R \int_{V_R}^{V_{RE}} \frac{1}{V} dV \right) = -1.45 \cdot 10^6 \; J \tag{19}$$

(Again, this numerical result is based on C_R=1 g/L, C_S=30 g/L and V_S=V_R = 1m^3)
The result from *Eq. (19)* is the same as the calculated value from the entropy increase W_E in *Eq. (9)*. This is due to the fact that the theory of PRO is based on the same physical principles as thermodynamics.

Nomenclature

a	mean activity
C	concentration (mol/m^3)
C_w	specific heat of water (4187 J·kg^{-1}·K^{-1})
d	number of moles transported in the RED process
F	Faraday constant (96485 C/mol)
G	free enthalpy (J)
H	enthalpy (J)
m	total number of moles per m^3 (55555 mol/m^3)
n	number of moles
Q	electric charge (C)
R	gas constant (8.314 J·mol^{-1}K^{-1})
R_i	internal resistance (Ω)
R_u	external resistance (Ω)
t	time (s)
S	entropy (J/K)
T	temperature (K)
U	voltage (V)
V	volume (m^3)
V_{SE}	end volume concentrate (m^3)
V_{RE}	end volume diluate (m^3)
W	work (J)
x	mole fraction of ions
y	mole fraction of water
z	valency of an ion

Greek symbols

α	permselectivity of the ion exchange membrane
ρ_{H2O}	density of water (~1000 kg/m^3)
Π	osmotic pressure (Pa)
φ	Nernst potential(V)

Subscripts

x	ions
y	water
S	sea (or concentrate)
R	river (or diluate)
M	equilibrium (or mixture)

Abbreviations

AEM	anion exchange membrane
CD	capacitive deionization
CEM	cation exchange membrane
ED	electrodialysis
MT	mechanochemical turbine
PRO	pressure-retarded osmosis

RCD	reverse capacitive deionization
RED	reverse electrodialysis
RO	reverse osmosis
VPDU	vapor pressure difference utilization

Chapter 3

Reducing power losses caused by ionic shortcut currents in reverse electrodialysis stacks by a validated model*

Abstract

Both in electrodialysis and in reverse electrodialysis ionic shortcut currents through feed and drain channels cause a considerable loss in efficiency. Model calculations based on an equivalent electric system of a reverse electrodialysis stack reveal that the effect of these salt bridges could be reduced via a proper stack design. The critical parameters which are to be optimized are ρ/r and R/r; where ρ is the lateral resistance along the spacers, R is the resistance of the feed and drain channels between two adjacent cells, and r is the internal resistance of a cell. Because these two parameters (ρ/r and R/r) are dimensionless, different stacks can be easily compared. The model is validated with two experimental stacks differing in membrane type and spacer thickness, one with large ionic shortcut currents and one where this effect is less. The loss in efficiency decreased from 25% to 5% for a well designed stack. The loss of efficiency in reverse electrodialysis and in electrodialysis can be reduced with the aid of the design parameters presented in this chapter.

**** Published as***

J. Veerman, J. W. Post, M. Saakes, S.J. Metz, and G.J. Harmsen

Reducing power losses caused by ionic shortcut currents in reverse electrodialysis stacks by a validated model

Journal of Membrane Science 310 (2008) 418-430

3.1. Introduction

Reverse electro dialysis (RED) is one of the possible processes for generating energy from the salt gradient between river and sea water[1]. Already in 1953 Pattle showed the possibility of this method[2]. A typical RED stack consists of a variable number of alternating cation and anion exchange membranes. The compartments between the membranes are fed in turn with a concentrated and a diluted salt solution, for instance of sea and river water. In *Figure 3.1* the situation is drawn for a stack with four cells.

Parasitic currents, also called current leakage, cause a loss in performance in both electrodialysis (ED) and reverse electrodialysis. There are two sources of these parasitic currents. Firstly in an ion exchange membrane, besides the wanted transport of the counter-ions, there is a transport of co-ions due to the fact that membranes are not 100% selective. Secondly, there are ionic shortcut currents, arising from the transport of ions through the feed and drain channels. These channels act as salt bridges between the compartments. Transport of ions through these salt bridges occurs due to an electrochemical potential difference between adjacent cells. Both types of parasitic currents cause a reduction of power and a decrease in energy efficiency in a RED stack. Reduction of the co-ion transport is a matter of membrane optimization and is left out of consideration in this chapter. However, the effect of the ionic shortcut currents is strongly related to the stack design and is discussed here.

That ionic shortcut can cause efficiency loss in electrodialysis was understood already in an early stage of the development of ED. Mandersloot and Hicks made already in 1966 a mathematical model of an ED stack and concluded that it is important to have a low

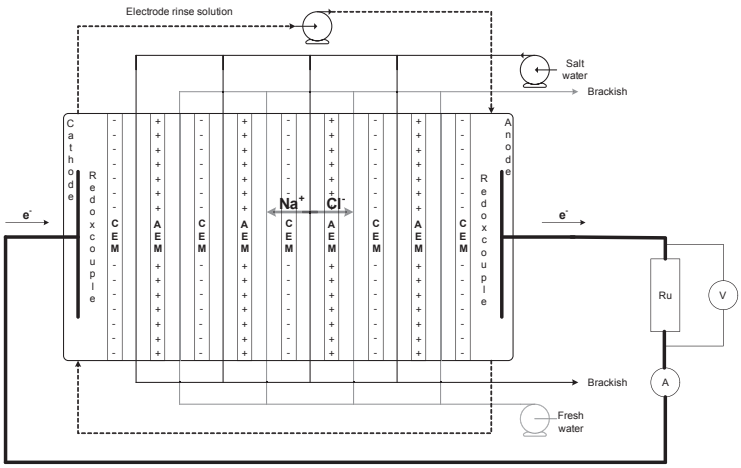

Figure 3.1. Schematic representation of a reverse electrodialysis stack with four cells.

channel conductivity between the compartments[3]. The efficiency loss is more drastic if the salt concentration becomes higher. Some measures to restrict the ionic shortcut currents are suggested:

- In Japan already in the sixties all edible salt was produced from seawater with electrodialysis. The high salt concentrations used in this process cause severe ionic shortcut losses in the system. Yamane et al. have found that the use of separate unit cells in the production of brine from sea water can reduce the ionic shortcut current by more than 30%[4]. The individual cells have separate feed tubes. The long conductive paths through these tubes give enough resistance to reduce the parasitic currents effectively.
- Air bubbles can be added to the feed. This decreases the ionic shortcut currents and has less effect on the water transport in the stack.
- Rotating valves which act as barriers to the electrolytic currents[5].
- An alternative method is the serial feed. The sea water is directed successively through all sea water compartments of the stack. These compartments are connected alternating at the top and at the bottom, causing a zigzag flow. The same holds for the river water. In this case a possible ionic shortcut current should pass a much longer pathway and is therefore significantly reduced. However, this causes also a much higher fluid resistance. However, a combination of parallel and serial feed can be realistic for an optimal design.
- The use of spiral wound modules makes the feed and drain channels superfluous. In fact there are only two compartments: the diluate and the concentrate[6,7,8].

Especially for bipolar cell stacks, the electrical leakage has been studied by different groups. In 1979 Kuhn and Booth reviewed the state-of-art in that field[9] and calculated the ionic shortcut currents as function of the place in a bipolar cell stack. Pretz and Staude[10] used a RED system with bipolar membranes and observed a limiting value of the open circuit voltage (OCV) with the increase of the number of membranes. Rubinstein[11] explained this effect by ionic shortcut currents.

The objective of this work is to quantify the efficiency losses due to ionic shortcut currents in (reverse) electrodialysis. These effects can be modeled via an equivalent electrical circuit and are validated experimentally. Experiments are performed with two different stack designs, one with a large ionic shortcut current and another where this effect is less. The model is calibrated by experiments with small stacks (1, 2 .. 5 cells) and validated by experiment with large stacks (10, 20 .. 50 cells). Model and experiments are in good agreement and this shows the possibility of managing the ionic shortcut currents within acceptable proportions.

3.2. Theory

3.2.1. Reverse electrodialysis

A RED stack with four cells is drawn in *Figure 3.1*. Each cell contains a cation exchange membrane (CEM), a compartment with a concentrated salt solution, an anion exchange membrane (AEM), and a compartment with a lower salt concentration. The last cell is closed with an extra cation exchange membrane. The 'fuel' consists of a concentrated and a diluted salt solution, for instance sea and river water.

The Na^+ ions from the sea water tend to diffuse through the cation exchange membranes and cause a positive potential on the left side of the stack. In the same way, the Cl^- ions diffuse through the anion exchange membrane in the reverse direction, also resulting in a positive potential on the left side of the stack. Transport of ions through the membranes occurs if an electrical load is connected to the electrodes. Externally there is a normal electrical current but in the cell this is an ionic current. The ionic current in the cells is converted to an electron current at the electrodes by redox reactions.
These redox reactions can be facilitated by means of a solution of $K_4Fe(CN)_6$ and $K_3Fe(CN)_6$ (potassium hexacyanoferrate (II) and potassium hexacyanoferrate (III)) in a bulk of NaCl in combination of inert electrodes. The iron(III) complex is reduced on the cathode and the iron(II) complex is reoxidized on the anode. Because the electrode rinse is recirculated through both electrode compartments, the original Fe(III)/Fe(II) ratio is maintained and there is no net chemical reaction.

$$Fe(CN)_6^{3-} + e \quad \leftrightarrows \quad Fe(CN)_6^{4-}, \quad E_0 = 0.36\ V$$

3.2.2. The electromotive force

The theory about reverse electrodialysis was formulated by Weinstein and Leitz[12], Clampitt and Kiviat[13], Jagur-Grodzinski and Kramer[14] and Lacy[15]. The potential to the left of a given cation exchange membrane in *Figure 3.1*, generated by the diffusion of Na^+ ions , is given by:

$$E = \alpha_{CEM} \frac{RT}{zF} \ln\left(\frac{a_c^+}{a_d^+}\right) \tag{1}$$

where E is the generated electromotive force (EMF), α_{CEM} the permselectivity of the cation exchange membrane, z the valency (z=1 for Na^+), R the gas constant, F the Faraday constant and a^+_c and a^+_d the activities of the sodium ion in the concentrated and diluted compartments. This formula holds also for the potential caused by the diffusion of Cl^- ions through an anion exchange membrane if α_{AEM} is taken for the permselectivity and a^-_c and

a^-_d for the activity of the Cl^- ion. Activities can be calculated with the extended Debye-Hückel formula[16]. With Eq. (1), the voltages across a 100% selective membrane can be calculated. For pure NaCl solutions of 1 and 30 g/L this gives values of 0.080 V for a CEM and 0.078 V for an AEM, or 0.158 V for a complete cell.

3.2.3. Ionic shortcut currents

A proper RED stack has a high power output characterized by the specific power (P_{spec}), which is the power generated at one square meter of membrane. An equally important process parameter is the energy efficiency: the amount of obtained energy in relation to the theoretical maximum for a given amount of fuel.

As explained in the introduction, there are two kinds of parasitic currents: firstly co-ion transport through the membranes due a restricted selectivity and secondly ionic shortcut currents, arising from the transport of ions through the feed and drain channels (*Figure 3.2*). Both types of parasitic currents cause a loss of power as well as a reduction of the energy efficiency in a RED stack.

Three ionic shortcut currents can be identified in a RED stack: i) In the electrode rinse solution. The anode compartment is connected with the cathode compartment by the electrode rinse loop as shown in *Figure 3.1*. This shortcut current is easily prevented by choosing an appropriate length of the tubing causing a higher resistance. ii) Between the river water compartments. This shortcut current has been neglected because the salt

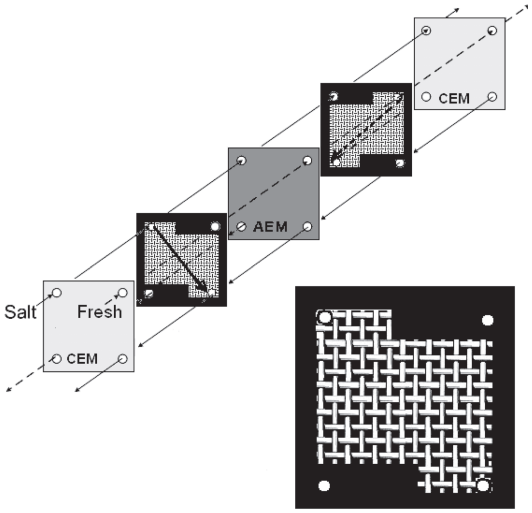

Figure 3.2. Fluid transport through the feed and drain channels of a reverse electrodialysis stack. The solid lines represent the salt water flow and the dashed lines the fresh water flow. The membranes (CEM and AEM) are separated by woven spacers surrounded by the gaskets (black). Insert: woven spacer and gasket.

concentration is too low to cause a significant shortcut current. iii) Between the seawater compartments. These latter shortcut currents are shown in *Figure 3.3*. Reducing these shortcut currents is the subject of this chapter.

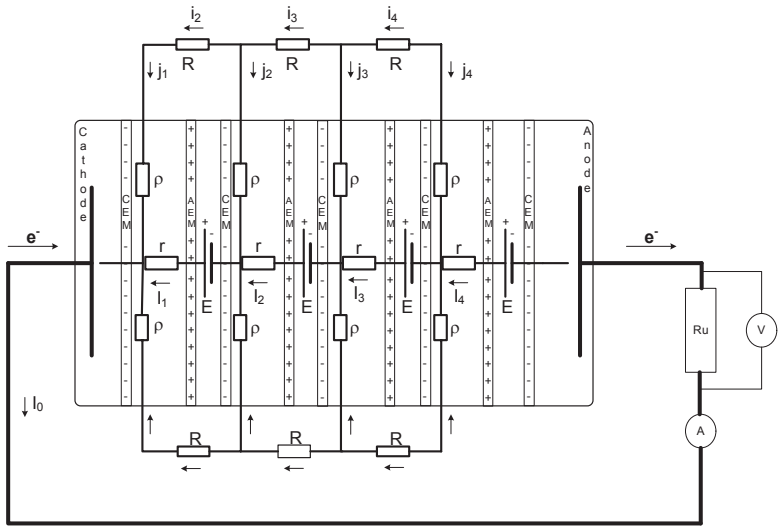

Figure 3.3. Ionic currents. The currents designated with i_n (n=2,3,4) and j_n, (n=1..4) are unwanted shortcuts. All given currents are positive except j_3 and j_4 which are negative.

In *Section 3.2.4* the theory of the power production in small stacks is formulated. In these stacks shortcut currents are not significant because the resistance of the bypass circuit is relatively high. The model is simple and the calculation of the power production can be done easily. In *Section 3.2.5* a model is introduced involving the shortcut currents in the salt water system. This model should be used if the stack has a large number of cells, but can be applied also to small and to very large stacks. In *Section 3.2.6* the model is simplified for very large stacks resulting in a simple equation for the relative power (Eq. (15)).

3.2.4. Internal resistance and power production of small stacks

In ideal stacks there are no ionic shortcut currents. In practice, these stacks consist of only a few cells. Stacks with a maximum of 5 cells are considered as ideal in this chapter. The internal resistance R_i of an ideal stack depends on the cell resistance r, the number of cells N and the resistance of the electrode system R_{el}.

$$R_i = N \cdot r + R_{el} \tag{2}$$

In the electrode resistance R_{el} is also included the resistance of one of the outer membranes (the other outer membrane is formally part of one of the cells).

The cell resistance r is the sum of the resistances of two membranes (R_{AEM} and R_{CEM}) and two water compartments (R_{river} and R_{sea}).

$$r = R_{AEM} + R_{CEM} + R_{river} + R_{sea} \tag{3}$$

If there is no spacer in the water compartment, the resistance of the water compartments, R_{comp} can be calculated from the specific conductivity σ (S/m) of the salt solution, the area A_{cell} (m^2) and the thickness δ (m) of the compartment. A correction is used for the volume occupied by the spacer material. The void factor f_v expresses the relative volume available for the salt solution (void volume).

$$R_{comp} = \frac{1}{f_v}\frac{1}{\sigma}\frac{\delta}{A_{cell}} \tag{4}$$

An ideal RED installation without complicating shortcut currents, behaves like a normal battery and its current I is given by:

$$I = \frac{E}{R_i + R_u} \tag{5}$$

where E is the electromotive force, R_i the internal resistance of the stack and R_u the external load resistance.

The power dissipated in the external resistance R_u in this ideal system is:

$$P_u = I^2 R_u = \left(\frac{E}{R_i + R_u}\right)^2 R_u \tag{6}$$

From Eq. (6) it follows that a maximum of P_u arises if $R_u = R_i$. In this case the terminal voltage is V_t = ½E. The efficiency (Eff) is the fraction of the power delivered to R_u and the total power dissipation in R_i and R_u.

$$Eff = \frac{I^2 R_u}{I^2 R_i + I^2 R_u} = \frac{R_u}{R_i + R_u} \tag{7}$$

At the condition for maximal power ($R_u = R_i$) even in an ideal system the efficiency is no higher than 50%. A higher efficiency can be achieved (by taking $R_u > R_i$) at the expense of a decreased power output.

3.2.5. Modeling the stack

An equivalent circuit model for a real stack with four cells and all shortcut circuits caused by the concentrate feed, is given in *Figure 3.4*. This stack is connected to an external load. The nomenclature of the symbols follows the model of Rubinstein et al.[11]. The directions

of the currents are arbitrarily designated. The resistors ρ are the lateral resistances along the spacers, from the middle to the drain and the feed. The resistors R are the resistances of the feed and drain channels through the stack and r is the internal resistance of a cell. For simplicity, only the shortcut by the sea water is taken into account. Shortcut by the river water is ignored because the conductivity in this part is much lower.
In fact, the equivalent circuit model in *Figure 3.4* is a summary of the circuit drawn in *Figure 3.3*. For reasons of symmetry, this model is simplified by omitting the lower part from *Figure 3.3*.

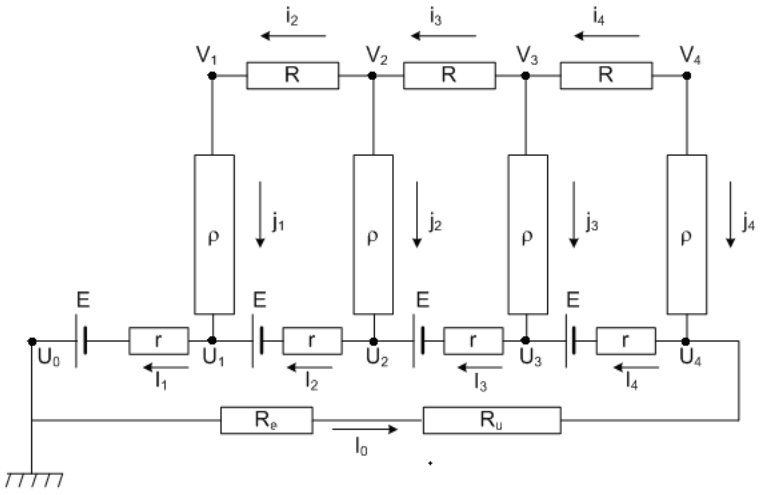

Figure 3.4. Equivalent circuit model for a RED stack with 4 cells. r is the internal resistance of a cell, ρ the resistance across a salt water space, R the resistance in the feed and drain channels between two salt water compartments, R_e the resistance of the electrode system, R_u the external load, I is the current through the membrane, i the current through the feed and drain channels, j the lateral current leakage along the membrane surface, U the potential at the centre of the membrane, V the potential in the feed and drain channel, and E the electromotive force of one cell.

Rubinstein et al.[11] have given an approach for solving a system like this in a sophisticated way. However, their model did not include an external load and only the open circuit voltage (OCV) could be calculated.

But adding a load to the system the method of Rubinstein is not applicable and a different method is necessary. This model involves many unknowns: each cell in the stack involves three currents (I, i and j) and two potentials (U and V). The five equations for solving these unknowns are three times the Law of Ohm (over r, over R and over ρ) and two times the law of Kirchhoff (in the junctions U and V). In Mathcad these equations are solved numerically.

3.2.6. An approximation for very large stacks

There are good ion conducting paths: first the main route through the cell (resistances r)

and next the bypass through the feed and drain channel (resistances R). The connection between both paths consists of the lateral spacer resistances (ρ) with a relative high resistance. However, a circuitry of many of such parallel connections result in a relatively low substitution resistance, well enough (in relation to the channel resistance) to realize an ionic shortcut current intruding into the feed and drain channels.

In this case the greater part of the resistance of the ionic shortcut current is formed by the resistances of the feed and drain channels and the lateral spacer resistance can be ignored. In *Figure 3.5* the model with this approximation is drawn. The EMF of the source,

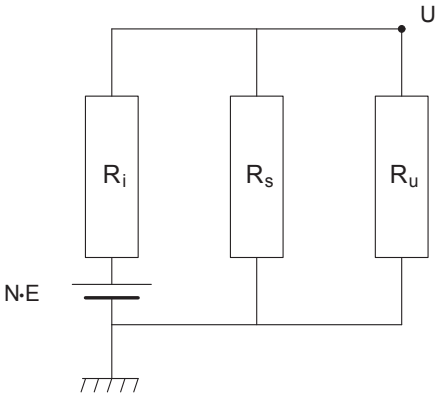

Figure 3.5. Simplified equivalent circuit model for a very large stack. The stack EMF is N times the cell EMF. R_i is resistance of the N cells, R_s the feed and drain channel resistance and R_u the external load. Because the stack is very large, the number of lateral spacer resistances connected parallel is so large that these can be omitted from the model.

the internal resistance of the stack (R_i) and the total bypass resistance (R_s) can be calculated from the cell parameters (E, r, R) and the number of cells (N): EMF=N·E, R_i=N·r and R_s=N·R. This little network, easily accessible for a straightforward calculation, gives the next results:

The maximum external power is achieved if the resistance of the load (R_u) equals the internal resistance of the parallel resistances R_i and R_s

$$R_u = \frac{R_i R_s}{R_i + R_s} \tag{8}$$

Figure 3.5 shows a very large stack with N cells. The internal resistance is R_i, the shunt resistance (from the shortcut circuit) is R_s and the load (the external resistance) is R_u. We can apply the voltage divider rule to calculate the voltage on point U relative to the ground:

$$U = \frac{R_s \parallel R_u}{R_i + R_s \parallel R_u} N \cdot E \tag{9}$$

The sign ‖ means adding two parallel resistances:

$$R_s \,||\, R_u \equiv \frac{R_s R_u}{R_s + R_u} \tag{10}$$

From this the generated power in R_u can be stated:

$$P_u = \frac{U^2}{R_u} = \left[\frac{R_s \,||\, R_u}{R_i + R_s \,||\, R_u} N \cdot E \right]^2 \frac{1}{R_u} \tag{11}$$

To generate maximum power in R_u, the external load R_u should be equal to substitution value of the internal load and the shunt resistance:

$$R_u = R_i || R_s \tag{12}$$

Substituting this value for R_u in the foregoing equation leads to

$$P_{\max} = \frac{R_s}{4R_i(R_i + R_s)} N^2 E^2 \tag{13}$$

In an ideal stack, the bypass resistance is infinite, resulting in a maximum external power P_{ideal}

$$P_{ideal} = \frac{1}{4R_i} N^2 E^2 \tag{14}$$

The power can also be expressed in relation to this value of P_{ideal}: the power ratio (P_R). The method has been tested on all 75 combinations, mentioned in *Section 3.4.4*. It follows that this approximation is suitable if satisfied to the condition N·R/ρ>1. In this case the approximation gives a maximal deviation of 10% downward.

$$P_R = \frac{P}{P_{ideal}} = \frac{R}{R + r} \qquad if \qquad \frac{N \cdot R}{\rho} > 1 \tag{15}$$

From the experiments, it appeared that the criterion N·R/ρ>1 is satisfied at N=50 for poor stacks and at N=1000 or more for well designed stacks.

3.2.7. Validation of the model for salinity power production

The optimization with respect to shortcut currents also holds for a salinity power production when the concentrated solution is depleted with ions and the diluted solution is enriched with ions. This causes a decrease of the shortcut currents in the concentrated compartments and an increase in the diluted compartments. If the conductivity of the salt solutions changes linearly with concentration, the net loss due to shortcut currents is equal to net loss that is the case when there is no transport of ions. Moreover, during mixing the internal resistance (r) also decreases, causing increased ratio of R/r and ρ/r and

a reduced power loss via shortcut currents. Therefore, optimization of the cell with respect to ionic shortcut currents also holds when ions are transported and salt concentrations are changing.

3.3. Experimental

3.3.1. Stack configuration

3.3.1.1. Stacks

The functional dimensions of the membranes in both types were 10 cm x 10 cm. On the outsides of the stacks cation exchange membranes prevent the transportation of negatively charged iron complexes.

Two types of stacks were used both with a variable number of cells. First stacks with Ralex anion and cation exchange membranes (MEGA a.s. Czech Republic) with a thickness of 0.65 mm. The stacks were equipped with regular nonwoven spacers of 1 mm. The radius of the holes in the membranes for the water supply and drain are 5 mm. These stacks are denoted *R1.0* in this chapter.

Next stacks were used with Fumasep anion and cation exchange membranes FAD and FKD with a thickness of 0.082 mm (Fumatech, Germany). The stacks were provided with polyamide woven spacers with a thickness of 200 µm (Nitex 03-300/51, Sefar, the Netherlands). The radius of the supply holes in the membranes are 4 mm in this case. The stacks of this type are designated as *F0.2* .

3.3.1.2. Electrode system

The electrode compartment consisted of a solution of NaCl (1 mol/L) with $K_4Fe(CN)_6$ (0.05 mol/L) and $K_3Fe(CN)_6$ (0.05 mol/L) (All chemicals were technical grade and purchased from Boom, Meppel, the Netherlands). This electrolyte is pumped through the anode and cathode compartment at a rate of 60 mL/min. Used were Ru-Ir mixed metal oxide electrodes, obtained from Magneto (Magneto Special Anodes b.v., the Netherlands).

3.3.1.3. Set up

The tests with the R1.0-stacks were done in a recirculating system with centrifugal pumps. Flows in the stack with 50 cells were about 2 L/min for both types of water. For the experiment with the F0.2-stacks, peristaltic pumps were used. The stack with 50 cells was fed with 700 mL/min. In both cases, smaller stacks were fed with proportional lower flow rates. This lower flow rate in the F0.2 stems from a higher hydrodynamic resistance of the thinner spacers. The temperature was about 24-25 °C for all experiments. The used salt concentrations were 1 and 30 g/L of NaCl.

3.3.1.4. Power measurements

On the R1.0-stacks, the voltage was measured between the work and the counter electrode. The F0.2-stacks were fitted with two little platinum electrodes in the middle of the work and the counter electrode. Stack potentials were measured in the anolyte and catholyte between these reference Pt electrodes whereas the current was applied to the working and counter electrode.

Measurements were done with an Ivium potentiostat (Ivium Technologies, Eindhoven, the Netherlands) in the galvanostatic mode. From the measured U(I)-curves the power was calculated as the maximum of the product from U and I and the resistance was calculated as the slope of the U(I) curve at the maximum power.

3.3.3. Calculation of the resistances r, R and ρ in a single cell

For comparing the electric characteristics of a R1.0-stack with a F0.2-stack it is necessary to know the resistances r, R and ρ. These parameters, which are typical cell properties, were calculated as well as possible. Afterwards the internal resistance r was experimentally determined in small stacks with 0,1..5 cells.

3.3.3.1. The internal resistance r

The internal resistance can be calculated from the membrane specifications at 0.5 mol/L NaCl (near to 30 g/L), given by the membrane supplier. The ionic resistance for Ralex membranes (8 $\Omega.cm^2$) is 10 times higher than the Fumasep membranes (0.8 $\Omega.cm^2$). It is assumed that the area resistance is independent of the salinity. A void factor $f_v = 0.80$ is used for the resistance of the water compartments.

Table 3.1 shows that the stack resistance is only reduced significantly if low resistance membranes are combined with thin spacers.

Table 3.1 Resistance (Ω) of one cell of 0.01 m2 for various cell designs

	Spacer: 1.0 mm		Spacer: 0.2 mm		Spacer: 0.1 mm	
	Ralex	Fumasep	Ralex	Fumasep	Ralex	Fumasep
AEM	0.080	0.008	0.080	0.008	0.080	0.008
CEM	0.080	0.008	0.080	0.008	0.080	0.008
Sea (30 gNaCl /L)	0.026	0.026	0.005	0.005	0.003	0.003
River (1 g NaCl/L)	0.629	0.629	0.126	0.126	0.063	0.063
Total	0.815	0.671	0.291	0.147	0.225	0.081
Ratio Ralex/Fumasep	1.21		1.98		2.77	

3.3.3.2. The feed and drain channel resistance R

As explained earlier, only the salt water channels are taken in account. The channel resistance R is calculated from the dimensions of the cylindrical bore through the cell and the conductivity of the salt water. In fact on the place where the channel crosses a spacer, the width of the channel increases. If we assign a zero resistance to this passage, the channel resistance is somewhat lower than the formerly calculated value. A good approximation is the average of the two mentioned values. Because R stands for two parallel resistances (feed and drain) in the model, this resistance value should be halved. The resistances calculated in this manner are 3.9 Ω for the R1.0-stack and 0.81 Ω for the F0.2-stack.

3.3.3.3. The lateral spacer resistance ρ

Figure 3.6 shows the configuration of the salt water compartment with the inlet and outlet in two opposite corners. From each point in the compartment there is a useful current perpendicular to the membranes through the cell and small lateral ionic shortcut currents in the direction of the feed and drain channels. In principle this is a three-dimensional potential flow problem. However, the described equivalent circuit model asks for only one single value of a spacer resistance (ρ). To estimate ρ, some approximations are applied. First, the resistance between inlet and outlet is calculated with a two dimensional potential flow model. The second step is the assumption that the current source lies on the diagonal d. In that case the resistance from the diagonal to the corner is half the corner-to-corner resistance. The results of the calculations are: ρ=142 Ω for the R1.0-stack and ρ=710 Ω for the F0.2-stack.

3.3.3.4 All calculated resistances together

In *Table 3.2* the calculated resistances for R, ρ and r are summarized.

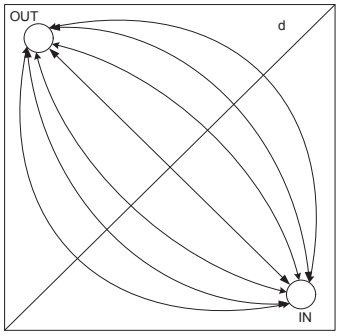

Figure 3.6. The lateral ionic shortcut currents in a seawater compartment. These currents originate from each point in the compartment and are directed by the electrical field to the inlet and outlet holes.

Table 3.2 Calculated resistances

	R1.0	F0.2
r cell (Ω)	0.815	0.147
R channel (Ω)	3.9	0.81
ρ spacer (Ω)	142	710

3.3.4. Experimental procedure

The equivalent circuit model was calibrated and validated (*Figure 3.7*). The calibration was performed successively with a stack of 5, 4 .. 0 cells. In the case of a small number of cells (N), the ionic shortcut currents through the spacers (ρ) and the channels (R) are negligible. Therefore, the calculation of E and r is rather straightforward. For each stack, the OCV was measured and the internal resistance (R_i) at maximal power was measured. From the slope of the regression lines of OCV versus N and R_i versus N, the EMF (E) and the cell resistance (r) were determined.

For the validation, experiments were done with larger stacks with 50, 40 .. 10 cells. Here the OCV and the maximal power were measured. These values were compared with the forecasted values calculated with the equivalent circuit model. In this model the EMF (E) and the cell resistance (r) from the calibration procedure were used together with the channel resistance (R) and the lateral spacer resistance (ρ) from the calculations in the previous *Sections* (*3.3.3.2* and *3.3.3.3*).
The procedure is performed with the two types of stacks. In each case the series was started with the complete stack of 50 cells and ended with the small stacks.

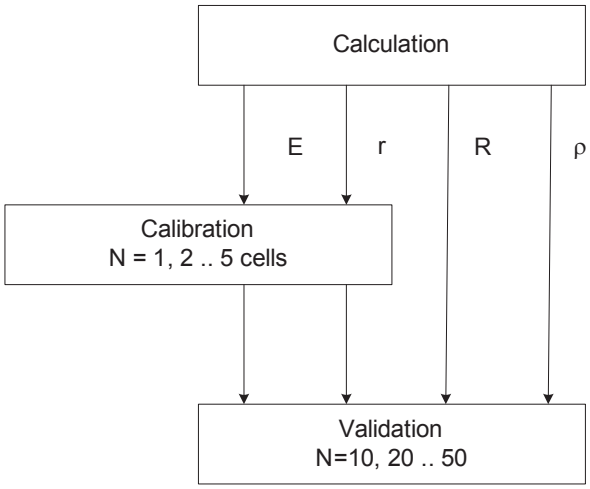

Figure 3.7. The validation procedure of the equivalent current model.

3.4. Results and discussion

3.4.1. Calibration: measurement of r and E

a) The R1.0-stack

The resistance is measured in a RED stack with 4, 3, 2, 1 and 0 cells (*Figure 3.8A*). In the case of 0 cells, only one cation exchange membrane (CEM) is placed between the electrode compartments. As seen in *Table 3.3*, at N=0, the resistance of the electrode system together with one CEM is 2.62 Ω and the resistance of one RED cell is 1.54 Ω. The EMF of a single cell (E) was obtained from the slope of the OCV regression line (*Figure 3.8C*).

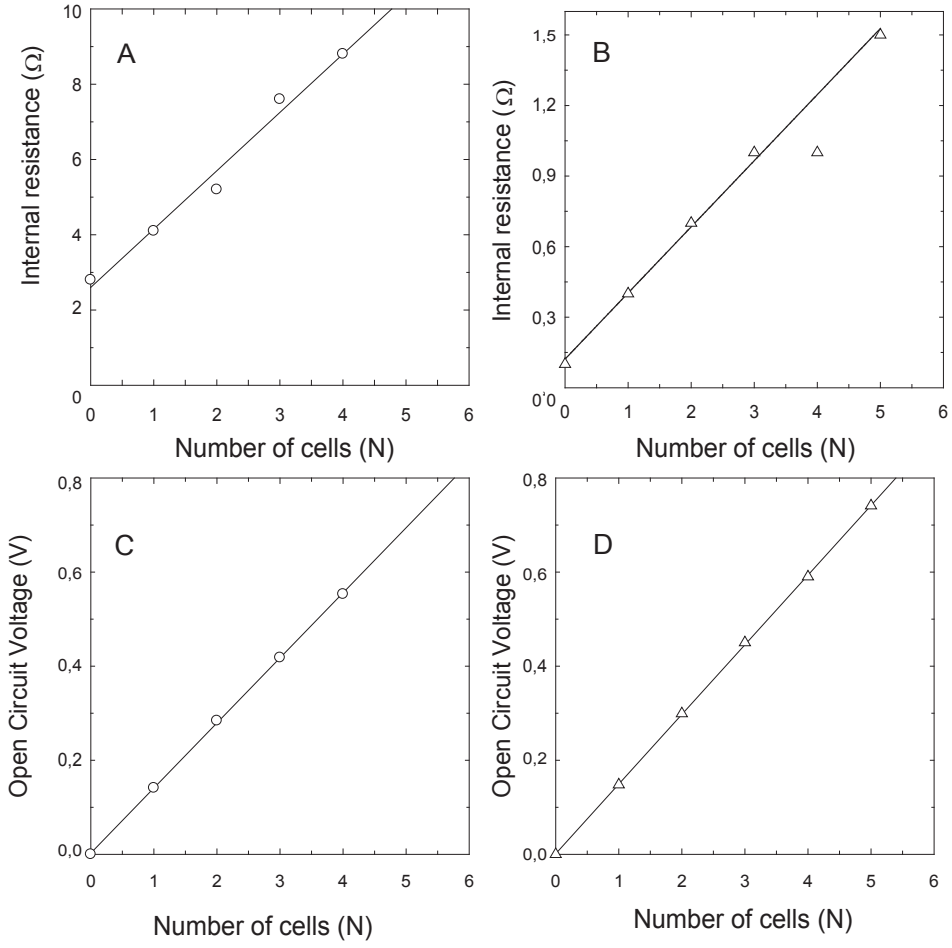

Figure 3.8 A and B: measured stack resistances. A: Resistance of R1.0-stacks measured between the working electrode and the counter electrode. B: Resistance of the F0.2-stacks measured between two platinum reference electrodes. For the calculation of the regression line, the point at N=4 is considered as an outlier and omitted. C and D: measured open circuit voltages. C: OCV of a R1.0-stack. D: OCV of a F0.2-stack.

b) The F0.2-stack

In *Figure 3.8B*, the result is shown for stacks with 5, 4 .. 1 cells. Because the voltage is measured between the platinum electrodes, the intercept of the R_i-axis is equivalent to the resistance of only one CEM. *Figure 3. 8D* shows the OCV regression line from which the E value is calculated. All regression results are listed in *Table 3.3*.

Table 3.3 Measured internal resistances (Ri) and OCV's as a function of the number of cells (N)

R1.0	F0.1
$R_i = 1.54\ N + 2.62 \quad R^2 = 0.9830$	$R_i = 0.28\ N + 0.12 \quad R^2 = 0.9977$
$OCV = 0.139\ N + 0.003 \quad R^2 = 0.9998$	$OCV = 0.148\ N + 0.001 \quad R^2 = 0.9999$

The EMFs are lower than the calculated value of 0.158 V for a cell with ideal membranes. The ratio between measured and calculated values can be interpreted as an average permselectivity α of the CEM and AEM. The ratios calculated from these values are α=0.88 for the Ralex membranes in the R1.0-stacks and α=0.94 for the Fumasep membranes in the F0.2-stacks.

In the R1.0-stack with 1 mm spacers the measured value of the cell resistance is almost twice the calculated value with Eq. (3) (measured 1.54 Ω; calculated 0.815 Ω). The same holds for the F0.2-stack (measured: 0.28 Ω; calculated 0.147 Ω). For these differences between the calculated and measured values some reasons are suggested:

- The membrane specifications hold for membranes immersed in 0.5 M NaCl solution. This value is near the used seawater concentration of 30 g/L. But the membranes in the stack are immersed between solutions of 1 and 30 g/L. A lower salt content increases the resistance of the membranes. A model is suggested by Zabolotsky and Nikonenko[17] in which homogeneities are present on micro scale. The included water phase and the solid membrane phase are described as a resistor network. The salt concentration in the water part of this network is dependent on the external concentration, causing an overall concentration dependent resistance.
- The ionic current through the spacer grid is not straightforward, but tortuous.
- Stagnant depletion and enrichment layers can be formed on both sides of the membranes.
- The membranes are covered partly by the spacer material. This is sometimes called the shadow effect.

3.4.2. Validation of the model

With the two types of stacks, experiments were done with a variable number of cells (N) in the range from 10 to 50. With the described model the stack performance was also calculated. The values of the used parameters are listed in *Table 3.4*. *Figure 3.9* shows the measured open circuit voltage and the power, plotted against the number of cells (N).

Table 3.4 Used input parameters in the model

	source	R1.0	F0.2
E (V)	experimental (N=1,2..5)	0.139	0.148
r (Ω)	,,	1.54	0.281
R (Ω)	calculated	3.9	0.81
ρ (Ω)	,,	142	710

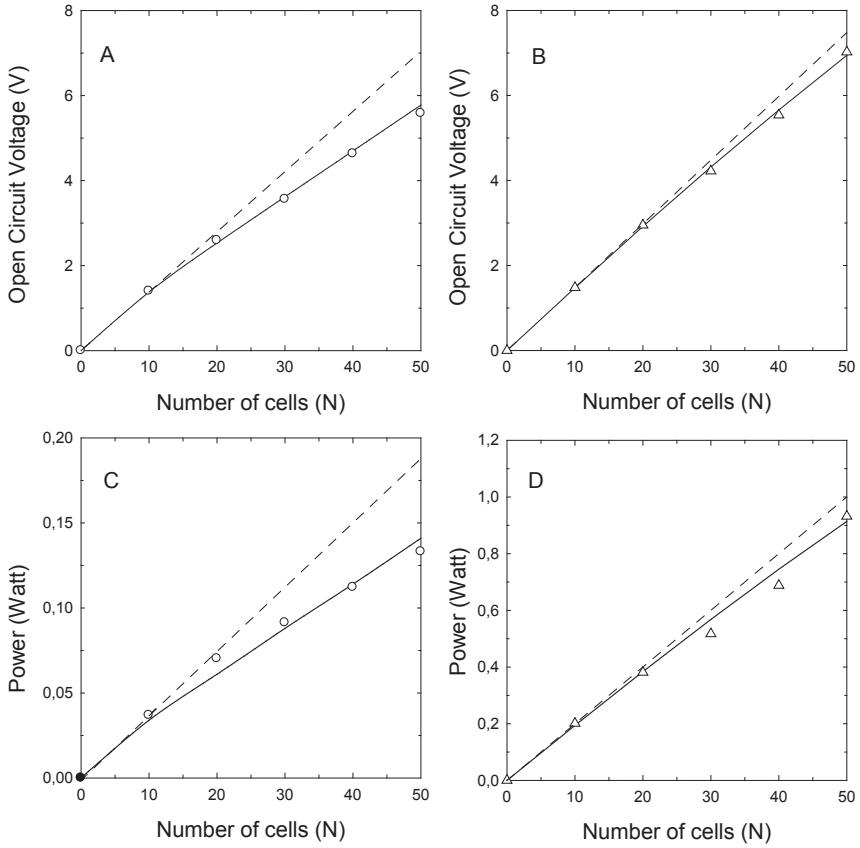

Figure 3.9 A and B. Measured and calculated Open Circuit Voltage (A: R1.0-stacks; B: F0.2-stacks). The solid lines represent the calculated values, the symbols represent the measured values, and the dashed line is the extrapolation of the first two measured data points. C and D: Equivalent graphs for the dissipated power (C: R1.0-stacks; D: F0.2-stacks).

Each graph shows the measured data (squares), the forecasted values by the equivalent circuit model (the solid line) and the extrapolation of the first two data points (the dashed line). The dashed lines represent an 'ideal stack'. Calculated and measured data are very close together, indicating that the model is valid.

3.4.3. Implementation of the model

For the used R1.0-stack, currents and dissipated powers are calculated with the equivalent circuit model for a stack containing 4 and 50 cells. The external resistance was adjusted such that a maximal power was achieved. The values used are ρ=142 Ω, R=3.9 Ω, r=1.54 Ω and E=0.150 V. With the same resistances the calculations are repeated for a stack of 50 cells. *Figure 3.10A* shows all currents in a R1.0-stack with 50 cells as function of the position n in the stack (1≤n≤N). In *Figure 3.10B* the cell voltage is plotted for the same stack. The distribution of the dissipated power in the different parts of R1.0-stacks with 4 and 50 cells is given in *Table 3.5*.

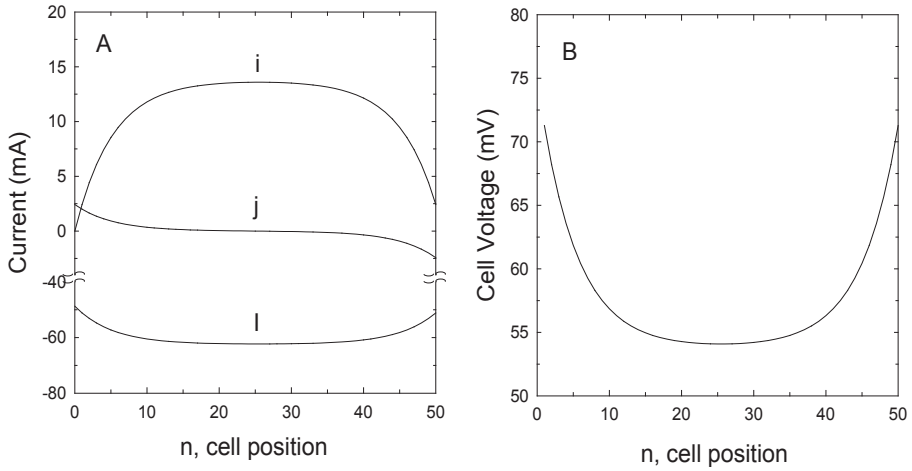

Figure 3.10 A. Calculated currents (j, i and I) in a R1.0-stack with 50 cells through the different resistances (ρ, R and r). The cell position n indicates the location in the stack. B: The calculated voltage over the individual cells in a R1.0-stack.

Table 3.5 Calculated generated external power (P_u) and dissipated power P_{dis} in % in different parts of a R1.0-stack with 4 and 50 cells

	N = 4	N = 50
P_u	46.7%	31.3%
P_{dis} in r	51.7%	61.9%
P_{dis} in R	0.1%	5.9%
P_{dis} in ρ	1.5%	1.2%
Total	100.0%	100.0%

The ionic shortcut currents cause a voltage drop over the individual cells (*Figure 3.10B*). Also here a flattening is seen in the middle of the stack. *Figure 3.10A* shows the same flattening effects, discussed already in *Section 3.2.6* for very large stacks. Only the first and final ten lateral spacer currents (j) appear to be significant. Assuming a number of 10 lateral spacer resistances of 142 Ω at the beginning, the result is a connection between the main route and the bypass of 14.2 Ω. This value is low compared to the resistance of the bypass channel (50·3.9=145 Ω).

It is evident that longer stacks have a more serious loss of power by shortcut currents but they do not exceed the limit values of very large stacks. If the saturation of the shortcut current is not reached already, an improvement of the efficiency can be achieved by an increase of both R/r as ρ/r.

The test value (N·R/ρ) and the efficiency at N=50 and at very large values of N for both studied stacks are summarized in *Table 3.6*. With the used test (N·R/ρ=1.6), the R1.0-stack with 50 cells is already 'very large' and operates near the efficiency limit. In this case of very large cells an improvement can be achieved only by increasing the ratio R/r. A higher ρ/r ratio has less effect on the efficiency.

Table 3.6 The efficiency at stacks with 50 cells and with a very large number of cells

	R1.0	F0.2
test value N·R/ρ (N=50)	1.6	0.06
efficiency at N=50	77%	94%
efficiency at N →∞	72%	74%

A stack consists of an electrode system and N cells. It is shown above that the shortcut currents are minimal at low N. The electrochemical parameters of the used electrode system are important for calculation of the optimal number of cells. Moreover, at real (economically-operating) RED installations the price of the electrode system should be taken into account in the optimization as well, resulting in a value of N that is as large as possible, and that is only restricted by the available space. *Table 3.6* shows that for such large stacks, the efficiency reaches a limiting value.

3.4.4. The validated model expressed in one plot

The equivalent circuit model has been used to calculate various stack designs. The maximum power is calculated for 75 combinations of the channel resistance R (1, 3 and 10 Ω), the spacer resistance ρ (1, 3, 10, 100, 300 Ω) and the number of cells n (2, 3, 10, 30 and 50). The following assumptions were used for the calculation: E = 0.15 Volt and r = 1 Ω for a single cell. The ideal power (P_{ideal}) is also calculated for each number of cells N by applying

large values for ρ and R in the model. Power is expressed as the power ratio (P_R=P/P_{ideal}).

In fact, by taking one of the resistances unity (r=1), the values of ρ and R can be considered as the relations ρ/r and R/r. So the power ratio is a function of these two relative resistances and of the number of cells N:

$$P_R = f(\rho/r, R/r, N) \quad (16)$$

The three variables form a three-dimensional space and at some points in this space the P_R-values (in %) are given in circles to give a kind of a four dimensional plot (*Figure 3.11*). The data for the described two stacks: the R1.0-stack (R/r=2.5; ρ/r=94) and the F0.2-stack (R/r=2.9; ρ/r=2580) is given in the plot as well. The F0.2-stack operates at 94% efficiency with 50 cells. Expansion of the stack to 250 cells will cause an estimated efficiency drop to about 80% going to a limit of 74% for very large stacks. A 50-cell R1.0-stack operates at an efficiency of 77% near to the limit of 72% for large stacks.

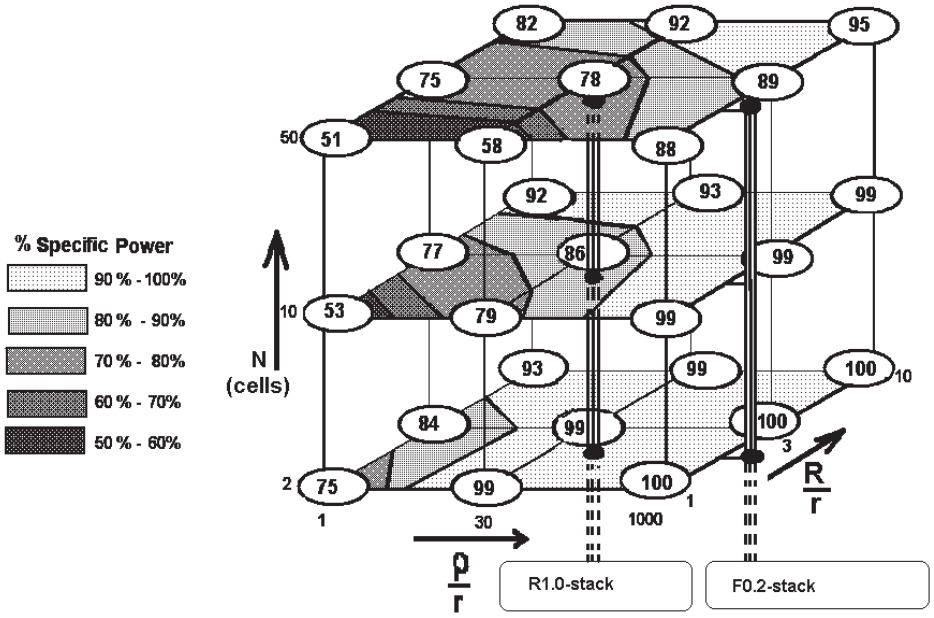

Figure 3.11. Power ratio (the values in the circles in %) as function of N, R/r and ρ/r. The lines between the different colors are the 90% borders, the 80% borders and so on.

From this plot it follows that at stacks with a medium number of cells, R/r and ρ/r should be as high as possible. This can be achieved by: a) increasing R by narrowing the channels, b) increasing ρ by taking thinner spacers (especially in the sea water compartment)

c) decreasing r by using low resistive membranes and thin spacers (especially the river water compartment). The possibilities to maximize R are limited because the hydro dynamical resistance in the channels increases with narrowing of the channels. In a cylindrical tube with radius r, the electrical resistance is proportional with r^2 whereas the fluid resistance is related to r^4, assuming Poiseuille flow dynamics. A benefit with a factor x in the electrical resistance is paid for with a factor x^2 in the fluid resistance. Increasing ρ influences the relative power only marginal in large stacks as explained in the previous section. However, decreasing r seems to be very opportune as it causes not only a higher efficiency but also an expansion of the specific power.

In addition to the theory described in *Section 3.2.6* for very large stacks, improvements can be obtained by optimizing R/r. Decreasing r by minimization of both compartments and both membrane thicknesses results in an equal decrease of R resulting in an unaffected ratio R/r. However, *Table 3.1* shows the river water compartment is the bottleneck in the resistance. In very large stacks reduction ρ/r is not opportune, so there is no need for thinning the sea water compartments. However, with given membrane and river water compartment dimensions, decrease of only the thicknesses of the sea water compartment results in (i) a higher R/r ratio and therefore in a higher efficiency (ii) a lower r, so a higher specific power of the stack.

3.5. Conclusions

In this work, a model for the ionic shortcut currents in a reverse electrodialysis stack is presented. The model is calibrated and validated on two different stacks. Our main findings are:

- Measured cell resistances are about a factor two higher than calculated. This deviation might stem from (i) a strong concentration dependent behavior of the membranes, (ii) a restricted ionic transport in the spacers, (iii) a stagnant depletion and enrichment layers on both sides of the membranes, (iv) a shadow effect from the spacer on the membranes.
- It is possible to describe the ionic shortcut loss with only three parameters: (i) the number of cells N, (ii) the channel resistance in proportion to the cell resistance R/r, (iii) the lateral spacer resistance in proportion to the cell resistance ρ/r.
- The equivalent circuit model was calibrated and validated with two different kinds of stacks. One type was built with Ralex membranes and 1 mm spacers, the other stack contained Fumasep membranes and spacers of 0.2 mm. Calibration was done with small stacks of 1, 2 to 5 cells and validation with large stacks of 10, 20 to 50 cells. The calculated and measured values of power and OCV's were in very good agreement.

- With the used Fumasep stack with 0.2 mm spacers, the loss caused by ionic shortcut currents is 6% for a stack with 50 cells, showing that the ionic shortcut currents are manageable.
- In very large stacks, increase of the ratio between the channel resistance and the cell resistance (R/r) is the most efficient measure for reduction of the ionic shortcut current loss.

Acknowledgement

The Noordelijke Hogeschool Leeuwarden has facilitated this research by detaching the first author. Also the Senter Novem organization is gratefully acknowledged for their grant. We thank all members of the energy theme from Wetsus for their support and fruitful discussions and especially the participating companies Nuon, Magneto, Triqua, Landustrie, Frisia Zout and the Waterlab Noord for their support.

Nomenclature

a	activity
a^+	activity of the sodium ion
a^-	activity of the chloride ion
A_{cell}	cell area (m^2)
E	electromotive force of one cell (V)
Eff	efficiency of a RED battery
F	Faraday constant (96485 C/mol)
f_v	void factor
N	number of cells in a stack
n	position of a special cell in a stack ($1 \leq n \leq N$)
I	electrical current perpendicular on the membranes (A)
i	the current through the feed and drain channels (A)
j	the lateral current leakage along the membrane surface (A)
P_{dis}	dissipated power (W)
P_{ideal}	ideal power (W)
P_{max}	maximum external power
P_R	power ratio
P_{spec}	specific power (W/m^2)
P_u	external power (W)
R_i	internal resistance (Ω)
R_u	external resistance (Ω)
R_{el}	electrode system resistance (Ω)
R_{AEM}	cation exchange membrane resistance (Ω)
R_{CEM}	cation exchange membrane resistance (Ω)
R_{sea}	sea water compartment resistance (Ω)
R_{river}	river water compartment resistance (Ω)
R_{comp}	compartment resistance (Ω)

R_{rel}	relative resistance
R_s	total bypass resistance (Ω)
r	cell resistance (Ω)
R	gas constant (8.31432 $Jmol^{-1}K^{-1}$)
R	channel resistance of one cell in a stack (Ω)
R^2	determination coefficient
T	temperature (K)
U	the potential at the centre of the membrane (V)
OCV	open circuit voltage (V)
V	the potential in the feed and drain channel (V)
V_t	terminal voltage (V)
z	valency

Greek symbols

α_{CEM}	permselectivity of the cation exchange membrane
α_{AEM}	permselectivity of the anion exchange membrane
δ	compartment thickness (m)
σ	specific conductivity (S/m)
ρ	lateral spacer resistance (Ω)

Abbreviations

AEM	anion exchange membrane
CEM	cation exchange membrane
ED	electrodialysis
EMF	electromotive force (V)
RED	reverse electrodialysis
R1.0	stack with Ralex membranes and 1 mm spacers
F0.2	stack with Fumasep membranes and 0.2 mm spacers

Definitions

compartment	space between the membranes
cell	combination of two membranes and two compartments
electrode system	the anode, cathode, electrode rinse and also one terminating membrane
stack	a number of cells with an electrode system

References Chapter 3

1 J.W. Post, J. Veerman, H.V.M. Hamelers, G.J.W. Euverink, S.J. Metz, K. Nymeijer, C.J.N. Buisman, *Salinity-gradient power: Evaluation of pressure-retarded osmosis and reverse electrodialysis.* J. Membr. Sci. 288 (2007) 218-230

2 R.E. Pattle, *Improvements relating to electric batteries.* Patent GB731729 (1955)

3 W.G.B. Mandersloot, R.E. Hicks, *Leakage currents in electrodialytic desalting and brine production.* Desalination 1 (1966) 178-194

4 R. Yamane, M. Ichikawa, Y. Mizutani, Y. Onoue, *Concentrated brine production from sea water by electrodialysis using ion exchange membranes.* Ind. Eng. Chem. Process Design Develop. 8 (1969) 159-165

5 B.R. Bligh, *Reverse electrodialysis.* Patent GB2197116A (1988)

6 T. Wen, G.S. Solt, Y.F. Sun, *Spirally wound electrodialysis (SpED) modules*. Desalination 101 (1995) 79-91

7 T. Wen, G.S. Solt, Y.F.Sun, *Modelling the cross flow spirally wound electrodialysis (SED) process. D*esalination 103 (1995) 165-176

8 T. Wen, G.S. Solt, D.W. Gao, *Electrical resistance and coulomb efficiency of electrodialysis (ED) apparatus in polarization.* J. Membr. Sci. 114 (1996) 255-262

9 A.T. Kuhn, J.S. Booth, *Electrical leakage currents in bipolar cell stacks.* J. Appl. Electrochem. 10 (1980) 233-237

10 J. Pretz, E. Staude, *Reverse electrodialysis (RED) with bipolar membranes , an energy storage system.* Ber. Bunsen-Ges. Chem. 102 (1988) 676-685

11 I. Rubinstein, J. Pretz, E. Staude, *Open voltage in a reverse electrodialysis cell.* Phys. Chem. Chem. Phys. 3 (2001) 1666-1667

12 J.N. Weinstein, F.B. Leitz, Electric *power from differences in salinity: The dialytic battery.* Science 191 (1976) 557-559

13 B.H. Clampitt, F.E. Kiviat, *Energy recovery from saline water by means of electrochemical cells.* Science 194 (1976) 719-720

14 J. Jagur-Grodzinski, R. Kramer, *Novel process for direct conversion of free energy of mixing into electric power*. Ind. Eng. Chem. Process Des. Dev. 25 (1986) 443-449

15 R.E. Lacey, *Energy by reverse electrodialysis*. Ocean Eng. 7 (1980) 1-47

16 D.C. Harris, *Quantitative Chemical Analysis*, 6th edition, W. H. Freeman & Company (2003)

17 V.I. Zabolotsky, V.V. Nikonenko, *Effect of structural membrane inhomogeneity on transport properties. J*. Membr. Sci. 79 (1993) 181-198

Chapter 4

Reverse electrodialysis: Evaluation of suitable electrode systems*

Abstract

Reverse electrodialysis (RED) is a method for directly extracting electrical energy from salinity gradients, especially from sea and river water. For the commercial implementation of RED, the electrode system is a key component. In this chapter, novel electrode systems for RED were compared with existing systems on safety, health, environment, technical feasibility and economics.

Systems with inert electrodes and a NaCl–HCl supporting electrolyte with the reversible Fe^{2+}/Fe^{3+} redox couple or the $[Fe(CN)_6]^{4-}/Fe(CN)_6]^{3-}$ couple achieved the highest ranking. Improvements of the electrode system are also discussed such as the use of special stable metal electrodes, graphite electrodes, other reversible redox couples, capacitive electrodes and electrolytes with carbon particles.

*** Published as**

J. Veerman, M. Saakes, S.J. Metz and G.J. Harmsen

Reverse electrodialysis: evaluation of suitable electrode systems

Journal of Applied Electrochemistry 40 (2010) 1461-1474

4.1. Introduction

Energy can be generated from the reversible mixing of salt solutions with different concentrations and is called salinity gradient power (SGP). The energy that theoretically can be generated per m^3 river water is 1.7 MJ when mixed with the same volume sea water or even 2.5 MJ when mixed with a large surplus of sea water (*Chapter 5: Table 5.1*). Post et al. proved experimentally that it is possible to convert 85% of this potential energy into useful electricity[1]. Wick and Schmitt[2] estimated the total global salinity power to be 2.6 TW, which is sufficient to supply the global electricity demand (2 TW) or 16% of the total present energy consumption[3].

There are two membrane technologies capable of converting this potential energy into electricity: reverse electrodialysis (RED)[4,5,6] and pressure retarded osmosis (PRO)[7,8]. Both PRO and RED are sustainable technologies without CO_2 or other emissions. The only product is brackish water which is also formed when a river flows directly in the sea. Moreover, there is no thermal pollution: the conversion of entropy into electrical energy causes a slight decrease of the water temperature of about 0.1 K if all the potential energy is extracted (*Chapter 6*). Post et al.[9] showed that in the case of using seawater with river water, RED is a good choice. In 1954 Pattle already[4,5,6] showed the possibilities of this method.

A RED stack consists of a large number of cells. An example of a RED stack with only one cell is shown in *Figure 4.1*. The cell consists (from left to right in the figure) of an anion exchange membrane (AEM), a sea water compartment, a cation exchange membrane (CEM) and a river water compartment. On the right side, the stack contains an extra AEM. The ions in the sea water diffuse through the membranes to the river water: the Na^+ ions through the CEM and the Cl^- ions through the AEM. The positive Na^+ movement to the right and the negative Cl^- movement to the left add together to a positive ionic current to the right. The electromotive force of such a cell is 175 mV if pure NaCl solutions are used of 1 and 30 g l^{-1} and ideal membranes are applied; practical cell voltages under conditions of maximal power generation are about 60 mV (*Chapter 5*). In practice, a large number of cells (N) would be used, in the range from 50 in laboratory equipments to 1000 or more in commercial RED plants (*Chapter 5*).

The N cells together are designed as 'generating system' (GS). At the electrodes, the ionic current is converted into an electron current. The electrode system (ES) consists at least of four parts: (i) electrodes, (ii) anolyte and catholyte, (iii) outer membranes, and (iv) technical equipment for recirculating the electrode rinse solution. Eventually the electrode rinse solution is controlled by an additional system.

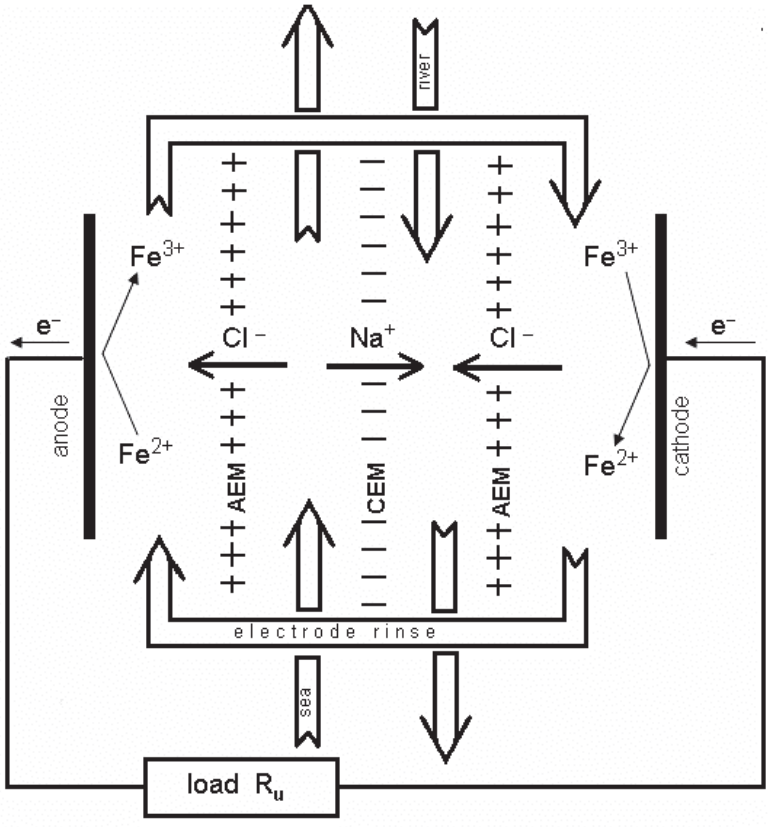

Figure. 4.1. A RED stack with only one cell.

In principle, the recirculation system of the electrode rinse solution can cause short-circuiting of the RED stack. However, if the resistance of this recirculation system is much higher than the internal resistance of the stack, this effect can be ignored. This can be done by applying relatively long tubes to the recirculating system.

The electrode system as shown in *Figure 4.1* is equipped with inert electrodes with a reversible redox couple containing Fe^{2+}/Fe^{3+} ions in a NaCl–HCl supporting electrolyte. The potential difference needed for reduction of Fe^{3+} to Fe^{2+} on the cathode is counterbalanced by the oxidation of Fe^{2+} to Fe^{3+} at the anode. Under zero current conditions, the total cell electromotive force (EMF) is obtained at the working electrodes. The Fe^{3+}/Fe^{2+} ratio is kept constant by recirculation the combined anolyte and catholyte through the electrode compartments. This type of redox system is called a homogeneous charge transfer reaction because all reactants are present in the same phase. In order to reduce the relative power loss of the electrode system, RED stacks should have a large number of cells.

In literature many electrode systems are described for RED. These systems are all used on laboratory scale and none of these systems have been evaluated for their practical applicability on a commercial scale. Many aspects of the electrode system are important for its operation: electrochemical reactions, energy consumption, transport through the membranes of the electrode system, reversibility etc. The objective of this chapter is to compare these electrode systems for their suitability for RED. The evaluated systems include those already described in literature, but also contains electrode systems as used in supercapacitors, redox flow battery, electrodialysis and capacitive deionization, which might also be useful for RED.

4.2. Electrode systems for RED

4.2.1. Classical systems

To be fair to the pioneers of RED, it should be mentioned that their electrode systems were designed for laboratory use and were *not* developed for real applications. However, we have used their systems in our comparison because their solutions vary so widely.

4.2.1.1. Overview

Table 4.1 shows the different published electrode systems for RED. These electrode systems can be classified into two groups: with or without opposite electrode reactions. First, for systems with opposite electrode reactions and a recirculating electrode rinse, there is no net chemical reaction. These systems have a zero equilibrium voltage. A RED system with such an electrode system can generate electrical energy with only a few cells because there is no energy consumption for a net chemical reaction. Another advantage is that there is no loss of chemicals (except for transport through the outer membranes) and no gas production. Pattle[5,6] used copper gauze electrodes in a $CuSO_4$ solution. On the cathode the dissolved Cu^{2+} was reduced to metallic copper and at the anode the copper was oxidized to Cu^{2+}. With a typical RED current density of 50 A/m^2 this effect on the thickness of electrodes is about 2 mm per week. Jagur-Grodzinski and Kramer[10] and Audinos[11,12] used zinc electrodes with a $ZnSO_4$ electrode rinse solution. In another experiment Audinos used Ag/AgCl electrodes in a NaCl solution[11,12].

In all these processes the electrodes play an active role in the redox process: one electrode is growing and the other is dissolving. In such systems the feed waters should be interchanged periodically to invert the direction of the electrical current and with that the electrode processes. This imposes limitations on the stack design: the stack should be equipped with identical sea and river water compartments. A less attractive solution is to mechanically perform the periodical interchange of anode and cathode.

Table 4.1. Electrode systems described in literature .┤ refers to the anode, ├ to the cathode, ≡ stands for a cation exchange membrane and ‡ for an anion exchange membrane. The repeating unit is underlined. S stands for sea water and R for river water. Direction of the ions through the membranes is designated by arrows.

	anode	anolyte + bulk		repeating unit	catholyte + bulk	cathode	*author* electrode reactions
described systems in iterature							
1	Cu ┤	$CuSO_4$	‡ ← Cl^-	S ≡ R ‡ → ← Na^+ Cl^-	$CuSO_4$	├ Cu	*Pattle [4, 5, 6]* cath.: $Cu^{2+} + 2e \rightarrow Cu$ anode: $Cu \rightarrow Cu^{2+} + 2e$ net: nil
2	metal ┤	sea		≡ R ‡ S → ← Na^+ Cl^-	sea	├ metal	*Weinstein/Leitz [13]* cath.: $2\,H_2O + 2e \rightarrow H_2 + 2OH^-$ anode: $2\,Cl^- \rightarrow Cl_2 + 2e$ net: $2H_2O + 2\,Cl^- \rightarrow H_2 + 2OH^- + Cl_2$
3	Ag/AgCl ┤	NaCl	‡ ← Cl^-	S ≡ R ‡ → ← Na^+ Cl^-	NaCl	├ Ag/AgCl	*Audinos [11, 12]* cath.: $AgCl + e \rightarrow Ag + Cl^-$ anode: $Ag + Cl^- \rightarrow AgCl + e$ net: nil
4	Zn ┤	$ZnCl_2$	‡ ← Cl^-	S ≡ R ‡ → ← Na^+ Cl^-	$ZnCl_2$	├ Zn	*Jagur–Grodzinski/Kramer [10]* cath.: $Zn^{2+} + 2e \rightarrow Zn$ anode: $Zn \rightarrow Zn^{2+} + 2e$ net: nil
5	C/Pt ┤	NaCl	≡ R → Na+	‡ S ≡ R ‡ ← → ← Cl^- Na^+ Cl^-	NaCl	├ C/Pt air	*Jagur–Grodzinski/Kramer [10]* cath.: $½O_2 + 2H^+ + 2e \rightarrow H_2O$ anode: $H_2O \rightarrow ½O_2 + 2H^+ + 2e$ and $2Cl^- \rightarrow Cl_2 + 2e$ separated anolyte and catholyte
6	Ti/Pt ┤	Na_2SO_4	≡ → Na+	R ‡ S ≡ ← → Cl^- Na^+	Na_2SO_4	├ Ti/Pt	*Turek [19, 20]* cath.: $2H_2O + 2e \rightarrow H_2 + 2OH^-$ anode: $H_2O \rightarrow ½\,O_2 + 2\,H^+ + 2e$ net: $H_2O + \rightarrow 2\,H_2 + ½\,O_2$
7	C ┤	sea		≡ R ‡ S → ← Na^+ Cl^-	sea	├ C	*Suda [17]* cath.: $2\,H_2O + 2e \rightarrow H_2 + 2OH^-$ anode: $2Cl^- \rightarrow Cl_2 + 2e$ net: $2H_2O + 2\,Cl^- \rightarrow H_2 + 2OH^- + Cl_2$
used systems by author							
8	Ti/RuIr ┤	Fe^{2+}/Fe^{3+} NaCl / HCl	‡ ← Cl^-	S ≡ R ‡ → ← Na^+ Cl^-	Fe^{2+}/Fe^{3+} NaCl / HCl	├ Ti/RuIr	*Veerman et al. [this chapter]* cath.: $Fe^{3+} + e \rightarrow Fe^{2+}$ anode: $Fe^{2+} \rightarrow Fe^{3+} + e$ net: nil
9	Ti/RuIr ┤	$Fe(CN)_6^{3-}$ / $Fe(CN)_6^{4-}$ NaCl	≡ → Na^+	R ‡ S ≡ ← → Cl^- Na^+	$Fe(CN)_6^{3-}$ / $Fe(CN)_6^{4-}$ NaCl	├ Ti/RuIr	*Veerman et al. [Chapter 3 and 5]* cath.: $Fe(CN)_6^{3-} + e \rightarrow Fe(CN)_6^{4-}$ anode: $Fe(CN)_6^{4-} \rightarrow Fe(CN)_6^{3-} + e$ net: nil
10	Ti/RuIr ┤	NaCl	≡ → Na^+	R ‡ S ≡ ← → Cl^- Na^+	NaCl $Fe(CN)_6^{4-}$ NaCl	├ Ti/RuIr	*Veerman et al. [Chapter 6]* cath.: $2\,H_2O + 2e \rightarrow H_2 + 2OH^-$ anode: $2Cl^- \rightarrow Cl_2 + 2e$ net: $2H_2O + 2\,Cl^- \rightarrow H_2 + 2OH^- + Cl_2$
suggested systems							
11	graphite ┤	Fe^{2+}/Fe^{3+} NaCl / HCl	‡ ← Cl^-	S ≡ R ‡ → ← Na^+ Cl^-	Fe^{2+}/Fe^{3+} NaCl / HCl	├ graphite	*Veerman et al. [this chapter]* cath.: $Fe^{3+} + e \rightarrow Fe^{2+}$ anode: $Fe^{2+} \rightarrow Fe^{3+} + e$ net: nil
12	graphite ┤	$Fe(CN)_6^{3-}$ / $Fe(CN)_6^{4-}$ NaCl	≡ → Na^+	R ‡ S ≡ ← → Cl^- Na^+	$Fe(CN)_6^{3-}$ / $Fe(CN)_6^{4-}$ NaCl	├ graphite	*Veerman et al. [this chapter]* cath.: $Fe(CN)_6^{3-} + e \rightarrow Fe(CN)_6^{4-}$ anode: $Fe(CN)_6^{4-} \rightarrow Fe(CN)_6^{3-} + e$ net: nil

This reversal can be avoided by taking a homogeneous redox couple with inert electrodes. This may be platinized titanium for both electrodes, special coated titanium for specific anode and cathode and carbon or steel for the cathode. Jagur-Grodzinski and Kramer used platinized carbon electrodes in their so called 'REF system', a combination of a RED system and the electrode system of a fuel cell. At the anode water is oxidized to O_2 and at the cathode oxygen from air is reduced to water. Because the electrode solution contained NaCl, it is also possible that Cl_2 is evolved at the anode. Veerman et al. used a system with $FeCl_2$ and $FeCl_3$ in a NaCl bulk as described in *Section 4.2.2.1*, the system $K_4Fe(CN)_6$ with $K_3Fe(CN)_6$ in a NaCl bulk (*Chapter 3* and *5*) and also a H_2/Cl_2 generating system with only NaCl (*Chapter 6*).

Second, the alternative for the systems with opposite electrode reactions are the systems with gas generation. The disadvantage of these systems is the loss of energy due to these reactions; a significant number of cells are required to overcome the cell equilibrium voltage before electricity production is possible. On laboratory scale the problem can be solved by using a small number of cells together with an external power supply. The virtual RED voltage (the voltage without the losses at the electrodes) is obtained from a pair of reference electrodes in the electrode compartments near to the outer membranes. Weinstein and Leitz[13], Wick[14], Loeb[15], Metha[16] and Suda et al.[17] reported such systems. At the cathode hydrogen is evolved and at the anode chlorine is evolved if a NaCl solution (or sea water) is used in the electrode compartments. A possible succeeding reaction is hypochlorite and chlorate formation[18]. Turek et al. avoided the formation of chlorine by using an electrode rinse solution with Na_2SO_4[19,20]. In this case oxygen is generated at the anode.

4.2.1.2. Membranes of the described electrode systems

The sequence of the membranes in a RED stack is always alternating, but for the outer membranes – confining the electrode system - there are some requirements. The systems described in literature are given in *Table 4.1*. Some authors (Weinstein and Leitz[13] and Suda et al.[17]) used seawater in the electrode compartments and applied two different outer membranes, ensuring in this way an alternating system of sea and river water compartments. However, the generated Cl_2 and ClO^- are discharged into the sea water which is unacceptable from the viewpoint of safety, health and environment (SHE). Also the formation of Cl_2 requires the application of chlorine resistant outer membranes.

Another possibility is to use a closed electrode system; we used a closed electrode rinse containing NaCl with CEMs as outer membranes (*Chapter 6*). In this case the negative ClO^- is confined together with the Cl_2 in the electrode rinse. Although there is no direct discharge

of these products to sea water, the problem of disposing these chemicals is not solved. Pattle[6] used a $CuSO_4$ solution and in *Table 4.1* it is seen that the Cu^{2+}-ions are maintained in the electrode compartments by the outer AEMs. Al though an AEM (with positively fixed charges) is slightly permeable for monovalent (positive) co-ions, the bivalent positively charged Cu^{2+}-ions are strongly excluded and Cu^{2+}-loss is expected to be relatively low but not to be negligible in terms of SHE. The SO_4^{2-} in the electrode system will be exchanged rapidly for Cl^- from the sea water. This exchange has no effect on the functioning of the system as long as the Cu^{2+} ions stay in the electrode compartments.

Jagur-Grodzinski and Kramer[10] also used active metal electrodes (zinc) but their design was improved by taking Cl^- as anion. Turek and Bandura[19] described a system with a Na_2SO_4 electrode rinse in combination with anion exchange outer membranes, evolving H_2 at the cathode and in first instance O_2 at the anode. In such systems the SO_4^{2-} can be exchanged for Cl^-. This can cause generation of Cl_2 because after some time there is enough Cl^- in the electrode rinse solution (>5 g/L) to generate Cl_2.

We conclude: if there is a closed electrode rinse loop, it is possible to contain only one type of ion (anion or cation) in the combined electrode compartments. In this case, the outer membranes should be of the same kind (both AEM or both CEM) and the ionic charge transport between the water compartments to the electrode rinse solution is done respectively by Cl^- or by Na^+.

4.2.2. Self-developed systems

In our laboratory, we used three different electrode rinse solutions, always with the same DSA (dimensionally stable anode) type electrodes: titanium mesh electrodes, coated with Ru–Ir mixed metal oxides. These electrodes are suitable as anode as well as cathode and therefore current reversal is allowed. The first electrode rinse solution was unpractical for laboratory use; the other two are described in *Chapter 3*, *5* and *6*.

4.2.2.1. Fe^{2+} / Fe^{3+} in NaCl–HCl

In order to avoid the large overvoltages of gas generating systems, we first used the system Fe^{2+}/Fe^{3+} in a NaCl bulk together with the mentioned inert electrodes. For an electrode rinse containing $FeCl_2$ (0.05 mol.l^{-1}), $FeCl_3$ (0.05 mol.l^{-1}) and NaCl (0.5 mol.l^{-1}), the resulting pH was 2.4. The disadvantage of this system is that O_2 oxidizes Fe^{2+} to Fe^{3+} and H^+ diffuses through the outer membranes, both causing an increase of the pH. After prolonged use, the electrode rinse solution assumed a red brownish color which can be explained by the formation of iron(III) oxyhydroxides. Oxidation can be decreased by means of an airtight system and the formation of insoluble salts can be avoided by controlling the pH to a

low value (<2.3) by the addition of HCl. However, buffering with HCl is difficult because anion exchange membranes are somewhat permeable for H^+ and a constant supply of HCl is necessary. In this way the pH of the effluent decreases which is unacceptable from an environmental viewpoint. A possible solution is the use of an external electrodialysis system with bipolar membranes, generating NaOH as well as HCl. The NaOH can be directed to the output stream and the HCl to the electrolyte. This process is pH neutral and there are no environmental implications. An internal electrodialysis system with bipolar membranes (built in the RED stack) for the same purpose is patented by Hamelers et al.[21].

4.2.2.2. $[Fe(CN)_6]^{4-}$ / $[Fe(CN)_6]^{3-}$ in NaCl

For the development and testing of RED systems in the laboratory the Fe^{2+}/Fe^{3+} appeared to be rather unpractical. Therefore, we changed to a quite stable system: the hexacyanoferrate system:

$$[Fe(CN)_6]^{3-} + e \quad \leftrightarrows \quad [Fe(CN)_6]^{4-} \; ; \; E^0 = 0.356\,V \text{ vs. she (standard hydrogen electrode)}$$

This system is described in *Chapter 3*, *5* and *6*. Again, the inert electrodes were used as described in *Section 4.2.2*. To prevent loss of the iron complex we used CEMs as outer membranes. As long as the electrolyte is not in contact with the AEMs, there are no problems to be expected. However, in case of internal leakages, hexanoferrate ions may poison the AEMs in the stack by irreversible binding, eventually resulting in a decreased performance[22].

4.2.2.3. NaCl

To prevent the poisoning of the membranes, we changed to a pure NaCl solution in the electrode compartments. With this system, we characterized some membrane pairs for the use in RED stacks (*Chapter 6*). By applying CEMs as outer membranes, the generated Cl_2 and OCl^- was kept within the electrode system.

4.2.3. Proposal for a novel system: Fe^{2+}/Fe^{3+} in NaCl–HCl with graphite electrodes

The formerly used DSA type electrodes (as described in *Section 4.2.2*) are designed for gas generation with low overvoltages. However, in our electrode systems with a reversible redox couple (the Fe^{2+}/Fe^{3+} system and the $[Fe(CN)_6]^{4-}$/ $[Fe(CN)_6]^{3-}$ system) gas evolution is undesirable.

Therefore, we suggest the use of graphite electrodes in these systems. Graphite electrodes have been extensively studied for use in redox flow batteries. One of these energy storage systems – the Fe/Cr system - uses the Fe^{2+}/Fe^{3+} couple in the positive half-cell at low pH.

It appears that this system is well reversible in electrochemical sense[23]. Graphite felt is tested until current densities of 7000 A/m^2[24] whereas the optimal current density at RED is much lower; we measured 40 A/m^2 for our experiments (*Chapter 5*).
Advantages of carbon electrodes to Ti/Ru/Ir electrodes are:
- No use of exhaustible precious metals.
- High overpotentials for gas formation. There is no risk of evolvement of dangerous and aggressive gasses (H_2, O_2 and Cl_2). Even with a reversible redox couple this may be the case if the flow of the electrode rinse solution is obstructed locally.
A disadvantage of graphite may be the lower mechanical stability with respect to DSA-type electrodes during longer operation times and the need for a proper current collecting system. Therefore, graphite electrodes may be advantageous for the Fe^{2+}/Fe^{3+} system as well as for the $[Fe(CN)_6]^{4-}/[Fe(CN)_6]^{3-}$ system. We added such systems to *Table 4.3* (column 11 and 12). The rather good end scores encourages further research on these systems.

4.2.4. Symmetry in RED stacks

If the sea and river water inlets of a RED stack are interchanged, the polarity of the generated voltage is reversed. Consequently, the performance of the RED stack is unaltered if the generating system (GS) and the electrode system (ES) are both symmetrical. It is evident that the symmetrical properties of GS and ES are related.

4.2.4.1. Reversal of the electrical current

For some electrode systems periodical reversal is obligatory as for systems with participating (one dissolving and one growing) electrodes. These electrode systems are designated as *'obligatory reversal'* or ES_1. Other systems consist of 'universal' electrodes where reversal is possible but not obligatory and are called '*facultative reversal*' or ES_2. A third case consists of the specific electrodes that are only suitable as cathode or as anode and in which reversal of the electrical current is not possible. These are denoted as *forbidden reversal* or ES_3.

4.2.4.2. Interchange of the feed water in RED stacks

Just as with the electrode system, we distinguish for the generating system between three types:

GS_1: obligatory interchange

In RED, growth of microorganisms in the stacks may be a serious problem. One approach to prevent this, is the periodical interchange of the river and sea water inputs. A comparable method is used for normal electrodialysis for desalination purposes and is called 'electrodialysis reversal' (EDR)[25,26]. From experiments in the future, it may be proven that such

a procedure is necessary and we denote this system as '*obligatory interchange*" or as GS_1.

GS_2: facultative interchange
If it should be proved that feed water interchange is not beneficial for prevention of microbial growth or for breaking down polarization layers, then this interchange is not obligatory. If the GS is also symmetrical (with identical sea and river water compartments), the interchange of sea and river water is also not forbidden. In this case we have a '*facultative interchange*' system or GS_2.

GS_3: forbidden interchange
Bottlenecks in stack design for RED are the hydrodynamical fluid resistance in all compartments and electrical resistance in river water compartments (*Chapter 5*). Optimization can lead to an asymmetric stack: sea water compartments may be thicker than river water compartments to reduce hydrostatic resistance without affecting electrical resistance substantially; also length and width can differ. In such a stack interchanging sea and river water is possible for cleaning purposes but during this interchange the power production is low. We call this a '*forbidden interchange*' system GS_3; although the adjective forbidden should not to be interpreted strictly.

4.2.5. Voltage losses in electrode systems

Electrode systems introduce a voltage loss in the RED system due to an overpotential, concentration polarization, an ohmic potential and a Nernst potential in each electrode compartment. In RED, current densities are relatively low (in our own experiments about 40 A/m^2 (*Chapter 5*)) and the losses due to concentration polarization and the ohmic potential are minimal. This is a general property of all studied electrode systems for RED. Further, with respect to voltage losses, these systems can be divided into low, high and medium loss electrode systems.

Low loss. In systems with opposite electrode reactions and a recirculating electrode rinse, there is no net chemical reaction and the Nernst voltages on both electrodes cancel each other out. In most of these systems no gas reactions are involved and the overpotentials are low. The total voltage loss in the whole electrode system is about 0.1 V; which is comparable to the generated voltage of 1-2 cells.

High loss. Electrode systems with gas evolution have higher voltage losses. For the electrolyses of water, the needed voltage based on the Nernst equation is 1.23 V, and the overpotentials are 0.03 V for H_2 and 0.52 V for O_2 evolution at a current density of 100 A/m^2[227], together 1.78 V. Because the typical cell voltage is about 60 mV under power

generating circumstances, a number of 30 cells is used to overcome the voltage loss of this electrode system.

Medium loss. A special case is the so called 'REF system' of Jagur-Grodzinski and Kramer[10] (system 5 in *Table 4.1*). At the anode O_2 is evolved and at the cathode O_2 is consumed, so there is no net generation of O_2. Because there are separated anode and cathode compartments, the net reactions is: $H_2O \rightarrow H^+ + OH^-$. This water dissociation in ions consumes about 15 kJ per mole[28], much lower less than the 286 kJ per mole as necessary for splitting of water in H_2 and O_2[29]. Therefore, this system is classified in the category 'medium loss'.

It should be noted that electrode losses are only important in stacks with a small number of cells as in laboratory equipments. In a stack with 1000 cells the loss of a high loss system is only 3%. High loss systems are assessed with minus 1 point with respect to low loss systems (*Section 4.3.2-A_5* and *Chapter 4-Appendix A_5*).

4.3. Criteria for electrode systems

4.3.1. Method of assessment

In the assessment of electrode systems, all relevant aspects concerning safety, health, environment (SHE), technical feasibility and economics are taken into account. In total 13 of these aspects were considered. A judgment in a scale from 0 (unacceptable) to 5 (good) is given. Because a commercial RED power plant was never built so far, there is no experience with the different systems under real economical power producing circumstances. Nine different electrode systems for RED are described in literature. To rank the quality of different systems, there are a large number of methods. Data envelopment analysis (DEA) is a powerful method, especially because the different weight factors are determined by the method itself. However, the consequence is that the method is only applicable if the number of systems is larger than the number of the aspects[30,31] and that is not the case in our current topic.

Often a much more simple system is used: the end result is calculated as the arithmetic mean of the different marks. However, to prevent compensation of bad marks by other good aspects, we achieved the total rating by calculating the geometric mean A of all (n) parts A_i. Each aspect A_i is judged with a mark in the range from 0 (unacceptable) to 5 (good).

$$A = \left(\prod_{i=1}^{n} A_i \right)^{\frac{1}{n}} \quad (1)$$

In fact, the geometric mean is closely related to the logarithmic mean with the difference that the first method can cope with zeros and the second method cannot. The advantages of this way of ranking are: (i) unacceptable systems are mentioned (judged as 0 on a single criterion) but always remain at the lowest level of the ranking, (ii) there is no need for ambiguous weight factors (iii) very different variables can be used for different items; even nominal and ordinal data can used together (iv) masking bad properties by averaging with good properties hardly occurs.

For most items, the generating system (N cells of the stack) is independent of the electrode system: each generating system can be combined with each electrode system. An important exception to this rule is the aspect of reversal as discussed in *Section 4.3.2*. This aspect requires a separate ranking system for stacks with obligatory, facultative and forbidden river and sea water reversal.

4.3.2. Assessed aspects

In this paragraph, different aspects are summarized. Applied criteria are included in the appendix. Aspects are classified in three groups: i) technical feasibility (5 aspects), ii) safety, health and environment (SHE; 5 aspects) and iii) economics (3 aspects). A larger number of aspects in a group make this group more important in the end score. Sometimes the classification is rather arbitrary.

A Technical feasibility

A_1 Reversal of the electrical current / interchange of the feed water

Discussed in *Section 4.2.4* are three types of electrode systems and three types of generating systems. Interchange of the feed water of a GS has consequences for the electrode system: by the reversal of the direction of the electrical current the anode becomes cathode and vise versa. *Table 4.2* shows the scores of the different combinations. All combinations are permitted except GS_3-ES_1.

Table 4.2. Marking the different combinations of generating systems with electrode systems.

		reversal direction of the electrical current		
		ES_1: obligatory	ES_2: facultative	ES_3: forbidden
interchange of the water inlets	GS_1: obligatory	4	5	1
	GS_2: facultative	5	5	5
	GS_3: forbidden	0	5	5

made of different materials like stainless steel and graphite; however, the requirements for anodes are much higher than for cathodes. Special mixed metal oxide electrodes based on thin layers of precious metals on titanium can act both as anode and as cathode but their lifetime is severely lowered if current reversal is applied[32,33]. In some patents for electrodialysis (ED), systems are described with composite electrodes[34-36]. These electrodes consist of an alternate array of strips of anode and cathode material. The power supply can be connected to the proper array on each side, dependent on the electrical current direction. In this way each used electrode material, as used in normal ED, can also be used also in the EDR mode, an ED method where the current is reversed periodically to prevent scaling on the membranes. Composite electrodes can be used in principle also for RED to cope with current reversal due to interchange of sea water and river water. Therefore, this 'forbidden' combination GS_1-ES_3 is judged with 1 point.
The combination GS_1-ES_1 is not a definitely ideal because the GS and the ES may demand different switch frequencies and therefore, only 4 points are noted.

A_2 Stability of anolyte/catholyte
Most anolytes/catholytes as listed in *Table 4.1*, contain only stable inorganic ions. The exception is the electrolyte with the hexacyanoferrate redox system. The complex ions in this solution are able to decompose and to form stable insoluble complexes with many multivalent metal ions with the risk of poisoning the membranes.

A_3 Gas formation at the electrodes
Gas formation (Cl_2 and O_2 at the anode and H_2 at the cathode) can cause problems at the electrodes (electrical obstruction) and Cl_2 is highly corrosive. Besides this, Cl_2 formation has a negative environmental value (again called in aspect B_3) and H_2 is an explosion hazard (again called in aspect B_1).

A_4 Participating electrodes
Participating electrodes are already counted at the reversal item. However, dissolving and plating (growing) should be reversible many thousands of times. For example, it is known that Zn is a difficult metal in this aspect and special provisions should be taken with the electrode rinse.

A_5 Electrical properties of the electrode system

Voltage loss
As stated in *Section 4.2.5,* electrode systems can cause low, medium or high losses. If at both electrodes opposite electrochemical reactions occur in the same electrolyte, the

voltage loss is low; otherwise this loss is high. For a large stack, this voltage loss is a minor problem.

Resistance of the electrode system
Electrodes are normally made from good conducting materials. An exception is the Ag/AgCl electrode with a thick AgCl layer where the Ag^+ has to diffuse from the solution to the Ag surface. This system was described by Audinos[11,12] and included as system nr. 3 in *Table 4.1*.

B Safety, health and environment

B_1 Safety
H_2 is explosive and especially dangerous in closed spaces as sea containers or units for underwater operation.

B_2 Health
Toxicity is judged in case of skin and eye contact, swallowing and inhalation. Especially organic redox couples like hydroquinone/1,4-benzoquinone can be a risk if in contact with the skin. The same holds true for acidified solutions of the couple Fe^{2+}/Fe^{3+}. Nearly all electrolytes are toxic if swallowed except NaCl solutions. The most probable danger of inhalation is Cl_2; HCN can be evolved under extreme conditions (low pH, UV-light) from the $[Fe(CN)_6]^{4-}/[Fe(CN)_6]^{3-}$ couple.

B_3 Environment: normal exhaust of Cl_2, ClO^- and ClO_3^-
If sea water or NaCl is used in the electrode system without a reversible redox couple, Cl_2 can be evolved at the anode and H_2 at the cathode. If anolyte and catholyte are combined, ClO^- is formed and there is the possibility of formation of ClO_3^- [18]. Sometimes these products are useful (e.g. as biocide) but mostly they are unwanted. To prevent contamination of the outlet streams with ClO^- and ClO_3^-, the outer membranes should be of the CEM type. However, due to the non ideal behavior of these membranes, there is also a small transport of these anions into the effluent. If other 'safe' salts (Na_2SO_4, $NaNO_3$ etc.) are used in the electrode rinse solution, there is still the danger of Cl_2 evolvement because Cl^- can diffuse from the sea water compartment to the electrode compartment through the CEM.

Even in the presence of a redox couple, Cl_2 formation is not excluded totally if Cl^- is present in the electrode rinse solution because the redox couple can be exhausted locally due to obstructions in the flow path in the electrode compartment.

If seawater is used as electrolyte, there is the possibility of a closed electrode rinse loop or an open single pass system. The last system is unacceptable from environmental viewpoint due to the discharge of Cl_2.

B_4 Environment: normal exhaust other chemicals

In principle, ions can be blocked by a proper choice of the outer membranes although blocking of co-ions is not 100%. Especially protons can easily pass the most types of AEMs. Technically, the problems of transport from unwanted species from the electrode compartments to the sea or river water compartments and vice versa can be solved by using double outer membranes. Between these outer membranes a guard electrolyte is recirculated. Disadvantageous is the need of conditioning this guard electrolyte.

B_5 Environment: accidental exhaust

Loss of anolyte/catholyte may occur by accident: rupture of the outer membranes, human errors and defects in the electrode rinse pumping system are possible causes. The effects of outer membrane damaging can be decreased by using double outer membranes as described above under B_4. Defects in the electrode rinse system can be controlled by leakage tanks. Moreover, a RED installation is built modular and in event of an accident only a small part of the electrolyte is drained.

C Economics

C_1 Special provisions for the anolyte/catholyte

The most frequent measures to be taken are:

a) pH control

At low pH, H^+ can diffuse easily through AEMs to the output stream and new H^+ should be added to the electrolyte. This can be achieved by adding HCl; an environmentally better way is the use an external electrodialysis system with bipolar membranes generating NaOH and HCl. The NaOH can be directed in the output stream and the HCl to the electrolyte. This process is pH neutral.

b) Redox control

In redox systems as Fe^{2+}/Fe^{3+}, the optimal Fe^{2+}/Fe^{3+} ratio is about unity. However, by oxidation by air this ratio may be affected. An airtight system should be used and/or a reduction system should be incorporated.

c) Concentration control

In fact, each anolyte/catholyte should be controlled, especially electrolytes containing monovalents ions like NO_3^- which can be exchanged rapidly with Cl^- from the sea water.

C_2 Price of the electrodes

Inert electrodes can be made of massive platinum, sometimes with added ruthenium or iridium for mechanical strength. Such electrodes are used in laboratories as measuring electrode or as working electrode in different analytical processes. These electrodes are very expensive and efforts have been made to platinize other metals or carbon in such a way that the inert properties of platinum are combined with the economics of other metals. This resulted in platinum coated titanium with 20-50 grams platinum per square meter. These electrodes are rather expensive and not catalytic enough for gas evolving processes. The next step was the invention of the so called 'dimensional stable electrode' (DSA) for the chlor-alkali membrane process[37].

Modern stable electrodes consist of a metal support (mostly titanium) with a mixed metal oxide (MMO) layer[38]. The MMO consist of two components: one is a catalytic and conducting (e.g. RuO_2, IrO_2, $PtO_{0.12}$), the other is inert and nonconducting (e.g. TiO_2). The catalytic part of the electrode cover is developed for special electrochemical purposes like Cl_2 or O_2 evolution. On these electrodes the amount of precious metal is only 10-12 g/m^2. Moreover the price of iridium and especially of ruthenium is much lower than of platinum. This may result in acceptable prices.

A further reduction of electrode price can be achieved by using partial electrodes: electrodes with a reduced surface by a proper dimensioning of a stretched metal process. In RED, partial electrodes can be used because the current density in the RED process is much lower than in other electrochemical processes for which these electrodes are developed.

Graphite electrodes are rather inexpensive. However, at larger surfaces, current collection may be a problem and results in a higher price.

C_3 Lifetime of the electrodes

Marks for the aspects of price (C_2) and lifetime (C_3) are generally opposite. In our used criteria (*Appendix*) all DSA type electrodes get the same judgment (mark=5). The actual lifetime of these electrodes is dependent on current direction (anodic or cathodic use), electrolyte and current density. Fields of application of electrodes with long erasing time are water desalination with electrodialysis (ED) and the chlor-alkali process. In normal

ED for desalination, a 5-year life of a platinum plated electrode is normal. Anode life was generally less than cathode life[39]. In fact all modern electrodes are MMO covered on titanium (DSA type). For chlorine evolving DSAs, as used in the chlor-alkali industry, typical current densities are more then 3000 A/m^2 in the membrane cell process[40]. In this case the lifetime of DSAs is guaranteed to be up to 10 years[41]. In contrast, optimal current densities in our RED process were 40 A/m^2 (*Chapter 5*). Therefore, lifetime of chlorine evolving DSAs may be expected to be much more than 10 years for RED. For oxygen evolution, Chen and Chen[42] predicted for their Ti/RuO_2–Sb_2O_5–SnO_2 electrode a lifetime of 8.3 years at a current density of 200 A/m^2 and even 27 years at 100 A/m^2. These lifetimes are also an indication for use in RED electrode systems. The foregoing refers to unidirectional use of the electrodes. Current reversal (as in EDR) generally decreases electrode lifetime substantially[39,43].

4.4. Discussion

4.4.1. Described electrode systems

Described electrode systems in literature for RED are not yet suitable for use in economical operated RED systems. A RED system should fulfill the requirements on safety, health, environment, technical feasibility and economics. In *Table 4.3* the formulated criteria are applied to the different described electrode systems from *Table 4.1* (for GS_1 in bold, for GS_2 regular and for GS_3 in italics). The row 'reversal to the electrical current' (A_1) is split up in three parts for the combination of the different generating systems with the electrode system in question. The same goes for the rows with the end-scores and ranks.

Table 4.3 shows that from the described used systems (column 1-10), the iron system with Ti/Ru,Ir electrodes (column 8) is the best system in combination with each of the three generating systems.
The hexacyanoferrate system with the same electrodes (column 9) may be useful in laboratory equipment. The table also indicates that by application of graphite electrodes the score of these systems is approached (column 11 and 12).

4.4.2. Proposal for improved electrode systems

Possible improvements are:

a) Use of graphite electrodes
As indicated in the *Sections 4.2.3* and *4.4.1,* the use of graphite electrodes in combination with homogeneous redox system like Fe^{2+}/Fe^{3+} has good prospects.

Table 4.3. Ranking the systems described in literature for practical use. The marks in the rows A1 are dependent on the generating system (GS_1, GS_2 or GS_3). The same holds for the score/rank rows at the bottom.

		described systems in literature							used systems by author			suggested systems	
		1	2	3	4	5	6	7	8	9	10	11	12
	anolyte / catholyte	Pattle	Weinstein	Audinos	Jagur-G	Jagur-G	Turek	Suda	Veerman	Veerman	Veerman	Veerman	Veerman
	bulk	$CuSO_4$	NaCl	NaCl	$ZnCl_2$	NaCl	Na_2SO_4	NaCl	Fe^{3+}/Fe^{2+} NaCl-HCl	HCF #) NaCl	NaCl	Fe^{3+}/Fe^{2+} NaCl-HCl	HCF #) NaCl
	cathode	Cu	Ti/Pt *)	Ag/AgCl	Zn	$C/Pt/O_2$	Ti/Pt	C	Ti/Ru,Ir	Ti/Ru,Ir	Ti/Ru,Ir	graphite	graphite
	anode	Cu	Ti/Pt *)	Ag/AgCl	Zn	C/Pt	Ti/Pt	C	Ti/Ru,Ir	Ti/Ru,Ir	Ti/Ru,Ir	graphite	graphite
	type	ES1	ES2	ES1	ES1	ES3	ES2	ES2	ES2	ES2	ES2	ES2	ES2
Technical feasibility													
GS_1	**A_1 Reversal of the el. current**	**4**	**5**	**4**	**4**	**1**	**5**	**5**	**5**	**5**	**5**	**5**	**5**
GS_2	A_1 Reversal of the el. current	5	5	5	5	5	5	5	5	5	5	5	5
GS_3	*A_1 Reversal of the el. current*	*0*	*5*	*0*	*0*	*5*	*5*	*5*	*5*	*5*	*5*	*5*	*5*
all	A_2 Stability of anolyte/catholyte	5	5	5	5	5	5	5	5	3	5	5	3
all	A_3 Gas formation	5	2	5	5	4	4	2	5	5	2	5	5
all	A_4 Participating electrodes	4	5	3	2	5	5	5	5	5	5	5	5
all	A_5 Electrical properties	5	4	4	5	3	4	4	5	5	4	5	5
Safety, health and environment (SHE)													
all	B_1 Hydrogen formation	5	3	5	5	5	3	3	5	5	3	5	5
all	B_2 Toxicity	4	3	5	4	3	5	3	4	4	3	4	4
all	B_3 Normal exhaust of Cl_2 etc.	5	0	5	5	4	4	0	5	5	1	5	5
all	B_4 Normal exhaust other chem.	4	5	4	4	5	5	5	4	4	5	4	4
all	B_5 Accidentally exhaust.	3	5	5	4	5	5	5	4	3	5	4	3
Economics													
all	C_1 Special provisions	4	3	4	4	2	4	3	3	4	3	3	4
all	C_2 Price of the electrodes	5	1	2	5	1	1	5	4	4	4	3	3
all	C_3 Life time of the electrodes	2	4	2	2	4	4	2	5	5	5	3	3
GS_1	**Score**	**4.1**	**0.0**	**3.9**	**4.0**	**3.2**	**3.9**	**0.0**	**4.5**	**4.3**	**3.5**	**4.2**	**4.1**
	Rank	**4**	**11**	**7**	**6**	**10**	**7**	**11**	**1**	**2**	**9**	**3**	**5**
GS_2	Score	4.2	0.0	4.0	4.1	3.6	3.9	0.0	4.5	4.3	3.5	4.2	4.1
	Rank	4	11	7	6	9	8	11	1	2	10	3	5
GS_3	*Score*	*0.0*	*0.0*	*0.0*	*0.0*	*3.6*	*3.9*	*0.0*	*4.5*	*4.3*	*3.5*	*4.2*	*4.1*
	Rank	*8*	*8*	*8*	*8*	*6*	*5*	*8*	*1*	*2*	*7*	*3*	*4*

*) Ti/Pt assumed

#) HCF = hexacyanoferrate = $Fe(CN)_6^{3-}/Fe(CN)_6^{4-}$

b) Improved electrodes of the DSA type

- Longer lifetime.

For our experiments we used titanium mesh end electrodes, coated with Ru–Ir mixed metal oxides (*Chapter 3, 5* and *6*). These electrodes are reversible (i.e. current reversal is possible) and therefore usable for all types of stacks. Lifetime of these electrodes is more than 10 years under the applied current density (40 A/m^2). An improvement of the lifetime with a factor 5 can be achieved with special Ir-MMO (mixed metal oxide) coated titanium anodes and Ru-MMO coated cathodes; another option is to use the extra stability of these electrodes for reducing the cost of these electrodes by decreasing the surface of the electrodes (the so called partial electrodes). A limitation of this system is that frequent current reversal during longer times is not possible with these electrodes.

- High overvoltages for Cl_2 / O_2 evolution

The success of DSA type electrodes is due to a combination of high mechanical and electrochemical stability with good catalytic properties and low overvoltages for special electrode reactions. Especially such anodes are developed for Cl_2 and O_2 generation. However, in a RED process with a homogeneous redox couple (e.g. the Fe^{2+}/Fe^{3+} or the system $[Fe(CN)_6]^{4-}$ / $[Fe(CN)_6]^{3-}$), these reactions are unwanted. Therefore, high overvoltages for gas evolution are favorable to the process. It requires some extra development to realize this with DSA type electrodes.

- Specific composite electrodes for RED

For use in normal electrodialysis some systems with composite electrodes are patented[34-36]. These systems allow current reversal with electrodes which are specifically usable as cathode or anode. In each current direction only one part of each electrode is used. Eventually the unused part can be protected with a low potential difference between this part and the adjacent part in operation.

c) New homogeneous redox couple

Homogeneous redox systems (e.g. the system $[Fe(CN)_6]^{4-}$ / $[Fe(CN)_6]^{3-}$) do not cause net chemical reactions and therefore the power losses are low. Most organic homogeneous redox couples involve protons in their reactions and special measures should be taken to control the pH. However, there are many iron complexes and possibly candidates are available that satisfy all mentioned criteria. The use of graphite electrodes may be considered again in this case.

d) Capacitive electrodes

In the last decades, special high ion absorbing carbon has been developed for use in

super capacitors[44-46] and in capacitive deionization (CDI)[47,48]. If this material is used as electrode in a RED stack, during a certain time an internal ionic current can persist. The electrodes behave as a capacitor and during that time there is also an external electrical current. After some time, the process should be inverted by changing the sea water and the river water feed. It is obvious that the changing time is related to the residence time in the system. Assuming that time to be one minute, then a half period (the time between two feed interchanges) should be at least about 60 minutes. Current RED stacks operate at maximum power output with a current density of about 40 A/m^2 or 144000 Coulomb per m^2 per hour. The cathode should adsorb then 144000/F= 1.5 mol Na^+ and on the anode the same amount of Cl^- (F is the Faraday constant; 1 F = 96 485 C/mol). Typical specific capacitances are reported of 100–200 F/g carbon in aqueous solution[44-46]. Using the highest value of 200 F/g, for an uploading to 1 V, there is 200 C/g carbon needed. For a one hour operation, the electrodes should consist of 720 grams carbon per m^2. This seems a realistic value for further development of such a system.

In principle, the method is very clean and sustainable. Carbon aerogel electrodes may have lifetimes of more than 10 years[49]. A restriction of this system is the obligatory interchange. For optimal performance, the connected load should be adapted continuously during one cycle. This is possible with modern DC-DC converters. For normal electrodialysis, such a system is patented by Wei et al.[50].

Brogioli succeeded in the *reversal of the capacitive deionization* (CD) technique[51]. The capacitor is formed by two activated carbon electrodes, immersed in the feed solution, alternately salt and fresh water. When filled with salt water, it is charged, and with fresh water it is discharged. Charging and discharging are promoted by the diffusion of ions and consequently there is a net energy gain.

e) Systems with an electrode rinse solution containing carbon particles and/or ion exchange resin particles

These systems are described by Kedem et al. for use in normal electrodialysis and patented[52,53]. The electrode rinse solution contains about 1% (w/w) active carbon and 1% (w/w) cation exchange resin in a NaCl solution of about 2% (w/w). The authors suggest that this system is based on the reversible system

$$H^+ + e \leftrightarrows \tfrac{1}{2} H_2$$

The H_2 gas, as evolved at the cathode is adsorbed by the carbon and transported to the

anode where the reverse reaction proceeds. The involved H^+ is transported by the ion exchange resin:

$RH + Na^+ \leftrightarrows RNa + H^+$

where RH is the resin in the acid form and RNa the resin in the salt form.
The net reaction at the cathode and at the anode is therefore:

$RH + Na^+ + e \leftrightarrows RNa + \frac{1}{2} H_2$

4.5. Conclusions

In this work, self-developed electrode systems and electrode systems described in literature are compared on safety, health, environment, technical feasibility and economics. A robust system of judging the different systems is presented. Applying this system to the described and used systems, a ranking was made of the different electrode systems. It is shown that the applicability of an electrode system is related to the generating system. Three types of generating systems can be distinguished: systems with (i) obligatory, (ii) facultative and (iii) forbidden interchange of the feed water inlets. The highest rankings for all the three generating systems are found for the Fe^{2+}/Fe^{3+} couple in a NaCl–HCl supporting electrolyte with bidirectional Ru/Ir covered titanium electrodes.

This system is not ideal and may be improved for application in commercially operating, large scale RED. There are five interesting topics: (i) improved stable metal electrodes (with longer lifetime, suitable for current reversal and high overpotential for gas evolvement), (ii) a new homogeneous redox couple (e.g. an iron complex), (iii) a system with capacitive electrodes, (iv) a system with an electrolyte, containing carbon particles and/or ion exchange resin particles, and (v) the Fe^{2+}/Fe^{3+} couple in combination with graphite electrodes. The last improvement seems to be the most realistic alternative; however, duration test should be performed under real RED conditions to prove that it has sufficient mechanical and electrochemical stability.

Acknowledgement
This work was performed in the TTIW-cooperation framework of Wetsus, centre of excellence for sustainable water technology (www.wetsus.nl). Wetsus is funded by the Dutch Ministry of Economic Affairs, the European Union Regional Development Fund, the province of Fryslân, the city of Leeuwarden and the EZ/Kompas program of the "Samenwerkingsverband Noord-Nederland". The first author would like to thank the Noordelijke Hogeschool Leeuwarden who facilitated this research by detaching him to Wetsus and the participants of the theme "Energy" for their fruitful discussions and their financial support.

Nomenclature

Abbreviations

AEM	anion exchange membrane
DC	direct current
CEM	cation exchange membrane
CDI	capacitive deionization
DEA	data envelopment analysis
DSA	dimensionally stable anode
ED	electrodialysis
EDR	electrodialysis reversal
EMF	electromotive force
ES	electrode system
GS	generating system
MMO	mixed metal oxide
PRO	pressure retarded osmosis
RED	reverse electrodialysis
she	standard hydrogen electrode
SHE	safety, health and environment
SGP	salinity gradient power

Definitions

compartment	space between the membranes
cell	combination of two membranes and two compartments
generating system	a number of N cells without the electrode system
electrode system	anode, cathode, electrode rinse and outer membranes
stack	a number of N cells with an electrode system

References Chapter 4

1 J.W. Post, H.V.M. Hamelers, C.J.N. Buisman, *Energy recovery from controlled mixing salt and fresh water with a reverse electrodialysis system.* Environ. Sci. Technol. 42 (2008) 5785-5790

2 G.L. Wick, W.R. Schmitt, *Prospects for renewable energy from sea.* Mar. Technol. Soc. J. 11 (1977) 16-21

3 Energy information administration; official energy statistics from the U.S. government, www.eia.doe.gov

4 R.E. Pattle, *Production of electric power by mixing fresh and salt water in the hydroelectric pile.* Nature 174 (1954) 660-660

5 R.E. Pattle, *Electricity from fresh and salt water - without fuel.* Chem. Proc. Eng. 35 (1955) 351–354

6 R.E. Pattle, *Improvements to electric batteries.* Patent GB 731.729 (1955)

7 S. Loeb, *Osmotic power plants.* Science 189 (1975) 654–655

8 S. Loeb, *Production of energy from concentrated brines by pressure retarded osmosis.1. Preliminary technical and economic correlations.* J. Membr. Sci. 1 (1976) 49–63

9 J.W. Post, J. Veerman, H.V.M. Hamelers, G.J.W. Euverink, S.J. Metz, K. Nymeijer, C.J.N. Buisman, *Salinity-gradient power: Evaluation of pressure-retarded osmosis and reverse electrodialysis.* J. Membr. Sci. 288 (2007) 218–230

10 J. Jagur-Grodzinski, R. Kramer, *Novel process for direct conversion of free energy of mixing into electric power.* Ind. Eng. Chem. Process Des. Dev. 25 (1986) 443–449

11 R. Audinos, *Inverse electrodialysis. Study of electric energy obtained starting with two solutions of different salinity.* J. Power Sources 10 (1983) 203–217

12 R. Audinos, *Electric power produced from two solutions of unequal salinity by reverse electrodialysis.* Ind. J. Chem. 31A. (1992) 348–354

13 J.N. Weinstein, F.B. Leitz, *Electric power from differences in salinity: the dialytic battery.* Science 191 (1976) 557–559

14 G.L. Wick, *Power from salinity gradients.* Energy 3 (19878) 95-100

15 S. Loeb, *Method and apparatus for generating power utilizing reverse electrodialysis.* Patent US 4.171.409 (1979)

16 G.D. Metha, *Performance of present-day ion-exchange membranes for power generation using a saturated solar pond.* J. Membr. Sci. 11 (1982) 107-120

17 F.Suda, T. Matsuo, D. Ushioda, *Transient changes in the power output from the concentration difference cell (dialytic battery) between seawater and river water.* Energy 32 (2007) 165-173

18 L.R. Czarnetzki, L.J.J. Janssen, *Formation of hypochlorite, chlorate and oxygen during NaCl electrolysis from alkaline solutions at an RuO_2/TiO_2 anode.* J. Appl. Electrochem. 22 (1992) 315-324

19 M. Turek, B. Bandura, *Renewable energy by reverse electrodialysis.* Desalination 205 (2007) 67-74

20 M. Turek, B. Bandura, P. Dydo, *Power production from coal-mine brine utilizing reversed electrodialysis.* Desalination 221 (2008) 462-466

21 H.V.M. Hamelers, J.W. Post, S.J. Metz, *Device and method for performing a reversed electrodialysis process.* Patent WO 2007/094659 A1 (2007)

22 R.E. Lacey, *Energy by reverse electrodialysis.* Ocean Eng. 7 (1980) 1-47

23 M. Lopez-Atalaya, G. Codina, J.R. Perez, J.L. Vazquez, A. Aldaz, *Optimization studies on a Fe/Cr redox flow battery.* J. Power Sources 39 (1992) 147-154

24 V. Pupkevich, V. Glibin, D. Karamanev, *The effect of activation on the electrochemical behaviour of graphite felt towards the Fe^{3+}/Fe^{2+} redox electrode reaction.* Electrochem. Comm. 9 (2007) 1924-1930

25 W.E. Katz, *The electrodialysis reversal (EDR) process*. Desalination 28 (1979) 31-40

26 V.D. Grebenyuk, O.V. Grebenyuk, *Electrodialysis, from an idea to realization.* Russ. J. Electrochem. 38 (2002) 906-910

27 International Critical Tables 1929, 6, 339

28 K. Nagasubramanian, F.P. Chlanda, Kang-Jen Liu, *Use of bipolar membranes for generation of acid and base - an engineering and economic analysis.* J. Membr. Sci. 2 (1977) 109-124

29 D.R. Lide (editor), *Handbook of chemistry and physics,* (CRC-press), 85th d (2004-2005), p. 5-18

30 A. Charnes, W.W. Cooper, E. Rhodes, *Measuring the efficiency of decision making units*. Eur. J. Operational Research 2 (1978) 429-444

31 N. Adler, L. Friedman, Z. Sinuany-Stern, *Review of ranking methods in the data envelopment anaysis context*. Eur. J. Operational Research 140 (2002) 249-965

32 J.X. Qu, S.M. Liu, *Electrode for electrodialysis.* Desalination 46 (1983) 233-242

33 A.T. Kuhn, C.J. Mortimer, *The efficiency of chlorine evolution in dilute brines on ruthenium dioxide electrodes.* J. Appl. Electrochem. 2 (1972) 283-287

34 W. Kwo-Weo Chen, *Electrodialysis apparatus for fluid treatment.* Patent US 3.192.148 (1965)

35 K. Mihara, M. Kato, *Polarity reversing electrode units and electrical switching means therefore.* Patent US 3.453.201 (1969)

36 S.M. Jain, *Polarity reversal electrodes.* Patent US 4.461.693 (1984)

37 H.B. Beer, *Electrode and coating therefore.* Patent US 3.632.498 (1972) and *Electrode having platinum metal oxide coating thereon, and method of use thereof*. Patent US 3.711.385 (1973)

38 C.H. Comninellis, G.P. Vercesi, *Characterization of DSA-type oxygen evolving electrodes: choise of a coating.* J. Appl. Electrochem. 21 (1991) 335-345

39 K. Price (ed.) (2003), *Desalination handbook for planners*, 3rd edn Ch. 4.8.9 RosTek Associates, Tampa, Florida

40 T.F. O'Brien, T.V. Bommaraju, F. Hine (2005) *Handbook of Chlor-Alkali Technology*, Volume 1, p. 33 Springer

41 S. Trasatti, *Electrocatalysis: understanding the success of DSA*. Electrochim. Acta 45 (2000) 2377-2385

42 X. Chen, G. Chen, *Stable Ti/RuO_2-Sb_2O_5-SnO_2 electrodes for O_2 evolution*. Electrochim. Acta (2005) 4155-4159

43 A. Kraft, *Electrochemical water disinfection: a short review. Electrodes using platinum group metal oxides*. Platinum Metals Rev. 52 (2008) 177-185

44 G. Lota, T.A. Centeno, E. Frackowiak, F. Stoeckli, *Improvement of the structural and chemical properties of a commercial activated carbon for its application in electrochemical capacitors.* Electrochim. Acta 53 (2008) 2210-2216

45 E. Frackowiak, F. Béguin, *Carbon materials for the electrochemical storage of energy in capacitors. Carbon* 39 (2001) 937-950

46 C. Kim, Y.O. Choi, W.J. Lee, K.S.Yang, *Supercapacitor performances of activated carbon fiber webs prepared by electrospinning of PMDA-ODA poly(amic acid) solutions.* Electrochim. Acta 50 (2004) 883-887

47 J.C. Farmer, D.V. Fix, G.V. Mack, R.W. Pekala, J.F. Poco, *Capacitive Deionization of NaCl and $NaNO_3$ solutions with carbon aerogel electrodes.* J. Electrochem. Soc. 143 (1996) 159-169

48 L.D. Zou, L.X. Li, H.H. Song, G. Morris *Using mesoporous carbon electrodes for brackish water desalination.* Water Research 42 (2008) 2340-2348

49 T.J. Welgemoed, C.F. Schutte, *Capacitive Delonization Technology (TM): An alternative desalination solution.* Desalination 183 (2005) 327-340

50 C. Wei, D. Yu, C. Wei, R. Xiong, L. Cao, *Non-Faraday based systems, devices and methods for removing ionic species from liquid.* Patent WO 2008/030646 A2 (2008)

51 D. Brogioli, *Extracting Renewable Energy from a Salinity Difference Using a capacitor.* Phys. Rev. Lett. 103 (2009) 058501 1-5

52 O. Kedem, G. Tanny, Y. Maoz, A s*imple electrodialysis stack*. Desalination 24 (1978) 313-319

53 O. Kedem, T. Robinson, *Electrodialysis device.* Patent US 4.226.688 (1978)

Appendix

Applied criteria.

The used marks are: good=5; reasonable=4; acceptable=3; poor=2; bad=1 and unacceptable=0.
In some cases minus signs are used. These mean that their value should be subtracted from the maximal score of 5.

A.Technical feasibility

A_1. Reversal of the electrical current
score: Already given in *Table 2*

A_2 Stability of the anolyte/catholyte
score:

no instable ions	5
$[Fe(CN)_6]^{4-}$, $[Fe(CN)_6]^{3-}$	4

A_3. Gas formation at the electrodes
score:

no gas	5
O_2 formation	-1
Cl_2 formation	-2
H_2 formation	-1

A_4. Participating electrodes
score:

no participating electrodes	5
participating without problems (Cu)	4
participating with minor problems (Ag/AgCl)	3
participating with more severe problems (Zn)	2
participating with severe problems	0

A_5. Electrical properties of the electrode system
score:

no problems	5
net chemical reaction	-1

high overvoltage	-1
slow redox couple	-1
high electrode resistance	-1

B. Safety, health and environment (SHE)

B_1. Hydrogen formation at the cathode

score:	
no gas formation	5
H_2 formation	3

B_2. Toxicity

score	
no danger	5
skin danger	-1
swallowing danger	-1
inhalation danger	-2

B_3. Environment: normal exhaust of Cl_2, ClO^- and ClO_3^-

score	
no Cl_2 generation	5
minor Cl_2 production in closed circuit	4
major Cl_2 production in closed circuit	1
minor Cl_2 production in open system	1
major Cl_2 production in open system	0

B_4. Environment: normal exhaust other chemicals

score	
no emission	5
low emission	4
above emission norm	0

B_5. Environment: accidentally exhaust

score	
Na^+, Cl^-, HCO_3^-, Mg^{2+}, Ca^{2+}	5
Zn^{2+}, Fe^{2+}, Fe^{3+}	4
$[Fe(CN)_6]^{4-}$, $[Fe(CN)_6]^{3-}$, Cu^{2+}	3
quinone, pyrocatechol, hydroquinone etc.	2

C. Economics

C_1. Special provisions for the anolyte/catholyte

score:	
no provisions	5
pH control	-1
concentration control	-1
air supply	-1
Cl_2, ClO^- and ClO_3^- discharge	-2

C_2. Price of the electrodes

score:	
Ti, C, Zn, Cu	5
DSA type	4
graphite	3
Ag	2
platinized Ti or C	1

C_3. Lifetime of the electrodes

score:	
DSA type	5
platinized Ti or C	4
graphite	3
participating electrodes, carbon	2

Chapter 5

Reverse electrodialysis: Performance of a stack with 50 cells on the mixing of sea and river water

Abstract

The purpose of reverse electrodialysis (RED) is to produce electricity upon the mixing of two solutions. We studied the power density (W/m^2) and the energy efficiency (the amount of energy produced from specified volumes of river and sea water in relation to the thermodynamic maximum). With a stack of 50 cells (of 10 cm X 10 cm), a power density of 0.93 W/m^2 was obtained with artificial river water (1 g NaCl/L) and artificial sea water (30 g NaCl/L), which is the highest practical value reported for RED. This value is achieved due to an optimized cell design using a systematic measurement protocol.

The main factor in the power density is the cell resistance. With the used membranes (Fumasep FAD and FKD) and a spacer thickness of 200 µm, a cell resistance of 0.345 Ω is measured under RED conditions. This is about one and a half times the value as expected from the contribution of the individual components. This high value is probably caused by the shielding effect of the spacers. The largest contribution to this resistance (about 45%) is from the river water compartment.

The hydrodynamic loss resulted in a maximal net power density of about 0.8 W/m^2 at a flow rate of 400 mL/min. At this optimum the consumed power for pumping is 25% of the total generated energy. The majority of the pump power is lost in the manifolds.

Multistage experiments were performed at maximal power conditions (a current density of about -30 A/m^2 and at a flow rate of 300 mL/min). At these conditions the theoretical energy efficiency is maximal 50%. In practice however, the energy efficiency of a single stack is 9%. The effluent concentrations of the so operated stack are used for a second experiment and so on, simulating a multi stage operation. With 3 stages a cumulative energy efficiency of 18% is achieved. A fourth stage did not increase this value. The power density of the 3 stages together was 50% of the power density of the first stage, indicating that energy efficiency and power density are counteracting.

Further increase of power density and energy efficiency can be obtained with a better spacer and manifold design. A more open spacer is beneficial for RED in two ways: less shielding and lower pressure drop. Less shielding decreases the electrical resistance of the cell. A lower pressure drop permits the use of thinner water compartments, resulting again in a decreased electrical resistance of the cell and an improvement of the power density.

Published as
J. Veerman, M. Saakes, S.J. Metz and G.J. Harmsen
Reverse electrodialysis: performance of a laboratory device with 50 cells on the mixing of sea and river water
Journal of Membrane Science 327 (2009) 136-144

5.1. Introduction

In 1954 Pattle[1] wrote: *The osmotic pressure of sea-water is about 20 atmospheres, so that when a river mixes with the sea, free energy equal to that obtainable from a waterfall 680 ft. high is lost. There thus exists an untapped source of power which has (so far as I know) been unmentioned in the literature.* This 'salinity power' is in principle clean and sustainable and gives no thermal pollution and no CO_2 exhaust. The energy that theoretically can be generated per m^3 river water is 2.5 MJ when mixed with a large surplus of sea water or 1.7 MJ when mixed with 1 m^3 sea water (*Table 5.1*). Wick and Schmitt[2] estimated the total global salinity power to be 2.6 TW, which is sufficient to supply the global electricity demand (2 TW) or 16% of the total present energy consumption[3]. There are different methods to extract energy from the mixing of sea and river water. Described techniques are reverse electrodialysis (RED)[1,4,5], pressure retarded osmosis (PRO)[6,7], vapor pressure difference utilization[8], mechanochemical methods[9], the so called 'hydrocratic generators'[10], membrane-less hydro-voltaic cells[11] and cryoscopic techniques like freezing temperature difference utilization[12]. RED as well as PRO are promising techniques for the generation of energy from a salinity gradient. Post et al.[13] showed that in the case of sea water with river water, RED is very promising.

In principle, RED is a seemingly simple technique. Nevertheless, only 8 groups have published in scientific journals on their experimental results with RED operating on sea and river water[1,4,5,12,14-20] during a period encompassing more than 50 years. In these papers RED has been proven on lab scale. However, the reported power densities were relatively low and the efficiency of the process (energy efficiency) was not taken into account. Meanwhile, the knowledge of ion exchange membranes has increased and many ion exchange membranes with good properties have been developed. Furthermore, energy demand, and therewith also the problems concerning chemical and thermal pollution as well as greenhouse problems caused by CO_2 exhaust, has grown enormously. The investigation of this technique using state of the art membranes and the improvement of the operational properties of the process is aimed at providing a solution to these problems.

The objective was to study the behavior of a RED stack with commercially available membranes with respect to two operational important parameters: energy efficiency (the gained power in relation to maximal thermodynamic value) and power density (the power generated per m^2 membrane). These two response factors are dependent on membrane properties (conductivity, selectivity, osmotic behavior), cell properties (compartment thickness, spacer type), stack design parameters (way of feed, electrode

system), operating conditions (flow rates, electrical load) and water quality (salt content, impurities, temperature, polyvalent ions). These parameters are conflicting in many ways. This chapter focuses on the main parameters affecting power density and energy efficiency: (i) current density, (ii) membrane and spacer resistance, and (iii) feed flow rate. In order to obtain a maximal power density we used commercial membranes with a low resistance. Experiments were performed with a custom made RED stack with a variable number of cells. The largest stack consisted of 50 cells with a total effective membrane area of 1 m^2, generating a power output of 0.93 W which is the highest power density ever reported for RED operating on river and sea water.

5.2. Theory

5.2.1. Reverse electrodialysis

A typical RED system consists of a variable number of alternating cation and anion exchange membranes in a stack. *Figure 5.1* shows such a system with only one cell. Every cell consists of a cation exchange membrane (CEM), a salt water compartment, an anion exchange membrane (AEM) and a fresh water compartment. Positive ions from the sea water diffuse through the CEMs to the river water compartment and build up a positive potential on one side of the stack. The negative ions from the sea water diffuse through the AEMs to the river water compartment on the other side and cause a negative potential in this location. The potential difference between the two solutions can be calculated using the Nernst equation. If sea water is considered as a solution of 30 kg NaCl /m^3 and river water as a solution of 1 kg NaCl/m^3, this potential difference is 140-160 mV per cell. If there is an external circuit connected to the end electrodes, electrical power can be extracted from the system. The ionic current in the cells is then converted to an external electron current via redox reactions at the electrodes.

5.2.2. Power density determination

The theory about reverse electrodialysis was formulated by Weinstein and Leitz[14], Clampitt and Kiviat[21], Jagur-Grodzinski, and Kramer[17] and Lacey[22] and is summarized by Veerman et al. (*Chapter 3*). Key parameters of a RED cell are the electromotive force, internal resistance and delivered power. The voltage across a 100% selective membrane can be calculated if pure NaCl solutions of 1 and 30 g/L at 298 K are used, giving values of 0.080 V for a CEM and 0.078 V for an AEM, or together E_{cell} = 0.158 V for a cell.

The power efficiency (η_p) is the fraction of total power that is delivered to an external power consumer with resistance R_u:

$$\eta_P = \frac{I^2 R_u}{I^2 R_i + I^2 R_u} = \frac{R_u}{R_i + R_u} \quad (1)$$

At the condition of maximal power output ($R_u = R_i$), the power efficiency is not higher than 50%. A higher efficiency can be achieved (by taking $R_u > R_i$) at the cost of a decreased power output.

The power density P_d of a RED system is defined as the external (P_u) power per membrane area (W/m^2) and is maximal under the condition of $R_u = R_i$:

$$P_d = \frac{P_u}{2A} = \frac{I^2 R_u}{2A} = \left(\frac{E_{cell}}{R_i + R_u} \right)^2 \frac{R_u}{2A} = \frac{E_{cell}^2}{8AR_i} = \frac{E_{cell}^2}{8A(R_{AEM} + R_{CEM} + R_{river} + R_{sea})} \quad (2)$$

where P_u stands for the external power, A for the active cell area, and 2A for the total membrane area (AEM and CEM) in a cell. R_{AEM}, R_{CEM}, R_{river} and R_{sea} are the resistances of the AEM, CEM, river water compartment and sea water compartment, respectively.

5.2.3 The mixing entropy of seawater and river water

In order to determine the amount of energy extracted from mixing, it is necessary to calculate the chemical potential between 2 solutions of different concentrations. The Gibbs free energy of mixing (ΔG_{RED}) of river water (V_R (m^3) ; NaCl concentration: C_R (mol/m^3)) with sea water (V_S (m^3); NaCl concentration: C_S (mol/m^3)) is given by[23,24]:

$$\Delta G_{RED} = 2RT \left[V_R C_R \ln \frac{C_R}{C_M} + V_S C_S \ln \frac{C_S}{C_M} \right] \quad (3)$$

with

$$C_M = \frac{V_R C_R + V_S C_S}{V_R + V_S} \quad (4)$$

where R is the gas constant ($R=8.31\ J \cdot mol^{-1} K^{-1}$) and T the temperature (K); the origin of the factor 2 is the dissociation of one mole NaCl in two moles of ions. C_M is the equilibrium concentration, gained at total mixing. *Eq. (3)* is an approximation: the entropy increase of the water is not included and the activity coefficients are taken to unity but both effects tend to counterbalance.

For a zero salt concentration in the river water (C_R=0), *Eq. (3)* can be simplified to:

$$\Delta G_{RED}(C_R = 0) = 2RT \left[V_S C_S \ln \frac{V_S + V_R}{V_R} \right] \quad (5)$$

In an ideal RED process, all the Gibbs free energy is liberated as electrical energy. *Table 5.1* shows this amount of energy produced for different mixing ratios of sea water (30 kg NaCl/m^3) and river water (0 kg NaCl/m^3) at 298 K. With 1 m^3 sea water and 1 m^3 of river water 1.76 MJ can theoretically be generated. With a large surplus of sea water this value is 2.55 MJ. *Table 5.1* also shows that in cases where the amount of salt water is the limiting factor, using an excess of river water is very useful (compare the 6.1 MJ of the V_R:V_S=10:1 combination with the 2.42 MJ for V_R:V_S=1:10). Such cases may be industrial processes with a brine effluent together with river or sea water.

In case of river water used with sea water, *Table 5.1* suggests the use of a surplus of sea water. However, the costs of pretreatment, transport and pumping through the stack should also be taken in account from an economical viewpoint. Assuming these costs are equal per m^3 for each type of water, the optimal ratio V_S/V_R can be obtained by substituting V_R=1 in *Eq. (3)* and subsequently differentiating the equation with respect to V_S. Solving $d(\Delta G_{RED})/d(V_S)=0$ gives $V_R/V_S=e-1\approx1.72$. This ratio results in a slightly higher energy compared to the 1:1 mixture with the same total volume of 2 m^3 as shown in *Table 5.1* (in italics).

Table 5.1. Gibbs free energy from mixing V_R (m^3) river water (S_R = 0 kg NaCl/m^3) with V_S (m^3) sea water (S_S = 30 kg/m^3) at 298 K.

V_R	V_S	V_R/V_S	ΔG_{RED}
[m^3]	[m^3]	[–]	[MJ]
∞	1	∞	∞
10	1	10	6.1
2	1	2	2.8
1	1	1	1.76
1.26	*0.74*	*1.72*	*1.87*
1	2	0.5	2.06
1	10	0.1	2.43
1	∞	0	2.55

By substituting the flows rates Φ for volumes V, *Eq. (3)* can used for calculating the free Gibbs energy per second before and after mixing in the RED stack:

$$X = 2RT\left[\Phi_R C_R \ln\frac{C_R}{C_M} + \Phi_S C_S \ln\frac{C_S}{C_M}\right] \quad (6)$$

The equilibrium concentration C_M can be obtained with *Eq. (4)* by using flow rates instead of volumes.

The available free energy is also called 'exergy'. The consumed free energy per second for the RED installation is obtained by taking the difference of output and input free energy per second:

$$X_{cons} = X_{in} - X_{out} \tag{7}$$

5.3. Experimental

The RED cell which was used in our experiments is shown in *Figure 5.1*. The specific components are described in the following sections.

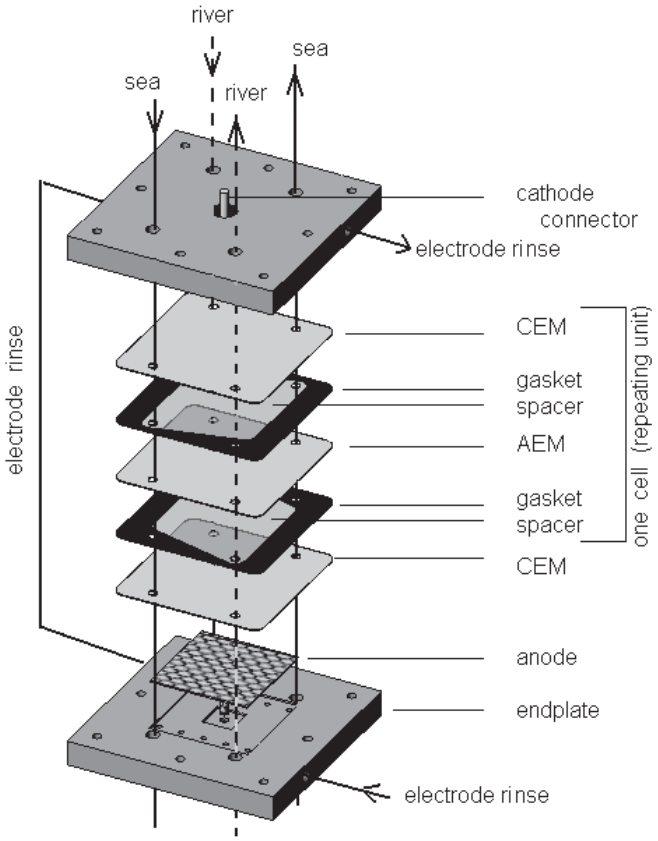

Figure 5.1. A reverse electrodialysis stack with one cell.

5.3.1. Endplates

Electrode compartments are situated inside the endplates. Endplates were milled from reinforced phenol formaldehyde (Epratex HGW 2082, Eriks, The Netherlands). Stainless steel bolts were used to close the stack. The distance between the end plates was about 33 mm in the case of 50 cells with 200 μm spacers and 200 μm gaskets.

5.3.2. Cells

The functional area of one membrane was 100 cm^2. On the outsides of the stacks cation exchange membranes were used as shielding membranes to prevent the transportation of negatively charged iron complexes. Fumasep anion and cation exchange membranes FAD and FKD with a thickness of 0.082 mm (obtained from Fumatech, Germany) were used. The stacks were equipped with polyamide woven spacers with a thickness of 200 µm. The membranes, gaskets and spacers were made at their correct size by means of a punch and a press.

5.3.3. Electrode system

The electrode compartments contained a solution of NaCl (1 mol/L) with $K_4Fe(CN)_6$ (0.05 mol/L) and $K_3Fe(CN)_6$ (0.05 mol/L). This electrolyte was pumped through the anode and cathode compartment at a rate of 60 mL/min. All chemicals used were technical grade and purchased from Boom, Meppel, The Netherlands. Titanium mesh end electrodes, coated with Ru–Ir mixed metal oxides with dimensions of 10cm X 10cm were used (Magneto Special Anodes b.v., Schiedam, the Netherlands. These electrodes are suitable as anode as well as cathode and therefore current reversal is possible.

5.3.4. Sea and river water

Demineralized water with technical grade sodium chloride (Boom, Meppel) was used. 'Sea water' consisted of 30 g NaCl/L and 'river water' of 1 g NaCl/L. A conduction meter with a Tetracon 325 cell (WTW, Weilheim, Germany) was used. To convert conductivities to salt content, a second-order calibration line was made in the 0–30 kg NaCl/m^3 range at 298 K. Peristaltic pumps (Masterflex L/S, Cole Parmer Instrument Company) were used for the delivery sea and river water and for recirculation of the electrode rinse. The stack with 50 cells was fed with 700 mL/min. Smaller stacks were fed with proportional lower flow rates, thereby maintaining the same flow velocity along the membrane surface. The temperature was controlled at 298±1 K for all experiments.

5.3.5. Reference electrodes

Platinum electrodes (diameter 1 mm) were inserted near the centre of the working and counter electrode through the meshes of the electrode grid and adjusted until the end was in plane with the inner surface of the end electrode. The Pt-wire was covered with epoxy and the end was scoured and polished afterwards. The measuring system based on Pt-electrodes was compared with a system of Ag/AgCl reference electrodes and showed the same results.

5.3.6. Electrical measurements

The measurements were carried out with an Ivium potentiostat (Ivium Technologies, Eindhoven, The Netherlands) in the galvanostatic mode. The galvanostatic scan rate was always set to 2 mA/s. Initially, the voltage (E) as function of the electrical current (I) was measured, resulting in an EI-plot. The reference current direction is chosen so that a positive current causes normal electrodialysis; RED is associated with a negative current. In most graphs in this chapter, the electrical current is transformed to the current density (J) and galvanostatic scans appear as EJ-curves.

5.4. Results and discussion

5.4.1. Variable cell number experiments

In order to determine the maximum power output of a RED stack, the stack voltage as function of the current density was measured. The applied current was controlled via a potentiostat. The optimal load (the external electrical resistance) for a maximal power density was determined with these values. The power output is maximal when the load equals the internal resistance (*Eq. (1)*. EJ-curves plotted of a full stack with 50 cells, with 40 cells and so on (N=50, 40, 30, 20, 10 and 0) are shown in *Figure 5.2*. A stack with 0 cells contained only 1 CEM between the electrode compartments. The voltage at the end electrodes (the working and the counter electrode) is represented by the dashed lines, the voltage on the reference electrodes by solid lines. At zero current density, both voltages are equal; at lower current densities the voltage on the end electrodes is slightly lower due to overpotentials at the electrode and a voltage drop inside the electrode compartment.

Figure 5.3 shows the power as function of the current density derived from *Figure 5.2* for different stacks (the solid lines). This power is determined from the potential measured at the reference electrodes multiplied by the current density throughout the stack. The potential measurement on the reference electrodes does not contain energy loss due to redox processes at the electrode. Therefore, this value gives the actual power obtained from the mixing of sea and river water via the RED stack. The 50 cell stack contains a total membrane area of 1 m^2 and therefore also represents the power density; the maximal (0.93 W/m^2) is reached at a current density of –28 A/m^2. At this point the theoretical energy efficiency is not more than 50%. Between 0 and –28 A/m^2, the energy efficiency is higher but the power density is lower. The obtained power density (0.93 W/m^2) is substantially higher than the power densities for the river water / sea water RED system published so far (*Table 5.2*). Furthermore, it can be observed from *Figure 5.3* that the power increases almost linearly with the number of cells (N=10: P=0.20 W; N=20: P=0.40 W; . . . ; N=50: P=0.93 W). This indicates that the loss due to leaking currents is minimal (*Chapter 3*). The

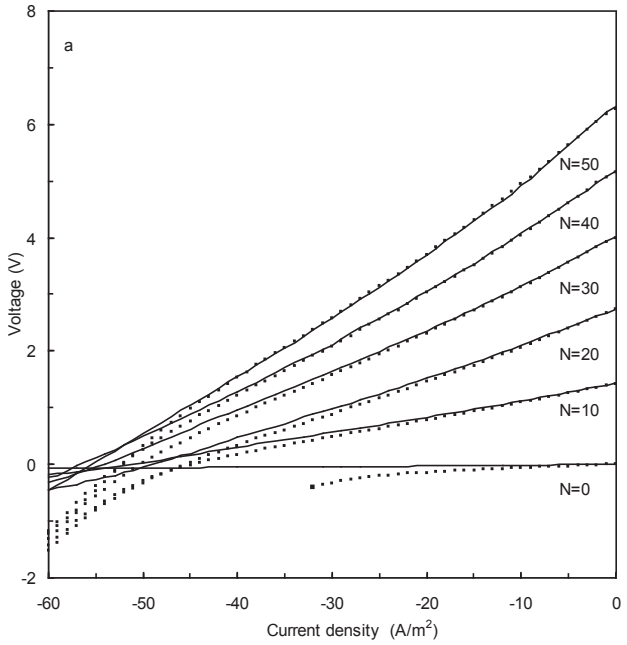

Figure 5.2. EJ–curve curves for a stack with 0, 10 .. 50 cells. Each curve is measured on the reference electrodes (solid lines) and on the end electrodes (dashed lines).

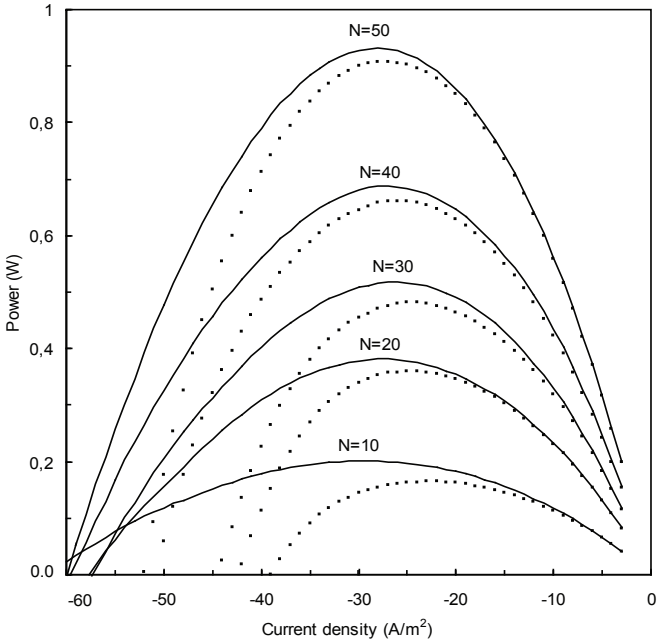

Figure 5.3. Measured power of stacks with 10, 20..50 cells. The solid line is the power generated by the stack and the dashed line is the output on the work electrodes.

Table 5.2. Reported power density P_d (W/m^2) and spacer thickness δ_M (mm) with solutions of 1 and 30 g NaCl/L by different authors.

Author	Year	Power density [W/m^2]	Membrane thickness (mm)
Pattle[4]	1955	0.05	0.7
Weinstein and Leitz[14]	1976	0.17	1
Audinos[15]	1983	0.40[a]	3
Jagur–Grodzinski and Kramer[17]	1986	0.41	0.55
Turek[18]	2007	0.46	0.19
Suda[19]	2007	0.26	1
Veerman et al. (this paper)	2008	0.95	0.2

[a] with seawater of 295 g/L

differences between the solid and the dashed lines represent the loss due to electrode reactions and an Ohmic drop in the electrode compartments. This loss is relatively low for large stacks as is shown by the experiment with the 50 cells.

5.4.2. Factors affecting the cell resistance

Central in the considerations about power density is the cell resistance, the denominator in *Eq. (2)*. The cell resistance should be minimal in order to obtain a maximal power output. The resistance of a RED stack can theoretically be determined by the addition of the resistances of the individual components: the resistances of an AEM, a CEM, a river water compartment and a sea water compartment. Membrane resistances are tabulated normally for 0.5 M NaCl conditions which is comparable to the sea water concentration. It is proven that the membrane resistance depends on concentration[25,26]. Measurements by Długołęcki et al.[27] show this concentration effect for the membranes used in the experiments described in this chapter (*Table 5.3*). The values determined by Długołęcki are obtained for equal concentrations on both sides of the membrane. However, in the case of RED, there exists a concentration profile over the membrane. An estimation of the membrane resistance during RED operation is made by fitting the membrane resistance

Table 5.3. Experimental area resistances of FAD and FKD ion-exchange membranes. The resistances between sea and river water (in italics) are calculated.

salt content [kg/m^3]		area resistance [Ωcm^2]	
A	B	FAD	FKD
30	30	0.88	3.75
1	1	11.5	44.7
1	30	*1.63*	*5.9*

as a function of concentration and integrating this over the whole membrane thickness (*Chapter 5 - Appendix A*). It follows that the estimated membrane resistance under RED conditions (between NaCl solutions of 30 g/L and 1 g/L) is about twice the resistance under normal membrane test conditions (between identical NaCl solutions of 30 g/L).

If the sea and river water compartments did not contain any spacer, 'spacer-less resistances' of these compartments could be established from the dimensions of the compartment and the specific resistance of the concerning salt solution. However, spacers inhibit the ion flow. The woven spacers used in the experiments described in this chapter occupy 33% of the volume and 49% of the area in a plane projection, resulting in obstruction factors f for the ionic current of 1/(1−0.33)=1.49 or 1/(0.49)=1.96. The first value is an underestimation because the ionic current follows a tortuous path between the threads of the spacer. The second value is an overestimation because the current can follow curved paths. Therefore, for the calculation of cell resistance all 'spacer-less resistances' were multiplied with obstruction factor f (the average of both values: f=1.72). The calculated and measured resistances of a single cell (10cm·10cm; spacers of 200 μm) are shown in *Table 5.4*. The table shows the resistance for the case where both compartments are fed with sea water (SS), both with river water (RR) and with sea and river water (SR). From *Table 5.4*, it follows that under normal RED operation (column SR), the river water compartment has the largest contribution to the total

These theoretical values were compared with the experimental data which were determined for 3 different cases when the different compartments are filled with: (i) both with sea water , (ii) both with river water and (iii) one with sea water and the other with river water (the normal RED operation) (*Figure 5.4*). The current density is varied from -60 to 0 A/m^2 in order to determine the cell resistance from the slope of the EJ-curves.

Table 5.4. Calculated and measured resistance and power density of a cell (A=0.01 m^2) with Fumasep membranes (FAD and FKD). The cell is fed with sea and river water (SR, left column), with sea and sea water (SS, middle column) and with river water with river water (RR, right column).

	feed	SR	SS	RR
calculated	FAD (Ω)	0.016	0.009	0.115
	FKD (Ω)	0.059	0.038	0.447
	sea water comp.(Ω)	0.007	0.007	0.155
	river water comp.(Ω)	0.156	0.007	0.155
	cell resistance (Ω)	0.238	0.061	0.872
	power density (W/m^2)	1.18	-	-
experimental	cell resistance (Ω)	0.345	0.067	0.734
	power density (W/m^2)	0.93		

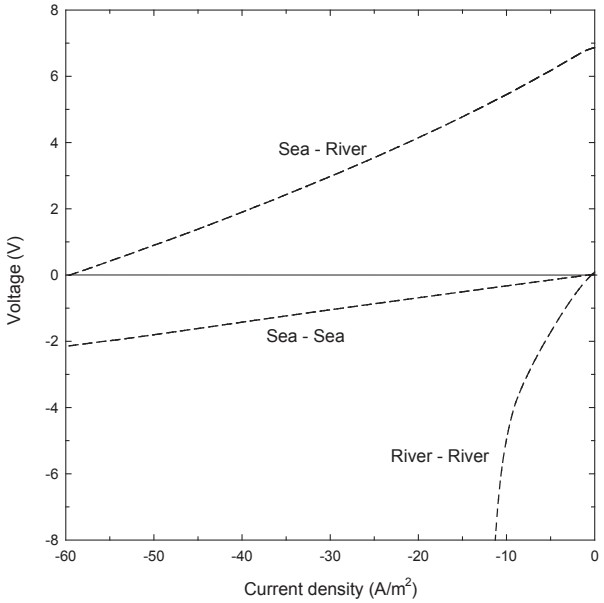

Figure 5.4. EJ–curves at the Pt-reference electrodes for a stack with 50 cells: a) normal b) sea–sea c) river–river.

As shown in *Figure 5.4*, there is no potential difference for sea/sea and river/river at zero current density. In fact, the operation mode here is not RED but normal ED resulting in a salt depletion in one compartment and an enrichment in the other. In the river/river case, this disproportion of the salt concentration causes an extremely high resistance and sharply curved lines at higher (negative) current. In the normal RED operation (sea/river) the opposite effect occurs: at a high negative current there is a NaCl transport from the sea water to the river water compartments resulting in a lower resistance at increased negative current.

From these EJ-curves the cell resistance can be obtained at different current densities. The experiment is done with a cell of 50, 30, 20, . . .1 cell. The results are presented in *Figure 5.5*. The resistances were calculated near J=0 by calculating $\Delta E/\Delta I$ over the range −50 mA to 0 mA of the scan. The single cell resistance is the slope of the different lines and is 0.73 Ω for the river/river system, 0.35 Ω for the sea/river system (normal RED) and 0.067 Ω for the sea/sea system and tabulated in *Table 5.4*.

In *Table 5.4* the calculated power density (1.18 W/m^2) has been added according *Eq. (2)*; for the cell voltage E_{cell} is taken the value of 0.150 V, based on a permselectivity of both membranes of 0.95 and on an ideal cell voltage of 0.158 V (*Chapter 3*). Measured power density (0.93 W/m^2) is 21% less than the calculated value, which is close to the theoretical values if the obstruction of the spacer is taken into account. If no spacer would be used

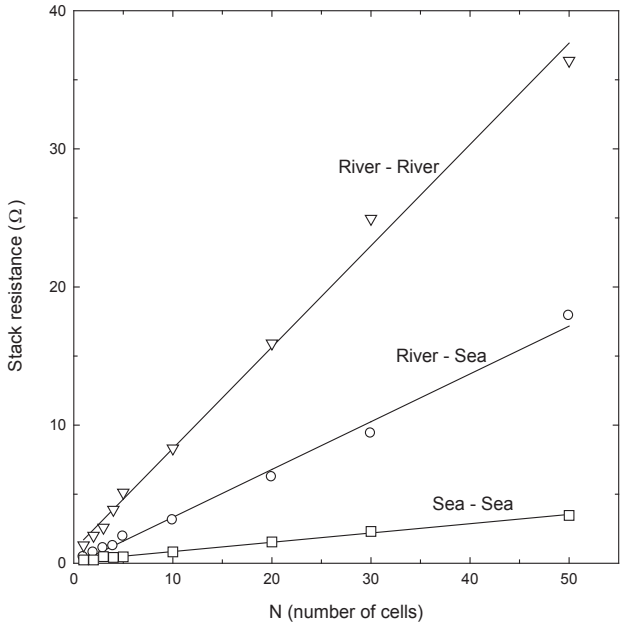

Figure 5.5. Stack resistance of stacks with different numbers of cells.

and the compartment thickness would be unaffected, a theoretical value of 1.65 W/m^2 is possible. This shows that further improvement of the power density of RED is obtainable with a more open spacer material or no spacer at all. Długołęcki et al.[27] presented a power density model dependent on spacer thickness and area resistance and permselectivity of the membranes. With the best available commercial membranes and spacers of 150 μm, they estimated a power density of about 5 W/m^2.

5.4.3. Effect of the flow rate on the power density

The net power output (P_u) is determined by subtracting the hydrodynamic loss from the produced power output. *Figure 5.6* shows the results in the range 200–1000 mL/min together with their difference, the net power. High flow rates of sea and river water maintain high concentration differences across the membranes and reduce concentration polarization. On the other hand, high flow rates cause higher pressure losses and lower the net power output. There exists an optimal flow regime for a given cell configuration, where the net power output is maximal. In *Figure 5.6* the electrical power P_u is fitted to the flow rate (Φ) by the following function (*d* and *e* are fit variables).

$$P_u = d - \frac{e}{\Phi} \tag{8}$$

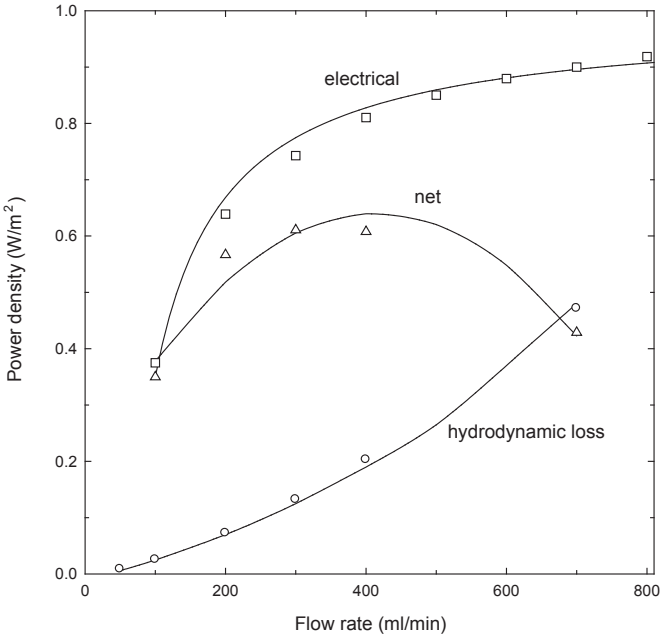

Figure 5.6. Generated electrical power, hydrodynamic loss and the supplied net power in a 50 cell stack.

The hydrodynamic power losses are fitted by a parabolic function:

$$P_{pump} = a\Phi^2 + b\Phi + c \tag{9}$$

where *a*, *b* and *c* are specific constants for the system. The maximal net electrical power is reached near 400 mL/min (0.7 cm/s). At this optimum the consumed power for pumping is 25% of the total generated electrical energy. The hydrodynamic loss is relatively high in these experiments where the pressure was measured outside the stack. Experiments with pressure measurements in the spacer compartments show a much lower pressure drop[28]. The residual pressure losses are caused by the internal manifolds. Experiments with pressure measurements within cells showed pressure losses in the manifolds of 80% of the total pressure drop over the whole cell. The design of the manifolds is very critical and these locations are subject to obstruction by pollution and mechanical deformation of the stack. Besides improving the manifolds, the pressure drop can be decreased by using more open spacer material. Another approach is the use of relatively thick sea water spacers: if they are five times thicker than the river water spacers, then the fluid resistance and the electric resistance are negligible compared to the river water compartment. However, the resulting decrease in lateral electrical resistance that causes an increased ionic shortcut current is a point of attention (*Chapter 3*).

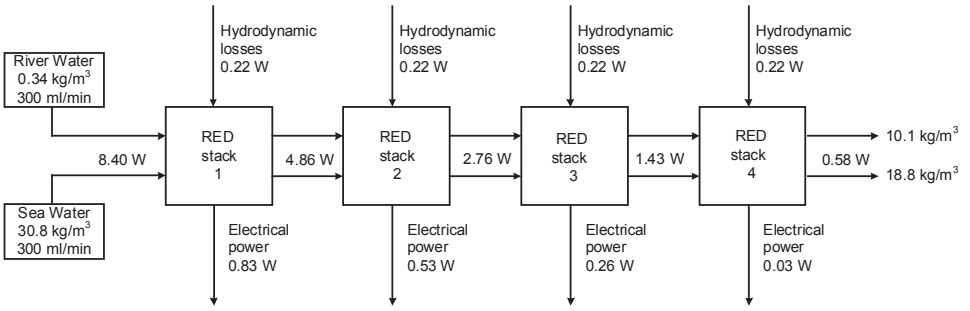

Figure 5.7. In- and outgoing potential salinity power, the delivered electric power and the hydrodynamic losses in a four stage experiment with a 50 cell stack with a total membrane area of 1 m^2.

5.4.4. Cascade operation

Multistage RED experiments were performed as shown in *Figure 5.7*. Instead of using 4 separate RED stacks in series as *Figure 5.1* suggests, experiments were done with only one RED stack, each time operating with inlet concentrations equal to effluent concentrations of the preceding experiment. This way a four 4 stage operation was simulated. The first stack was fed with solutions of 0.34 g/L (river water) and 30.8 g/L (sea water), both with a flow rate of 300 mL/min. All stacks were operated with the same electrical current of −300 mA to simulate a real serial operation of the four stages. Determined at this current were: (i) the salt concentrations of the in and outgoing streams (from the conductivity) (ii) the water flow rates (iii) the pressure drop between outlet and inlet of the stack (iv) the ingoing water temperatures (v) the potential salinity power from mixing as calculated from *Eqs. (6)* and *(7)* (vi) the delivered electrical power (from the voltage at the reference electrodes) and (vii) the hydraulic loss (from the flow and pressure drop).

In each stage, the electricity was generated near maximal power conditions (the external electrical resistance is equal to the internal resistance) with the consequence that 50% of the potential salinity power is lost in any case. Another part of the salinity power is lost by NaCl transportation and osmosis through the membranes, by ionic shortcut currents (*Chapter 3*) and by irreversible mixing due to internal leakage in the stack.
The generated electrical power density (gross power) and the net electrical power (gross power minus pressure losses) from each stage in *Figure 5.7* are plotted in *Figure 5.8*.
The gross energy efficiency is defined as follows:

$$Y_{gross} = \frac{P_u}{X_{\max}} \tag{10}$$

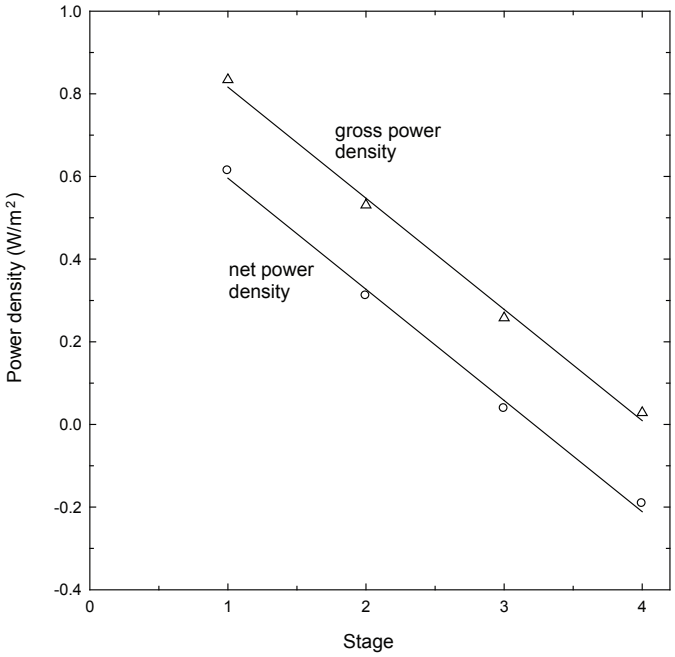

Figure 5.8. Power density and the hydraulic loss for each stage at a four stage experiment in a 50 cell stack with a total membrane area of 1 m^2.

with P_u the generated (and usable) electric power. The flow ratio (the sea water flow divided by the river water flow) and a possible addition of NaCl to the river water are not prescribed.

In the net energy efficiency Y_{net}, a correction for the hydrodynamic loss is made as well:

$$Y_{net} = \frac{P_u - P_{pump}}{X_{\max}} \tag{11}$$

Figure 5.8 indicates that only two stages are useful. However, in the case of a large reduction of the hydraulic losses, the third stage can also contribute to the net energy yield. In this scheme the electrical power consumed by the electrode system is not included. This dissipated power is about 10% of the generated electrical power for a stack with 50 cells and is marginal in large stacks.
Figure 5.9 shows the effect of multiple stages on the cumulative gross power density and the cumulative gross energy efficiency: it follows that both important RED parameters are counteracting. However, these values depend on the mode of operation (current density) and the stack design (pressure drop).

The most important response variables of a RED stack are the power density P_d and the

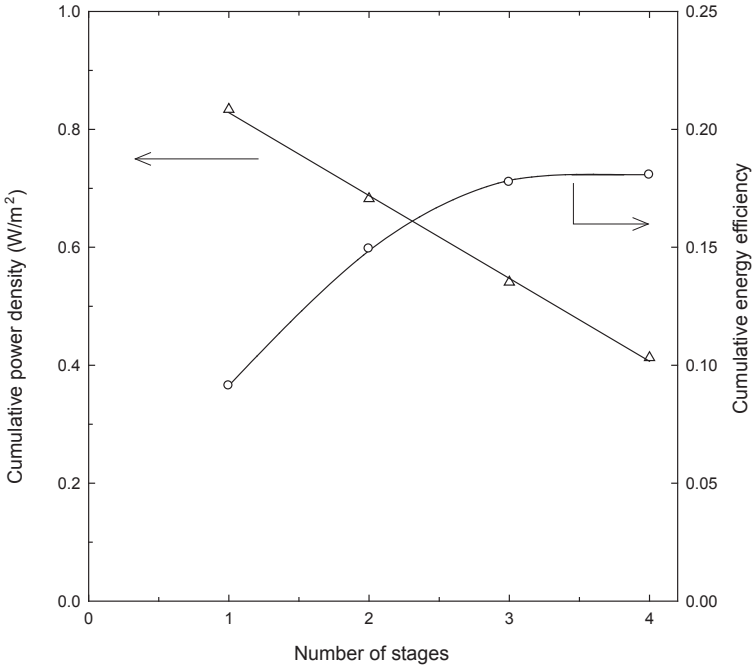

Figure 5.9. Cumulative power density and cumulative gross energy efficiency in of a system with 1, 2, 3 and 4 stages.

net energy efficiency Y_{net}. A commercial RED installation should operate at high power generation and low water consumption. These requirements are conflicting in many ways. A high power density is preferred when the equipment costs are the main costs and there is an excess of river water. However, when the pretreatment costs of water are substantial or the amount of river water is limited, it may be interesting to operate at a lower power density, thereby increasing the energy efficiency. There are many factors that influence both goals, such as flow rates, spacer thickness, stack design, river water concentration, current density, and so on. Maximizing the power of a special installation gives well-defined values of different parameters; minimizing the fuel (water) consumption requires low flow rates and a high external load while the power output is relatively low.

5.4.5. Comparison of RED and ED

The most important difference between RED and ED (as used for desalination) is the product: electrical power or drinking water. The market price of these products dictate in general the design differences between the techniques and to a less order the requirements of the product and operational differences.

Table 5.1 shows the generated amount of energy for different mixing ratios: for the most realistic 1:1 ratio there can be generated a theoretical maximum of 1.7 MW. Compared

to fossil fuels this is a very low energy density. To operate on an economical base, high power densities and high energy efficiencies should be achieved. This requires a very sophisticated design with tuned operational variables. These are low electrical resistance (thin compartments, thin membranes), low fluid friction (well designed spacers and manifolds), high energy efficiency (high permselective membranes), a high degree of exhaustion of the feed water (multi stage operation), an efficient electrode system. At this moment there are no membranes and spacers designed specifically for RED.
In contrast the suitability of the ED technique is dictated by the water price and by product requirements. Energy consumption is a second interest. For making drinking water, all materials should satisfy to food quality regulations. This concerns pumps, piping, spacers and especially the membranes. This is only possible with a rather robust and over dimensioned structure.

5.5. Conclusions

In this chapter we show that the actual power density of a RED stack operated on artificial sea and river water is 0.93 W/m^2, which is the highest reported value for a real stack operation. This value is obtained with low resistance membranes, good sealing of the compartments, with small compartment thickness (200 μm) and an accurate method to determine the stack performance. 25% of this produced power is lost by pressure drop by using commercially available spacers. We show that this pressure drop is mainly caused by the resistance of the manifolds. The net produced power also depends on the flow rate. At high flow rates, it increases due to reduced concentration polarization, and decreases due to higher pressure losses. The optimal value is found at 400 mL/min (0.7 cm/s). The total cell resistance is one and a half times higher than expected from the sum of the contribution of the individual components. This may be caused by the shielding effect of the spacer. A more open spacer is beneficial for RED in 2 ways: less shielding and lower pressure drop. The membrane resistance is of minor importance in the tested stacks, because the 200 μm river water compartment has a dominant influence on the total cell resistance. The energy efficiency of 4 cells which are operated in series is also shown. A gross energy efficiency of 18% is achieved in a 4 stage operation at maximal produced power. This value was achieved under conditions of maximal power density were the maximal energy efficiency is 50%. The results are encouraging for further efforts on the improvement of the system.

5.6. Recommendations

Power density and energy efficiency are counteracting. Nowadays there is plenty of unused fuel (river water) and a RED installation is at present rather expensive. The first goal

is to increase the power density, but proving the possibility of a high energy efficiency is likewise necessary in order to make reverse electrodialysis a substantial energy source in the future.

The described results are encouraging and are the basis of further investigations. The central theme will be describing the power density and the energy efficiency in terms of membrane and spacer properties, stack and cell dimensions, fluid velocities and so on. Furthermore, the search for improved membranes, spacers, gaskets and electrode systems is ongoing. Also the use of real sea and river water in RED and its effect on the performance, fouling, spacers and membranes needs to be investigated. Fouling should be prevented by a balanced basic pre-treatment and improved, very open spacers. The goal is an economical performing RED installation operating on river water and sea water.

Acknowledgement

This research was performed at Wetsus, centre of excellence for sustainable water technology. Wetsus is funded by the city of Leeuwarden, the province of Fryslân, the European Union European Regional Development Fund and by the EZ/Kompas program of the Samenwerkingsverband Noord-Nederland. The first author would like to thank the Noordelijke Hogeschool Leeuwarden who facilitated this research by detaching him to Wetsus and the participants of the energy theme for their interest and financial contribution.

Nomenclature

A	cell area (m^2)
a, b, c	fit variables for P_{pump}
C	concentration (mol/m^3)
d, e	fit variables for P_u
E	voltage (V)
E_{cell}	electromotive force of one cell (V)
f	obstruction factor
F	Faraday constant (96 485 C/mol)
G_{RED}	free energy of the RED process (J)
I	electrical current (A)
J	electrical current density (A/m^2)
M	mol mass NaCl (0.0584 kg/mol)
N	number of cells in a stack
P_d	power density (W/m^2)
$P_{d\text{-}net}$	net power density (W/m^2)
P_{max}	maximum external power (W)
P_u	external power (W)
P_{pump}	hydrodynamic loss (W)
R_{AEM}	cation exchange membrane resistance (Ω)
R_{CEM}	cation exchange membrane resistance (Ω)
R_{area}	area resistance of a membrane (Ωm^2)
R_{eff}	effective area resistance of a membrane (Ωm^2)
R_i	internal resistance (Ω)
R_u	external resistance (Ω)
R_{river}	river water compartment resistance (Ω)
R_{sea}	sea water compartment resistance (Ω)
R^2	determination coefficient
R	gas constant ($8.31432\ J{\cdot}mol^{-1}K^{-1}$)
t_w	electro-osmotic water transport number (mol/F)
S	salt content (kg/m^3)
T	temperature (K)
OCV	open circuit voltage (V)
p, q, r	fit variables for R_{eff}
V	volume (m^3)
X_{in}	free energy per second of the inlet (W)
X_{out}	free energy per second of the effluent (W)
X_{cons}	consumed free energy per second (W)
X_{max}	maximal available free energy per second (W)
Y	energy efficiency
Y_{gross}	gross energy efficiency

Greek symbols

α	permselectivity of the ion exchange membrane
δ_C	compartment thickness (m)
δ_M	membrane thickness (m)
η_P	power efficiency
Φ	flow (m^3/s)

Superscripts

i	in
o	out

Subscripts

S	sea
R	river
M	equilibrium

Abbreviations

AEM	anion exchange membrane
CEM	cation exchange membrane
ED	electrodialysis
EMF	electromotive force (V)
RED	reverse electrodialysis

Definitions

compartment	space between the membranes
cell	combination of two membranes and two compartments
electrode system	the anode, cathode and electrode rinse
stack	a number of N cells with an electrode system

References Chapter 5

1 R.E. Pattle, *Production of electric power by mixing fresh and salt water in the hydroelectric pile.* Nature 174 (1954) 660

2 G.L. Wick, W.R. Schmitt, *Prospects for renewable energy from sea.* Mar. Technol. Soc. J. 11 (1977) 16-21

3 Energy information administration; official energy statistics from the U.S. government. www.eia.doe.gov

4 R.E. Pattle, *Electricity from fresh and salt water - without fuel.* Chem. Proc. Eng. 35 (1955) 351–354

5 R.E. Pattle, *Improvements to electric batteries.* Patent GB731729 (1955)

6 S. Loeb, *Osmotic power plants.* Science 189 (1975) 654–655

7 S. Loeb, *Production of energy from concentrated brines by pressure retarded osmosis.1. Preliminary technical and economic correlations.* J. Membr. Sci. 1 (1976) 49–63

8 M. Olsson, G.L. Wick, J.D. Isaacs, *Salinity gradient power - utilizing vapor-pressure differences.* Science 206 (1979) 452–454

9 M.V. Sussman, A. Katchalsky, *Mechanochemical turbine: a new power cycle.* Science 167 (1970) 45–47

10 W. Finley, E. Pscheidt, *Hydrocratic generator.* US Patent 6.313.545 B1 (2001)

11 G. Lagger, H. Jensen, J. Josserand, H.H. Girault. *Hydro-voltaic cells. Part 1. Concentration cells.* J. Electroanal. Chem. 5445 (2003) 1–6

12 V. Kniajev, *Energy of salinity gradient - new source of energy with minimal environmental impact.* Abstracts from the International Workshop "Result of Fundamental Research for Investments" (IWRFRI'2001'), St. Petersburg. Russia (2001)

13 J.W. Post, J. Veerman, H.V.M. Hamelers, G.J.W. Euverink, S.J. Metz, K. Nymeijer, C.J.N. Buisman. *Salinity-gradient power: Evaluation of pressure-retarded osmosis and reverse electrodialysis.* J. Membr. Sci. 288 (2007) 218–230

14 J.N. Weinstein, F.B. Leitz, *Electric power from differences in salinity: the dialytic battery.* Science 191 (1976) 557–559

15 R. Audinos, *Electrodialyse inverse. Etude de l'energie electrique obtenue a partir de deux solutions de salinites differentes.* J. Power Sources 10 (1983) 203–217

16 R. Audinos, *Electric power produced from two solutions of unequal salinity by reverse electrodialysis.* Ind. J. Chem. 31A. (1992) 348–354

17 J. Jagur-Grodzinski, R. Kramer, *Novel process for direct conversion of free energy of mixing into electric power.* Ind. Eng. Chem. Process Des. Dev. 25 (1986) 443–449

18 M. Turek, B. Bandura, *Renewable energy by reverse electrodialysis.* Desalination 205 (2007) 67–74

19 F. Suda, T. Matsuo, D. Ushioda, *Transient changes in the power output from the concentration difference cell (dialytic battery) between seawater and river water.* Energy 32 (2007) 165–173

20 J. Veerman, J. W. Post, S.J. Metz, M. Saakes, G.J. Harmsen. *Reducing power losses caused by ionic shortcut currents in reverse electrodialysis stacks by a validated model.* J. Membr. Sci. 310 (2008) 418-430

21 B.H. Clampitt, F.E. Kiviat, *Energy recovery from saline water by means of electrochemical cells.* Science 194 (1976) 719–720

22 R.E. Lacey, *Energy by reverse electrodialysis.* Ocean Eng. 7 (1980) 1–47

23 C. Forgacs, *Generation of electricity by reverse electrodialysis.* BGUN-RDA – 178-78 Ben-Gurion University, Israel (1978)

24 C. Forgacs, R.N. O'Brien, *Utilization of membrane processes in the development of non-conventional renewable energy sources.* Chem. Can. 31 (1979) 19-21

25 V.I. Zabolotsky, V.V. Nikonenko, Effect *of structural membrane inhomogeneity on transport properties.* J. Membr. Sci. 79 (1993) 181–189

26 L. X. Tuan, C. Buess-Herman, *Study of water content and microheterogeneity of CMS cation exchange membrane.* Chem. Phys. Letters 434 (2007) 49-55

27 P. Długołęcki , K. Nymeijer, S. Metz, M. Wessling, *Current status of ion exchange membranes for power geration from salinity gradients*. J. Membr. Sci. 319 (2008) 214–222

28 M.H. Dirkse, W.K.P. van Loon, J.W. Post, J. Veerman, J.D. Stigter, G.P.A. Bot, *Extending Potential Flow Modelling of Flat-Sheet Geometries as Applied in Membrane-Based Systems.* J. Membr. Sci. 325 (2008) 537-545

Appendix A. Resistance of a membrane between two solutions with different concentration.

Długołęcki[27] et al. have measured the area resistance of FKD and FAD membranes at different NaCl concentrations. We fitted exponential functions to these data points:

$$R_{area}(C) = p + q \cdot e^{-rC} \tag{1}$$

where R_{area} is the area resistance of the membrane, C the concentration and p, q and r fit parameters.

Fitting resulted in $R_{area}=4.37+99.4e^{-53.1C}$ for the FKD and $R_{area}=0.91+17.6e^{-29.8C}$ for the FAD membrane. The effective area resistance R_{eff} can be determined by integrating the exponential function between the concentration boundaries C_1 and C_2.

$$R_{eff} = \frac{1}{C_2 - C_1}\int_{C_1}^{C_2}(p + q \cdot e^{-r \cdot C})dC = \frac{1}{C_2 - C_1}\left[pC - \frac{q}{r}e^{-C}\right]_{C_1}^{C_2} = 1 - \frac{q}{r}\frac{e^{-pC_1} - e^{-pC_2}}{C_2 - C_1} \tag{2}$$

The resulting effective area resistances are 5.90 Ωcm^2 for the FKD and 1.63 Ωcm^2 for the FAD if used NaCl concentrations of C_2=0.51 mol/L (=30 g/L) and C_1=0.017 mol/L (=1 g/L). For the used membranes it follows that the resulting resistance is about twice the resistances between solutions of 0.5 mol NaCl/L.

Chapter 6

Reverse electrodialysis: Comparison of six commercial membrane pairs on the thermodynamic efficiency and power density*

Abstract

Reverse electrodialysis (RED) generates electricity through the entropy increase from the mixing of sea and river water. Two important RED process parameters were investigated: power density (in Watts per square meter membrane) and the thermodynamic efficiency. Beside this, we quantified losses in a RED stack experimentally: co-ion transport, osmosis and internal loss as a function of current density and related those to the energy loss due to mixing. Six different commercial available membrane pairs - *Qianqiu Heterogeneous Ion Exchange Membrane* (AEM and CEM), *Qianqiu Homogeneous Ion Exchange Membrane* (AEM and CEM), *Fumasep* (FKD and FAD), *Selemion* (AMV and CMV), *Neosepta* (ACS and CMS) and *Neosepta* (AMX and CMX) - were compared. It was found that at maximal power density, the thermodynamic efficiency was between 14% and 35%, where 50% is the maximum theoretical value at at maximal power density. The highest score (35%) is achieved with the Neosepta (ACS-CMS) pair. The power density of the different membrane pairs varied from 0.5 to 1.2 W/m^2. The maximal value was found for Fumasep (FAD and FDK) and Selemion (AMV and CMV) pair. For ranking purpose, we have combined the two response parameters to a single one by multiplying the power density and the thermodynamic efficiency. This response parameter is the highest (34 $W/m^2 \cdot \%$) for the Selemion (AMV and CMV) pair.

**** Published as***
J. Veerman, R.M. de Jong, M. Saakes, S.J. Metz, G.J. Harmsen
Reverse electrodialysis: Comparison of six commercial membrane pairs on the thermodynamic efficiency and power density
Journal of Membrane Science 343 (2009) 7–15

6.1. Introduction

Salinity power, using river and sea water, is a clean and sustainable source of energy. One of the technologies for generating energy from this source is reverse electrodialysis (RED). The basic theory of RED is described by different authors in literature[1-18]. A RED stack consists of alternating CEMs (cation exchange membranes) and AEMs (anion exchange membranes). These membranes are separated by spacers that keep the membranes in a fixed position, ensure defined water compartments and act as turbulence promoters. Sea and river water are alternately supplied through the spacer compartments. Positive charged ions diffuse from the sea water to the river water through the CEMs in one direction and negative charged ions diffuse through AEMs in the other direction. These ionic currents are converted in an electron current at the electrodes of the stack by proper redox reactions. Power can be withdrawn by connecting an external load to these electrodes. Maximal power is delivered if the resistance of the external load equals the internal stack resistance.

Theoretically, the maximal amount of energy that can be harvested from 1 m^3 fresh water and a large surplus salt water (30 g NaCl/L) is 2.55 MJ (*Chapter 5*). However, transport of large amounts of seawater to and through the stack consumes a large amount of energy. Therefore, it is more realistic to mix 1m^3 fresh water with 1m^3 seawater, generating 1.76 MJ (*Chapter 5*). In the Netherlands, the Rhine has an average flow rate of 2200 m^3/s and has a power potential (P_{pot}) of 3.9 GW, about 30 % of the electricity consumption in the Netherlands. The amount of produced power by RED depends on the availability (Q) of the river water and on the energy efficiency of the process. The fraction of the theoretical maximal energy that can be obtained from given volumes salt and fresh water with given concentrations is the energy efficiency Y. Therefore, the total generated power is $P= Q \cdot Y \cdot P_{pot}$. It is clear that energy efficiency is a key parameter in the RED process.

In this chapter, we focus on the energy balance during the RED process at maximal power. In order to obtain a maximal power density, relative high flow rates are used and a low degree of mixing is achieved. At these circumstances, the energy efficiency Y – the produced energy in relation to the exergy of the feed - is low and rather useless. Therefore, we introduce the term 'thermodynamic efficiency' (η_T, which is defined as the produced energy in relation to the difference of exergy of the incoming and outgoing water. The second key parameter is the power density P_d, the generated amount of power per square meter of membrane. It is a measure of the power per invested euro because the membranes (and spacers) form a substantial part of the price of a RED power plant.

In fact power density and energy efficiency interact in a conflicting way. If only electrical aspects are taken into account, it can easily be seen that for maximal power density the external resistance (the load) is equal to the internal resistance of the stack. Therefore, the energy efficiency cannot exceed 50% (*Chapter 3*). The RED process is most energy efficient at low current densities when the external resistance is much higher than the stack resistance. High power densities demand a maximal concentration difference over the membrane. This can be achieved with high flow rates, which is limited by an increase in pump power (*Chapter 5*). Therefore, there exists an optimal flow rate for maximal energy efficiency.

Many authors have studied the power density of a RED stack[2,3,8,9,15,16]. In these studies no systematic approach on the effect of membrane properties on the total performance was made. Długołęcki et al.[18] presented a theoretical model of the power density in relation to spacer thickness, area resistance of the membranes and permselectivity of the membranes. They concluded that a high power density could be obtained with small membrane spacing and low membrane resistance. Our goal is to compare different commercial membrane pairs in a real RED stack and relate the measured power density and energy efficiency of mixing from a RED stack to the membrane properties (area resistance and permselectivity).

6.2. Experimental

6.2.1. Endplates

The RED stack that was used in our experiments is shown in *Figure 6.1*. This experimental setup is described in great detail in *Chapter 3* and *5*. Electrode compartments are situated inside the endplates. Endplates were milled from reinforced phenol formaldehyde (Epratex HGW 2082, Eriks, The Netherlands). Stainless steel bolts were used to close the stack.

6.2.2. Cells

The functional area of one membrane was 100 cm^2. On the outsides of the stacks CEMs were used. The studied ion exchange membranes were:

(a) Qianqiu Heterogeneous Ion Exchange Membrane AEM and CEM (Hangzhou QianQiu Industry Co, China)
(b) Qianqiu Homogeneous Ion Exchange Membrane AEM and CEM (Hangzhou QianQiu Industry Co, China)
(c) Fumasep FKD and FAD (Fumatech, Germany)
(d) Selemion AMV and CMV (Asahi Glass Company, Japan)
(e) Neosepta ACS and CMS (Tokuyama Corporation, Japan)
(f) Neosepta AMX and CMX (Tokuyama Corporation, Japan)

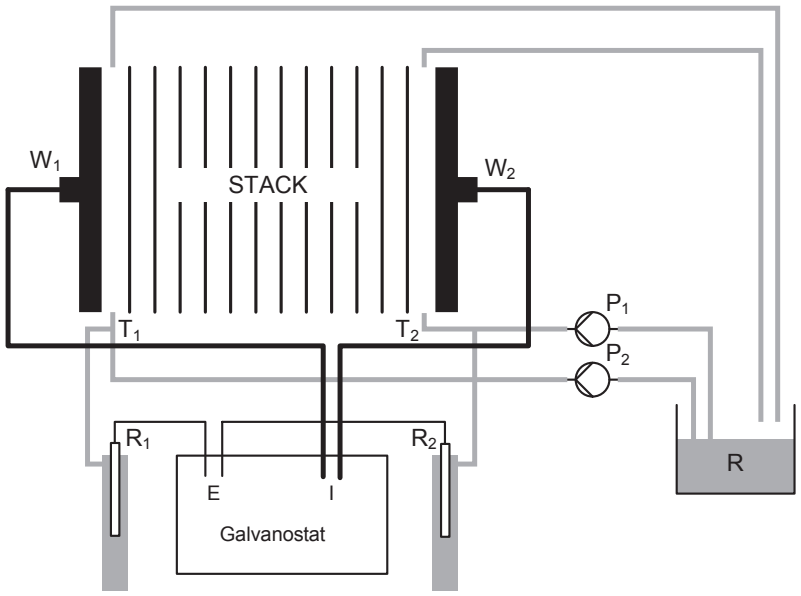

Figure 6.1. Configuration of the experimental set-up.The electrode rinse R is circulated with pumps P1 and P2 to the electrode compartments of the stack. The Ag/AgCl reference electrodes R1 and R2 are inserted in two vessels which are connected to the inlets with the T-connectors T1 and T2. The galvanostat is electrically connected to the reference electrodes R1 and R2 and to the working electrodes W1 and W2. The river and sea water flows through the stack are not shown.

The radius of the feed and drain channels through the membranes was 4 mm. The stacks were equipped with nylon woven spacers with a thickness of 200 µm (Nitex 03-300/51, Sefar, The Netherlands). Gaskets were made of silicon micro film with a thickness of 200 µm (SSF-MLTN-940, Specialty Silicone Fabricators, Paso Robles, USA). Stacks were made with 25 cells (Fumasep and Qianqiu homogeneous) or 5 cells (the other membrane pairs). The membranes, spacers and gaskets were made at their correct size by means of a punch and a press.

6.2.3. Electrode system and electrical measurements

The electrode compartments contained a NaCl solution of 15 g/L (technical grade; Frisia Salt, Harlingen, The Netherlands). For the anode and cathode compartment a separate electrode rinse circuit was used with a common supply vessel (*Figure 6.2*). The anolyte and catholyte flow rate was about 100 mL/min. Titanium mesh end electrodes, coated with Ru-Ir mixed metal oxides with dimensions of 10cm x 10cm were used (Magneto Special Anodes, Schiedam, the Netherlands). These electrodes are suitable as anode as well as cathode and therefore current reversal is allowed. Ag/AgCl gel filled reference electrodes (QM711X, ProSense, Oosterhout, the Netherlands) were inserted in small vessels. The vessels were connected via thin tubes to the inlet tubes of anolyte and catholyte, just

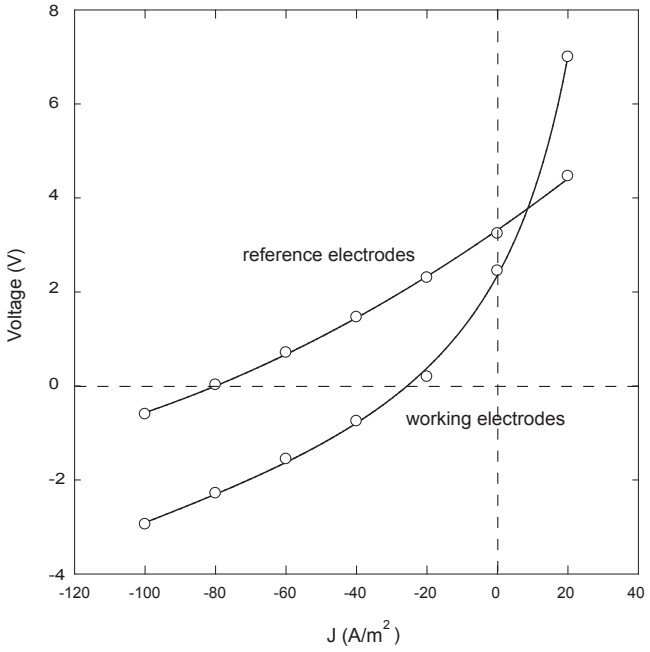

Figure 6.2. Voltages as function of the current density J of a RED stack with 25 cells with Fumasep membranes.

before the inlet points of the stack (*Figure6.1*). The galvanostatic measurements were carried out with an Ivium potentiostat (Ivium Technologies, Eindhoven, the Netherlands).

6.2.4. Artificial sea and river water

The artificial 'sea water' consisted of 30 g NaCl/L and the artificial 'river water' of 1 g NaCl/L. A conductivity meter with a Tetracon 325 cell (WTW, Weilheim, Germany) was used. To convert conductivities to salt content, a second order calibration line was used in the 0-30 g NaCl/L range at 298 K. For the delivery of sea and river water and for recirculation of the electrode rinse, peristaltic pumps are used (Masterflex L/S, Cole Parmer Instrument Company). The stack with 25 cells was fed with 700 mL/min. Smaller stacks were fed with proportional lower flow rates, thereby maintaining the same flow velocity along the membrane surface. The temperature was controlled at 298±1K for all experiments.

6.2.5. Improvement of the electrode rinse solution

In previous experiments as described in *Chapter 3* and *5*, we used an electrode rinse, containing the hexacyanoferrate redox couple $[Fe(CN)_6)^{3-}$ / $[Fe(CN)_6]^{4-}$ in a bulk of NaCl. In this system there is a risk of poisoning the membranes[7]: especially at the AEM the negatively charged hexacyanoferrate ions can accumulate in the membrane with the positive fixed amino groups. Although the outer membranes are CEMs, and there is no

direct contact between the electrode rinse and the AEMs, the sea water is circulated through the stack and hexacyanoferrate ions can leak to the sea water and contact the AEMs in this way. To be sure that the membranes are not affected by the electrolyte, only a pure NaCl solution is used in the electrode compartments. The salt content in the electrode compartments was maintained at 15 g/L, the mean of the concentrations in sea and river water. In this way a rather constant salt concentration in the electrode rinse is assured.

The potential difference over the former stacks - with the reversible hexacyanoferrate system - was measured between platinum electrodes. This is not possible in the NaCl system because a reversible electrochemical couple is lacking here. Therefore, standard Ag/AgCl reference electrodes were used, inserted in small vessels outside the stack. These vessels were connected to the electrode compartments with thin tubes.

A further improvement was the use of silicon gaskets. With this material no leakage was observed. Because these gaskets do not require coating to prevent leakage, the thickness of the gaskets is not affected.

6.3. Results and discussion

6.3.1. Experiments with a Fumasep stack of 25 cells

In this section experiments are described with a stack of 25 cells and Fumasep membranes. In the next paragraph (*Section 6.3.2)* the properties of this Fumasep FAD/FKD pair are compared with other commercial membrane pairs. We studied power density, thermodynamic efficiency, and ion transport behavior for different RED stacks. Typical experimental results (voltage and power density as function of the current density) are shown in *Figure 6.2* and *Figure 6.3*.

6.3.1.1. Determination of the power density.

The RED stack was connected to the potentiostat and measurements were performed at fixed current densities. At each current density we determined the (i) flow rates of the outlets, (ii) water conductivities and temperatures at the inlets and outlets, (iii) voltage on the working electrodes, and (iv) voltage on the reference electrodes. Conductivities were converted in concentrations.

In *Figure 6.2* and following, positive current density implies normal electrodialysis (ED) operation; the negative current densities are related to RED. Current densities lower than the short cut current (<80 A/m^2) cause a negative potential on the reference electrodes.

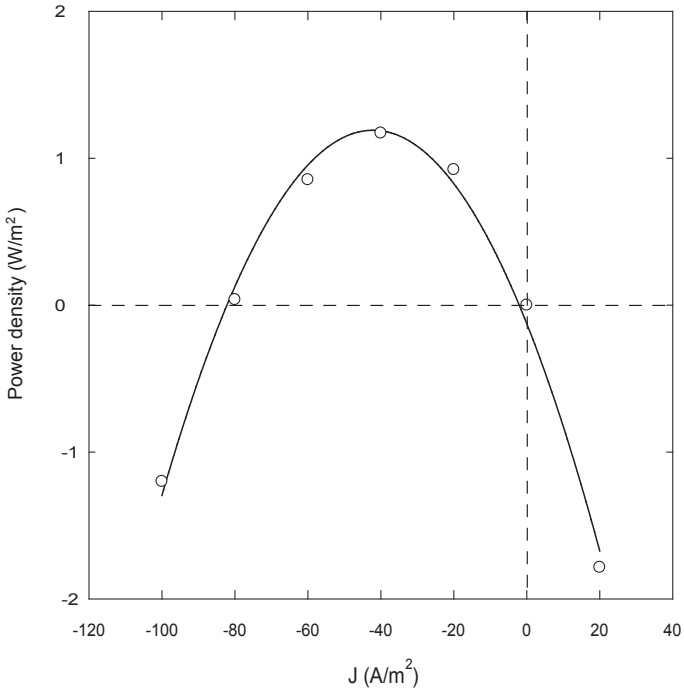

Figure 6.3. Generated power density of a RED stack with 25 cells with Fumasep membranes.

The region with current densities lower than –80 A/m^2 can be called 'forced RED'. In *Figure 6.2* voltages are shown between the working electrodes and between the reference electrodes. At low current densities (J<–24 A/m^2) the difference between both curves is about 2 V, representing the used voltage for the electrolysis process at the electrodes (generating Cl_2 and H_2). This loss is negligible in practice, since an economically operated stack should have hundreds of cells. Then, the loss caused by electrode reactions is marginal with respect to the generated voltage as measured on the reference electrodes. If the main topic is the behavior of the stack (the membranes and the water compartments) and not the electrode system, the voltage on the reference electrodes is the most important value.

In *Figure 6.3* the generated power - as calculated from the applied current and the voltage on the reference electrodes - is plotted against the current density. From this figure, a maximal power density of 1.18 W/m^2 at a current density J=–42 A/m^2 is found. This is a significant improvement compared to earlier experiments. The better performance is ascribed to the use of silicon rubber gaskets (prevention of leakage) and of electrode rinse solution (no membrane poisoning by hexacyanoferrate ions).

6.3.1.2. Ionic and water transport in a RED stack

6.3.1.2.1. Transport curves. The transport of ions through the membranes can be determined using a mass balance from the flows entering and leaving the stack. In *Figure 6.4* results are presented for a stack containing 25 cells. In *Figure 6.4* the NaCl transport (in $mmol \cdot m^{-2}s^{-1}$) to the sea water and to the river water is plotted as a function of the current density J (A/m^2). Transport of salt is negative to the sea water and positive to the river water. The dashed lines represent the case of an ideal process (i.e. 100% selective membranes and no osmosis). Two deviations of the ideal behavior are observed: (i) at zero current density there is salt transport and (ii) the transport curves are not symmetrical with respect to the x-axis. The regression lines of the experimental data have high correlation coefficients (R^2=0.999) indicating that these deviations are not ascribed to random errors.

6.3.1.2.2. Osmosis. The difference between the ideal transport and the measured transport in *Figure 6.4* is larger for the sea water compartment than for the river water compartment. This is most likely caused by the transport of water from the river water compartment to the sea water compartment through the membranes (osmosis). The transport curves shown in *Figure 6.4* are reproducibly determined for 10 different stacks indicating the

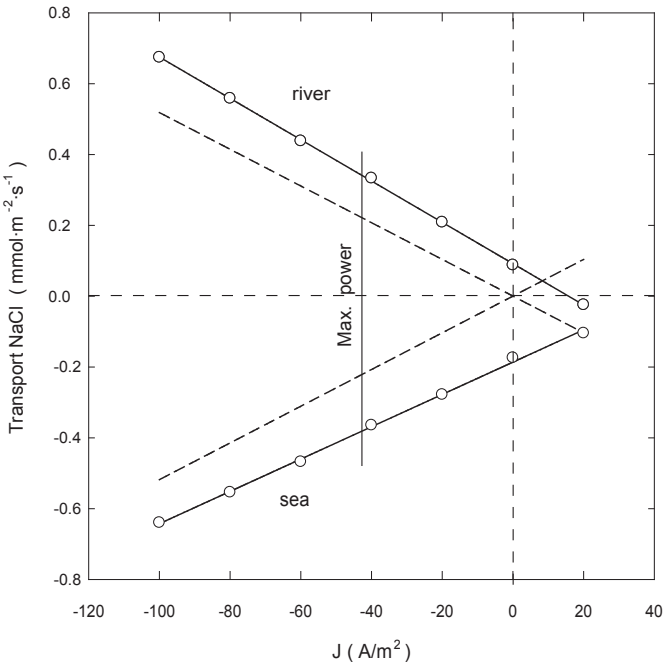

Figure 6.4. NaCl flux through the membranes in a stack with 25 cells with Fumasep membranes. The dashed lines show the ideal case (100% selective membranes and no osmosis). The transport causes a positive increase of the salt content in the river water and a negative increase in the sea water.

asymmetry cannot be ascribed to leakage between the gaskets and membranes.
Figure 6.4 shows that the asymmetry of the transport lines is relatively small but nevertheless very clear: At this point the plot suggests that more salt had disappeared from the sea water than transported to the river water. This effect of osmosis can be quantified as follows:

For each RED process the salt balance can be written:

$$\Phi_S^o C_S^o + \Phi_R^o C_R^o = \Phi_S^i C_S^i + \Phi_R^i C_R^i \tag{1}$$

where Φ is the flow rate (m^3/s) and C the concentration (mol/m^3). The subscripts *S* and *R* stand for *sea* and *river* and the superscripts *i* en *o* for *in* and *out*.

Concentrations in feed and effluent are obtained accurately by electrical conductivity measurement. Experimentally, outgoing flow rates are much better to measure than the ingoing ones. However, if we consider that the announced asymmetry can be ascribed to osmosis, we can write the following flow rate balances:

$$\Phi_S^o = \Phi_S^i + \Phi_{osm} \quad ; \quad \Phi_R^o = \Phi_R^i - \Phi_{osm} \tag{2}$$

where Φ_{osm} is the osmotic flow rate.

Substituting these equations in *Eq. (1)* result in:

$$\Phi_S^o C_S^o + \Phi_R^o C_R^o = (\Phi_S^o - \Phi_{osm}) C_S^i + (\Phi_R^o + \Phi_{osm}) C_R^i \tag{3}$$

or

$$\Phi_{osm} = \frac{\Phi_S^o (C_S^i - C_S^o) + \Phi_R^o (C_R^i - C_R^o)}{C_S^i - C_R^i} \tag{4}$$

Figure 6.5 shows the calculated osmotic flux as function of the applied current density. The osmosis at J=0 A/m^2 (where no electro-osmotic effects are expected) can be compared with the values of some other ion-exchange membranes. The osmosis at J=0 A/m^2 is 9.03 $mmol \cdot m^{-2} s^{-1}$. Osmosis most likely has a negative effect on the power density in reverse electrodialysis by counteracting the diffusion of the counter ions (by drag) through the membranes and by dilution of the boundary layer on the sea water side of the membrane. Osmosis also decreases the thermodynamic efficiency. Both effects (osmosis and co-ion transport) can be described - analogous to the effects in normal batteries - as self discharge.

The diffusion constant D_{water} for these membranes is calculated based on the given salt concentrations:

$$D_{water} = J_w^0 \frac{\delta_M}{\Delta C_{water}} \approx J_w^0 \frac{\delta_M}{-\Delta C_{salt}} \quad (5)$$

with J^0_w the measured water flux (mol·m^{-2}s^{-1}), δ_m the membrane thickness (m). ΔC_{water} and ΔC_{salt} are the differences of water and the NaCl concentration in the two solutions (in mol/L). From concentration tables it follows that ΔC_{water} is almost equal to $-\Delta C_{salt}$ for solutions with a concentration less than 0.5 mol NaCl/L.

In principle, for the determination of diffusion constants the concentration gradient in the membrane should be used and not the concentration difference of the bulk phases. The existence of boundary layers causes an extra transport resistance. However, in our experiments, we have used rather high flow rates to obtain a maximal power in combination with spacers acting as turbulence promoters. The consequence is that the boundary layers are very thin and our diffusion constants (obtained from bulk concentrations) are rather good estimates. *Table 6.1* shows that our determined values are in the same range as those determined in literature.

6.3.1.2.3. Electro-osmosis. Figure 6.5 shows that the water flux depends on the current density. In comparison with the zero current density behavior, the water transport through the membranes decreases when the cell operates in the RED mode (with a negative current) and at J=–80 A/m^2 (near to the shortcut current density), the water transport vanishes. This is caused by electro-osmosis: water is transported with the ions of the salt in a direction opposite the normal osmotic flow. The slope of the regression line (y=0.121x+9.03) is the transport of water per coulomb and given in *Table 6.1* as t_w, the water transport number (mol/F). Electro-osmosis counterbalances the negative effect of normal osmosis.

6.3.1.2.4. Co-ion transport. The reason that both lines in *Figure 6.4* do not cross the origin (0 A/m^2) is the imperfect behavior of the membranes. Ion-exchange membranes are slightly permeable for co-ions (ions with the same charge as the fixed ion exchange groups). Transport of co-ions at zero current condition appears as NaCl diffusion through the ion-exchange membranes and can be compared with the self-discharge of normal electric batteries. The intersection of the two (solid) transport lines at J=+15 A/m^2 in *Figure 6.6* indicates the place were migration is balanced by co-ion transport. At higher current density the electrodialysis process is possible. At current densities J<0 A/m^2, the reverse electrodialysis process starts. Between 0 and +15 A/m^2 the discussed loss phenomena

Table 6.1. Osmosis values and salt diffusion measured for some ion–exchange membranes.

membrane C=CEM, A=AEM A/C=mixed values	Reference	salt	δ_m (m)	D_{water} (m^2/s)	t_W (mol/F)	D_{salt} (m^2/s)
A/C: Fumasep FAD/FKD	This chapter	NaCl	8.0E–05	1.3E–09	11.7	1.3E–11
A/C: Qianqiu homogen.	This chapter	NaCl	2.5E–04	7.9E–09	–	3.2E–11
A/C: Qianqiu heterogen.	This chapter	NaCl	5.8E–04	3.9E–09	6.0	2.0E–11
A/C: Neosepta ACS/CMS	This chapter	NaCl	1.3E–04	9.0E–10	10.1	<2.0E–12
A/C: Neosepta AMX/CMX	This chapter	NaCl	1.5E–04	5.8E–10	4.6	5.5E–11
C: JJC–82	Jagur–	NaCl	2.0E–05	5.8E–11	–	8.0E–14
A: JJA–72	Grodzinski[9]	„	2.0E–05	8.0E–11	–	1.8E–14
A: JJA–5/2PVP	„	„	2.0E–05	1.4E–10	–	7.3E–13
C: Nafion 450	Visser[19]	NaCl	4.5E–04	2.0E–09	5.3	9.0E–12
A: Neosepta AFN	Tasaka[20]	KCl	1.6E–04	2.4E–09	–	–
C: Neosepta C66–10F	Tasaka[21]	KCl	3.6E–04	5.8E–10	–	–
C: Flemion AR1.25	„	„	1.0E–04	1.7E–09	–	–
C: Nafion 417	„	„	4.3E–04	3.2E–09	–	–
C: Nafion 120	Narebska[22]	NaCl	3.0E–04	2.4E–09	5.3	3.0E–11
C: Selemion CMV	Schoeman[23]	NaCl	1.3E–04	2.4E–09	10.4	–
A: Selemion AMV	”	„	1.3E–04	2.4E–09	10.4	–
A/C Selemion AMV/CMV	This chapter	NaCl	1.2E–04	1.2E–10	5.1	3.1E–12
C: MC–40–8	Berezina[24]	–	–	–	6.5	–
C: MC–40–6	„	–	–	–	7.0	–
C: MC–40–4	„	–	–	–	9.2	–
C: MC–41–8	„	–	–	–	6.7	–
A: MA–41–9	„	–	–	–	5.0	–
CL–25T	Gnusin[25]	NaCl	–	–	–	1.5E–11
MC–40	„	„	–	–	–	7.0E–12
Nafion–117	„	„	–	–	–	6.0E–12
MF–3SC	„	„	–	–	–	5.0E–12
SPEEK–1	„	„	–	–	–	1.5E–12
SPS–2	„	„	–	–	–	5.0E–13

(osmosis and co-ion transport) wins the competition with electrodialysis. This range is of less importance from the viewpoint of RED (no energy production) as well as from the viewpoint of ED (no separation).

The total mass transport T_{total} (mol/s) of NaCl from the sea to the river side in the stack is obtained from the difference between the output and input flow of the river water:

$$T_{total} = \Phi_R^o C_R^o - \Phi_R^i C_R^i \qquad (6)$$

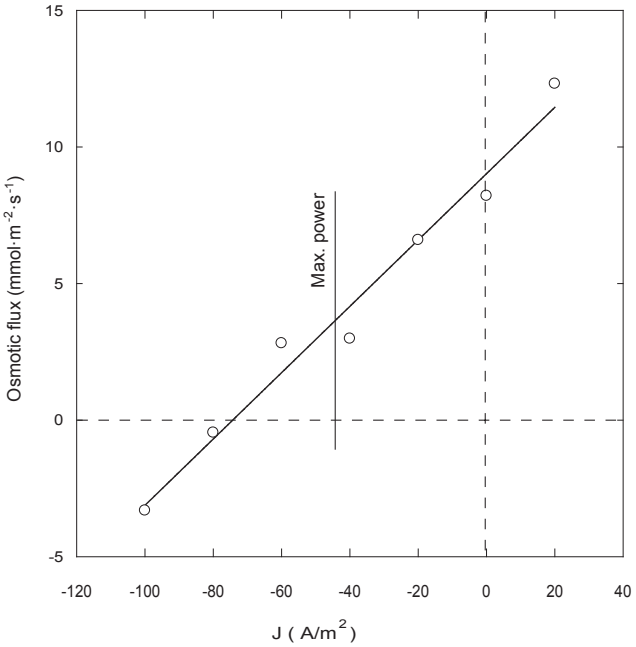

Figure 6.5. Osmotic flux in a stack with 25 cells with Fumasep membranes.

The mass transport of NaCl is due to two contributions: a coulombic part (T_{coul}) and the part due to the co-ion transport (T_{cit})

The coulombic part is obtained from the electrical current through the stack (F is the Faraday constant):

$$T_{coul} = \frac{I}{F} \tag{7}$$

At RED conditions, the co-ions move through the membranes from the sea water to the river water compartment in the same direction as the counter ions and are measured as an extra salt transport T_{cit}. This part is obtained by:

$$T_{cit} = T_{total} - T_{coul} \tag{8}$$

The transport of NaCl from sea to river water is corrected for the osmotic flow of water. The results are presented in *Figure 3.6.* The transport of NaCl can be described by the linear relationships y=±0.0053x+0.080 with R^2=0.9997. The slopes are very near to the ideal values (y=±0.0052x). At zero current the NaCl flux (J^0_{salt}) is 0.080 mmol·m^{-2}s^{-1}. This value is only due to co-ion transport and referred in literature as 'NaCl diffusion'. It is remarkable

to note that the water flux (on mol base) in the other direction is more than 100 times the NaCl diffusion.

Besides the NaCl flux, the diffusion constant D_{salt} (in m^2/s) can be calculated:

$$D_{salt} = J^0_{salt} \frac{\delta_M}{\Delta C_{salt}} \quad (9)$$

with J^0_{salt} the measured NaCl flux ($molm^{-2}s^{-1}$), δ_m membrane thickness (m) and ΔC_{salt} the difference of salt concentration on both sides of the membrane (mol/m^3). *Table 6.1* shows measured diffusion data of the investigated membrane pairs (in fact the average of the anion and the cation exchange membrane values) compared with data of other membranes. Most data are in the same range.

6.3.1.3. Thermodynamic exergy losses in the system

Exergy in our RED system is the maximal amount of electrical energy that can be generated from a given amount of river water and sea water. However, in practice the fraction of generated electrical energy of the exergy content of the incoming water (Y) is less than 100%. The causes are threefold: (i) the reversible mixing of the water is not complete (especially at high flow rates), (ii) reversible mixing is only possible at infinitesimally small current density and (iii) membranes are not ideal (there is an exergy loss by co-ion transport and by osmosis).

Because energy balances are the central theme in this work, the exergy content of the outlet of the RED stack should also to be considered. Therefore, we introduced the concept thermodynamic efficiency (η_T), defined as the generated electrical energy divided by the exergy decrease of the water after passing the RED stack. For a system with ideal membranes, η_T can be 0.5 at maximal power density and may be higher at if the external resistance is increased, resulting in a lower power density.

The effect of co-ion transport and osmosis on η_T in a Fumasep cell is investigated in this paragraph.

Diluted salt solutions like river water and sea water can be considered as ideal and on irreversible mixing of the solutions, the temperature effect is small. The consequence is that when electrical energy is extracted during reversible mixing (as in a RED stack), the temperature of the water should decrease because the total energy is conserved. However, the effect on temperature is small: the maximum amount of energy on reversible mixing of 1 m^3 sea water (30 g NaCl/L) with 1 m^3 river water (0 g NaCl/L) is 1.6 MJ (*Chapter 5*)

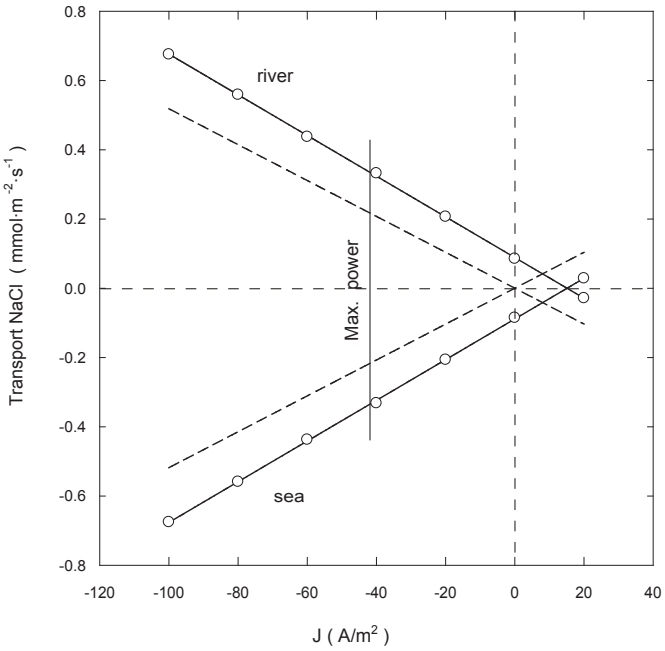

Figure 6.6. NaCl flux corrected for the osmotic flux in a stack with 25 cells with Fumasep membranes.

and correspondents with a decrease of 0.2 degree. Thus, although the RED process is an adiabatic process, good estimation of entropy changes can be achieved with an isothermal approximation.

6.3.1.3.1. Exergy losses. The exergy content of two volumes of water with different concentrations and the same temperature is derived from the entropy increase on total mixing of these volumes. The exergy flow rate X of two water streams with different salt concentration is the power potential and is presented in Watt. The exergy flow rate X^i into a RED stack is given by (Chapter 5; [5,6]):

$$X^i = 2RT\left[\Phi_R^i C_R^i \ln\frac{C_R^i}{C_M^i} + \Phi_S^i C_S^i \ln\frac{C_S^i}{C_M^i}\right] \quad (10)$$

In this equation, C^i_M is the hypothetical resulting concentration on total mixing of both streams*:*

$$C_M^i = \frac{\Phi_R^i C_R^i + \Phi_S^i C_S^i}{\Phi_R^i + \Phi_S^i} \quad (11)$$

During the residence time in the RED stack, the exergy content of the feed (sea water and

river water) decreases. The exergy flow on the outlet (X^o) is obtained analogous to *Eq. (10)* with the same equation by changing the superscript *i* into *o*.

The consumed exergy per second (X_{cons}) is obtained by subtracting both exergy flow rates:

$$X_{cons} = X^i - X^0 \tag{12}$$

In *Figure 6.7A* the value X_{cons} per m^2 membrane is plotted as function of the current density J (curve *a*). The figure shows that even at zero current density there is exergy decrease. This can be ascribed to osmosis and NaCl diffusion (by the mechanism of co-ion transport). The contribution of each effect can be specified.

6.3.1.3.2. Osmotic part of the exergy loss. At each value of the current density J, the osmotic flow rate Φ_{osm} is obtained by *Eq. (4)*. Hypothetical effluent concentrations ($C^o_{S,osm}$ and $C^o_{R,osm}$) can be determined by taking into account only osmosis and no salt transport between the compartments. These output concentrations can be obtained via the NaCl-balance:

$$C_{S,osm} = C_S^i \frac{\Phi_S^i}{\Phi_S^o} \quad ; \quad C^o_{R.osm} = C^i_R \frac{\Phi^i_R}{\Phi^o_R} \tag{13}$$

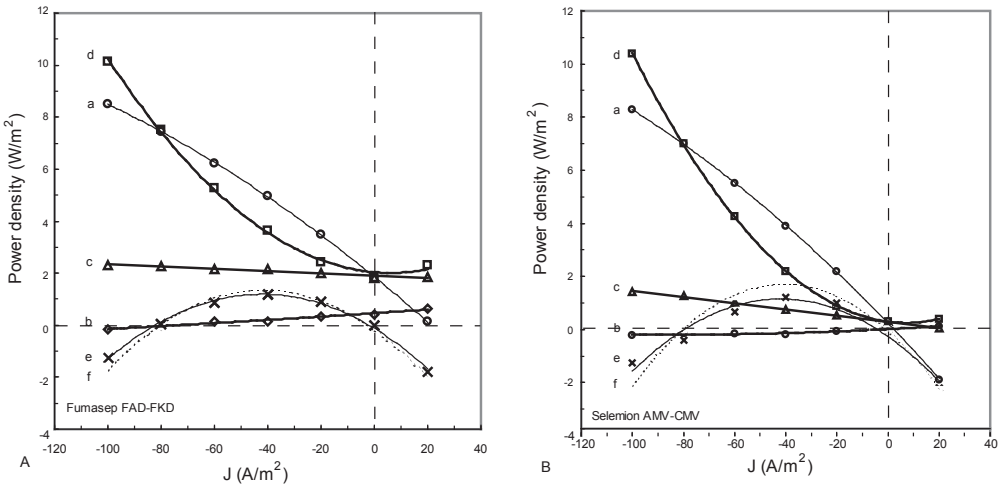

Figure 6.7. Consumed exergy flux and produced power density of two RED stacks as function of the current density. A (left): with Fumasep membranes (FAD/FKD, B (right): with Selemion membranes (AMV/CMV). All plotted variables are referred to 1 m^2 membrane. a) exergy decrease of the feed water on passing the stack, b) exergy loss due to osmosis c) exergy loss due to osmosis plus co-ion transport d) exergy loss due to osmosis, co-ion transport and internal power dissipation, e) produced electrical power density. The difference between curves a and d (curve f) should in principle be equal to curve e. All parabolic regression lines are used to guide the eye.

With these output concentrations in combination with the measured parameters (input concentrations, output flow rates) and the derived input flow rates, the osmotic part of the output exergy flow rate (X^o_{osm}) is obtained and with that the osmotic loss X_{osm} (using *Eq. (10)* and *Eq. (11)*:

$$X_{osm} = X^i - X^o_{osm} \tag{14}$$

The obtained osmotic part of the exergy decrease is plotted per square meter used membrane in *Figure 6.7A* (curve *b*). At zero current density the osmotic part of the exergy loss is 26% of the total exergy loss and at the optimal current density (J=-42 A/m^2) this is only 5%.

6.3.1.3.3. Ionic part of the exergy loss. The difference between the measured NaCl transport lines (the solid lines) and the calculated ideal lines (the dashed lines) in *Figure 6.6A* is the NaCl diffusion due to co-ion transport. The exergy flow rate loss of this part is obtained as follows.

Assuming salt transport is caused only by co-ion transport (T_{cit}), a balance can be written for the sea and river water stream. $C_S^{co,o}$ and $C_R^{co,o}$ are the hypothetical effluent concentrations:

$$C^o_{S,cit}\Phi^i_S = \Phi^i_S C^i_S - T_{cit} \quad ; \quad C^o_{R,cit}\Phi^i_R = \Phi^i_R C^i_R + T_{cit} \tag{15}$$

In the case of no osmosis, output flow rates ($\Phi_S^{co,o}$ and $\Phi_R^{co,o}$) would be equal to the input flow rates:

$$\Phi^o_{S,cit} = \Phi^i_S \quad ; \quad \Phi^o_{R,cit} = \Phi^i_R \tag{16}$$

Now the output concentrations are known:

$$C^o_{S,cit} = \frac{\Phi^i_S C^i_S - T_{cit}}{\Phi^i_S} \quad ; \quad C^c_{R,cit} = \frac{\Phi^i_R C^i_R + T_{cit}}{\Phi^i_R} \tag{17}$$

With this output concentrations, output exergy flow rate (X^o_{cit}) can be calculated. The exergy loss due to co-ion transport X_{cit} can be obtained with (using *Eq. (10)* and *Eq. (11)*:

$$X_{cit} = X^i - X^o_{cit} \tag{18}$$

In *Figure 6.7A* the sum of the osmotic part and the co-ion transport part is plotted (curve *c*). In this case co-ion transport costs much more exergy then osmosis.

6.3.1.3.4. Internal power dissipation exergy losses. The next exergy loss is the internal power dissipation (P_i) due to the ionic current through the cell. This part can be obtained by the square of the current and the internal resistance (R_i):

$$P_i = I^2 R_i \tag{19}$$

Because the harvested power (P_u) is related to the external resistance (R_u):

$$P_u = I^2 R_u \tag{20}$$

It follows that

$$\frac{P_i}{P_i + P_u} = \frac{R_i}{R_i + R_u} \tag{21}$$

Maximal power output is achieved at P_u=P_i (*Chapter 3*): in first instance the conclusion seems to be that in this case heat is generated in the RED stack (numerical equal to the electric output power). However, it should be emphasized that in the RED process all generated electrical power is equivalent to the decreased heat content of the feed water. Internal dissipation of heat is in fact a decrease of the cooling of the feed water. From a thermodynamical viewpoint, the mixing process is partially reversible and partially irreversible; at maximum power both parts are 50% and at very small current densities the part of reversible process approaches 100 %.

In practice, the experiments were performed with a potentiostat instead of an external resistance. The voltage measured at zero current is the open circuit voltage (OCV). At current I, the internal power dissipation is calculated by

$$P_i = (OCV - E)I \tag{22}$$

where E stands for the voltage on the reference electrodes. This loss is added again to the aforementioned losses (due to osmosis and NaCl leak) and plotted in *Figure 6.7A* as curve *d*.

6.3.1.3.5. Extractable part of the exergy. The counterpart of the internal dissipated power - as given by *Eq. (22)* - is the produced electrical power P_u which is determined *as:*

$$P_u = EI \tag{23}$$

Curve *d* in *Figure 6.7A* includes all exergy losses and curve *a* is the measured exergy loss; the difference between curve *d* and *a* can be extracted as usable energy. To verify this statement, the generated power density is also added to the figure (curve *e*). It is now evident now that the difference between the curves *a* and *d* is near to the power curve *e*. Especially important is the power density balance at the current density of maximal power density (J=–42 A/m^2). *Table 6.2* (*column c)* specifies the contribution of the different parts, expressed in percent of the exergy decrease of the feed water. *Table 6.2* shows a produced power of 23% of the exergy decrease at optimal current density. We will refer to this value as 'thermodynamic efficiency' (η_T).

$$\eta_T = \frac{P_u}{X^o - X^i} = \frac{P_u}{X_{cons}} \tag{24}$$

A related value is the energy efficiency Y:

$$Y = \frac{P_u}{X^i} \tag{25}$$

In this chapter we focus on thermodynamic efficiency. This parameter describes the losses in the cell and is less sensitive to variations of the river and sea water flow rate. However, for a real operating RED power plant, the energy efficiency is a more important process parameter.

6.3.2. Experiments with other membrane pairs

The experiments of Section *6.3.1* with Fumasep membranes were repeated with other membrane pairs: *Qianqiu Heterogeneous Ion Exchange Membrane* (AEM and CEM), *Qianqiu Homogeneous Ion Exchange Membrane* (AEM and CEM), *Selemion* (AMV and CMV), *Neosepta* (ACS and CMS) and *Neosepta* (AMX and CMX). The results and derived data are summarized in *Table 6.2* and estimated diffusion parameters are added to *Table 6.1*. All exergy and energy data are expressed as power per m^2 membrane area (W/m^2).

A new parameter (R_p) is introduced in *Table 6.2*. This response parameter is a product of the power density and the thermodynamic efficiency (*Eq. 26*) and is a measure for the most optimal membrane stack configuration for RED.

$$R_P = P_d \eta_T \tag{26}$$

This response parameter allows for an easy ranking of the performance of a RED stack. For RED a high power density and energy efficiency are preferred. Post et al. showed[17] that a high efficiency (> 80%) could be obtained at a low current density. This would yield a low value of the response product. This highest power density shown in *Table 6.2* (1.18 W/m^2)

Table 6.2. Data for all studied membrane pairs at 25 ±1 °C.

		a Qianqiu heterog.	b Qianqiu homog.	c Fumasep FAD/FKD	d Selemion AMV-CMV	e Neosepta ACS-CMS	f Neosepta AMX-CMX
values at optimal current density ($J=J_{opt}$)							
exergy decrease feed (X_{cons})	W/m^2	1.88	5.09	5.05	4.07	1.70	4.80
thermodynamic exergy eff. (η_T)	%	26	21	23	29	35	14
power density (P_d)	W/m^2	0.49	1.05	1.17	1.18	0.60	0.65
response product ($R_P=P_d \cdot \eta_T$)	$W/m^2 \cdot \%$	13	22	27	34	21	9
values at open circuit (J=0)							
open circuit voltage per cell (OCV)	V	0.141	0.132	0.133	0.156	0.158	0.143
mean permselectivity (α_{mean})	%	87	90	88	97	100	94
other values							
optimal current density (J_{opt})	A/m^2	-16	-39	-42	-42	-18	-23
short cut current (SCC)	A/m^2	-32	-78	-84	-84	-34	-49
membrane properties							
diffusion const. of water (D_{water})	10^{-10} m^2/s	39±6	79±4	13±2	1±3	9±6	6±6
electro-osm.water transport nr (t_W)	mol/F	6.0±1.1	–	11.7±2.1	5.1±2.2	10.1±3.4	4.6±3.2
diffusion const. of NaCl (D_{salt})	10^{-10} m^2/s	0.20±0.06	0.32±0.05	0.13±0.01	0.031±0.005	<0.02	0.55±0.02

is the highest reported in literature up to now. This value can be further improved by optimizing the hydrodynamics in a RED stack (*Chapter 5*). *Table 6.2* also shows the open circuit voltage (OCV), which is a measure for the selectivity of the membrane stack. A 100% selective membrane pair would yield an OCV of 0.158 V. Also shown are the optimal current density at maximal power density and the short cut current. Both values are high for a stack with a high current density. *Table 6.2* also lists the membrane transport properties, which are in the same range as those reported in literature (see *Table 6.1*).

Figure 6.7B shows the exergy flux diagram for the Selemion cell. In comparison to the similar plot of the Fumasep cell in *Figure 6.7A* it is noticeable that the osmotic and co-ion transport losses are much less in the Selemion stack, yielding a higher thermodynamic efficiency.
As can be seen from *Table 6.2* there is no clear relationship between the thermodynamic efficiency and the mean membrane pair selectivity. This is because the thermodynamic efficiency not only depends on the exclusion of co-ions but also on the chemical nature of the membranes, which affects transport phenomena like osmosis and membrane resistance.

The relation between membrane transport properties and structure is not straightforward. We refer to the detailed study on membrane properties in relation to membrane structure to Długołęcki et al.[18] and especially on water transport to Berezina at al.[26]. Długołęcki et al.[18] studied the relation between membrane properties and the theoretical performance of a RED stack. They showed that the charge density influences membrane permselectivity and resistance but these relations are not linear and depend on the type of membrane. Moreover, they showed that heterogeneous membranes have a relative large membrane resistance due to their membrane structure and a relative low charge density. In our experiments, we found for the only heterogeneous membrane pair in our tests (the Qianqiu heterogeneous pair) indeed a low power density, about 50% lower compared to the other membrane pairs.

6.4. Conclusions

In this chapter we show the experimental thermodynamic efficiency determined at maximal power density for 6 different commercial membrane pairs. The stacks were operated on artificial river and sea water of 1 and 30 g NaCl/L. The highest obtained power density is 1.2 W/m^2 for the Fumasep (FAD and FDK) and Selemion (AMV and CMV) combinations. These values are the highest reported in literature for this concentration gradient. The thermodynamic efficiency (η_T) is ranged between 14% and 35% where 50%

is the maximal possible value at maximal power output. We demonstrated that this non-ideal behavior of the membranes is due to osmosis and co-ion transport and we were able to quantify each effect. Higher efficiencies can be obtained if the stack is operated at lower current densities.

Introduced is the response product (R_p), the product of the response parameters. It combines the benefits of high power density with high thermodynamic efficiency and may be a useful ranking parameter. The highest R_p (34 $W/m^2 \cdot \%$) is achieved with the Selemion (AMV-CMV) pair.

There is no clear relationship between the membrane selectivity and the thermodynamic efficiency, since many membrane properties like membrane resistance, osmosis and co-ion transport affect the transport process. Osmosis and co-ion transport cause a loss in thermodynamic efficiency. The loss in efficiency due to osmosis is small compared to co-ion transport. Osmosis is current dependent and is especially low at a current density of maximal power density.

Membranes for RED should combine a low resistance with a high permselectivity. Until now, special RED membranes have not been developed. It is the challenge to develop such membranes for an economically acceptable price.

Acknowledgement
This research was performed at Wetsus, centre of excellence for sustainable water technology. Wetsus is funded by the city of Leeuwarden, the province of Fryslân, the European Union European Regional Development Fund and by the EZ/Kompas program of the Samenwerkingsverband Noord-Nederland. The first author would like to thank the Noordelijke Hogeschool Leeuwarden who has facilitated this research by detaching him to Wetsus, and the participants of the energy theme for their interest and financial contribution. We thank Maarten Biesheuvel (Wetsus) for his comment and contribution to the final text.

Nomenclature

C	concentration (mol/m^3)
D_{salt}	diffusion constant of NaCl (m^2/s)
D_{water}	diffusion constant of water (m^2/s)
E	voltage (V)
E_{cell}	electromotive force of one cell (V)
E_{ideal}	voltage of a cell with ideal membranes (V)
F	Faraday constant (96485 C/mol)
I	electrical current (A)
J	electrical current density (A/m^2)
J^0_w	water flux at zero current (mol·m^{-2}s^{-1})
J^0_{salt}	NaCl flux at zero current (mol·m^{-2}s^{-1})
N	number of cells in a stack
P	power (W)
P_d	power density (W/m^2)
P_i	internal dissipated power (W)
P_u	external power (W)
P_{pot}	power potential of a river or country (W)
Q	fraction of river water available for RED
R^2	determination coefficient
R	gas constant (8.314 J·mol^{-1}K^{-1})
R_i	internal resistance (Ω)
R_u	external resistance (load) (Ω)
R_P	response product (W/m^2)
t_w	electro-osmotic water transport number (mol/F)
T_{total}	total mass transport of NaCl (mol/s)
T_{coul}	coulombic part of the NaCl transport (mol/s)
T_{cit}	co-ion transport current of NaCl (mol/s)
T	temperature (K)
OCV	open circuit voltage (V)
SCC	short circuit current (A)
X^i	exergy flow rate of the inlet (W)
X^o	exergy flow rate of the effluent (W)
X_{cons}	consumed free energy per second (W)
Y	energy efficiency

Greek symbols

α	permselectivity of the ion exchange membrane
δ_m	membrane thickness (m)
η_T	thermodynamic efficiency
Φ	flow rate (m^3/s)

Superscripts

i	in
o	out

Subscripts

S	sea
R	river
M	equilibrium
osm	osmotic
cit	co-ion transport

Abbreviations

AEM	anion exchange membrane
CEM	cation exchange membrane
ED	electrodialysis
EMF	electromotive force
OCV	open circuit voltage
RED	reverse electrodialysis
SCC	short circuit current

Definitions

compartment	space between the membranes
cell	combination of two membranes and two compartments
electrode system	the anode, cathode and electrode rinse
stack	a number of N cells with an electrode system

References Chapter 6

1 R.E. Pattle, *Production of electric power by mixing fresh and salt water in the hydroelectric pile.* Nature 174 (1954) 660

2 R.E. Pattle, *Electricity from fresh and salt water - without fuel.* Chem. Proc. Eng. 35 (1955) 351-354

3 J.N. Weinstein, F.B. Leitz, *Electric power from differences in salinity: the dialytic battery.* Science 191 (1976) 557-559

4 B.H. Clampitt, F.E. Kiviat, *Energy recovery from saline water by means of electrochemical cells.* Science 194 (1976) 719-720

5 C. Forgacs, *Generation of electricity by reverse electrodialysis.* BGUN-RDA 178-78 Ben-Gurion University, Israel (1978)

6 C. Forgacs, R.N. O'Brien, *Utilization of membrane processes in the development of non-conventional renewable energy sources.* Chemistry in Canada 31 (1979) 19-21

7 R.E. Lacey, *Energy by reverse electrodialysis.* Ocean Eng. 7 (1980) 1-47

8 R. Audinos, *Electrodialyse inverse, etude de l'energie electrique obtenue a partir de deux solutions de salinites differentes*. J. Power Sources 10 (1983) 203-217

9 J. Jagur-Grodzinski, R. Kramer, *Novel process for direct conversion of free energy of mixing into electric power.* Ind. Eng. Chem. Process Des. Dev. 25 (1986) 443-449

10 R. Audinos, *Electric power produced from two solutions of unequal salinity by reverse electrodialysis.* Ind. J. Chem. 31A (1992) 348-354

11 I. Rubinstein, J. Pretz, E. Staude, *Open voltage in a reverse electrodialysis cell*. Phys. Chem. Chem. Phys. 3 (2001) 1666-1667

12 J.W. Post, J. Veerman, H.V.M. Hamelers, G.J.W. Euverink, S.J. Metz, K. Nymeijer, C.J.N. Buisman. *Salinity-gradient power: Evaluation of pressure-retarded osmosis and reverse electrodialysis.* J. Membr. Sci. 288 (2007) 218-230

13 J. Veerman, J. W. Post, S.J. Metz, M. Saakes, G.J. Harmsen, *Reducing power losses caused by ionic shortcut currents in reverse electrodialysis stacks by a validated model.* J. Membr. Sci. 310 (2008) 418-430

14 J. Veerman, M. Saakes, S.J. Metz, G.J. Harmsen, *Reverse electrodialysis: performance of a stack with 50 cells on the mixing of sea and river water.* J. Membr. Sci. 327 (2009) 136-144

15 M. Turek, B. Bandura, *Renewable energy by reverse electrodialysis.* Desalination 205 (2007) 67-74

16 F. Suda, T. Matsuo, D. Ushioda, *Transient changes in the power output from the concentration difference cell (dialytic battery) between seawater and river water.* Energy 32 (2007) 165–173

17 J.W. Post, H.V.M. Hamelers, C.J.N. Buisman, *Energy recovery from controlled mixing salt and fresh water with a reverse electrodialysis system.* Environ. Sci. Technol. 42 (2008), 5785–5790

18 P. Długołęcki, K. Nymeijer, S.J. Metz, M. Wessling, *Current status of ion exchange membranes for power generation from salinity gradients.* J. Membr. Sci. 2008 (2008) 214-222

19 R.C. Visser, *Electrodialytic recovery of acids and bases, Multicomponent mass transfer description*. Thesis, Groningen 2001

20 M. Tasaka, T. Urata, R. Kiyono, Y. Aki, *Solvent transport across anion-exchange membranes under a temperature difference and an osmotic pressure difference.* J. Membr. Sci. 67 (1992) 83-91

21 M. Tasaka, T. Hirai, R. Kiyono, Y. Aki, *Solvent transport across cation-exchange membranes under a temperature difference and an osmotic pressure difference.* J. Membr. Sci. 71 (1992) 151-159

22 A. Narebska, S. Koter, W. Kujawski, *Ions and water transport across charged Nafion membranes. Irreversible thermodynamic approach.* Desalination 51 (1984) 3-17

23 J.J. Schoeman, J.F. van Staden, *Electro-osmotic pumping of sodium chloride solutions.* J. Membr. Sci. 132 (1997) 1-21

24 N. Berezina, N. Gnusin, O. Dyomina, S. Timofeyev, *Water electrotransport in membrane systems. Experiment and model description.* J. Membr. Sci. 86 (1994) 207-229

25 N.P. Gnusin, N.P. Berezina, N.A. Kononenko, O.A. Dyomina, *Transport structural parameters to characterize ion exchange membranes*. J. Membr. Sci. 243 (2004) 301-310

26 N.P. Berezina, N.A. Kononenko, O.A. Dyomina, N.P. Gnusin, Characterization *of ion-exchange membrane materials: Properties vs structure.* Adv. Colloid Interface Sci. 139 (2008) 3-28

Chapter 7

The performance of a scaled-up reverse electrodialysis stack*

Abstract

A scaled-up test stack for reverse electrodialysis was developed with an output of 11 Watt with 50 cells with active membrane dimensions of 25x75 cm^2. This is the largest dimension of a reverse electrodialysis stack published so far. The stack was equipped with 3 pairs of electrodes, Qianqiu ion exchange membranes and woven polyamide spacers. We investigated the effect of flow rate, flow path length (25 or 75 cm), operation mode (co-current or counter-current), spacer thickness and segmentation of electrodes. Results were compared with those from small stacks. The main finding was that the key parameter for power density is the residence time of fluids in the cell compartments. Spacers with a thickness of 200 µm were optimal for small stacks (10x10 cm^2) but showed high hydrodynamic losses in cells with a flow path length of 25 cm. The novel stack generated more power in co-current flow than in counter-current flow operation. Co-current flow has other advantages: local pressure differences between sea and river water compartments are low, hence preventing leakage around the internal manifolds and through pinholes in the membranes. Low pressure differences also enable the use of very thin membranes (with low electrical resistance) as well as very open spacers (with low hydrodynamic losses) in the future.

**** Submitted to Environmental Science & Technology in condensed form as:***
J. Veerman, M. Saakes, S.J. Metz and G.J. Harmsen
Electrical power from sea and river water by reverse electrodialysis:
a first step from the laboratory to a real power plant

7.1. Introduction

Salinity gradient power (SGP) is a potentially clean and sustainable form of energy; and can be generated from the reversible mixing of sea water and river water, producing brackish water and electrical energy. The theoretical energy content of mixing 1 m^3 river water with a large surplus of sea water is 2.5 MJ or 1.7 MJ when mixed with 1 m^3 sea water (*Chapter 5*). The global potential of SGP is estimated to be 2.6 TW[1] which is more than the global electricity consumption. There are two membrane-based technologies which can convert this potential energy into useful electricity: reverse electrodialysis (RED) and pressure retarded osmosis (PRO). It has been shown that, in the case of river water with seawater, RED is a promising technique[2].

Figure 7.1 shows the principle of RED. A number of alternately stacked cation exchange membranes (CEM) and anion exchange membranes (AEM) are separated by spacers. These spacers are open structures that are needed for structural stability of the stack and the promotion of turbulence within the compartments. The spacer filled compartments are fed alternately with seawater and river water. The positive ions diffuse from sea to river water compartments through the CEMs and the negative ions through the AEMs in the

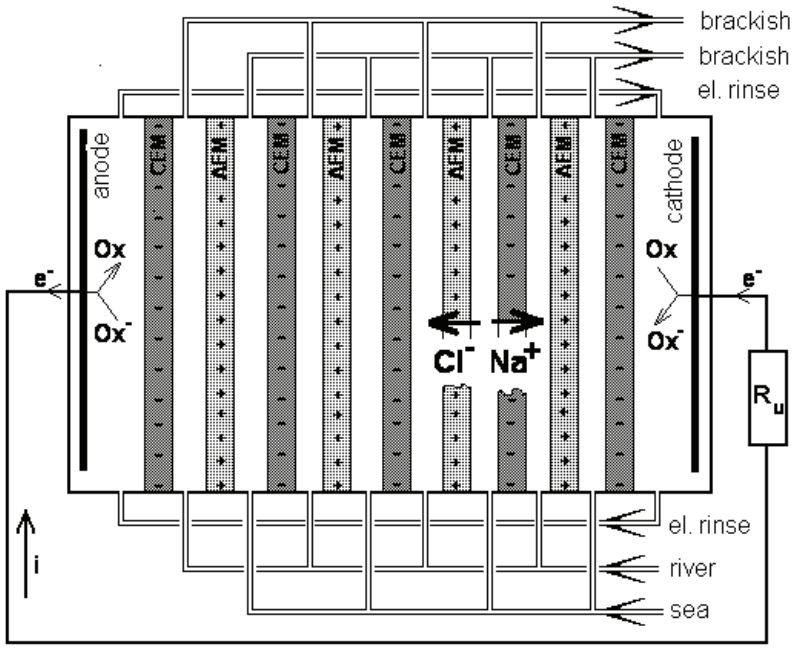

Figure 7.1. Principle of RED. Positive ions diffuse through CEMs from seawater to river water compartments in the direction of the cathode, negative ions diffuse through the AEMs in the opposite direction. The ion current in the stack is converted to an electron current at the electrodes via the reversible redox reaction: $Ox + e \Leftrightarrow Ox^-$.

opposite direction. The ion current in the stack is converted to an electron current at the electrodes by redox reactions.

For optimal performance, a RED power plant should generate maximal power from a given river water feed at lowest investment and operational costs. Related to these economical aspects, three response parameters are important: power density, energy efficiency and net power. A high power density (power generated per m^2 membrane) decreases investments not only in membranes but in the whole stack. High energy efficiency (the percentage of the generated energy from a given amount of feed water compared with the theoretical limit) is favorable for the optimal use of the available water sources. Power density and energy efficiency are conflicting: for high energy efficiency large membrane areas at a low power density are necessary (*Chapter 5*; [3]). Hydrodynamic losses due to the pumping of water through a RED stack should be kept to a minimum. A key parameter for the hydrodynamic resistance is the length of the flow channel. If only power density and energy efficiency are maximized, the result of an optimization procedure may be a very small stack with a low power production. Therefore, the total generated power of the stack (the net power) is also an important response parameter.

Post et al. showed that it is possible to extract 85% of the potential energy in a system with recirculating feed water, however, at the price of a low power density[4]. They also showed the effect of multivalent ions on the power output[4]. Veerman et al. showed that internal short-cut currents are controllable by a proper stack design (*Chapter 3*); they also quantified the power losses by co-ion transport and osmosis in a RED stack and showed that these losses are substantial (*Chapter 6*). Długołęcki et al. made an overview of the properties of commercial membranes as possible candidates for application in RED[5] and were able to specify the contributions of electrical stack resistance, concentration polarization and spacer shadow effects with electric impedance spectrometry, and suggested improvements on the current systems[6]. Dirkse et al. modeled water flows in the compartments using the potential flow theory[7]. With this validated model it is possible to achieve the residence time distribution in a RED compartment.

Up to now all our published experimental work on RED has been done with relatively small stacks (10x10 cm^2). In this work we compare the performance of these small laboratory stacks with a scaled-up 25x75 cm^2 stack. With this larger stack we will also study new aspects affecting the performance, such as: residence time, flow direction (co- or counter-current), flow velocity, segmentation of electrodes (various current densities as a function of the position in the stack).

7.2. Theoretical

In a RED stack, electricity is produced directly at the working electrodes. A part of the generated energy is lost due to electrode reactions. However, in stacks with a large number of cells, as will be used in a commercially operated RED stack, these losses are relatively low. Besides the working electrodes, stacks were equipped with reference electrodes in the electrode compartments. By measuring the voltage between the reference electrodes, the voltage drop at the working electrodes was eliminated. We used this voltage for determining the stack power.

$$P_{hydr} = \Phi_R \Delta P_R + \Phi_S \Delta P_S \tag{1}$$

where Φ_R and Φ_S are flow rates of river and sea water (m^3/s) and ΔP_R and ΔP_S the pressure drop (Pa) over the river and sea water compartments

The feed water entering a RED stack represents a certain amount of exergy X^i (*Chapter 5* [8,9]);

$$X^i = 2RT\left[\Phi_R C_R \ln\frac{C_R}{C_M} + \Phi_S C_S \ln\frac{C_S}{C_M}\right] \tag{2}$$

where X^i is the exergy flow rate if the feed (W), R is the gas constant (8.314 $J \cdot mol^{-1}K^{-1}$), T temperature (K), Φ_R and Φ_S flow rates of river and sea water (m^3/s) and C_R and C_S the salt concentrations in the river and sea water (mol/m^3). C_M is the equilibrium concentration, obtained at total mixing of river and sea water:

$$C_M = \frac{\Phi_R C_R + \Phi_S C_S}{\Phi_R + \Phi_S} \tag{3}$$

The energy efficiency Y is the part of the incoming exergy flow rate that is converted to electrical power:

$$Y = \frac{P_u}{X^i} \tag{4}$$

where P_u is the generated electrical energy.

The net energy efficiency is the amount of generated electrical power (P_u) minus the hydrodynamic loss (P_{hydr}) related to the exergy of the feed water:

$$Y_{net} = \frac{P_u - P_{hydr}}{X^i} = \frac{P_{net}}{X^i} \tag{5}$$

Besides efficiency, other important process parameters are power density (P_d) and net power density (P_{d-net}):

$$P_d = \frac{P_u}{A} \quad ; \quad P_{d\text{-net}} = \frac{P_{net}}{A} \tag{6, 7}$$

where A stands for the total active membrane area (AEMs and CEMs together).
For theoretical considerations, the term thermodynamic efficiency (η_T) is used. Here the generated electrical power P_u is related to the difference of ingoing (X^i) and outgoing (X^o) exergy flow rate of the feed water.

$$\eta_T = \frac{P_u}{X^o - X^i} \tag{8}$$

7.3. Experimental

7.3.1. RED stacks

Two types of stacks were investigated. The 'small stack' is described in detail in *Chapter 5* and had a functional membrane area of 10x10 cm^2. In addition to this, we constructed a novel stack (called 'large stack') as shown in *Figure 7.2* and *Figure 7.3*. In this large stack three electrode compartments - each with its own electrodes - were located on each side

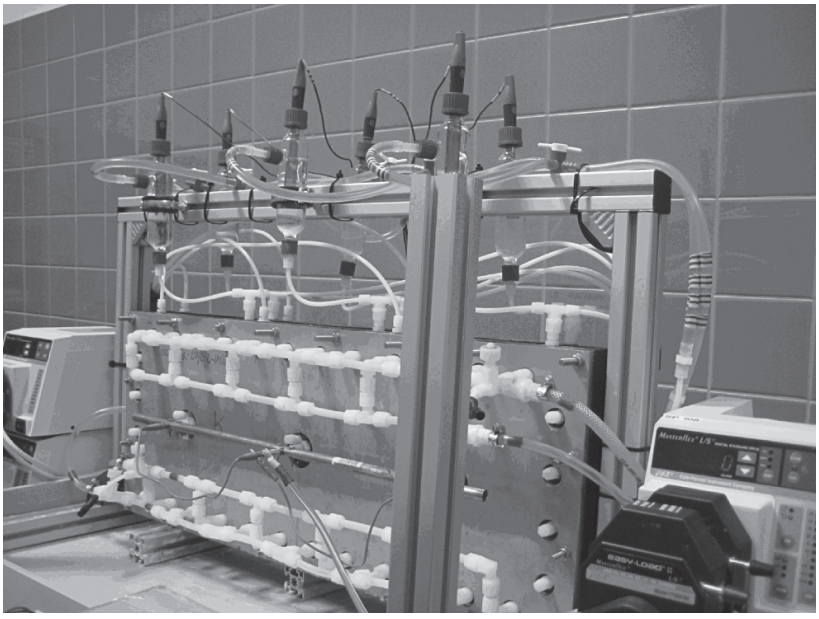

Figure 7 2. Large stack, equipped on the front side with the piping for sea and river water delivery (bottom) and drain (top). Dimensions of the stainless steel end plates are 87 cm by 35 cm. The copper bar in the front connects the 3 cathodes to the power supply. The reference electrodes in the vessels at the top are connected via capillaries to the anolyte and catholyte entrances.

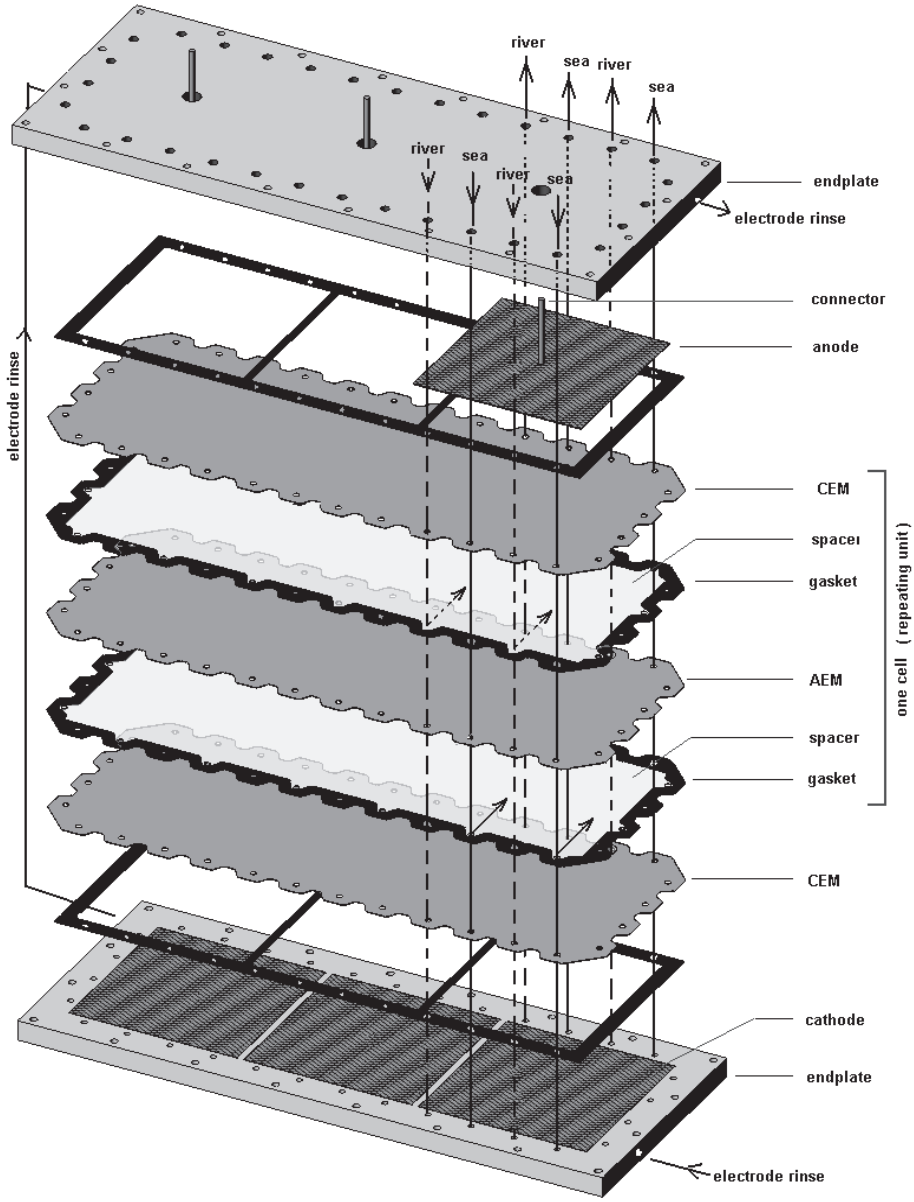

Figure 7.3. Exploded view of the large stack equipped with only one cell. The holes in the long end are used for water feed and drain in the short direction (with 25 cm flow path) as shown in the figure. Alternatively, the holes in the short side can be used for operation in the other direction (with 75 cm flow path).

inside the endplates. Endplates were milled from HDPE (high-density polyethylene). Not shown in this picture are the two stainless steel supporting plates, needed to prevent bending of the cell.

7.3.2. Cells

The functional area of one membrane in the large stack was 25x75 cm^2 =1825 cm^2. On the outsides of the stacks Fumasep FKD cation exchange membranes (Fumatech, Germany) were used as stable end membranes. These membranes are more resistant to chlorine, which evolved at the anode. The inner membranes were Qianqiu (Homogeneous AEM and CEM, Hangzhou Qianqiu Industry Co, China). The stacks were equipped with nylon woven spacers, thickness 200 µm (Nitex 03–300/51, Sefar, The Netherlands); in some experiments with the small stack, 100 µm spacers were used (Nitex 03–190/57). Gaskets were made of silicon micro film with a thickness of 200 µm (SSF-MLTN-940, Specialty Silicone Fabricators, Paso Robles, USA). The stack was equipped with 25 cells and later on expanded to 50 cells.

7.3.3. Electrode system and electrical measurements

The electrode system and the measurement method were analogous to those of the small stack, which is described in detail in *Chapter 5*. However, the electrodes used in the large stack were different. Anodes were coated with Ir mixed metal oxides and the cathodes with Ru mixed metal oxides (Magneto Special Anodes, Schiedam, The Netherlands). These electrodes are optimized for one current direction.

Galvanostatic measurements were carried out with an Ivium potentiostat in combination with an Ivium booster (Ivium Technologies, Eindhoven, the Netherlands) which permits measurements up to 20 A at 20 V.

Two types of electrode rinse solutions were employed. In some experiments a solution of (15 g/L) NaCl (0.25 mol/L) was used. This electrolyte is electrolyzed at the electrodes and the electrolysis consumes a large part of the generated energy. However, even in the case of a net negative power production, measurements were possible because a potentiostat was used.

The effect of segmentation of the electrode was studied with the hexacyanoferrate electrode solution ($K_4Fe(CN)_6$: 0.05 mol/L, $K_3Fe(CN)_6$: 0.05 mol/L, NaCl: 0.25 mol/L). With this system electrode losses are much lower than the generated power and therefore it was possible to use 3 variable resistors (slide rheostats of 22 Ω, 5 A) as electrical load instead of 3 potentiostats and boosters.

7.3.4. Sea and river water

'Sea water' consisted of 30 g NaCl/L and 'river water' of 1 g NaCl/L. A conductivity meter with a Tetracon 325 cell (WTW, Weilheim, Germany) was used. For the delivery of sea and river water and for recirculation of the electrode rinse, peristaltic pumps were used. Temperature was controlled at 298±1K for all experiments.

7.3.5. Flow rate and pressure measurements

Flow rates were determined gravimetrically. Pressure differences were measured with a Deltabar S (Endress + Hauser, Germany) differential pressure gauge between inlet and outlets. Hydrodynamic losses were determined as the product of flow rate and pressure difference.

7.4. Results and discussion

7.4.1. Effects of scale-up

In this part, we compare the experimental results of the scaled up (large) stack (25x75 cm^2) with the performance of the small stack (10x10 cm^2). In order to compare both stacks, identical experimental conditions were used.

7.4.1.1. Effect of the residence time on the power density

At high flow rates, it is expected that the power density is maximal because the concentration difference between the fresh and salt water on both sides of the membrane is nearly unaffected by the transport of salts through the membrane. However, it should be taken into account that hydrodynamic power losses lower the net power output and is minimal at low flow rates. So, there exists an optimal flow rate for the maximal net power density. This optimum was determined for the large stack, containing 50 cells with Qianqiu homogeneous membranes, at different flow rates. The flow direction was vertical (flow

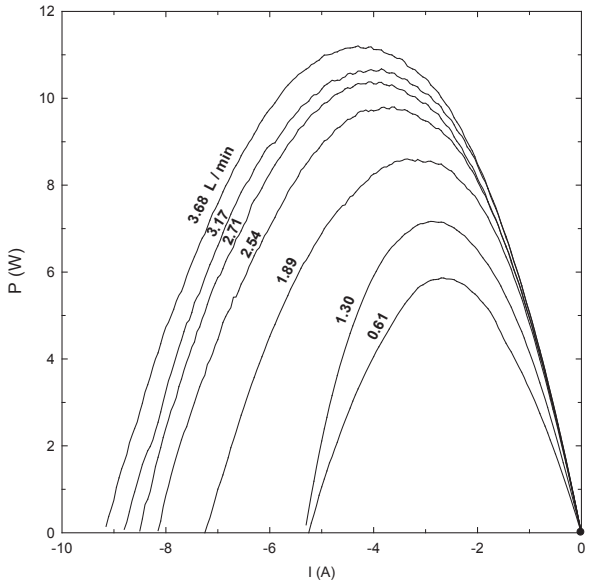

Figure 7.4. Power curves for a Qianqiu stack with 50 cells in the 'large stack'. Flow rates vary from 0.61 L/min (lowest line) to 3.68 L/min (upper line).

path 25 cm). On each flow rate, IE-curves were measured; E being the voltage measured on the reference electrodes and I the applied electrical current. The generated electrical power was obtained from the product of current and voltage and shown in *Figure 7.4* as a function of current density for various liquid flow rates.

Maxima of the power curves from *Figure 7.4* were used to determine power densities by dividing the power by the total active membrane area. The maximal power density proved to be 0.6 W/m^2 in the large stack and was achieved at a flow rate of 3.7 L/min or a linear velocity of 0.8 cm/s. Power densities are compared with data achieved in former experiments (*Chapter 5*) with a small stack with the same amount of cells (N=50). This showed that the large stack produced much lower power densities compared to the small stack. Although the membranes in this small stack are of a different type (Fumasep), this can not explain the differences because the membrane properties of both membrane pairs are comparable (*Chapter 6*).

However, if the power densities of both stacks are compared on basis of residence time (t_R), then the results become comparable. *Figure 7.5* shows the power density in the large stack (○) and in the small stack (●) as a function of the residence time. From this figure it is obvious that both cells deliver the same electrical power density (0.6 W/m^2) at a residence time of 30 s. *Figure 7.5* also shows the hydrodynamic losses in the large *(□)* and in the small

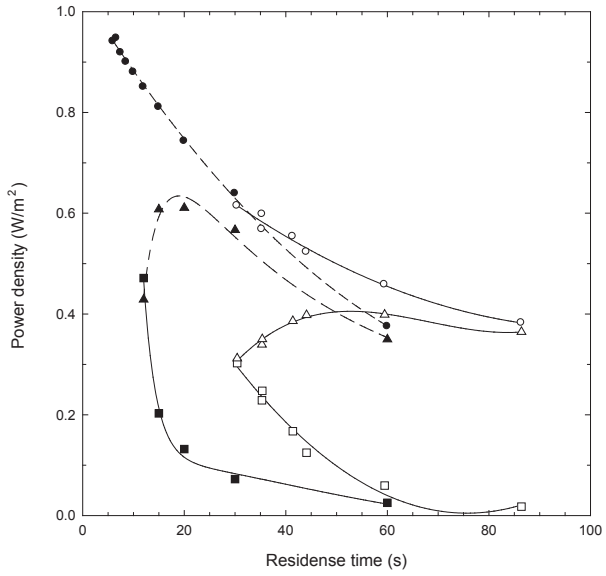

Figure 7.5. Generated electrical power density (○,●), hydrodynamic loss (□, ■) and net power density(Δ, ▲) in two different stacks, each with 50 cells: (a) Large stack with Qianqiu membranes (open symbols and solid regression lines) and (b) Small cell with Fumasep membranes (filled symbols and dashed regression lines).

stack *(■)*. Due to the longer flow path in the large stack, the hydrodynamic losses are also larger in this stack. Higher flow rates could not be obtained in this stack due to the higher hydrodynamic resistances in the large stack, and therefore residence times are generally higher.

Net power density, which is the difference between power density and hydrodynamic loss, is plotted in *Figure 7.5* for the large (Δ) and the small stack (▲). For the large stack a maximal net power density of 0.4 W/m^2 is achieved at a residence time of 50 s and the hydrodynamic loss is 13 % from the generated electrical power. For the small stack the maximal net power density of 0.6 W/m^2 is obtained at a residence time of 20 s and the hydrodynamic loss is 18%.

Figure 7.6 compares data of experiments with different process parameters. First, there is the small stack (□) equipped with Fumasep membranes and the large stack (Δ, ◊ and x) with Qianqiu membranes. Second, the flow directions are varied: the small stack (□) is operated in cross-current flow (the direction of the sea water and river water are perpendicular) and the large cell is operated with co-current flow (Δ and ◊) or with counter-current flow (x). Third, the number of cells differs: some experiments are performed with 25 cells (□ and Δ) other with 50 cells (◊ and x).

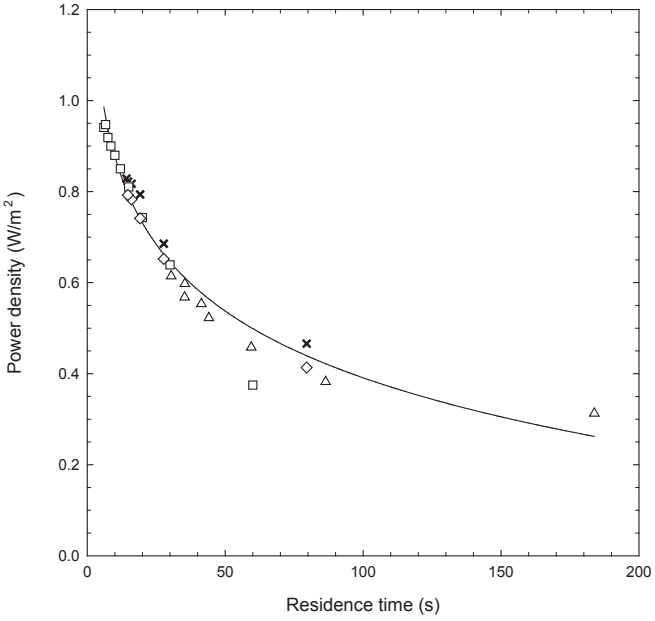

Figure 7.6. Power densities of different stacks and different operational modes. □: small stack (10x10cm^2), 50 cells, Fumasep membranes, cross current; Δ: large stack (25x75 cm^2), 50 cells, Qianqiu, co-current, ◊: large stack, 25 cells, Qianqiu, co-current, x: large cell, 25 cells, Qianqiu, counter-current. The logarithmic regression line is added to guide the eye.

The main conclusion from *Figure 7.5* and *Figure 7.6* is that the residence time is the key parameter governing the power density. The generated electricity in different stacks with the same spacers is largely independent of flow direction, membranes, cell dimensions and the number of cells. The small influence of the flow direction is discussed in 7.*4.1.2*. The independence of the membranes is most likely due to comparable membrane properties (electrical resistance, permselectivity) (*Chapter 6*) and by the fact that the electrical cell resistance is mainly determined by the electrical resistance of the river water compartment (*Chapter 5*). The effect of the number of cells in a stack (N) is probably too small for the two applied values of N (N=25 and N=50) to give different results due to shortcut currents (*Chapter3*).

Moreover, it is found that the application of spacers of 200 μm in combination with a flow path length of 25 cm causes unacceptable friction losses. With a thicker spacer these losses can be reduced; however, due to the increased electrical resistance of the river water compartment, the net power will be lower than the net power of the small stack.

7.4.1.2. Effect of the residence time on the energy efficiency

At low flow rates (long residence times), it is expected that the energy efficiency is maximal because the equilibrium concentrations can be approached and hydrodynamic power losses are minimal. However, at very low flow rates, losses due to co-ion transport and osmosis start to play a significant role (*Chapter 6*). Therefore, also for maximal energy efficiency, there exists an optimal flow.

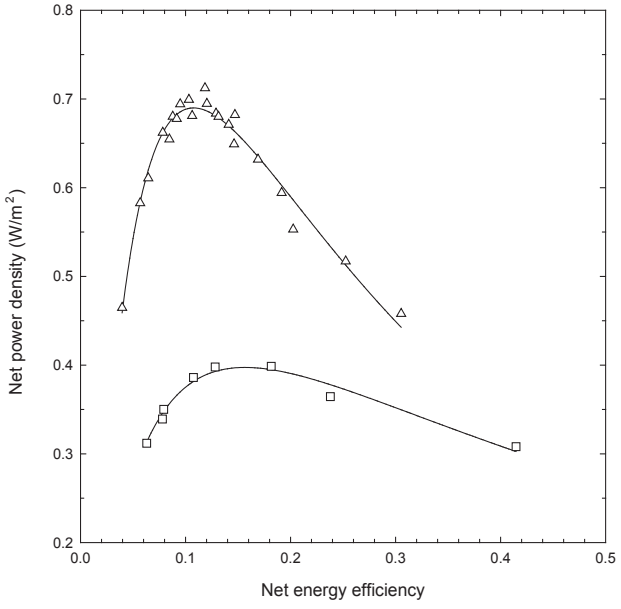

Figure 7.7. Net power density as function of the net energy efficiency in the small stack (Δ) and in the large stack (□).

Figure 7.7 shows the net energy efficiency (Y_{net}) of a small stack and a large stack on as a function of the delivered net power ($P_{d\text{-}net}$) It should be emphasized that all power measurements were done at maximal power density. At these conditions only 50% of the potential power is harvested. This can be explained with a classical electric cell model with an internal electrical resistance (R_i) and an electrical load R_u. Maximal power is delivered on R_u if R_u=R_i. In this case the 50% of the electricity is dissipated in R_i, the other 50% utilized in R_u (*Chapter 6*).

If maximal power is required, *Figure 7.7* is clear: the small stack performs the best. Maximal net power density for the small stack is 0.71 W/m^2, about twice the value of the large stack (0.40 W/m^2). The net energy efficiency is at this point for 12% for the small stack and 18% for the large stack; the part of energy lost in hydrodynamic friction is 13% respectively 16%.

Higher energy efficiency is possible by applying a lower flow rate. The upper graph of the small cell in *Figure 7.7* illustrates this: If a net energy efficiency is required of 30%, this is possible at the cost of a reduced net power density of 0.35 W/m^2.

7.4.2. Co-current or counter current

In many processes, like heat exchange and dialysis, the process can be performed in co-current and in counter-current mode. In most cases, counter-current operation is more efficient due to its higher driving force and it should be investigated whether this is also the case for RED.

Co-current and counter-current operation were tested in the large stack (*Figure 7.2* and *Figure 7.3*), equipped with 25 Qianqiu cells. The flow direction was vertical (flow path 25 cm); in the co-current mode, both sea and river water flow upwards and in the counter-current mode the direction of the river water flow is inverted. The electrode rinse solution contained NaCl (15 g/L) and the power was derived from the EI-curves. *Figure 7.8* shows the generated power density for both flow directions *Figure 7.8* shows that co-current operation yields a little higher power densities (about 0.05 W/m^2) compared to counter current flow. This is at first sight rather surprising, because in many processes, counter-current operation is more efficient.

A part of the explanation of this behavior is the existence of two counteracting effects on the generated power density in the cell. In co-current operation the generated voltage is maximal near to the inlet. However, the conductivity of the river water is small at this point, resulting in a rather small current. On the outlet side, the Nernst potential is lower

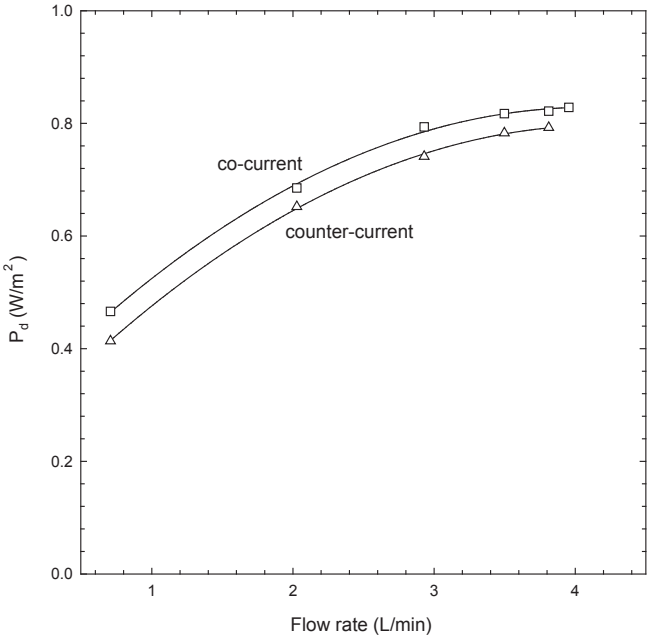

Figure 7.8. Co-current (□) and counter- current (Δ) operation of the large stack.

but the conductivity of the river water compartment is higher. This results in a relatively constant power density on each position in the cell. Another part of the explanation is the internal deformation in the stack. In counter-current operation the pressures between sea and river water compartments are very different; only in the middle of the stack, they are equal. Therefore, the spacers in the sea water compartments are compressed on one side of the stack and the river water spacers are compressed at the other side. This may result in local deformations of the flow path with an increase of the hydrodynamic loss and not optimal residence times.

The higher power densities in the co-current operation, have favorable implications on the design of large economical operated RED stacks. By using co-current feed, the pressure between the sea water and the river water compartments is very small. Therefore, leakage around the membranes in the surroundings of the manifolds inside the stack and leakage through pinholes in the membranes is minimal. Besides this, very thin and delicate low electrical resistance membranes can be used with the opportunity to give high power densities. For spacer materials the yielded profit is that they can be made with a delicate open structure, as necessary for low hydrodynamic losses, and are not compressed by high pressures differences.

In the small stack the supply of sea water and river water occurs through manifolds located near the corners and result in a diagonal flow direction (*Chapter 3*). The direction of the sea water flow is perpendicular to the river water flow. This 'cross-current' flow can be considered as intermediate between co- and counter-current operation and this holds also for the performance of a cross-current cell.

7.4.3. Segmentation of the electrodes

During the passage of the feed water through a RED stack, the salt concentration in the river water increases strongly whereas the relative decrease of the salt concentration in the sea water compartment is low. The consequence is that the electrical stack resistance on the inlet side of the river water is higher than on the outlet side. Because the ratio of the concentrations is the largest at the inlet side of the river water, the electromotive force (EMF) is maximal on this side. In order to generate maximal power density, the external load should be the same as the electrical stack resistance. It is evident that the value of the external resistance is a compromise and it is worth investigating whether it is possible to extract more power by means of dividing the electrode into a number of smaller electrodes, each with its own electrical load.

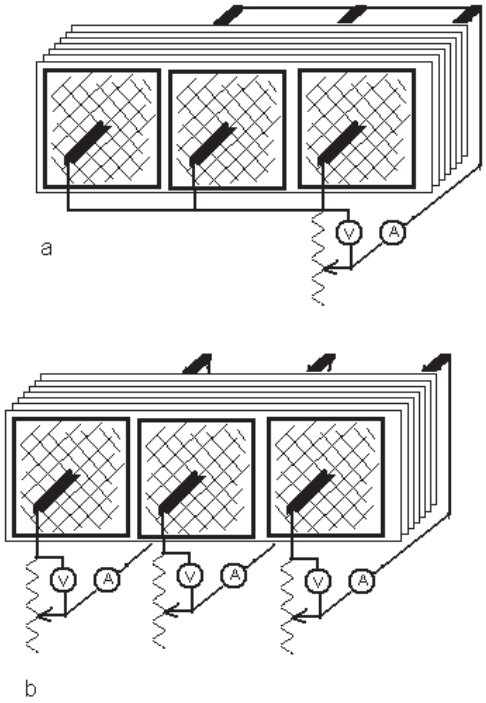

Figure 7.9. Unsegmented (top) and segmented (bottom) electrodes in a RED stack.

Horizontal operation of the large stack (with a flow path of 75 cm) enables experiments to study the effects of segmentation of the electrodes. *Figure 7.9(a)* shows the normal electrical connections of a single load to the large stack; there is effectively only one pair of electrodes. *Figure 7.9(b)* shows the connections of three slide rheostats to the three electrical separated segments. Each rheostat was adjusted in such a way that the power (the product of voltage and current) was maximal.

The system was equipped with variable resistors because otherwise three galvanostats and boosters should be used for this experiment. The consequence is that in this case an anolyte/catholyte should be used with a low overpotential and therefore minimal losses due to electrode reactions. Therefore, we used for this experiment the reversible $Fe(CN)_6^{4-}$ / $Fe(CN)_6^{3-}$ system (*Chapter 6*). The stack was operated with co-current feed in horizontal direction. Because the large stack consumes large quantities of feed water in this setup, we used another method to determine the power: first we measured the OCV (open circuit voltage) and after that we applied half of this value during some minutes until the current was constant.

The results are listed in *Table 7.1*. The power of an unsegmented stack is 8.23 Watt, whereas the power of the three segments of a system with divided electrodes is 4.30, 2.49 and 2.31 Watt, a total of 9.10 Watt or 11% more then in the unsegmented system. Because the stack was operated in horizontal direction with a long flow path and consequently high hydrodynamic losses, only relative low flow rates were possible. This implies relatively large concentration gradients along the flow paths in the stack. It is plausible that at higher flow rates – with more similar concentrations in the three parts - the effect of segmentation is less. Because segmentation requires additional complicated electronics, it may be questioned whether the small theoretical advantage also holds in practice.

Table 7.1. Segmentation of electrodes. The power of a unsegmented cell is 8.23 Watt, whereas the power of the three segments of a system with divided electrodes is 4.30, 2.29 and 2.31 Watt, a total of 9.10 Watt or 11% more.

		undivided	divided in 3 segments		
		parallel	segment 1	segment 2	segment3
open circuit voltage	(V)	4.88	5.35	3.89	3.50
terminal voltage	(V)	2.40	2.68	1.88	1.74
electrical current	(A)	3.42	1.60	1.33	1.33
generated power	(W)	8.23	4.30	2.49	2.31
internal resistance	(Ω)	0.71	1.67	1.47	1.32

7.4.4. Hydrodynamics; effect of flow path length

Hydrodynamic losses to and within the stack are important issues in the design of a RED generator. In this chapter we will focus on the stack and not on the supply of sea and river water from the sources (river and sea) to the stack. In our test equipment, pressure difference was measured between supply and drain, just outside the branching to the different inlets and outlets. Therefore, we measured pressure drop due to the fluid resistance in (i) the manifolds (the white tubing, visible in *Figure 7.2*), (ii) the bores through the stack, (iii) the spacer filled part of the compartments just around the supply and drain holes and (iv) the part of the spacer filled compartment where a rather uniform flow exists. Fluid resistance of the external tubing is negligible, because this system is well over-dimensioned. Likewise, the fluid resistance in the internal bore-holes is very low because these channels are only 3 cm deep. However, the resistance around the inlet and outlet holes in the spacer can be very high. All feed water enters the compartments radially from these holes with relative high fluid velocities[7]. We shall refer to this part as 'radial spacer resistance'. After passing some distance in the spacer filled compartment, the flow is reasonable uniform and we will call this 'uniform spacer resistance'.

The large stack makes it possible to distinguish between radial and uniform spacer resistance if vertical flow is compared with horizontal flow. The flow path in vertical direction is 25 cm and in horizontal direction 75 cm. However, the distance between the inlets (and also between the outlets) is the same in both directions.

Figure 7.10 shows pressure as function of the flow rate in the large stack for the two kinds of operation: horizontal (□) and vertical (Δ) (both in co-current mode). Data are obtained from different experiments. Regression lines are added to the figure: $y = 0.406x + 0.088$; $R^2 = 0.96$ for horizontal operation and $y = 0.169x + 0.005$; $R^2 = 0.93$ for vertical operation. The slope of the regression line for horizontal operation (0.406) is 2.4 times the slope for vertical operation (0.169). This is remarkable because at horizontal operation the length of the flow path is three times and the width of the flow path one third of the values at vertical operation (the reduction of the width causes a threefold fluid velocity at the same flow rate). If the 'uniform spacer resistance' contributes only to the total hydrodynamic resistance, a factor 9 should be expected.

As stated, a high fluid resistance is expected around the feed holes in the spacer material. In a specific compartment, the feed water enters the compartment at two places and leaves at two other outlet holes; in vertical operation there are 6 inlet and outlet holes. If these places would be the sole source of hydrodynamic resistance, we would expect a factor 3 for the slope ratio. The actual factor is close to this value and the conclusion is that

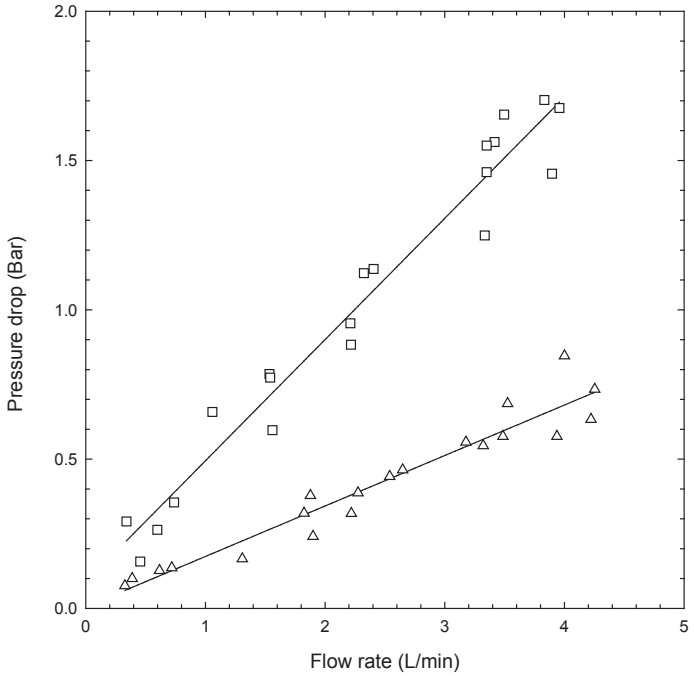

Figure 7.10. Pressure drop as function of the flow rate in the large stack for different lengths of the flow path. Squares (□) indicate horizontal operation (75 cm), triangles (Δ) vertical operation (25 cm). Data are obtained from different experiments as well as for sea water flow as for river water flow.

most of the fluid resistance can be ascribed to the direct surroundings of the inlet and outlet places within the spacer. Studies of Dirkse et al.[7] support this idea: pictures from modeled velocity fields show high velocities around these places.

There are some possible measures to decrease the fluid resistance. The total cross-sectional area of the supply and drain channels through the stack should not be increased, because in that case the effect of shortcut currents would be unacceptable (*Chapter 3*). However, it is possible to make more inlet and outlet places with the same total cross-sectional area. Another option is to use special very open spacers around the inlet and outlet holes.

7.4.5. Hydrodynamics; effect of spacer thickness

Spacer thickness is a key parameter in stack design. Although the fluid resistance can be decreased by application of thick spacers, the electrical cell resistance increases in that case and it is clear that there is an optimal spacer thickness for a given stack. However, the electrical area resistance is due to an ionic current perpendicular to the membranes and is independent of length and width of the cell, while the fluid resistance is lateral and increases with a longer flow path. Therefore, the optimal spacer thickness is dependent on the dimensions of the stack.

The effect of spacers was tested in the small stack. We equipped the small stack, containing 5 cells, successively with 200 µm and 100 µm spacers *(Table 7.2)*. The generated electrical power increased with 19% after the 200 µm spacers were replaced by the100 µm spacers. However, due the large hydrodynamic losses, this resulted in a negative net power. *Figure 7.11* shows a comparison between the hydrodynamic properties of the two spacers. The hydrodynamic resistance (as calculated from the average of the slopes of sea and river water flow) of the 100 µm spacer is 5.4 times higher than of the 200 µm spacer or 2.7 times higher if based on the same spacer thickness.

In order to compare the performance of the two spacer materials, which have different wire thicknesses and porosities, we determined the lateral transport through spacers (embedded between membranes). If there are two similar spacers A and B with thicknesses δ_A and δ_B, and wire diameter $\delta_A/2$ and $\delta_B/2$, the ratio of diameter of the water channels will be δ_A/δ_B. The straight lines in *Figure 7.11* indicate laminar flows within the compartments. Following the Hagen-Poiseuille equation for laminar flow, one may expect that at the same mean velocity, the relative pressure drop in A and B is $(\delta_B/\delta_A)^2$. In our case with

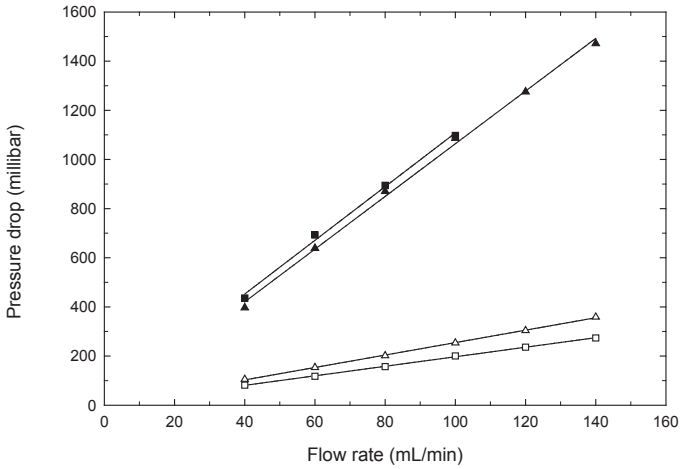

Figure 7.11. Pressure drop as function of the flow rate in the small stack for different spacer thicknesses. Squares (■, □) indicate sea water and triangles (▲, Δ) river water flow. Open symbols (□, Δ) refer to 200 µm and filled symbols (▲, ■) to 100 µm spacers.

Table 7.2. Used spacer materials. Spacers are woven from polyamide 6.6.

spacer type	thickness (µm)	porosity (%)	wire diameter (µm)
03-300/51	200	67	122
03-190/57	100	74	62

spacers of 100 µm and 200 µm we would expect a pressure drop factor of 4. We found only a factor 2.7. This may be ascribed to (i) the somewhat more open structure of the thin spacer (porosity 74%) in relation to the thick one (porosity 67%), (ii) deviations of the actual from the nominal spacer thickness and porosity in the tightly fastened stacks and (iii) the impossibility to use the Hagen-Poiseuille equation.

To verify the possibility of the existence of a laminar flow, the Reynolds number (Re), is calculated. Spacer filled compartments have some resemblance to packed beds and therefore we apply the concerning equation for Re[10]:

$$\mathrm{Re} = \frac{2}{3}\frac{\rho v_0 D_p}{\mu(1-\varepsilon)} \tag{9}$$

Here, ρ stands for density of the fluid, v_0 for superficial velocity (hypothetical velocity for the bed without filling but with the same volumetric flow rate), D_p for particle diameter, µ for dynamic viscosity and ε for porosity. Typical values in RED are: ρ=1000 kg/m^3, v_0=0.03 m/s, D_p=10^{-4} m, µ= 0.001 Pa·s and ε=0.7, resulting in Re=8. This value is low enough to ensure laminar flow, even around the inlet and outlet holes were the velocity may me much larger.

Although the packed bed theory was developed for more densely packed beds (0.35<ε<0.45) with spherical particles, we will use Ergun relation as an approximation of the pressure drop gradient (ΔP/L)[10]:

$$\frac{\Delta P}{L} = \frac{v_0^{\,2}}{D_p}\frac{1-\varepsilon}{\varepsilon^3}\left[170\frac{\mu}{v_0 D_p}(1-\varepsilon)+1.75\rho\right] \tag{10}$$

The left term between the brackets is due to laminar flow, the right term due to turbulence. With the typical RED values from the foregoing paragraph (v_0=0.03 m/s, D_p=10^{-4} m and ε=0.7) it proves that ΔP/L=1.0·10^5 Pa/m. For the 200 micron spacer we measured with the same velocity a pressure drop of 2.7·10^4 Pa. The distance between inlet and outlet hole is 0.15 m and the pressure gradient is, using this distance, 1.8·10^5 Pa/m. However, the concept of velocity is ambiguous in the small stack with a complicated velocity vector field and the calculated value is only an approximation.

It is more realistic to compare the two spacers if we assume that the velocity vector field in the two spacers is the same. With the discussed typical RED values it turns out that the contribution of the turbulence to the total pressure gradient is only 4% and therefore we can ignore the concerning part in *Eq. (10)*, resulting in:

$$\frac{\Delta P}{L} = \frac{v_0}{D_p{}^2} \frac{(1-\varepsilon)^2}{\varepsilon^3} 170\mu \quad (11)$$

For two spacers with the same porosity, the ratio of the pressure gradient is inversely proportional to $D_p{}^2$. With wire diameters of 62 μm and 122 μm for both spacers, the ratio is 3.9. However, the porosities are also different: ε=0.74 for the thin spacer and ε=0.67 for the thick spacer. With these different porosities the ratio is 1.8. The measured ratio is 2.4. The result of the Ergun equation is strongly dependent on the value of the porosity. Small variations in ε result in large deviations of dP/L; if taken the value ε =0.70 for the thin spacer in stead of ε =0.69, the result would be ΔP/L=2.5 Pa/m.

We conclude that:

- the pressure gradient is inversely proportional to the square of the wire thickness,
- deviations in our experiments from that relation can be probably ascribed to differences in porosity,
- an open spacer structure is very important for the pressure gradient.

7.4.6. Net power density and net energy efficiency in the large stack

For RED, there are three relevant response parameters: power, net power density and net energy efficiency. Power density and energy efficiency are counteracting to a certain degree and it can be questioned whether this also holds for *net* power density and *net* energy efficiency. For a high power density a rather constant concentration of sea and river water during the pass through the compartments is beneficial. This can be achieved by applying high flow rates. However, for the *net* power density ($P_{d\text{-}net}$) the hydrodynamic losses are subtracted from the power density and there should be an optimum flow rate. *Net* energy efficiency (Y_{net}) is dependent on $P_{d\text{-}net}$ and on the incoming exergy flow rate as stated in *Eq. (5)*. At high flow rates much of the exergy is unused but at low flow rates the effects of co-ion transport and osmosis result in irreversible mixing of the sea and river water. Therefore, also for Y_{net} there is an optimum flow. This may have implications for the design of the stack: optimal flow rates for a power full stack (high $P_{d\text{-}net}$) may be different for an energy efficient stack (high Y_{net}).

The experiments with the large stack enabled us to study the optimum residence time for both response parameters. In *4.2* we compared the net power density in the co-current mode with the counter-current mode. The effect on the power density seemed to be small and we pooled the results. In *4.4*. we investigated the pressure drop in vertical (25 cm) and horizontal (75 cm) operation. As stated in *4.2.1* the residence time is an important parameter for stack performance. Therefore, we made plots of net power density (*Figure 7.12*) and net energy efficiency (*Figure 7.13*) as function of the residence time.

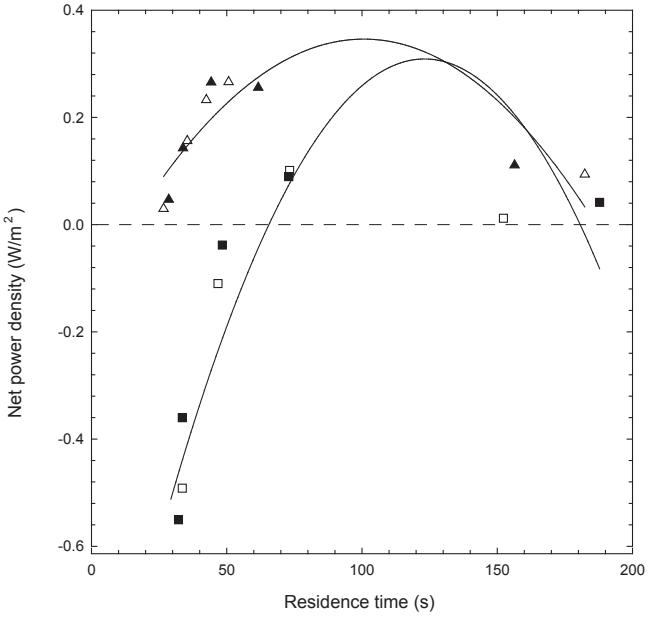

Figure 7.12 Net power density as function of the residence time. Triangles (▲, Δ) indicate vertical and squares (■, □) horizontal feed; open symbols (Δ, □) refer to co-current operation and filled ▲, ■) to counter current operation. The parabolic regression lines do not distinguish between co- and counter operation.

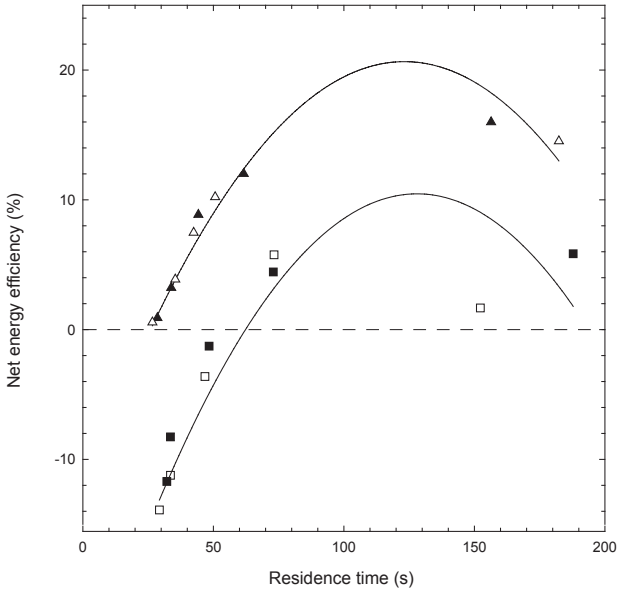

Figure 7.13. Net energy efficiency as function of the residence time. Triangles (▲, Δ) indicate vertical and squares (■, □) horizontal flow; open symbols (Δ, □) refer to co-current operation and filled symbols (▲, ■) to counter current operation. The parabolic regression lines do not distinguish between co- and counter operation.

As seen in *Figure 7.12* and in *Figure 7.13*, the maxima for net energy efficiency and for net power density were achieved at residence times between 100 and 130 s. This holds for horizontal as well as for vertical flow. The conclusion seems to be that optimizing with $P_{d\text{-}net}$ as response parameter gives roughly the same results as optimizing using Y_{net} for that purpose. To get a flexible design, suited on demand for power or for efficiency, a useful response parameter might be the response product $R_p = P_{d\text{-}net} \cdot Y_{net}$ (*Chapter 6*).

7.4.7. Thermodynamic efficiency of the large stack

In the theoretical section in this chapter, the thermodynamic efficiency η_T was introduced and defined in *Eq. (8)*. This variable is independent of hydrodynamic losses and also independent of electrode reactions because the stack voltage is measured using reference electrodes. Factors that affect η_T in a negative sense are fluid leakage, co-ion transport (*Chapter 6*), osmosis (*Chapter 6*), electrical power dissipation and parasitic currents (*Chapter 3*). Leakage can occur through pinholes in the membranes and around inlet and outlet holes. Electrical energy can be dissipated in the resistive parts of the cell: the membranes and the water compartments, especially the river water compartments. If power is generated at conditions of maximal power, the electrical resistance of the external load is equal to the internal resistance and only 50% of the exergy can be harvested (*Chapter 6*). *Figure 7.14* shows the thermodynamic efficiency η_T (as defined in *Eq. (7)*) for the four

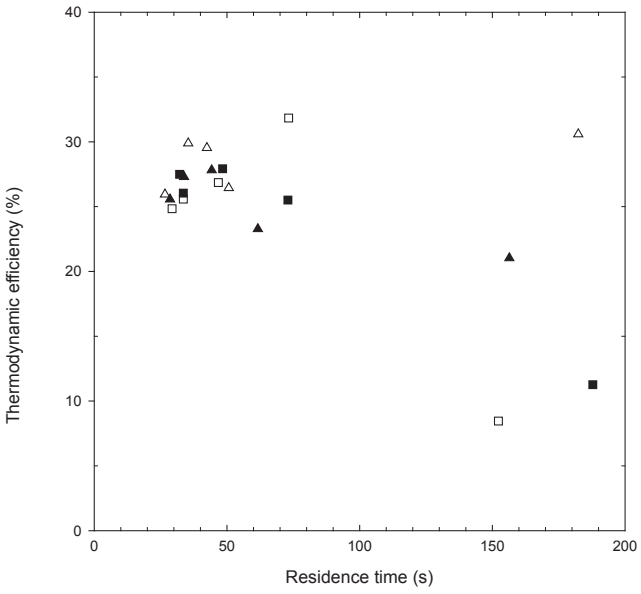

Figure 7.14. Thermodynamic efficiency as function of the residence time. Triangles (▲, Δ) indicate vertical and squares (■, □) horizontal feed; open symbols (Δ, □) refer to co-current operation and filled symbols (▲, ■) to counter current operation.

different cases. The value of η_T seems to be rather independent of flow direction and operational mode and is at lower residence times (t_R<100 s) in most cases between 25% and 30%.

With the same Qianqiu homogeneous membranes we formerly measured a thermodynamic efficiency of 21% in the small stack and the current data are consistent with this value. This is much less than the theoretical maximum of 50%. In the future, specially tailored membranes for RED should combine low electrical resistance with high permselectivity and low osmotic losses. If these membranes are combined with a thin, very open spacer for the river water compartment, is possible to achieve a higher thermodynamic efficiency.

7.5. Conclusions and outlook

1. For the objective of SGP, using the RED technology, we studied the effect of increasing the membrane size from 10x10 cm^2 to 25x75 cm^2. The key parameter on power density proved to be the residence time. In larger cells, with longer flow pathways, the linear velocity should be increased in order to maintain the same residence time. The consequence is that the hydrodynamic losses are higher in the enlarged cell. Larger cells demand thicker spacers for optimal performance, but the therewith introduced larger electrical resistance results in a lower generated electrical power.

2. In the large stack it was possible to compare co-current and counter-current operation. It appeared that the stack generated more power in co-current mode. This is an important result for further development of the RED technique because in the co-current mode, local pressure differences between sea and river water compartments are much smaller. Therefore, leakage around the internal manifolds is expected to be less. The same holds for leakage through possibly existing pinholes in the membranes. Low pressure differences permit also the use of very thin membranes (with low electrical resistance) as may be manufactured in the future for RED purpose. Another advantage is that delicate spacers with a very open structure (with low hydrodynamic losses) can be applied without being distorted by high pressure differences.

3. The power density of the stack is increased by segmentation of the electrodes. However, the effect is marginal and it should be questioned if the efforts made to do this, are economically justified.

4. A large part of the hydrodynamic spacer resistance is due to the inlet and outlet system. Attention should be paid to a more efficient system.

5. The relative effect of spacer thickness and porosity on the pressure gradient can be explained by the Ergun equation. For spacers with the same porosity, the pressure gradient is inversely proportional to the square of the wire thickness. The Ergun relation forecasts an extreme reduction in pressure if more open spacers are applied.

6. Maximum net power density and net energy efficiency are achieved with comparable residence times. A new response parameter (the response product) can be constructed by multiplying net power density and net energy efficiency. If the design is optimized for this response product, the stack is flexible enough to operate on demand for maximal net power density or for maximal energy efficiency.

7. A thermodynamic efficiency of about 20% - 30% has been measured, whereas 50% is the theoretical limit under conditions of maximal power. The low value can be ascribed to fluid leakage (through pinholes in the membranes and around inlets and outlets), co-ion transport, osmosis, electrical power dissipation (in the membranes and compartments) and to parasitic currents.

RED is a rather complex process with various electrical and hydrodynamic aspects. The response variables (power, power density and energy efficiency) are dependent on many input variables. In the next chapter, we will present a model which explains some of the properties and the behavior of the RED stack. With aid of such a model, it is possible to make a next step in the scaling-up process.

Acknowledgement

This work was performed in the TTIW-cooperation framework of Wetsus, centre of excellence for sustainable water technology (www.wetsus.nl). Wetsus is funded by the Dutch Ministry of Economic Affairs, the European Union Regional Development Fund, the province of Fryslân, the city of Leeuwarden and the EZ/Kompas program of the "Samenwerkingsverband Noord-Nederland". The first author would like to thank the Noordelijke Hogeschool Leeuwarden who facilitated this research by detaching him to Wetsus and the participants of the theme "Energy" theme for their fruitful discussions and their financial support. We thank the Redstack company for financing the large stack, Jan Valk for the making the CAD-CAM drawings of the large stack, Feiko Reinalda, Reinald de Jong, Jan Jansen and Tiara Stoker for their help with the experiments and Bertus Nobach for making Figure 3.

Nomenclature

A	total membrane area (m^2)
C	concentration (mol/m^3)
D_p	particle diameter (m)
I	electrical current (A)
J	electrical current density (A/m^2)
L	length of flow path (m)
N	number of cells in a stack
P_u	generated electrical power (W)
P_{hydr}	hydrodynamic loss (W)
P_d	power density (W/m^2)
$P_{d\text{-}net}$	net power density (W/m^2)
ΔP	pressure drop (Pa)
R	gas constant (8.314 $J{\cdot}mol^{-1}K^{-1}$)
R_i	internal resistance of a RED stack (Ω)
R_u	external load on a RED stack (Ω)
R_P	response product (W/m^2)
Re	Reynolds number
t_R	residence time (s)
X^i	exergy flow rate to the inlet (W)
X^o	exergy flow rate from the outlet (W)
Y	energy efficiency
Y_{net}	net energy efficiency
v	mean fluid velocity (m/s)
v_0	superficial velocity (m/s)

Greek symbols

Δ	spacer thickness (m)
ε	porosity (voidance)
η_T	thermodynamic efficiency
Φ	flow rate (m^3/s)
μ	dynamic viscosity (Pa·s)
ρ	density (kg/m^3)

Abbreviations

AEM	anion exchange membrane
CEM	cation exchange membrane
EMF	electromotive force (V)
RED	reverse electrodialysis
OCV	open circuit voltage
PRO	pressure retarded osmosis
SGP	salinity gradient power

Definitions

compartment	space between the membranes
cell	combination of two membranes and two compartments
electrode system	the anode, cathode and electrode rinse
segment	part of an electrode
stack	a number of N cells with an electrode system

References Chapter 7

1 G.L. Wick, W.R. Schmitt, *Prospects for renewable energy from sea.* Mar. Technol. Soc. J. 11 (1977) 16-21

2 J.W. Post, J. Veerman, H.V.M. Hamelers, G.J.W. Euverink, S.J. Metz, K. Nymeijer, C.J.N. Buisman, *Salinity-gradient power: Evaluation of pressure-retarded osmosis and reverse electrodialysis.* J. Membr. Sci. 288 (2007) 218-230

3 J.W. Post, H.V.M. Hamelers, C.J.N. Buisman, *Energy recovery from controlled mixing salt and fresh water with a reverse electrodialysis system.* Environ. Sci. Technol. 42 (2008), 5785-5790

4 J.W. Post, H.V.M. Hamelers, C.J.N. Buisman, *Influence of multivalent ions on power production from mixing salt and fresh water with a reverse electrodialysis system.* J. Membr. Sci. 330 (2009) 65-72

5 P. Długołęcki, K. Nymeijer, S.J. Metz, M. Wessling, *Current status of ion exchange membranes for power generation from salinity gradients.* J. Membr. Sc. 319 (2008) 214-222

6 P. Długołęcki, A.Gambier, K. Nijmeijer, M. Wessling, *Practical potential of reverse electrodialysis as process for sustainable energy generation.* Environ. Sci. Technol. 43 (2009) 6888-6894

7 M.H. Dirkse, W.P.K. van Loon, J.D. Stigter, J.W. Post, J. Veerman, G.P.A. Bot, *Extending potential flow modelling of flat-sheet geometries as applied in membrane-based systems.* J. Membr. Sci. 325 (2008) 537-545

8 C. Forgacs, *Generation of electricity by reverse electrodialysis.* BGUN-RDA – 178-78 Ben-Gurion University, Israel (1978)

9 C. Forgacs, R.N. O'Brien, *Utilization of membrane processes in the development of non-conventional renewable energy sources.* Chem. Can. 31 (1979) 19-21

10 W.J. Beek, K.M.K. Muttzall, J.W. van Heuven, *Transport phenomena*. John Wiley and Sons Ltd., (1999), 2nd ed.

Chapter 8

Modeling the performance of a reverse electrodialysis stack*

Abstract
Reverse electrodialysis (RED) is a technology to generate electricity using the entropy of mixing of sea and river water. A model is made of the process and this model is validated experimentally with various laboratory scale stacks and for various feed flow directions (co-current, counter-current and cross-current) and related to segmentation of the electrodes (single electrodes and electrodes divided into a number of segments). Input parameters are salt content and flow rate of the sea and river input streams, thickness and lengths of the compartments and various membrane properties (area resistance, NaCl and H_2O diffusion constants); response parameters are the delivered electrical power density and outlet concentrations. The model is in good agreement with the experiments.

The model is then used to design and optimize the RED process. The used response parameters for optimizing the cell dimensions and feed water flow rates are the net power density (the generated net power per m^2 membrane in W/m^2) and the net river water yield (the net amount of generated energy from 1 m^3 river water and an optimal amount of sea water in J/m^3).

The model predicts very small differences between counter- and co-current operation. It was decided to focus on co-current design because co-current operation causes smaller local pressure differences between the river and sea water compartments - hence smaller risk of leakages and the possibility to use very thin membranes with high fluxes and very open spacer structures with low hydrodynamic resistance.

Segmentation of the electrodes proved to increase the power density by about 15% under realistic operational conditions. As segmentation of the electrodes requires complicated electrical provisions, it was decided to design a system with undivided electrodes.

The model shows that with smaller systems - in terms of length of the flow path - higher power densities are possible. This effect is rather dramatical and poses a challenge for designing improved RED stacks on large commercial scale. It is suggested to reduce the flow path length by applying a fractal structure design of the spacers. Such structures can be made by profiling the membrane.

*** Submitted in condensed form to the Chemical Engineering Journal as:**
J. Veerman, M. Saakes, S.J. Metz and G.J. Harmsen
Reverse electrodialysis: a validated process model for design and optimization

8.1. Introduction

Salinity gradient power using river and sea water is a clean and sustainable source of energy. The recommended technology for harvesting this energy is reverse electrodialysis (RED)[1]. In the previous chapters, we presented our lab scale experimental results with a small cell (10x10 cm^2, 50 cells) (*Chapters 3, 5* and *6*) and with a large stack (25x75 cm^2; 50 cells) (*Chapter 7)*. In this chapter we describe a process model containing all key elements of hydrodynamics, membrane transport and the electrode system. This model is first validated with the experimental data of our various test facilities for all key parameters and then it is used to design and optimize a commercial scale RED process.

To clarify the subject of investigation in this chapter, first we will describe all essential elements. *Figure 8.1a* shows a RED stack, consisting (from left to right) of an anode, a number of alternately stacked anion exchange membranes (AEM) and cation exchange membranes (CEM), and a cathode. The compartments between the membranes are fed with sea and river water; the compartments between electrodes and outer membranes contain the electrode rinse solution which is circulated through anode and cathode compartments. The cells – consisting of an AEM, a sea water compartment, a CEM and a river water compartment - are the repeating units in a stack; the number of cells (N) may be small in a test setup or large (hundreds up to thousands) in a real economically operating stack. Cations from the sea water diffuse through the CEMs to the river water compartment and build up a positive potential on the cathode. The anions from the sea water diffuse through the AEMs to the river water compartment on the other side and cause a negative potential on the anode. Electrical power can be extracted from the system by an external circuit connected to the electrodes. The ionic current within the cells is then converted to an external electron current via redox reactions at the electrodes. These electrodes can be undivided as shown in *Figure 8.1a* or divided into some segments as shown in *Figure 8.1b*. With the undivided electrodes, there is only one load (i.e. an external resistance) R_u; in the system with the segmented electrodes, each electrode has its own load.

8.2. Process model description

8.2.1. Response variables

In a RED stack, there are three key response parameters. The first is the net produced power P_{net}, being the produced electrical power P_u minus the hydrodynamic loss P_{hydr} :

$$P_{net} = P_u - P_{hydr} \tag{1}$$

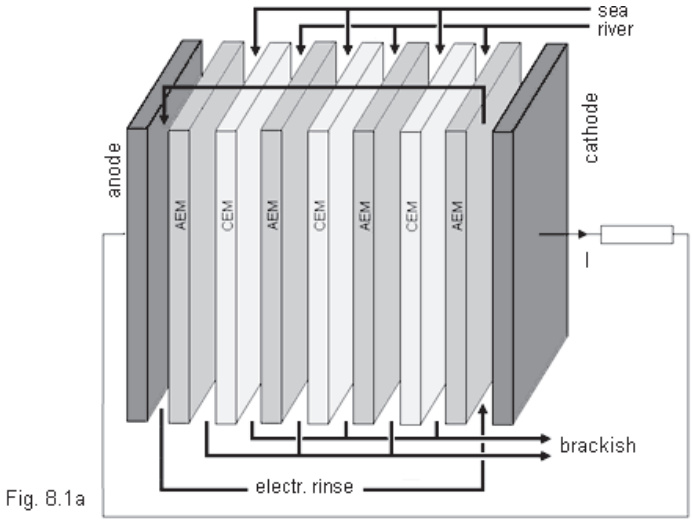

Fig. 8.1a

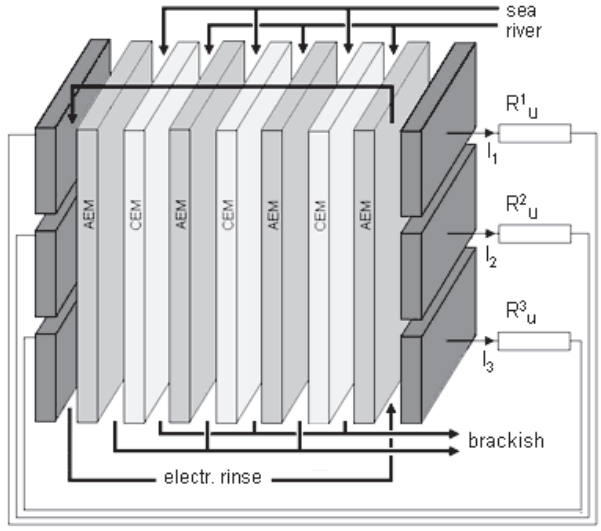

Fig. 8.1b

Figure 8.1. A RED stack with three cells.
Figure 8.1a. The stack with undivided electrodes and one external load R_u.
Figure 8.1b. The stack with electrodes divided into three segments and three loads (R^1_u, R^2_u and R^3_u).

P_u is the product of the voltage (U) over an external resistor and the current (I) through that resistor:

$$P_u = UI \tag{2}$$

P_{hydr} is the product of the pressure drop over the stack (ΔP_S and ΔP_R) and the flow rate (Φ_S and Φ_R) for the two feeds:

$$P_{hydr} = \Delta P_S \Phi_S + \Delta P_R \Phi_R \quad (3)$$

The second important response parameter is the power density P_d, the produced electrical power divided by the total (AEM and CEM) membrane area A_m. For the net power density P_{d-net}, this value is corrected for the hydrodynamic loss:

$$P_d = \frac{P_u}{A_m} \quad ; \quad P_{d-net} = \frac{P_{net}}{A_m} \quad (4, 5)$$

Power density is an important parameter, because the membrane area is related to the total investment costs of a RED power plant.

From the starting point that the availability of river water is the limiting factor, it is useful to define an efficiency measure directly from the consumed amount of river water. We call it 'net river water yield' (Z_{net}).

$$Z_{net} = \frac{P_{net}}{\Phi_R} \quad (6)$$

Maximization of Z_{net} may result to unpractical values: very long residence times in combination with low power densities. Therefore, we introduce the response product R_{PZ}:

$$R_{PZ} = P_{d-net} \cdot Z_{net} \quad (7)$$

8.2.2. Overview of the modeling of mass and charge transport, equivalent electrical circuits of systems with undivided and with segmented electrodes.

In order to simulate the performance of a RED stack, the transport of counter-ions through the membranes should be calculated: Na^+ through the CEMs and Cl^- through the AEMs from the sea water into the river water compartments. Two disturbing effects should be taken into account: co-ion transport (Na^+ through the AEMs and Cl^- through the CEMs) in the same direction and osmosis (H_2O transport from the river water to the sea water compartments). Of special interest are the influence of the flow direction (co-current or counter-current) and the degree of segmentation of the electrodes (n_e=1: undivided or n_e>1: segmented). We will focus on a single RED cell; effects of parasitic currents - as can be found in stacks with more cells - are not included in this model but were object of a former study (*Chapter 3*). This and the following sections will describe the system and the equations used to define the model and derive the properties of the model.

Figure 8.2 shows a single RED cell, consisting (from left to right) of an AEM, a sea water compartment, a CEM and a river water compartment. In the picture the AEM of the adjacent cell is drawn with dashed lines. The dimensions of the stack are described by

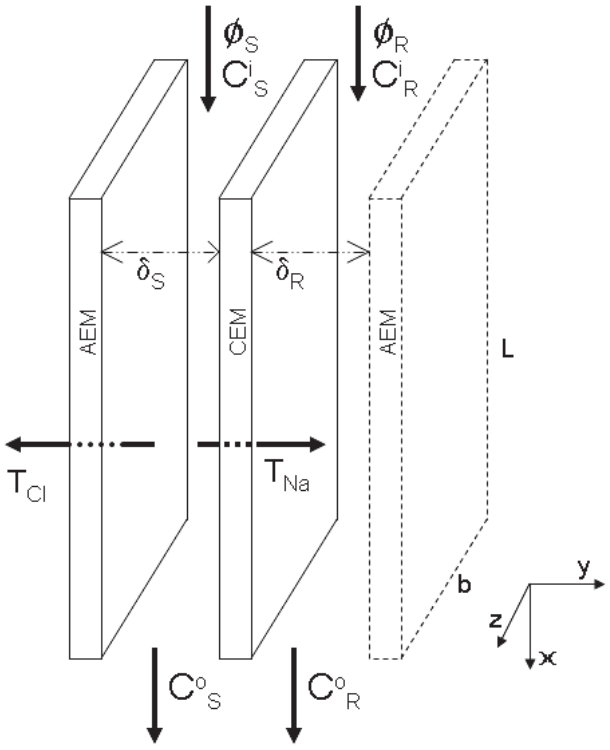

Figure 8.2. One cell in a RED stack. The solid part is the repeating unit; the dashed membrane is part of the adjacent cell.

length (L), width (b), thickness of sea water compartment (δ_S) and thickness of the river water compartment (δ_R). Flow rates of sea and river water are designated by Φ_S and Φ_R and input concentrations by C^i_S and C^i_R.

The cell of *Figure 8.2* is operated in co-current mode; near the feed water inlets, the electrical resistance is determined by the resistance of the river water compartment (the resistance of the river water is much higher than of the seawater). During the passage of the feed water through the cell, the salt concentration of the sea water decreases and of the river water increases. The consequences are (in the direction of the flow) a decreasing electrical cell resistance and a decreasing voltage. In most test stacks, all parts of the stack share the same electrodes (n_e=1) as shown in *Figure 8.1a*. This situation is not optimal because for maximal power the resistance of the load should be equal to the internal resistance. In the worst case it is imaginable that the upper part of the cell generates power, the middle part does nothing and the lower part acts in the reverse direction (like a normal electrodialysis (ED) unit).

In principle, the stack can be improved by electrode segmentation. In *Figure 8.1b* the electrode is divided into three parts (n_e=3), each with its own load (R_u). Maximal power is generated if each load R_u equals the internal resistance R_{cell} of a specific part of the RED cell (*Chapter 3*). Theoretically, the more the electrode is segmented, the higher the efficiency. In the following sections, a model is developed for both extreme cases: systems with unsegmented electrodes and systems with indefinitely segmented electrodes. The equivalent electrical circuits of systems with undivided and with segmented electrodes are shown in *Figure 8.3a* and *Figure 8.3b*.

8.2.3. Modeling of the salt and charge transport in a system with infinite segmented electrodes

Electrodes can be undivided as in *Figure 8.1a* and *Figure 8.3a* or segmented into three parts as in *Figure 8.1b* and *Figure 8.3b* or segmented to another degree (n_e). First we will present the theory for a system with an infinite degree of segmentation (n_e=∞), each segment with its own external load. This gives a simple continuous model by which several effects

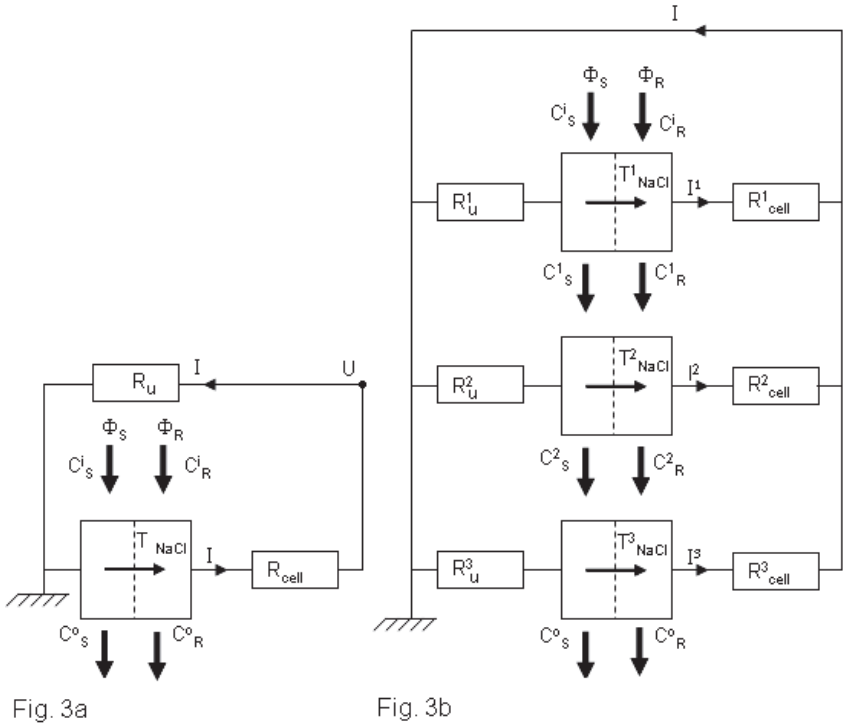

Figure 8.3 a/b. A RED cell in co-current operation.
Figure 8.3a With undivided electrodes and one external load R_u,
Figure 8.3b With 3 separate electrodes and 3 external loads, R^1_u, R^2_u and R^3_u. In the counter-current operation mode, the direction of the river water (Φ_R) is inverted.

of design variables on the response variables can be studied. The system of differential equations is programmed in *Berkeley Madonna (Chapter 8: Appendix A)*. *Section 8.2.5* explains how this program can be adapted to an undivided electrode system (n_e=1). The extreme values of the segmentation number (n_e=1 and n_e=∞) are sufficient for general conclusions concerning segmentation. In *Section 8.3.2.3* the effect of intermediate values of the segmentation number (n_e=1..7) on the power density is discussed.

In the first order approximation, it is assumed that the salt concentration in the compartments of the cell is uniform in the direction perpendicular to the membranes. Transport of salt from the seawater to the riverwater compartments is caused by diffusion of Na^+-ions through the CEM and of Cl^--ions through the AEM. In real membranes there is also a small co-ion transport: the diffusion of the ions through the 'wrong' membranes.

We describe the performance of the RED cell with the following system of 11 equations. Most variables are dependent on the place in the cell, expressed by x (x=0..L). The first of these equations (*Eq. (8)*) is the expression of the electromotive force of the cell (E_{cell}). This voltage is the sum of the Nernst potential difference over the CEM and over the AEM (*Chapter 3*).

$$E_{cell}(x) = \alpha_{CEM}\frac{RT}{F}\ln\frac{\gamma_S^{Na}(x)C_S(x)}{\gamma_R^{Na}(x)C_R(x)} + \alpha_{AEM}\frac{RT}{F}\ln\frac{\gamma_S^{Cl}(x)C_S(x)}{\gamma_R^{Cl}(x)C_R(x)} \tag{8}$$

In this expression, R is the gas constant (8.314 $J{\cdot}mol^{-1}K^{-1}$), T is the temperature and F is the Faraday number (96485 $C\,mol^{-1}$); α is the permselectivity of the membrane, a measure for the specificity of the membrane for the permeability of counter-ions. Concentrations (in mol/m^3) are denoted by C and activity coefficients by γ. Subscripts S and R indicate 'sea' and 'river'.

Activity coefficients are also dependent on the position in the cell and are obtained with the extended Debye-Hückel equation[2]:

$$log(\gamma(x)) = \frac{-0.51z^2\sqrt{\mu_{ion}(x)}}{1+\frac{A}{305}\sqrt{\mu_{ion}(x)}} \tag{9}$$

where γ is the activity coefficient of the ion, μ_{ion} the ion strength of the solution (mol/L), z the valency and A the effective hydrated ion radius in pm (A_{Na+}=450 pm and A_{Cl-}=300 pm).

The ionic strength μ is calculated from the molar concentration C_i and the valency z_i of

each ion. Because pure NaCl solutions are studied, the value of the ion strength is equal to the concentration in mol/L (z_i^2=1 for Na^+ and Cl^-). The factor 1000 is introduced to convert concentrations in mol/m^3 into the standard unit of mol/L as used usually in the ion strength.

$$\mu_{ion}(x) = \frac{1}{2}\sum_i z_i^2 \frac{C_i(x)}{1000} = \frac{C(x)}{1000} \tag{10}$$

The method holds for solutions to about 500 mol/m^3 (roughly the salt concentration in sea water).

From the molar conductivity Λ_m of a NaCl solution, the space dependent area resistances of the sea and river water compartments -$R_{a,S}(x)$ and $R_{a,R}(x)$- are calculated. In fact, Λ_m is dependent on the concentration C, but if a correct value of Λ_m is used for low concentrations, the calculated resistance of the river water compartment is reliable; the resistance of the sea water compartment, being much lower, has less influence on the total resistance:

$$R_{a,S}(x) = f\frac{\delta_S}{\Lambda_m C_S(x)} \quad ; \quad R_{a,R}(x) = f\frac{\delta_R}{\Lambda_m C_R(x)} \tag{11, 12}$$

In this equation δ_S and δ_R are the thicknesses of the sea and river water compartment (*Figure 8.2*). The obstruction factor f is a measure for the increase of the electrical resistance due to the negative effects of the spacer (tortuosity of the ion path, decrease of the amount conducting solution and shielding the membrane).

The area cell resistance is the sum of the compartment area resistances -$R_{a,S}(x)$ and $R_{a,R}(x)$- and the membrane area resistances (R_{AEM} and R_{CEM}).

$$R_{a,cell}(x) = R_{a,S}(x) + R_{a,R}(x) + R_{AEM} + R_{CEM} \tag{13}$$

For maximal power, the external resistance (load) should be equal to the internal resistance. Because the internal resistance of the cell is space dependent, the load ($R_{a,u}(x)$) should also be space dependent. This load – expressed in units of area resistance (Ωm^2) – is varying continuously in the x-direction:

$$R_{a,u}(x) = R_{a,cell}(x) \tag{14}$$

The current density (J) is now achieved with Ohm's law:

$$J(x) = \frac{E_{cell}(x)}{R_{a,cell}(x) + R_{a,u}(x)} \tag{15}$$

Salt transport from sea to river water compartment, T_{total}, is composed of a Coulombic part (T_{coul}) and a part due to co-ion transport, (T_{cit}). The Coulombic part is equal to J/F, where F is the Faraday constant (96485 C/mol). The co-ion transport can be obtained from the NaCl diffusion constant for the membranes (D_{salt}), the membrane thickness (δ_m). The factor 2 is due to the fact that the there are two membranes in a cell.

$$T_{total}(x) = T_{coul}(x) + T_{cit}(x) = \frac{J(x)}{F} + \frac{2D_{NaCl}}{\delta_m}\left[C_S(x) - C_R(x)\right] \tag{16}$$

This transport of NaCl causes changes in the sea and river water concentrations, determined by the mass balance equations:

$$\frac{d}{dx}C_S(x) = -\frac{b}{\Phi_S}T_{total}(x) \quad ; \quad \frac{d}{dx}C_R(x) = \frac{b}{\Phi_R}T_{total}(x) \tag{17, 18}$$

In these equations, Φ_S and Φ_R are the flow rates of sea and river water. In co-current operation, they have positive values; in the case of counter-current operation we assign a negative value to Φ_R.

The system – described by the equations 8 to 18 – is numerically solved with the program *Berkeley Madonna (Chapter 8: Appendix A)*. In the co-current mode, input concentrations $C_S(0)$ and $C_R(0)$ should be specified. In the counter-current mode (with a negative sign for the river water flow rate Φ_R) the significance of $C_R(0)$ in the model is the outlet concentration of the river water and the input concentration is given by $C_R(L)$; by adjusting $C_R(0)$ the specified input concentration $C_R(L)$ can be obtained.

Once the system is solved, the produced external power density function $P_d(x)$ is given by:

$$P_d(x) = \frac{1}{2}J^2(x)R_{a,u}(x) \tag{19}$$

The factor ½ is due to the double membrane area (CEM and AEM) in a cell. The total developed power P_{total} is obtained by integration over the length L in the x-direction:

$$P_{total} = b\int_o^L P_d\,dx \tag{20}$$

This results in an average power density ($\overline{P}_d$):

$$\overline{P_d} = \frac{P_{total}}{Lb} \tag{21}$$

Supply of feed water is expressed as flow rates Φ (m^3/s) or in velocities (m/s) or in the reverse unit residence time (t_R). For a compartment with dimensions L, b and δ:

$$v = \frac{\Phi}{Lb} \quad and \quad t_R = \frac{Lb\delta}{\phi} \tag{22, 23}$$

8.2.4. Correction of the model for the effects of water flow through the membranes by osmosis

Opposite to the salt flux, there is a water flux (T_{water}) due to osmosis (*Chapter 6*) of water from the river water compartment to the sea water compartment (analogous to the second term in *Eq. (16))*:

$$T_{water}(x) = -\frac{2D_{water}}{\delta_m}\left[C_S(x) - C_R(x)\right] \tag{24}$$

D_{water} stand for the diffusion constant of water in the membranes. The flux in *Eq. (24)* is expressed in $mol \cdot m^{-2} \cdot s^{-1}$. To convert this to a volumetric flux (T'_{water}), a factor M_{H2O}/ρ_{H2O} (molar mass over density) is added; in fact, this volumetric water flux is the superficial water velocity through the membrane.

$$T'_{water}(x) = -\frac{2D_{water}}{\delta_m}\left[C_S(x) - C_R(x)\right]\frac{M_{H2O}}{\rho_{H2O}} \tag{25}$$

The effect of salt transport on the concentrations in sea and river water is symmetric: If 0.1 gram NaCl is transported from 1 L sea water (30 g/L) to 1 L river water (1 g/L), the new concentrations are 29.9 and 1.1 g/L: the decrease in sea water equals the increase in river water. On the other hand, if 100 mL water is transported by osmosis in the opposite direction, the new concentrations are 30/1.1=27.3 and 1/0.9=1.11 g/L. In this case the concentration change in the sea water is much larger than in the river water.

Osmosis affects – in principle - salt concentrations as well as feed water flow rates. The impact of the concentration change on the stack performance is much larger. A typical value of the osmotic flux is about 10 $mmol \cdot m^{-2} \cdot s^{-1}$ (*Figure 6.5 in Chapter 6*), which is equivalent to a velocity of $2 \cdot 10^{-7}$ $m \cdot s^{-1}$. The feed water velocities through the compartments are typical 0.01 $m \cdot s^{-1}$, hence a factor 10^5 higher.

Therefore, we ignore the flow rate change during the passage of the cell and calculate

only the effect on the concentration.

Figure 8.4 shows the flow rate balance. The osmotic flow ($d\Phi_{osm}$) from the river water compartment (left) is directed through a small area of membrane ($dA = b \cdot dx$) to the sea water compartment (right). The osmotic flow rate is:

$$d\Phi_{osm} = b \cdot T'_{water} \cdot dx \tag{26}$$

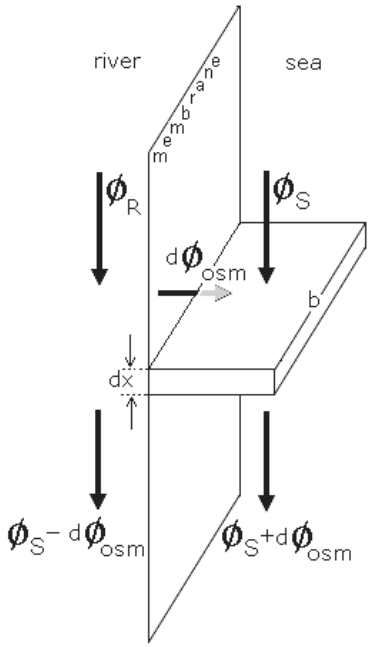

Figure 8.4. Flow rate balance; an osmotic flow $d\Phi_{osm}$ is directed from the river water compartment (left) through the membrane to the sea water compartment (right).

The incoming salt flow rate is $\Phi_S C_S$ (mol/s). This amount of salt also leaves the slice. In this place the concentration is given by:

$$C_S(x+dx) = \frac{\Phi_S C_S(x)}{\Phi_S + d\Phi_{osm}} = C_S(x) \frac{1}{1 + \frac{d\Phi_{osm}}{\Phi_S}} \approx C_S(x)\left(1 - \frac{d\Phi_{osm}}{\Phi_S}\right) \tag{27}$$

$$dC_S(x) = -C_S(x) \frac{d\Phi_{osm}}{\Phi_S} = -C_S(x) \frac{b \cdot T'_{water}}{\Phi_S} dx \tag{28}$$

For the increase of the salt content in the river water compartment, an analogous expression can be derived. To incorporate the effect of osmosis *Eq. (25)* should be added to the model *(*as described in *2.2.1) and Eq. (17)* and *Eq. (18)* should be replaced by:

$$\frac{d}{dx}C_S(x) = -\frac{b}{\Phi_S}T_{total}(x) - C_S(x)\frac{b \cdot T'_{water}}{\Phi_S} \tag{29}$$

and by

$$\frac{d}{dx}C_R(x) = \frac{b}{\Phi_R}T_{total}(x) + C_R(x)\frac{b \cdot T'_{water}}{\Phi_R} \tag{30}$$

8.2.5. Modeling of the system with undivided electrodes

The principle of this arrangement is shown in *Figure 8.3a*. The left electrode (anode) is grounded and the potential on the cathode (right) is assigned to be U volt. In this way, the current through the cells is determined, and also the current through the external load and the delivered power in that load. In the model U is adjusted manually to maximal power in the load. The used program is a modification of the used program for an infinite number of electrodes and presented in *Chapter 8 - Appendix A*. In the next section, the effect of segmentation on the performance of a RED stack will be shown.

8.2.6. Spatial effect within the cell: the effects of flow direction (co- or counter current) and segmentation (undivided or infinite segmented)

The power of the program as presented in *Chapter 8 - Appendix A*, is that several design options can be evaluated quickly, such as the effects of flow direction (co- or counter current) and segmentation (undivided or infinite segmented). To give a first impression of the behavior within a RED cell, the (not yet calibrated) model is used to simulate a small cell (10x10 cm^2), equipped with Fumasep membranes (FAD and FKD). Used parameters as obtained from precious work (*Chapter 6*) include: obstruction factor: f=2, membrane area resistances: $R_{CEM}=5.90 \cdot 10^{-4}$ Ωm^2 and $R_{AEM}=1.63 \cdot 10^{-4}$ Ωm^2, permselectivity: $\alpha=0.88$, spacer thickness (both compartments): $\delta_S=\delta_R=200$ µm and NaCl diffusion coefficient: $D_{salt}=0.13 \cdot 10^{-10}$ m^2/s. Input salt contents are 30 g/L (512.8 mol/m^3) for the sea water and 1 g/L (17.1 mol/m^3) for the river water; residence time is 60 s for sea and for river water.

Figure 8.5 shows some variables in cells with: (a) segmented with an infinite number of electrodes and co-current operation (b) undivided electrodes and co-current operation, c) segmented with an infinite number of electrodes and counter-current operation, and d) undivided electrodes and counter-current operation. Plotted are local concentrations

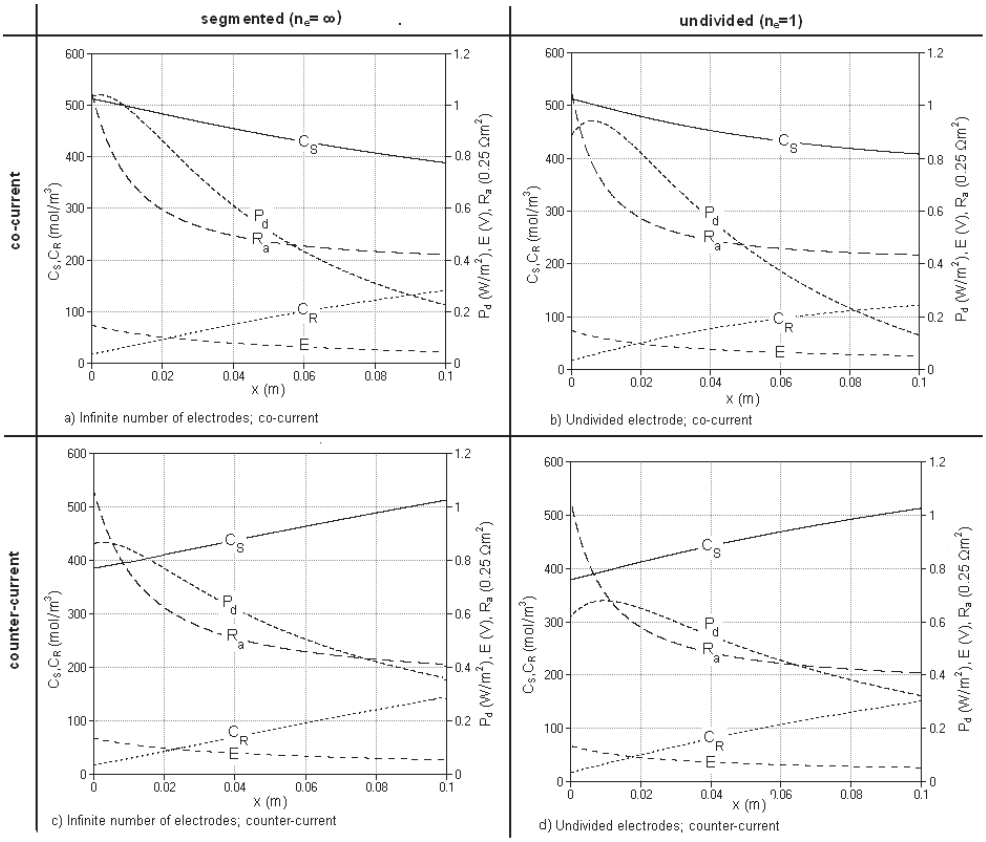

Figure 8.5. Model predictions for a stack with Fumasep membranes. Dimensions of the stack: 10x10 cm^2; spacer thickness 200 µm. A residence time of 60 seconds is used in the calculation. In each graph the following local values are shown: the salt concentration of sea water (C_S) and river water (C_R), both using the left axis, power density (P_d), open circuit voltage (E) and area resistance (R_a), all three using the right axis. The graphs show the effects of the relative flow direction and of the segmentation of the electrodes. The two left graphs (a and c) are related to systems with a high degree of segmentation of the electrodes; the right two graphs (b and d) to systems with undivided electrodes. The upper two graphs (a and b) describe the behavior of co-current feed and the lowest two (c and d) of counter-current feed.

in the sea (C_S (x)) and in the river water compartments (C_R(x)), together with local power density (P_d(x)), local open circuit voltage (E(x)) and local area resistance (R_a(x)). In each graph, the river water inlet is on the left side. In the co-current mode graphs (a and b) the sea water inlet is also on the left side. In the counter-current graphs (c and d), the sea water inlets are on the right side. Effects of osmosis are not incorporated in this model and therefore the graphs of the concentration in sea and river water (C_R and C_R) are symmetrical.

The graphs show the following aspects of the cell behavior; going from the river water inlet to the river water outlet (from left to right) we note:

- The salt concentrations in the sea and river water compartments (C_S and C_R) change more or less linearly.
- The electrical resistance (R_a) decreases sharply in the first quarter of the flow path and after that more slowly.
- The cell voltage decreases smoothly to about half the initial value.
- The generated power density (P_d) is maximal close to the river water inlet. The reason is that the input concentration of the river water is very low and the resulting high resistance limits the electrical current and thereby the power. In the models with undivided electrodes (plot *b* and *d*) this maximum is a bit delayed.
- With the segmented electrodes (plot *a* and *c*) the power density is higher over the whole length of the cell than with the undivided electrodes (plot *b* and *d*).

8.3. Model calibration and validation with laboratory scale experimental set-ups

The electrical model (with osmosis correction) as defined in *Sections 8 2.3* and *8.2.4* is calibrated and validated. In *Section 8.3.1* we shall discuss the calibration of the model and in *Section 8.3.2* the model is validated experimentally. *Figure 8.6* shows the calibration and validation procedure. In the model, parameters are used without fitting as much as possible. Fitting is restricted to some difficult accessible parameters (the obstruction factor f and the diffusion constants D_{salt} and D_{water}); this tuning process is called calibration. The relevant experiments with the small stack are described in *Chapter 5*; with the large stack in *Chapter 7*.

8.3.1. Calibration of the electrical model

Figure 8.7 shows the input variables and process parameters of the model. In general, most parameters are well defined but some are less reliable: the obstruction factor of the spacers (f) and the diffusion constants for salt (D_{salt}) and water (D_{water}). These parameters are found by fitting the model to experimental data. The obstruction factor describes the extra electrical resistance of the water compartments due to the influence of the spacer (*Chapters 5* ;[3,4,5]). The effect includes: (i) the increase of the electrical resistance due to the tortuosity of the ion path, (ii) decrease of the amount conducting salt solution in the compartments and (iii) the shielding effect of the spacer on the membrane on the contact places. D_{salt} and D_{water} should only describe the diffusion of ions and water in the membrane; however in practice also leakage (around the inlet holes) can contribute to these diffusion constants.

For the calibration, we used three small stacks (10x10 cm^2) with Qianqiu homogeneous membranes (25 cell, with cross current feed). For the fitting procedure the residue was

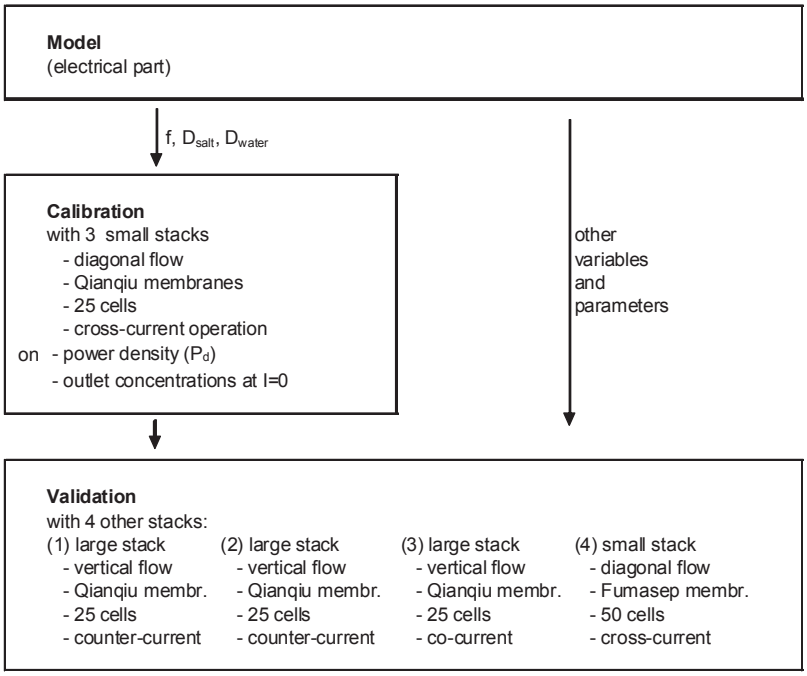

Figure 8.6. Scheme for calibration and validation. The shielding factor f and the diffusion constants D_{salt} and D_{water} are fitted with one stack for use in model predictions of other stacks.

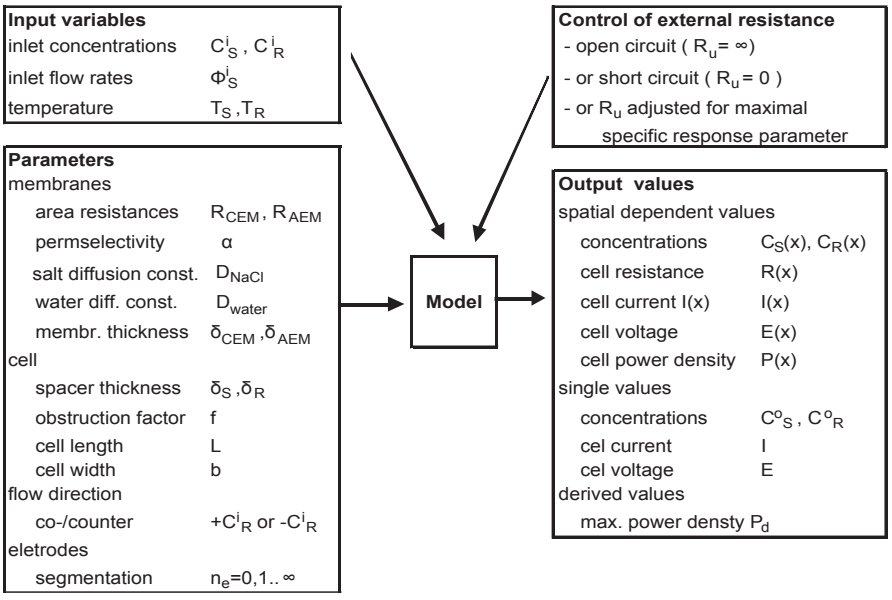

Figure 8.7. Input variables and parameters as used by the model for calculating the outlet values.

calculated from the maximal power density (P_d) and the outlet concentrations under open circuit conditions (no external load connected to the system) of the sea water(C_S^{open}) and river water (C_R^{open}):

$$Residue = \sum_i (\Delta P_{d,i})^2 \sum_i (\Delta C_{S,i}^{open})^2 \sum_i (\Delta C_{R,i}^{open})^2 \quad (31)$$

In this equation, $\Delta P_{d,i}$ is the difference of the measured and calculated power density etc. The parameters f, D_{salt} and D_{water} were adjusted until the minimal residue was achieved.

Figure 8.8 shows the measured values of the maximal power density and the outlet concentrations of the unloaded stacks together with the fitted data.
Fitted values are near to the formerly found data used as starting values. The following values are found: obstruction factor f=1.6 (starting value 1.7 from *Chapter 5*), salt diffusion constant $D_{salt}=2.5\cdot10^{-11}$ m^2/s (starting value $3.2\cdot10^{-11}$ m^2/s from *Chapter 6*) and water diffusion constant $D_{water}=3.5\cdot10^{-9}$ m^2/s (starting value $7.9\cdot10^{-9}$ m^2/s from *Chapter 6*). Both starting values and fitted values are in the normal range of diffusion constants in ion exchange membranes (*Chapter 6: Table 6.1*).

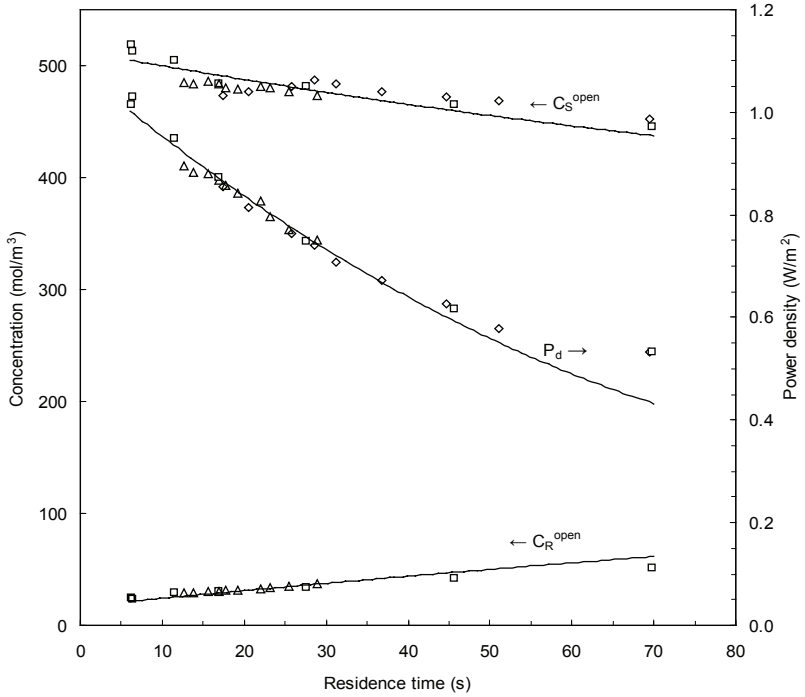

Figure 8.8. Calibration of the model. Computed (line) and measured (marked points) power densities and outlet concentrations of three small Qianqiu stacks of 25 cells as function of the residence time. Power densities (P_d) are measured on maximal power conditions; outlet concentrations (CR^{open} and CS^{open}) were determined with open circuit (unloaded) stacks. Different marks (□, Δ and ◊) refer to different stacks.

To *Figure 8.8* are added calculated outlet concentrations for stacks under condition of maximal power. In fact the model is developed for co- or counter-current operation and in contrast, in the small stack the relative directions of the sea and river water flows are perpendicular (cross-current operation). In *Section 8.3.2.2* it will be shown that differences between co- and counter-current operation are small. Therefore, it is reasonable to use the model also for the small stack because cross-current operation can be seen as an intermediate form between the co- and counter-current modes.

8.3.2. Validation of the electrical model

We have developed models for 4 different modes: two electrode system (undivided and segmented electrodes) and for each electrode system two flow directions (co- and counter-current).

Calculated data of the calibrated model are compared with experimental data. Three different aspects of the model are validated:
- Generated power as function of the residence time (discussed in *8.3.2.1*).
- Effect of the flow direction (discussed in *8.3.2.2*).
- Effect of the segmentation of the electrodes (discussed in *8.3.2.3*).

8.3.2.1. Validation of the electrical model - Model for co-current and undivided electrodes: generated power as function of the residence time

Power measurements were also made with the small stack equipped with Fumasep (FKD and FAD type) membranes (50 cells) and with the large stack with Qianqiu (homogeneous type) membranes in co-current mode (25 and 50 cells) and in counter-current mode (25 cells). *Figure 8.9* shows only small differences in behavior of the two flow directions (co- and counter current). The model prediction from *8.3.1* (the line marked with 'Pd' in *Figure 8.8*) is added to *Figure 8.9*.

Figure 8.9 shows a discrepancy between model (solid line) and measured data of 0.1 W/m^2. To investigate whether this could be due to different values for the diffusion coefficients or to the obstruction factor f, the model was fitted by adjusting $D_{water}=1.0\cdot10^{-8}$ m^2/s, $D_{salt}=0.5\cdot10^{-10}$ m^2/s and f=2.3, and resulting in the dotted line. Remarkable are the higher values of D_{salt} (2 times higher) and D_{water} (3 times higher). An explanation could be water leakage through pinholes in the membrane or along the inlets and outlets in the cells as used for validation (and resulted in the dashed line in *Figure 8.9)*.

The difference between the dotted and the solid line in *Figure 8.9* is independent of the residence time and apart from this offset, the calculated data fit well to the experimental

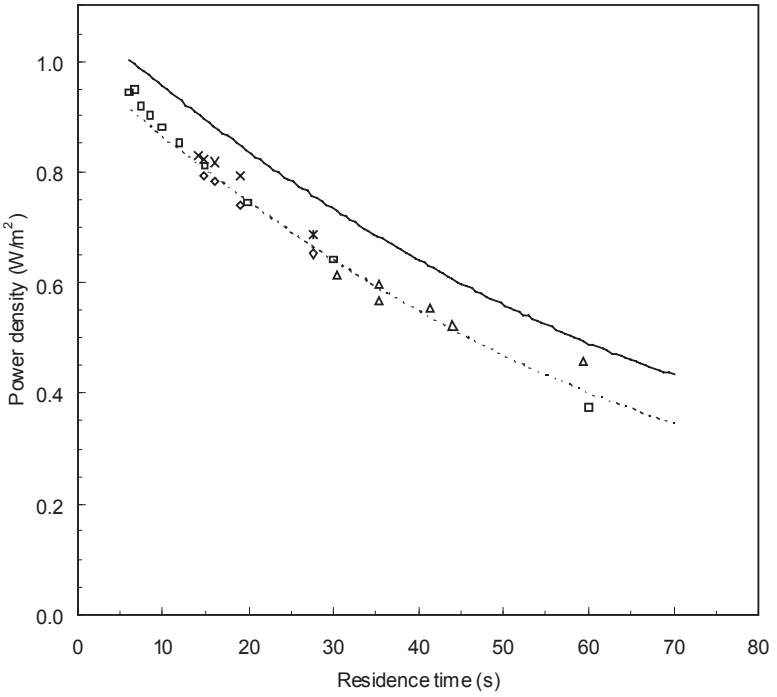

Figure 8.9. Validation of the model. Computed (line) and measured (marked points) power densities as function of the residence time. For the computed line a model for co-current operation with undivided electrodes is used; it is the same line as indicated with 'Pd' in Figure 8.8. The measured data include: (□) Fumasep, small stack, 50 cell, cross current; (Δ) Qianqiu, large stack, 50 cell, co-current; (◊) Qianqiu, large stack, 25 cell, counter-current; (x) Qianqiu, large stack, 25 cell, co-current.

data. As the difference is small, we did not analyze the cause of this. For the purpose in this stage of research the model is good enough.

8.3.2.2. Evaluation of the flow direction (co-current and counter-current)

Figure 8.10 shows computed data for two different flow directions (co- and counter-current) and two different electrode systems (undivided and segmented). The effect of the flow direction is small. For undivided electrodes, the differences are less than 1% in the studied residence time range. For the system with infinite segmented electrodes, the benefit of counter-current flow is maximally 2% better at long residence times (70 s).

Measured data, as shown in *Figure 8.9 (*and enlarged in *Figure 8.11)* show a slightly higher power density for co-current operation (4%) whereas the model shows no significant differences. This could be explained by the fact that the model is based on a rigid stack but the real stack is flexible. Counter-current operation introduces high local pressure

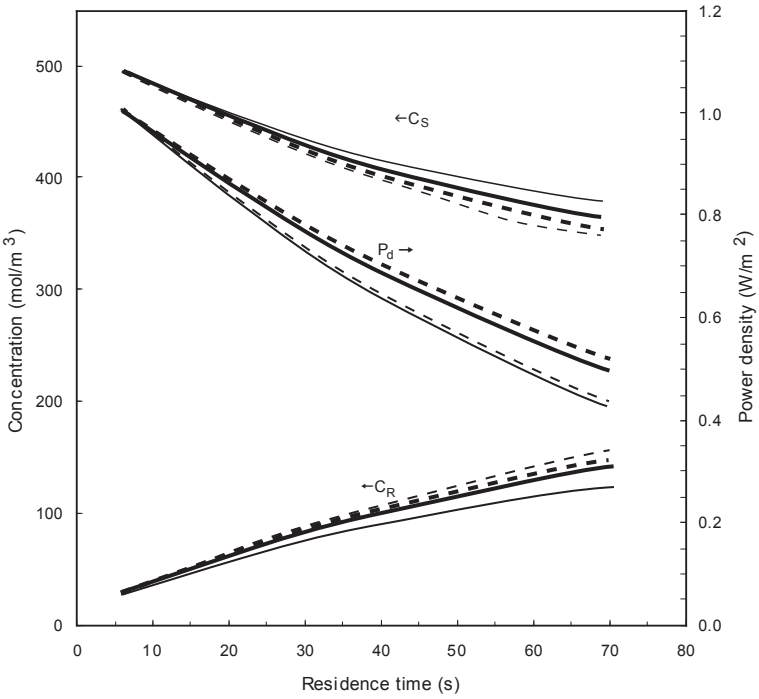

Figure 8.10. Computed values for different flow directions (co-current and counter current) and different electrodes (undivided and infinitely segmented). Solid lines stand for co-current and dashed line for counter current operation. Thin lines stand for undivided electrodes and thick lines for infinitely segmented electrodes.

differences between sea- and river water compartments. This can result in local obstructions for the fluid flow and in local deviations of the electrical conductivity (*Chapter 7*).

By taking into consideration that co-current operation causes smaller local pressure differences between the river and sea water compartments - hence smaller risk of leakages and the possibility to use very thin membranes with high fluxes and very open spacer structures with low hydrodynamic resistance - it was decided to focus on co-current design.

8.3.2.3. Benefit of the system with segmented electrodes

Experimentally, an increase of 11% is found (from 0.441 to 0.488 W/m^2) by dividing the electrode in three independent segments, each loaded with its own optimal resistance (*Chapter 7*0). As seen in *Figure 8.10*, the model forecasts also an increase of the power density by segmentation of the electrodes. The benefit of a system with an infinite segmentation and operated in the co-current mode, is (according to *Figure 8.10*) about 15% at a residence time of 70 s.

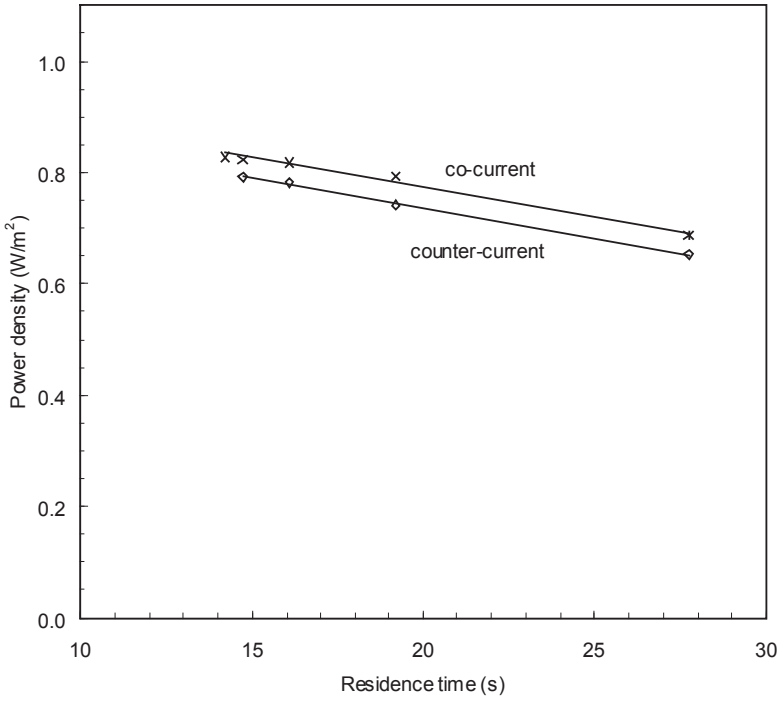

Figure 8.11. Effect of the residence time on the power density for co- and counter-current flow in the large stack.

We then used our model to study the effect of segmentation in detail. The results are shown in *Table 8.1*. Segmentation only yields a small gain in power density and segmentation, if any, should be limited to 2 segments. As segmentation of the electrodes requires complicated electrical provisions, it was decided to use a system with undivided electrodes.

Table 8.1. Average maximal power density (P_d) as function of the number of segments of the electrode. Added is the gain achieved by dividing process. Each segment has its own load, optimized for maximal power output.

Segments	P_d (W/m^2)	Gain (%)
1	0.434	0.0
2	0.490	12.9
3	0.502	15.7
4	0.505	16.4
5	0.506	16.6

8.4. Optimization of the river feed water inlet concentration, thicknesses and lengths of the water compartments and of the resident times

Key parameters in the design of a RED stack are the thicknesses and the length of the sea and river water compartments. In most experiments with our small stack, we used a spacer thickness of 200 μm for both compartments. In this case the electrical cell resistance is mainly determined by the river water compartment; the hydrodynamical loss with the used spacers is about 20% (*Chapter 5*). With thinner spacers the electrical resistance (perpendicular on the spacers) decreases but at the cost of a higher hydrodynamical resistance in the lateral direction.

It is not self-evident that optimal performance is achieved with equally sized spacers for both compartments. It seems reasonable that the spacer thickness of the seawater compartment can be taken some (e.g. 5) times thicker than that of the river water compartment. In this case the total electrical cell resistance is hardly influenced; on the other hand the hydrodynamical resistance of the sea water compartment is much lower than that of the river water compartment. In this way the total hydrodynamic loss is reduced to about half. A thicker seawater compartment permits also the use of a sea water flow rate that is higher than the river water flow rate: the amount of harvested energy per m^3 river water can increase from 1.8 MJ with a 1:1 ratio to 2.6 MJ with a large surplus of sea water (*Chapter 5*). However, a contraindication may be the increased parasitic ionic currents in the seawater system (*Chapter 3*).

A special property of the hydrodynamic loss is that it is affected by the length of the flow path L. If some ions diffuse (and generate energy) only in the second part of the flow path, these ions (together with the accessory amount of water) have traveled the first part in vain, only causing frictional losses there. Therefore L is a main design parameter.

The main finding in *Section 8.3* was that a stack in co-current operation with undivided electrodes is a good choice. Based on this configuration, we used the developed RED model for cells with two types of membranes and two spacer configurations. For each investigated cell we study the influence of the flow path length on the various response parameters, power density and energy efficiency. For each length, thicknesses of both compartments and flow rates of both feeds are adjusted for maximal output of the different response parameters.

In the following sections, we start in *8.4.1* with a brief discussion on the applied response parameters P_{d-net} and R_{PZ}. In *8.4.2* the influence or the salt concentration of the river feed

water is discussed. After that, we will discuss the contribution of de different parts (spacers and membranes) of the cell. We will start in *Section 8.4.3* with ideal membranes (no osmosis, no co-ion transport and no electrical resistance) with spacerless water compartments. To investigate the effect of spacers, in *Section 8.4.4* the model is used with ideal membranes and real spacers. In *Section 8.4.5* the model is applied to a cell with real membranes and with spacerless compartments and in *Section 8.4.6* the behavior of the cell with real membranes in combination with real spacers are studied. Finally, in *Section 8.4.7* we use the achieved information for new spacer concept: the fractal profiled membrane

8.4.1. Choice of response parameters for design and optimization

In *Section 8.2.1* we introduced various response parameters. They include net power density (P_{d-net}), the net river water yield Z_{net} and the response product $R_{PZ}= Z_{net}\cdot P_{d-net}$. Each response parameter has its own characteristics. Net power density (P_{d-net}) describes the produced net power per square meter of installed membrane. If we assume that the area of installed membrane is proportional to the total investment costs of a RED plant, then P_{d-net} is a measure for the economical performance. However, under conditions of maximal P_{d-net}, the efficiency of the used feed water is low. Therefore we introduced in Chapter 5 en 6 the 'net energy efficiency' (Y_{net}). This is the gained net energy as fraction of the theoretical maximum from a given amount of sea and river water. Because normally there is no limit in the availability of sea water, we suggest the net river water yield (Z_{net}) as a better alternative: the amount of energy generated from 1 m^3 of river water and an arbitrary amount of sea water. However, maximization of Z_{net} may result in extremely long residence times and very low power densities. A compromise between power density and efficiency is the product of both: the response product $R_{PZ}= Z_{net}\cdot P_{d-net}$.

We used the model for four cell configurations:
(A) without spacers and with ideal membranes
(B) with real spacers and with ideal membranes
(C) without spacers and with real membranes
(D) with real spacers and with real membranes

The ideal membranes have no electrical resistance, no osmosis and no co-ion transport and a permselectivity α=1. The real membranes are the Qianqiu homogeneous membranes. For spacerless cells, it is supposed to exist a laminar flow between the membranes as will be explained in detail in *Section 8.4.3*. The real spacers are similar spacers to those studied in *Section 8.3.1*.

In order to compare the four cell configurations in a similar way, in each configuration a

obstruction factor f=1, a flow path length L=0.25 m and input concentrations C_S=512.8 and C_R=17.1 mol/m^3 (i.e. 1 and 30 g/L) was used.

8.4.2. Optimization of the river feed water inlet concentration

The salt concentration of the river feed water at the inlet of the RED stack is variable to a certain degree. The lower limit is the natural concentration; it can be increased somewhat by premixing with sea water. With a very low salt concentration in the river water, the cell resistance is high and the produced power low. However, If the salt concentration is too high, the Nernst voltage is low and again the produced power is low. Consequently, there is a optimum salt concentration in the river water.

In early experiments we used a salt concentration of 17.1 mol/m^3 (1 g/L) for the river feed water inlet NaCl concentration. The main reason was that with this value a stable OCV (open circuit voltage) is achieved. We used the developed model for Qianqiu homogeneous membranes to investigate the effect of the river water inlet concentration. The net power density was maximized in a cell with a fixed flow channel length (L=0.25 m) by adjusting the two spacer thicknesses and the two residence times. *Figure 8.12* shows the net power density ($P_{d\text{-}net}$) and the net river water yield (Z_{net}) as a function of the river water concentration. From this figure it follows that optimal performance is achieved at a

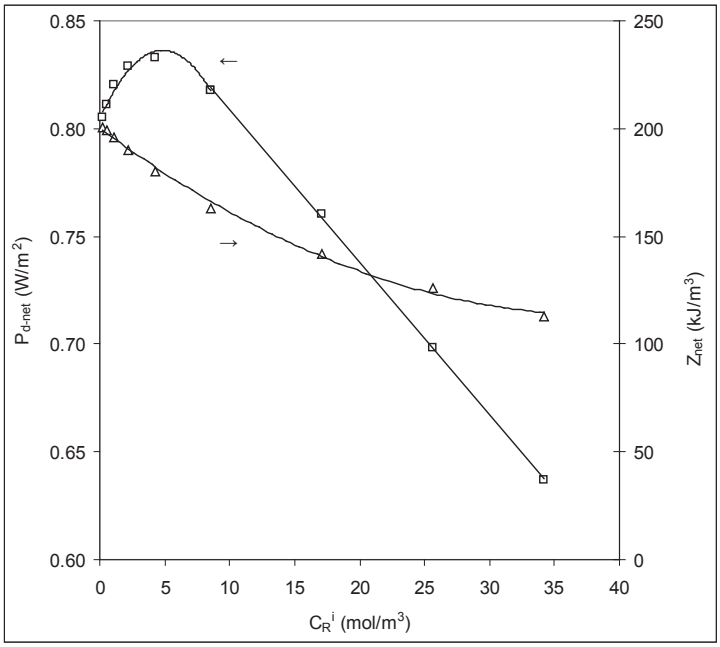

Figure 8.12. Calculated net power density ($P_{d\text{-}net}$; □) and the net river water yield (Z_{net}; Δ) as function of the river water concentration in a Qianqiu cell with a fixed length (L=0.25 m).

river feed water concentration between 0 mol/L (for maximal river water efficiency) to 5 mol/m^3 (=0.3 g/L) (for maximal power density).

8.4.3. Design optimization of flow channel dimensions without spacers and with ideal membranes (cell configuration A)

Normally, spacers are used between the membranes. They are needed for mechanical stability and may furthermore promote mixing within the compartments, thereby reducing the diffusion layers. However, in our ideal hydrodynamic model we ignore the effect of spacers in the compartments. Reynolds numbers are achieved with:

$$\mathrm{Re} = \frac{vD\rho}{\mu} \tag{32}$$

where v is the mean velocity, D the hydraulic diameter, ρ the density of the feed water and μ the dynamic viscosity ($0.9 \cdot 10^{-3}$ Pa·s for pure water at 25 ºC). For a flow between two parallel planes, the hydraulic diameter equals two times the distance between them. Applying *Eq. (32)* to a standard small cell as described in *Chapter 7* (dimensions 0.1x 0.1 m^2 with a compartment thickness of 200 μm), we obtain for a relative short residence time of 5 s (corresponding to a mean velocity of 2 cm/s) and a Reynolds number of 0.01, low enough to be sure of a laminar flow.

With a laminar flow between the membranes, the pressure drop over a compartment is:

$$\Delta P_S = \frac{2\mu L \Phi_S}{b\delta_S^3} \quad ; \quad \Delta P_R = \frac{2\mu L \Phi_R}{b\delta_R^3} \tag{33}$$

The hydrodynamic power loss P_{hydr} is then

$$P_{hydr} = \Delta P_S \Phi_S + \Delta P_R \Phi_R \tag{34}$$

The second assumed ideality of the cell is that they are equipped with membranes without electrical resistance and with permselectivity α=1 and no osmosis. Input concentrations are 1 g/L and 30 g/L (17.1 and 512.8 mol/m^3), temperature is 25°C.

The effect of path length L was studied for maximal power density; for each value of L, the thicknesses of the compartments (δ_S *and* δ_R) and the residence times (δ_S *and* δ_R) were adjusted in such a way that maximal net power density (P_{d-net}) was obtained (α-mode) or maximal response product (R_{PZ}) (β-mode). From these data were calculated the average fluid velocities (v_S and v_R), concentration of the outgoing water (C^o_S and C^o_R), the flow rate ratio (Φ_S/Φ_R), electrical power density (P_d), hydrodynamical loss density ($P_{d\text{-}hydr}$) and

net power density (P_{d-net}), net energy efficiency (Y_{net}), thermodynamical efficiency (η_T), net river water yield (Z_{net}), response product (R_{PZ}) and the Reynolds number in both compartments (Re_S and Re_R). The results for this cell configuration A are summarized in *Table 8.2*, the upper part concerning the α-mode and the lower part the β-mode.

name	maximization of
α-mode	power density (P_{d-net})
β-mode	response product (R_{PZ})

Table 8.2 shows some remarkable facts:

(a) The most important conclusion is that short cells perform better than long cells on net power density (P_{d-net}). This holds for the α-mode (*Table 8.2,* upper part*)* as well for the β-mode (*Table 8.2*, lower part).There is a simple relation between net power density (P_{d-net}) and length of the flow path (L):

Table 8.2. Cell configuration A: cell without spacers and with ideal membranes.
*Effect of the length of the flow path (L) on different cell parameters. Maximized values (printed in bold) are the power density (P_{d-net}) in the upper part (α-mode) and the response product (R_{PZ}) in the lower part (*β-mode*). Adjusted values (italics) include: compartment thicknesses (δ_S and δ_R) and residence times ($t_{R,S}$ and $t_{R,R}$). Normal printed values are calculated and include: linear average velocities (v_S and v_R), outlet concentrations (C^o_S and C^o_R), flow rate ratio (Φ_S/Φ_R), electrical power density (P_d), hydrodynamic loss (P_{d-hydr}), net power density (P_{d-net}), net river water yield (Z_{net}), response product (R_{PZ}) and the Reynolds numbers (Re_S and Re_R).*

L	δ_S	δ_R	$t_{R,S}$	t_{RR}	v_S	v_R	C^o_S	C^o_R	Φ_S/Φ_R	P_d	P_{d-hydr}	P_{d-net}	Z_{net}	R_{PZ}	Re_S	Re_R
m	μm		s		cm/s		mol/m^3			W/m^2			kJ/m^3			
α. Maximization of P_{d-net}																
0.010	*19*	*9*	*0.04*	*0.03*	25	35	456	100	2.8	75.2	15.0	**60.2**	371	22352	11	7
0.025	*29*	*15*	*0.10*	*0.07*	25	35	456	100	2.8	47.6	9.5	**38.1**	373	14202	17	11
0.050	*42*	*21*	*0.20*	*0.14*	25	35	456	100	2.8	33.7	6.8	**26.9**	373	10031	24	16
0.100	*59*	*29*	*0.40*	*0.29*	25	35	455	101	2.8	23.7	4.7	**19.0**	373	7091	33	23
0.250	*93*	*46*	*0.99*	*0.71*	25	35	455	100	2.8	15.1	3.0	**12.0**	372	4474	53	36
0.500	*131*	*65*	*1.97*	*1.42*	25	35	456	100	2.8	10.7	2.1	**8.5**	373	3173	75	51
1.000	*185*	*92*	*3.95*	*2.84*	25	35	455	100	2.8	7.5	1.5	**6.0**	373	2243	105	72
β. Maximization of R_{PZ}																
0.010	*23*	*9*	*0.04*	*0.05*	23	21	471	138	2.4	58.0	6.4	51.6	557	**28714**	12	4
0.025	*38*	*15*	*0.12*	*0.13*	22	19	472	135	2.2	35.6	3.3	32.3	560	**18064**	19	6
0.050	*52*	*20*	*0.22*	*0.24*	23	21	471	137	2.4	26.0	2.9	23.1	556	**12841**	27	9
0.100	*74*	*28*	*0.43*	*0.47*	23	21	471	138	2.4	18.4	2.1	16.3	555	**9080**	38	13
0.250	*117*	*45*	*1.08*	*1.21*	23	21	472	138	2.4	11.6	1.3	10.3	558	**5743**	61	21
0.500	*162*	*62*	*2.14*	*2.33*	23	21	471	138	2.4	8.3	1.0	7.3	553	**4059**	30	30
1.000	*232*	*89*	*4.31*	*4.75*	23	21	471	137	2.4	5.8	0.7	5.2	555	**2871**	121	42

$$P_{d-net} = p \cdot L^q \tag{35}$$

The value of the constants is p=–0.500 and q= 6.00 for the cell optimized for the α-mode and p=–0.500 and q=5.25 for the β-mode.

(b) In the α-mode as well in the β-mode, outlet concentrations are nearly independent of channel length (L). Also the required feed water velocities (v_S and v_R) are independent of the flow path length.

(c) Optimal channel thicknesses for sea water (δ_S) and river water (δ_R) are inversely proportional to the produced electrical power density. It is obvious that the sea water compartment should be thicker than the river water compartment due to the lower electrical resistance in seawater. It is noted is that in the α-mode the ratio δ_S/δ_R equals 2.0 and in the β-mode this ratio is 2.6. Optimal thickness of the river water compartment of both optimization modes (α and β) are about the same.

(d) Compartments of about 10 μm seem to be impractically thin at first. However, it should be emphasized that *Cell A* is equipped with spacerless water compartments. An option to construct these is the fractal profiled membrane, as discussed in *Section 8.4.7.*

(e) The amount of energy used for transport of the water (P_{hydr}/P_{electr}) through the cell is in all cases about 20 % of the generated electrical power in the α-mode and 11% in the β-mode.

(f) The low Reynolds numbers justify the laminar model used.

8.4.4. Design optimization of flow channel dimensions with real spacers and ideal membranes (cell configuration B)

The calculations are now made for systems with real spacers and ideal membranes. We will compare the pressure drop in spacer filled systems with spacerless systems and introduce a factor Q in *Eq. (33)*.

$$\Delta P = Q \frac{2\mu L \Phi}{b\delta^3} \tag{36}$$

From former experiments (*Chapter 7*) the hydrodynamic properties of a special woven polyamide spacer were determined experimentally with a large stack containing 50 cells (compartment thickness δ=200 μm, stack width b=0.75 m and length of the flow path L=0.25 m). The pressure drop in this stack was correlated with the flow rate: $\Delta P = 1.0 \cdot 10^9 \Phi$. From *Eq. (36)* the value of Q=715 is derived.

The used spacer in *Chapter 7* was of the 'balanced plain weave' type: warp and weft are made of threads of the same size at the same distance and are indistinguishable

in the fabric. We will restrict ourselves to similar spacers of this type, all with the same proportions between yarn diameter, mesh opening and thickness. It is then reasonable to assume that the resistance through the spacer in the lateral direction is – as in the case of the spacerless compartment– proportional to the third power of the thickness. Therefore, we can use *Eq. (36)* for the pressure drop over compartments with similar spacers with thickness δ. For pure water at 25 °C, *Eq. (36)* becomes:

$$\Delta P = 1.3\frac{L\Phi}{b\delta^3} \tag{37}$$

With this pressure drop the calculations of *Section 8.4.3* are repeated. In this cell configuration (configuration B) we use an "ideal membrane" and ignore also any shielding use in this cell configuration value (f=1). The results are listed in *Table 8.3*.

The conclusions from *Table 8.3* are mainly the same as from *Table 8.2* except for the numerical values for the net power density and the δ_S/δ_R ratio.
If *Table 8.3* is compared with *Table 8.2* there are two additional conclusions:
(i) The net power density in *Table 8.3* is decreased with a factor 5 with respect to *Table 8.2*.
(ii) The net river water yield is almost the same in *Table 8.3* and *Table 8.2*.
The difference between cell configuration A (*Table 8.2*) and B (*Table 8.3*) is the use of real spacers in cell configuration B. Consequently, we conclude that spacers affects only the net power density and not the river water yield.

Table 8.3. Cell configuration B: cell with real spacer and ideal membranes (additional notes at Table 8.2).

L	δ_S	δ_R	$t_{R,S}$	t_{RR}	v_S	v_R	C^o_S	C^o_R	Φ_S/Φ_R	P_d	$P_{d\text{-}hydr}$	$P_{d\text{-}net}$	Z_{net}	R_{PZ}
m	μm		s		cm/s		mol/m^3			W/m^2			kJ/m^3	
A. Maximization of $P_{d\text{-}net}$														
0.010	*96*	*48*	*1.1*	*0.8*	0.93	1.30	455	100	1.45	14.46	2.88	**11.58**	373	4319
0.025	*152*	*76*	*2.7*	*1.9*	0.94	1.30	456	100	1.45	9.16	1.83	**7.32**	372	2727
0.050	*216*	*107*	*5.4*	*3.9*	0.93	1.30	456	100	1.45	6.46	1.29	**5.18**	373	1929
0.100	*305*	*151*	*10.7*	*7.7*	0.93	1.30	456	100	1.45	4.57	0.91	**3.66**	373	1367
0.250	*483*	*239*	*26.8*	*19.2*	0.93	1.30	456	100	1.45	2.89	0.58	**2.32**	372	861
0.500	*683*	*338*	*53.5*	*38.4*	0.93	1.30	456	100	1.45	2.05	0.41	**1.64**	372	609
1.000	*965*	*478*	*107*	*77*	0.93	1.30	456	100	1.45	1.45	0.29	**1.16**	373	431
B. Maximization of R_{PZ}														
0.010	*121*	*46*	*1.2*	*1.3*	0.85	0.78	471	137	2.89	11.18	1.24	9.95	555	**5525**
0.025	*191*	*73*	*2.9*	*3.2*	0.86	0.78	471	137	2.90	7.08	0.80	6.29	555	**3494**
0.050	*271*	*103*	*5.8*	*6.5*	0.86	0.78	471	138	2.91	5.00	0.56	4.45	556	**2471**
0.100	*387*	*147*	*12*	*13*	0.85	0.76	472	138	2.95	3.51	0.38	3.13	558	**1747**
0.250	*606*	*232*	*29*	*33*	0.86	0.77	471	137	2.91	2.23	0.24	1.99	556	**1105**
0.500	*851*	*326*	*58*	*64*	0.86	0.78	471	137	2.88	1.58	0.18	1.41	555	**781**
1.000	*1200*	*461*	*116*	*128*	0.86	0.78	471	137	2.87	1.12	0.13	1.00	554	**552**

8.4.5. Design optimization of flow channel dimensions without spacers and with real membranes (cell configuration C)

To investigate the effect of the membranes, a configuration is used without spacers and with Qianqiu homogeneous membranes. Membrane values are used as described in *Section 8.3.1*. Again an obstruction factor f=1 is used. The results for this cell configuration C are listed in *Table 8.4*.

The effect of flow channel length on net power density (P_{d-net}) is less extreme than in the foregoing cell configurations. For the α-mode (maximization of P_{d-net}) the range is 2.43 to 1.27 for the investigated flow channel length; a factor of about 2 between the largest and smallest value. For the β-mode (maximization of the response product R_{PZ}) this factor is only 1.5. In contrast to the cell configurations A (*Table 8.2*) and B (*Table 8.3*), now the river water yield (Z_{net}) is strongly dependent on the flow channel length (L) in the α-mode and nearly independent from L in the β-mode. Te main conclusion is that short cells perform better than long cells

8.4.6. Design optimization of flow channel dimensions with real spacers and real membranes (cell configuration D)

Now the complete real cell configuration is used: a cell with real spacers and with Qianqiu

Table 8.4. Cell configuration C: cell without spacers and with Qianqiu homogeneous membranes (additional notes at Table 8.2)

L	δ_S	δ_R	$t_{R,S}$	t_{RR}	v_S	v_R	C^o_S	C^o_R	Φ_S/Φ_R	$\mathbf{P_d}$	$P_{d\text{-}hydr}$	$\mathbf{P_{d\text{-}net}}$	Z_{net}	R_{PZ}
m	μm		s		cm/s		mol/m^3			W/m^2			kJ/m^3	
α. Maximization of $P_{d\text{-}net}$														
0.010	*56*	*29*	*0.5*	*0.2*	2.0	5.3	504	23	0.75	2.52	0.09	**2.43**	32	77
0.025	*78*	*40*	*0.9*	*0.4*	2.7	6.8	502	25	0.77	2.35	0.11	**2.24**	41	93
0.050	*101*	*51*	*1.5*	*0.6*	3.3	8.1	499	26	0.80	2.20	0.12	**2.08**	51	105
0.100	*132*	*66*	*2.5*	*1.1*	4.0	9.4	497	29	0.84	2.04	0.13	**1.91**	61	117
0.250	*188*	*93*	*4.9*	*2.2*	5.1	11.5	493	33	0.90	1.80	0.14	**1.66**	77	128
0.500	*248*	*121*	*6.1*	*3.8*	8.2	13.2	489	37	1.27	1.60	0.14	**1.46**	91	133
1.000	*331*	*160*	*13.4*	*6.7*	7.5	15.0	485	41	1.03	1.41	0.14	**1.27**	105	133
β. Maximization of R_{PZ}														
0.010	*75*	*11*	*0.6*	*1.2*	1.64	0.81	507	84	13.86	1.30	0.01	1.29	290	**374**
0.025	*104*	*17*	*1.1*	*2.0*	2.19	1.28	505	85	10.77	1.25	0.01	1.24	293	**364**
0.050	*133*	*25*	*1.8*	*3.1*	2.72	1.61	504	87	8.89	1.21	0.01	1.20	295	**353**
0.100	*168*	*35*	*3.0*	*4.5*	3.38	2.25	501	88	7.30	1.17	0.02	1.15	295	**339**
0.250	*236*	*54*	*5.6*	*7.6*	4.46	3.28	498	91	5.90	1.09	0.03	1.06	297	**315**
0.500	*304*	*76*	*9.2*	*11.6*	5.43	4.30	494	94	5.02	1.01	0.03	0.98	298	**292**
1.000	*398*	*108*	*15*	*18*	6.62	5.46	491	99	4.49	0.92	0.03	0.88	300	**265**

homogeneous membranes. In fact, the cell configurations of *Sections 8.4.4* and *8.4.5* are combined in this configuration. The results for this cell configuration D are tabulated in *Table 8.5.*

We repeated the optimization procedure of cell D by maximization of R_{PZ} with fixed spacer thicknesses as found at the maximization of P_{d-net}. Under these conditions we achieved a net power density P_{d-net} and a net river water yield Z_{net} quite near the values achieved with optimized spacer thicknesses. This is an important finding. The conclusion is that a RED cell as designed for maximal net power output also can be used for maximal R_{PZ}, only by adjusting the flow rates of the sea and river water.

Table 8.5 shows that in each cell configuration, the optimal sea water compartment is thicker than the river water compartment. For fouling, the thinner river water compartment is thus more critical. Another finding is that in the α-mode river water compartments are thicker than in the β-mode. Therefore, it is advantageous to use the optimal spacer thicknesses as found for the α-mode.
The main conclusions of *Table 8.5* (real spacers with Qianqiu membranes) are:
(i) Short cells perform better than long cells on power density and on river water yield.
(ii) The Pd decreases continuously with increasing cell length for all cases.

Table 8.5. Cell configuration D: cell with real spacers and real (Qianqiu homogeneous) membranes (additional notes at Table 8.2)

L	δ_S	δ_R	$t_{R,S}$	t_{RR}	v_S	v_R	C^o_S	C^o_R	Φ_S/Φ_R	**P_d**	$P_{d\text{-}hydr}$	**$P_{d\text{-}net}$**	Z_{net}	R_{PZ}
m	μm		s		cm/s		mol/m^3			W/m^2			kJ/m^3	
α. Maximization of $P_{d\text{-}net}$														
0.010	*194*	*96*	*5.2*	*2.3*	0.19	0.43	492	33	0.90	1.78	0.14	**1.63**	78	128
0.025	*280*	*137*	*10.1*	*4.8*	0.25	0.52	487	38	0.98	1.52	0.14	**1.38**	97	134
0.050	*373*	*181*	*17.0*	*8.5*	0.29	0.59	483	43	1.03	1.32	0.14	**1.18**	111	131
0.100	*503*	*240*	*28.6*	*15.2*	0.35	0.66	478	49	1.11	1.13	0.13	**0.99**	126	125
0.250	*753*	*356*	*58.2*	*33.3*	0.43	0.75	471	58	1.21	0.88	0.12	**0.76**	142	109
0.500	*1030*	*486*	*100.3*	*60.7*	0.50	0.82	466	65	1.28	0.71	0.11	**0.61**	151	91
1.000	*1430*	*672*	*175*	*112*	0.57	0.89	459	74	1.36	0.56	0.09	**0.47**	156	73
β. Maximization of R_{PZ}														
0.010	*240*	*54*	*5.9*	*7.7*	0.17	0.13	497	92	5.76	1.08	0.03	1.05	298	**313**
0.025	*341*	*88*	*11.4*	*14.1*	0.22	0.18	493	96	4.79	0.97	0.03	0.94	300	**281**
0.050	*448*	*124*	*18.8*	*22.1*	0.27	0.23	489	101	4.25	0.88	0.04	0.84	300	**252**
0.100	*590*	*175*	*31.3*	*35.5*	0.32	0.28	485	106	3.82	0.78	0.04	0.74	299	**220**
0.250	*863*	*274*	*62.6*	*68.0*	0.40	0.37	478	114	3.42	0.64	0.04	0.59	294	**174**
0.500	*1160*	*388*	*107*	*114*	0.47	0.44	472	122	3.19	0.53	0.04	0.48	285	**138**
1.000	*1590*	*553*	*186*	*196*	0.54	0.51	466	130	3.03	0.43	0.04	0.38	272	**104**

(iii) The best cell dimensions are the achieved values from the maximization of the power density (the α-mode).

8.4.7. Novel compartment and cell design

Post et al.[6] showed that it is possible to generate energy from sea and river water with RED at a price comparable with the price of wind energy. They based their calculations on the assumption of a power density of 2 W/m^2 and an energy recovery of 70% (equivalent to a river water yield of 1.1 MJ/m^3). Our values with real membranes and real spacers (cell configuration D, *Table 8.5)* are much lower (1.6 W/m^2 and 0.08 MJ/m^3 in the α-mode or 1.1 W/m^2 and 0.30 MJ/m^3 in the β-mode) and it is obvious that the current spacers and membranes should be improved for use in economical operated RED stacks.

With the following reasoning, we arrived at the concept of fractal design. The reasoning points are:

(a) Compartments in current systems have two functions: they act as feed channels and as reactors. The first function requires thick and the other thin compartments. Therefore, both functions should be decoupled by a spatial separation between the supply part and the reactor part.
(b) The electrical specific resistance of sea water is comparable with ion exchange membranes and the specific resistance of river water is much higher. Therefore the most profits are achievable by improving the river water compartment. This should be as thin as possible.
(c) Spacers are unwanted due to their large hydrodynamic resistance.
(d) The shorter the channel length, the higher the produced power density.

These arguments lead to the concept of fractal profiled membranes. *Figure 8.13* shows a complete RED cell with a profiled AEM (beneath; serving as sea water compartment) and a profiled CEM (above; serving as river water compartment). To form an idea, the following dimensions can be imagined: the membrane thickness is 0.5 mm, in the membranes are pressed the feed channels with a depth of 0.4 mm and the reactor cannels with a depth of 0.1 mm. In the river water compartment, the electrical resistance is decreased by the use of thin compartments (0.1) mm. The reactor channels are short, and spacerless, and have a low hydrodynamic resistance. Because of the low electrical resistance of the sea water, the reactor channels in the sea water compartment can be deeper. A patent with all details has been submitted.

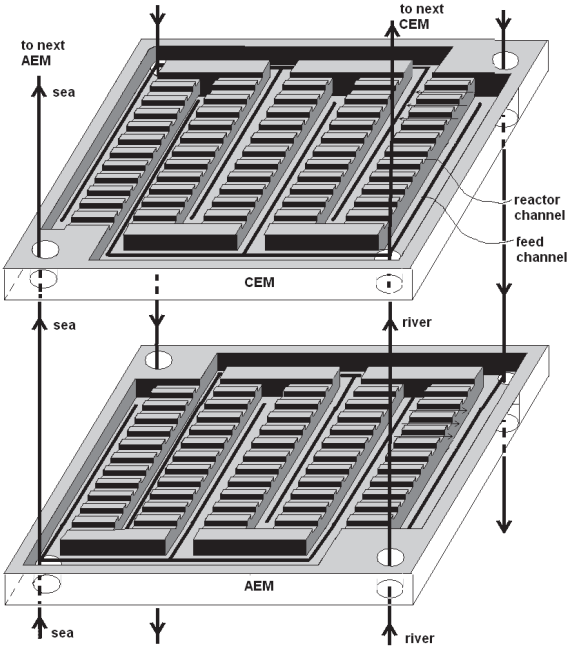

Figure 8.13. A RED cell with fractal profiled membranes. Feed channels are pressed in the membranes (thickness 0.5 mm) until a depth of 0.4 mm. Compartments are pressed with a depth of 0.1 mm. All cell dimensions are arbitrary, for illustration only.

8.5. Conclusions and outlook

8.5.1. Conclusions

A process model is developed and validated for laboratory experimental RED systems. The model is then used to study response parameters, suitable for optimization purposes. It was found that there are two response parameters that give useful results on maximization: first the net power density and second the product of power density and net river water yield. A RED stack as designed for maximal net power density is also suitable for a high river water yield. In this case other flow rates should be applied with an excess of seawater. It is reasonable to suppose that when the first economical RED plants are built, there is enough fresh water and high power density is more wanted than high river water yield. Therefore, a RED plant can be operated on high power density initially and a more energy efficient mode can be used eventually.

Performance of co-current and counter-current operation is almost identical. Therefore, co-current operation is preferred because in this mode the local pressure differences between the compartment are very low, which enables the use of very thin membranes and very open spacers. Thin membranes have a low electrical resistance but lack mechanical strength; open spacers have a low hydrodynamic resistance but are compressible. An extra benefit of the low pressure differences is that leakage through pinholes in the membranes and around the inlet and outlet holes is minimal.

Segmentation of the electrodes can increase the power density with about 15%. If divided into two parts, most of this percentage is achieved. The same effect can be achieved with two separate RED modules; for an optimal result, the length of the flow channel of both stages should be half the length of the original stack. However, both parts demand their own electronics and it is questionable if segmentation or staging would be economically interesting.

The model showed the huge negative influence of channel length on power density, the need for thin membranes with a low electrical resistance and the requirement of spacers with a very open structure (or no spacers at all). Therefore, fractal profiled membranes are very promising. They do not require spacers, the membrane is locally very thin, and the fractal structure allows larger cell dimensions.

8.5.2. Outlook

To bring RED for river water with sea water to maturity and suitable for economical applications, there are some challenges remaining:

Membrane integration

Integration of membranes, spacers and gaskets is the new challenge. Advantages of integration are: a more simple construction of stacks and less leakage. A special way to integrate, is using profiled membranes. In this way the advantage of conducting spacers is used[5]. A next level of profiling is the fractal profiling.

Special membranes for RED

Until now, special commercial membranes are not available for RED. However, RED has other requirements than the usual electrodialysis techniques and therefore special membranes should be developed. These membranes should be suitable for the profiling process.

Spiral wound RED stacks

Spiral wound stacks may be easer to produce on large scale. However, making test modes is a special challenge.

New electrode systems

In Chapter 4 of this thesis, a comparison is made between different electrode systems. Especially the Fe^{2+}/Fe^{3+} system should be tested to come to a decision about the best system.

Prefiltration
The price of prefiltration is a critical point. Moreover, prefiltration gives a waste stream that generates new costs. Therefore, a RED system should be designed with very low prefiltration needs.

Duration tests
RED stacks should be subject to extended duration tests with real river and sea water. Fouling, stability of the electrode system and mechanical stability should be monitored.

Scale-up
In our experiments, we achieved specific power densities of about 4 kilowatt per cubic meter stack volume. That is exclusive of pumps and tubing. One approach of a commercial SGP power plant is using a modular system. One module is built in a sea container in this concept; the largest commercially available types (45 feet High Cube) have an internal volume of 87.7 m^3. If this volume is used 100% with RED stacks, the power would be 350 KW. If tubing and pumps are located inside these containers, there is less room for the stack and the power is substantially less. It is clear that the development of systems with a higher specific power is welcome.

Power conversion and transport of the electrical power
The power from a RED stack is of the DC (direct current) type. Conversion to AC (alternating current) can be done on modular level or central dependent on economical considerations.

Electrical safety
A RED stack with thousands of cells generates a voltage of some hundred volts. A complication is that the feed channels are connected to the electrical circuit. Therefore, a special study on the safety of a RED module should be done.

If all questions are answered, the RED technique may be finished, however, for the application of SGP it is the starting point! Finding good locations for SGP, achieving political commitment and social agreement with all stakeholders and public acceptance are the following steps. Now it is the time for civil engineers who are directing water streams to and from the RED power plants.
In the beginning of a real SGP application, power density is the most important economical item. However, if the technique is proven and accepted, and more RED power is produced, there will be a time that the efficiency of the process will be the most important item. That is the time when SGP has found a place between other forms of renewable energy: all these forms have their own niches and together they are an answer to exhaustion of fossil fuels and the increase of the CO_2 content in the atmosphere.

Acknowledgement

This work was performed in the TTIW-cooperation framework of Wetsus, centre of excellence for sustainable water technology (www.wetsus.nl). Wetsus is funded by the Dutch Ministry of Economic Affairs, the European Union Regional Development Fund, the province of Fryslân, the city of Leeuwarden and the EZ/Kompas program of the "Samenwerkingsverband Noord-Nederland". The first author would like to thank the NHL Hogeschool who facilitated this research by detaching him to Wetsus and the participants of the theme "Energy" theme for their fruitful discussions and their financial support.

Nomenclature

A	cell area (m^2)
A_m	total membrane area (m^2)
A_{Na+}	effective hydrated ion radius of Na^+ (pm)
A_{Cl-}	effective hydrated ion radius of Cl^- (pm)
b	width of a cell (m)
C	concentration (mol/m^3)
D	hydraulic diameter (m)
D_{salt}	diffusion constant of NaCl (m^2/s)
D_{water}	diffusion constant of water (m^2/s)
E	voltage (V)
E_{cell}	electromotive force of one cell (V)
F	Faraday constant (96485 C/mol)
f	obstruction factor
I	electrical current (A)
J	current density (A/m^2)
L	length of a cell (m)
M_{NaCl}	mass NaCl (0.05844 kg/mol)
M_{H2O}	mol mass H_2O (0.01805 kg/mol)
N	number of cells in a stack
ne	degree of segmentation of electrodes
OCV	open circuit voltage (V)
P	power (W)
P_d	power density (W/m^2)
P_{d-net}	net power density (W/m^2)
P_{hydr}	hydrodynamic power loss (W)
P_i	internal dissipated power (W)
P_{net}	net produced power (W)
P_u	produced electrical power (W)
ΔP	pressure drop (Pa)
Q	pressure drop factor
R	gas constant ($8.314\ J{\cdot}mol^{-1}K^{-1}$)
R_a	area resistance (Ωm^2)
R_{AEM}	area resistance of the AEM (Ωm^2)
R_{CEM}	area resistance of the CEM (Ωm^2)
R_{cell}	cell resistance (Ω)
R_u	external resistance (Ω)
R_{PZ}	response product ($J^2m^5s^{-1}$)
Re	Reynolds number
S	salt content (kg/m^3)
T	temperature (K)
T_{NaCl}	flux of NaCl ($mol{\cdot}s^{-1}m^{-2}$)
T_{Na}, T_{Cl}	flux of Na^+, Cl^- ($mol{\cdot}s^{-1}m^{-2}$)
T_{water}	molar flux of water ($mol{\cdot}s^{-1}m^{-2}$)
T'_{water}	volumetric flux of water (m/s)
t_R	residence time (s)
T	temperature (K)
U	voltage (V)
v	average velocity (m/s)

x	flow path direction (m)
Z_{net}	net river water yield (J/m^3)
z	valency of an ion

Greek symbols

α	permselectivity of the ion exchange membrane
γ	activity coefficient
δ_m	membrane thickness (m)
δ_R	river water compartment thickness (m)
δ_S	sea water compartment thickness (m)
δ_m	membrane thickness (m)
Λ_m	molar conductivity ($S \cdot m^2/mol$)
ρ_{H2O}	density of water (1000 kg/m^3)
μ_{ion}	ion strength of a solution (mol/L)
μ	dynamic viscosity (Pa·s)
Φ	flow rate (m^3/s)

Superscripts

i	in
o	out

Subscripts

cit	co-ion transport
coul	coulombic
M	equilibrium
osm	osmotic
R	river
S	sea

Abbreviations

AEM	anion exchange membrane
CEM	cation exchange membrane
ED	electrodialysis
OCV	open circuit voltage
RED	reverse electrodialysis

Definitions

Compartment	space between the membranes
cell	combination of two membranes and two compartments
electrode system	the anode, cathode and electrode rinse
stack	a number of N cells with an electrode system
α-mode	a system optimized for maximal electrical power density (P_d)
β-mode	a system optimized for maximal net river water yield (Z_{net})

References Chapter 8

1 J.W. Post, J. Veerman, H.V.M. Hamelers, G.J.W. Euverink, S.J. Metz, K. Nymeijer, C.J.N. Buisman, *Salinity-gradient power: Evaluation of pressure-retarded osmosis and reverse electrodialysis.* J. Membr. Sci. 288 (2007) 218-230

2 D.C. Harris, *Quantitative Chemical Analysis*, 6th edition, W. H. Freeman & Company (2003)

3 J.W. Post, H.V.M. Hamelers, C.J.N. Buisman, *Energy recovery from controlled mixing salt and fresh water with a reverse electrodialysis system.* Environ. Sci. Technol. 42 (2008), 5785–5790

4 P. Długołęcki, A. Gambier, K. Nijmeijer, M. Wessling, *Practical Potential of Reverse Electrodialysis As Process for Sustainable Energy Generation.* Environ. Sci. Technol. 43 (2009) 6888-6894

5 P. Długołęcki, J. Dąbrowska, K. Nijmeijer, M. Wessling, *Ion conductive spacers for increased power generation in reverse electrodialysis.* J. Membr. Sci. 347 (2010) 101-107

6 J.W. Post, C.H. Goeting, J. Valk, S. Goinga, J. Veerman, H.V.M. Hamelers, P.J.F.M. Hack, *Towards implementation of reverse electrodialysis for power generation from salinity gradients.* Desalination and Water Treatment 16 (2010) 182–193

Appendix A

Program of the developed model for two flow directions (co- and counter) and two degrees of segmentation (undivided and infinitely segmented)

The process model is programmed in Berkeley Madonna. Standard, the program calculates with time dependent differential equations, but in line 4, time is replaced by x, the travelled distance in the flow path. In line 44 and 45 the mean effective hydrated ion radius A_{mean}=375 pm is used for both ions. In line 41 the mean permselectivity α_{mean} is used for both membranes.

In the four different modes, the program is used in the following way.

a) Infinite number of electrodes; co-current operation.
   Apply in line 16 the plus sign, activate line 57 and deactivate line 58.
   The program can be used directly. The constraint Re=Rcell (line 57) ensures that maximal output is gained by the RED process.
b) Infinite number of electrodes; counter-current operation.
   Apply in line 16 the plus minus, activate line 57 and deactivate line 58.
   In this operation mode 'INIT Cr' (line 40) refers to the outlet concentration of the river water. A slider should be defined to adjust for the initial river water concentration ('INIT Cr'). The input value of the salt concentration in the river water is seen as the last element of the Cr if the results are presented as a table. 'INIT Cr' is adjusted until the right input concentration is displayed.
c) Undivided electrodes; co-current operation.
   Apply in line 16 the plus sign, deactivate line 57 and activate line 58.
   A slider should be defined for the electrode potential ('U'). The value of U is adjusted in such a way that the concerning response variable is maximal.
d) Undivided electrodes; counter-current operation.
   Apply in line 16 the plus minus sign, deactivate line 57 and activate line 58. Sliders should be defined for the variables 'INIT Cr' and 'U'. In a cyclic way, 'INIT Cr' and 'U' are adjusted until a proper values for the input concentration (the last element of Cr) and a maximum of the concerning response variable are achieved.

```
{ 1} { A RED CELL  WITH  VARIABLE NUMBER OF ELECTRODES AND VARIABLE FLOW DIRECTION }
{ 2} {  j.veerman, september 2009 }
{ 3}  METHOD RK4 STARTTIME=0 {s}  STOPTIME=0.25  {s} DT=0.00002 {s}
{ 4}  rename time=x { conversion  seconds to meters s --> m}

{ 5 }  { === CONTANTS, PARAMETERS}
{ 6}  R=8.3143        { J/mol/K, gasconst.}
{ 7}  Temp=298        { K        , temperature }
{ 8}  Fad=96487       { C/mol  , Faraday const.}
{ 9}  visc = 0.891E-3 {Pa.s, viscosity water at 25 C}
{10}  Vwater=18E-6  { m3/mol. molar volume of water }
{11}  tR=6            { s       , residence time,  input by slider }
{12}  tS=6            { s       , residence time,  input by slider }
{13}  Fs= L*b*Hs/tS  { m3/s,  Flow rate sea water }

{14}  { === CO- OR COUNTER-CURRENT ====== }
{15}  { ***** Choose in next line  PLUS for co-current,  MINUS for counter-current  ********}
{16}  Fr= + L*b*Hr/tR  { m3/s,  Flow rate river water,   PLUS for co-current,  MINUS for counter-current }

{17}  { === MEMBRANE DATA  ===}
{18}  { ***** Choose line 19, 20 or 21 by desactivating the others  with semicolon ********}
{19}   {membr. area  resistance    permselect. diffusion  constants                  thickness     type  }
{20}  { Ohm.m2         Ohm.m2        -            m2/s              m2/s                m                    }
{21}  ; Raem=1.63E-4 Rcem=5.9E-4 a=0.88  Dnacl=0.13E-10  Dwater=10E-10 Hm=  80E-6 ; FAD & FKD
{22}   Raem=4.5E-4   Rcem=4.5E-4 a=0.9   Dnacl=0.35E-10 Dwater=35E-10  Hm=250E-6 ; QianQiu-homog
{23}  ; Raem=0         Rcem=0         a=1     Dnacl=0            Dwater=0          Hm= 1E-10  ; Ideal membrane

{24}  { === SPACER DATA  ===}
{25}  { ***** Choose line 26 or 27 by deactivating the other  with semicolon ********}
{26}  ; dPs = 2*visc*L*Fs/b/Hs^3  dPr  = 2*visc*L*Fr/b/Hr^3   ; No  spacer
{27}   dPs = 1.3*L*Fs/b/Hs^3      dPr  = 1.3*L*Fr/b/Hr^3      ; Real spacer

{28}  { === CELL DATA ===========}
{29} N=50             { number of cells =membrane pairs}
{30}  L=0.25          { m,             length flow path    }
{31}  b=0.10          { m,             width flow path     }
{32}  M=58.5/1000     { kg/mol,        molar mass NaCl  }
{33}  obstr =1        { -,             obstruction factor  }
{34}  Labda=0.01287  { m2/Ohm/mol, molar conductivity }
{35}  Hs=200E-6       { m,             spacer thickness ,  input by slider}
{36}  Hr=200E-6       { m,             spacer thickness,  input by slider}

{37}  { === CALCULATION ===========}
{38}  RRs=obstr*Hs/(Labda*Cs)  RRr=obstr*Hr/(Labda*Cr)    {Ohm.m2}
{39}  INIT Cs = 512.8   Cs0=512.8  {mol/m3  = 30 g/L}
{40}   INIT Cr = 17.1     Cr0=17.1     {mol/m3  =1 g/L ;…   Is outlet conc. in counter-Current mode !}
{41} E=a*2*R*Temp/Fad*logn(As /Ar)      {V,  electromotive force}
{42}  U=0.030                           {V, potential at electrode,  adjustable with slider }
{43}  Ra=Rcell*(L*b)*400                {only used for plot}
{44}  As=Cs*10^( -0.51 / (1.230 + sqrt(1000/Cs)))       {mol/m3, activity sea water}
{45}  Ar =Cr *10^( -0.51 / (1.230 + sqrt(1000/Cr)))       {mol/m3,  activity river water}
{46}  Rcell = RRs + RRr + Raem + Rcem     {Ohm.m2, cell resistance }
{47}  Tnacl = J/Fad  +  (Cs-Cr)*Dnacl/Hm*2  {mol/s/m2, NaCl flux }
{48}  Twater=-(Cs-Cr)*Dwater/Hm*2*Vwater    { m/s     }
```

```
{49} Cs' = - Tnacl/Fs*b   +  b*Twater*Cs/Fs   { mol/m4 }
{50} Cr' = + Tnacl/Fr*b   -  b*Twater*Cr/Fr   { mol/m4 }
{51} INIT I=0  I'=J*b                          { A      }
{52} Pd=J*U/2                                  { W/m2   }
{53} INIT Pd_el=0   Pd_el' = Pd/L              { W/m2 }
{54} Ptotal=Pd_el*2*L*b*N                      { W/m2   }

{55} { === SEGMENTED OR UNDIVIDED ELECTRODES  ===========}
{56} { ***** Choose line 57 or 58 by desactivating the other  with semicolon ********}
{57} ; Re=Rcell      J=E/(Rcell+Re)   Pd=J*J*Re/2 { infinitely segmented  }
{58}   J=(E-U)/Rcell  Re=U/(I+0.0000001)            { undivided  electrodes }


{59} Pd_hydr=(dPs*Fs+dPr*Fr)/2/L/b        { W/m2, hydrodynamic loss per m2 membrane }
{60} Pd_net=Pd_el - Pd_hydr               { W/m2, net power density }
{61} Cm      = (Fs*Cs0+Fr*Cr0)/(Fs+Fr)    { mol/m3, average concentration }
{62} { === EXERGY FLOW RATE  ===========}
{63} Ex_in   = (2*R*Temp*(Fr*Cr0*logn(Cr0/Cm) +  Fs*Cs0*logn(Cs0/Cm))  )/(2*L*b)  {W, in  }
{64} Ex_out  = (2*R*Temp*(Fr*Cr  *logn(Cr /Cm) +  Fs*Cs  *logn(Cs  /Cm))  )/(2*L*b)  {W, out}
{65} Ex_cons =  Ex_in - Ex_out                                                    {W, consumed}

{66} { === EFFICIENCY , RESPONSE PRODUCTS ========}
{67} EffEn    =  100* Pd_net/(Ex_in+0.000000001)    { -,  net energy efficiency}
{68} EffTh    =  100*Pd_el/(Ex_cons+0.000000001)   {     thermodynamic eff }
{69} RP       =  EffEn*Pd_net                      {W/m2, response product}
{70} XL = L  XHs=Hs   XHr=Hr  XtS=tS   XtR=tR  { print variables }
{71} WE  =Pd_net*L*b*2/Fr/1000 { kJ/m3,       river water yield}
{72} WEP=Pd_net*WE           { J2/m5/s,   second response product }

{73} XL = L  XHs=Hs   XHr=Hr  XtS=tS   XtR=tR  { print variables }

{
Optimizing tS, tR, Hs, and Hr for maximal Pd-net (or other response variable)
A) Infinite segmented electrode + co-current
   a) Make sliders for:  tS, tR, Hs and Hr
   b) Maximize Pd-net with tS, tR, Hs and Hr
B) Undivided  electrode + co-current
   a) Make sliders for:  tS, tR, Hs, Hr and U
   b) Maximize Pd-net  with tS, tR, Hs,  Hr and U
C)  Infinite segmented electrode + counter-current
   a) Make sliders for:  tS, tR, Hs, Hr and Cr
   b) Maximize Pd-net with tS, tR, Hs and Hr
      and adjust Cr to 17.1 (or other input value)
D)  Undivided electrode + counter-current
   a) Make sliders for:  tS, tR, Hs, Hr, U and Cr
   b) Maximize Pd-net with tS, tR, Hs, Hr and U
      and adjust Cr to 17.1 (or other input value)
}
```

Figure 8.14. Berkeley Madonna program listing for a RED cell.

Summary

There is a great need for new energy sources that are clean and sustainable without thermal or chemical pollution and without emission of CO_2. One of the potential sources is *salinity gradient power* (SGP), the power that can be generated from the reversible mixing of river water with sea water. The energy density of this 'fuel' is low compared to fossil fuels; nevertheless, the quantities involved are large and the total power – the product of energy density and quantity – is considerable. There are two main challenges: to find suitable locations for SGP and to develop a suitable technique for the conversion of SGP into usable energy. Our objective was the second one.

When we started the project in 2005, the literature revealed two serious candidates: *reverse electrodialysis* (RED) and *pressure-retarded osmosis* (PRO). At that moment only six scientific articles describing real experiments on RED had been published and for PRO there was about the same amount of literature. All described experiments concerned small laboratory generators with a power output of less than 1 Watt. From the two candidate techniques, RED seemed to be more attractive experimentally because using this method the conversion is rather simple, without the requirement of high pressure set-ups, pressure exchangers and turbines. Therefore, the first research question was:

Is RED better than PRO for generating energy from sea and river water?

In **Chapter 2** of this thesis (*Comparison of different techniques for salinity gradient power*), we proved that the amount of extractable energy using RED and PRO from specified quantities of diluate and concentrate is theoretically the same. However, from practical considerations, based on membrane properties as published in literature, it was found that RED is more attractive for power generation using river and sea water and PRO is more attractive using concentrated saline brines.

When performing the first experiments, we realized that there was energy loss due to three short circuits: the sea water feed channels, the river water channels and the electrode rinse solution. In principle parasitic currents can be prevented by the use of mechanical valves or air bubble injection, but it would be more practical to have a design with inherently low losses. Therefore, the next research question was:

Is it possible to manage power losses by ionic short-circuit through a proper stack design?

The positive answer is described in **Chapter 3** (*Reducing power losses caused by ionic shortcut currents in reverse electrodialysis stacks by a validated mode*l). We made a model

of a RED stack and validated this model experimentally with two types of RED stacks with different membranes and different spacers. It is possible to describe the ionic shortcut loss with only three parameters: (i) the number of cells N, (ii) the channel resistance in proportion to the cell resistance R/r, (iii) the lateral spacer resistance in proportion to the cell resistance ρ/r. With the used stack with 0.2 mm spacers and Fumasep membranes, the loss caused by ionic shortcut currents is 6% for a stack with 50 cells, showing that the ionic shortcut currents are manageable.

We found different electrode systems in the literature, therefore the next question is:

What are useful electrode systems for RED?

In **Chapter 4** (*Reverse electrodialysis: evaluation of suitable electrode systems*) an inventory was made for all aspects of electrode systems in terms of technical feasibility, SHE (safety, health and environment) and economics. All systems described in literature were evaluated as well as some novel systems used by the authors. The iron based systems (Fe^{2+}/Fe^{3} and $Fe(CN)_6^{4-}/Fe(CN)_6^{3-}$) with inert metal electrodes have the highest scores for use in commercial RED power plants. However, the use of graphite electrodes may also be a feasible option.

From the experiments described in Chapter 3, it was known that a system with thin spacers and thin membranes has the best performance. A new stack was built with those spacers and membranes and with enough cells to serve as a prototype of larger stacks. The purpose was to get an idea of the delivered power density, the hydrodynamical losses in the stack and the energy. Therefore, the next research question is:

What is the performance of a 10x10 cm^2 stack with 50 cells?

In **Chapter 5** (*Reverse electrodialysis: performance of a stack with 50 cells on the mixing of sea and river water*) the performance parameters of this stack were described. The total membrane area was 1 m^2. The obtained power density was 0.93 W/m^2, which was the highest reported value for a real stack operation; 25% of this produced power was lost by pressure drop in the stack. The energy efficiency (the conversion efficiency from potential energy to generated electricity) was 8%. With cascade operation of 4 stacks, a higher energy efficiency was achieved (18%) together with a lower power density (0.40 W/m^2).

These results were encouraging and the basis for further investigations. The central theme was describing the power density and the fuel efficiency in terms of membrane and

spacer properties, stack and cell dimensions, fluid velocities and so on. The performance of a stack is affected by two kinds of losses: hydrodynamical and electrical. The first are located in the manifolds and in the spacers, the second in the feed water supply (due to the parasitic currents as discussed in Chapter 3) and in the membranes. Membranes are of particular interest, because they include three sources of loss: osmosis, co-ion transport and membrane resistance. Therefore, it was time to have a closer look to the membranes:

What is the effect of osmosis, co-ion transport and membrane resistance on the generated power and efficiency of different membranes?

In **Chapter 6** (*Reverse electrodialysis: Comparison of six commercial membrane pairs on the thermodynamic efficiency and power density)* the experimental results are shown. It showed that the contribution of co-ion transport and of internal dissipation (due to the electrical resistance) on the total losses are comparable and the contribution of osmosis is much less. Introduced is the response product (RP), the product of the thermodynamic efficiency and the power density as ranking parameter. It combines the benefits of high power density with high thermodynamic efficiency and may be a useful ranking parameter. The highest RP was achieved with the Selemion membrane pair. However, the Qianqiu homogeneous membranes proved to be also rather good. That was good news, because their price was a factor ten lower than of the other membranes.

A new large stack was built with these Qianqiu membranes. The dimensions were 75x25 cm^2 and the stack was equipped with 50 cells (each cell containing two membranes) and three separate electrode pairs. With a total active membrane area of 18.75 m^2, it was the largest RED stack ever built. With this cell it was possible to study the effects of residence time, flow direction (co-current or counter-current), flow path length (75 cm at horizontal flow or 25 cm at vertical flow) and of electrode segmentation (undivided or separated in three segments). The research question was:

What is the effect of flow channel length, residence time, flow direction and of electrode segmentation on power density and efficiency of a RED stack?

In **Chapter 7** *(The performance of a scaled-up reverse electrodialysis stack)* the results of the concerning experiments are discussed. It proved that residence time is a key parameter for the stack performance. It turned out that a long flow path causes high hydrodynamic losses. Co-current flow appeared to result in higher power densities and the effect of segmentation of the electrodes is marginally positive.

The experiments as described in Chapter 7 have provided much data and are useful for the validation of a RED model. Therefore, the next research questions were:

How to model the RED process and how to optimize the design with this model?

A model is presented in **Chapter 8** *(Modeling the performance of a reverse electrodialysis stack)*. The model is validated and applied to different stacks. The model confirms the findings of the experiments as described in Chapter 7. The most important is that long flow paths induce unacceptably high hydrodynamic losses. With short flow paths, high power densities and acceptable energy efficiencies can be obtained but the total power production with such cells is inherently low. The conclusion is that the way to scale up of a RED stack is found by very short cells and by a fractal design of these cells. A patent has been applied for a fractal solution: an integration of spacers and membranes with a diverging system of flow channels. The required structures are pressed in the membrane.

Samenvatting

Er is een grote behoefte aan nieuwe energiebronnen die schoon en duurzaam zijn, geen thermische of chemische vervuiling geven en geen CO_2-emissie veroorzaken. Een van de potentiële bronnen is zoutgradiënt energie (*salinity gradient power,* SGP), de energie die gegenereerd kan worden door reversibele menging van rivierwater met zeewater. De energiedichtheid van deze 'brandstof' is laag vergeleken met die van fossiele brandstoffen; desalniettemin zijn er grote beschikbare hoeveelheden van en het totale vermogen – het product van energiedichtheid en hoeveelheid – is aanzienlijk. Er zijn twee belangrijke uitdagingen: het vinden van goede locaties voor de toepassing van SGP en de ontwikkeling van een geschikte techniek om die SGP om de zetten in een bruikbare energievorm. Ons doel was dit laatste.

Toen we het project startten in 2005, dienden zich twee serieuze kandidaten aan in de literatuur: omgekeerde elektrodialyse (*reverse electrodialysis*, RED) en drukvertraagde osmose (*pressure-retarded osmosis,* PRO). Toentertijd waren er slechts zes artikelen gepubliceerd die daadwerkelijke experimenten met RED beschreven; wat betreft PRO was er ongeveer dezelfde hoeveelheid literatuur. Van de twee kandidaat-technieken, leek RED experimenteel het meest aantrekkelijk omdat de conversie met deze techniek redelijk eenvoudig is, zonder dat er voorzieningen voor de hoge druk, drukwisselaars en turbines nodig zijn. Derhalve was de eerste onderzoeksvraag:

Is RED beter dan PRO voor de opwekking van energie uit zee- en rivierwater?

In **Hoofdstuk 2** van dit proefschrift (*Comparison of different techniques for salinity gradient power*) tonen we aan dat de hoeveelheid winbare energie met RED en met PRO met gespecificeerde hoeveelheden diluaat en concentraat theoretisch hetzelfde is. Vanuit praktische overwegingen echter, gebaseerd op membraaneigenschappen zoals gepubliceerd in de literatuur, werd er geconcludeerd dat RED de aangewezen techniek is al er rivier- en zeewater gebruikt wordt en dat PRO aantrekkelijker is als er geconcentreerde zoutoplossingen gebruikt worden.

Toen we de eerste experimenten uitvoerden, realiseerden we ons dat er energieverlies was door drie kortsluitcircuits: de toevoerkanalen voor zeewater, de toevoerkanalen voor rivierwater en de elektrodespoeling. In principe kunnen parasitaire stromen voorkomen worden door gebruik te maken van mechanische afsluiters of door luchtbel injectie, maar het zou praktischer zijn een ontwerp te hebben met inherent lage verliezen. Daarom luidde de volgende onderzoeksvraag:

Is het mogelijk het vermogensverlies door interne kortsluitstromen te beheersen door een adequaat ontwerp van de stack ?

Het bevestigende antwoord is beschreven in **Hoofdstuk 3** (*Reducing power losses caused by ionic shortcut currents in reverse electrodialysis stacks by a validated mode*l). We maakten een model van een RED-stack en valideerden dit model experimenteel met twee types RED-stacks met verschillende membranen en verschillende spacers. Het is mogelijk de interne kortsluitstromen te beschrijven met slechts drie parameters: (i) het aantal cellen N, (ii) de verhouding van de weerstand van het voedingkanaal en de celweerstand R/r, (iii) verhouding van laterale spacer weerstand en de celweerstand ρ/r. Met de gebruikte stack met 0.2 mm spacers en Fumasep membranen, was het verlies door interne kortsluitstromen 6% voor een stack met 50 cellen, wat aantoont dat deze kortsluitstromen beheersbaar zijn.

In de literatuur vonden we verschillende elektrodesystemen, daarom is de volgende vraag:

Wat zijn bruikbare elektrodesystemen voor RED?

In **Hoofdstuk 4** (*Reverse electrodialysis: evaluation of suitable electrode)* wordt een inventarisatie gemaakt van alle aspecten van elektrodesystemen in termen van technische haalbaarheid, SHE *(*safety, health and environment, ofwel veiligheid, gezondheid en milieu) en kostprijs. Alle in de literatuur beschreven systemen werden geëvalueerd alsmede enige nieuwe systemen die door de auteur gebruikt zijn. De op ijzer gebaseerde systemen (Fe^{2+}/Fe^{3} and $Fe(CN)_6^{4-}/Fe(CN)_6^{3-}$) met inerte metaalelektroden scoren het hoogst voor een economisch bedreven RED-centrale. Echter lijkt het gebruik van grafietelektroden ook een haalbare optie.

Uit experimenten zoals beschreven in Hoofdstuk 3 bleek dat systemen met dunne membranen en dunne spacers de beste prestaties leveren. Er werd een stack gebouwd met zulke spacers en membranen en met voldoende cellen om als prototype dienst te doen voor grotere stacks. Het doel was om een idee te krijgen van de geleverde vermogensdichtheid, de hydrodynamische verliezen in de stack en van de energie-efficiëntie van het systeem:

Wat zijn de prestaties van een 10x10 cm^2 stack met 50 cellen?

In **Hoofdstuk 5** (*Reverse electrodialysis: performance of a stack with 50 cells on the mixing of sea and river water*) zijn de prestaties van deze stack beschreven. Het totale membraanoppervlak was 1 m^2. De verkregen vermogensdichtheid was 0.93 W/m^2, wat de hoogste waarde was ooit verkregen met een RED-stack; 25% van dit geproduceerde vermogen werd gebruikt door de drukval in de stack. De energie-efficiëntie (de conversie-efficiëntie van potentiële energie naar opgewekte elektriciteit) was 8%. Met een cascadeschakeling van 4 stacks werd een hogere energie-efficiëntie verkregen (18%), echter met een lagere vermogensdichtheid. (0.40 W/m^2).

Deze resultaten waren bemoedigend en de basis voor verder onderzoek. Het centrale thema is de beschrijving van vermogensdichtheid en de brandstofefficiëntie in termen van membraan- en spacereigenschappen, stack- en celafmetingen, vloeistofsnelheden enzovoorts. De prestaties van een stack worden beïnvloed door twee typen verliezen: hydrodynamisch en elektrische. De eerste zijn gelokaliseerd in de waterkanalen en in de spacers, de tweede in het watervoorzieningsysteem (wegens de in Hoofdstuk 3 besproken lekstromen) en in de membranen. Membranen zijn van bijzonder belang omdat hier drie bronnen van verlies aanwezig zijn: osmose, co-ion transport en membraanweerstand. Daarom was de tijd aangebroken om dieper op de membranen in te gaan:

Wat is het effect van osmose, co-ion transport en membraanweerstand op het opgewekte vermogen en op de efficiëntie bij verschillende membranen?

In **Hoofdstuk 6** (*Reverse electrodialysis: Comparison of six commercial membrane pairs on the thermodynamic efficiency and power density)* werden de experimentele resultaten beschreven. Het blijkt dat de bijdrage van co-ion transport en van interne vermogensdissipatie (wegens de elektrische weerstand) aan de totale verliezen vergelijkbaar zijn en dat het aandeel van osmose veel minder groot is. Het begrip response product (RP), het product van thermodynamische efficiëntie en van vermogensdichtheid, wordt geïntroduceerd als beoordelingsparameter. De hoogste RP-waarde werd bereikt met het Selemion membraan paar. Echter bleken de homogene membranen van Qianqiu ook vrij goed. Dat was goed nieuws omdat de prijs daarvan een factor 10 lager was dan van de andere membranen.

Er werd een nieuwe stack gebouwd met deze Qianqiu membranen. De afmetingen waren 75x25 cm^2 en de stack werd voorzien van 50 cellen (elke cel met twee membranen) en drie afzonderlijke elektrodeparen. Met een totaal actief membraanoppervlak van 18.75 m^2 was het de grootste RED-stack die ooit gebouwd is. Met deze stack was het mogelijk de effecten te bestuderen van de verblijftijd, stroomrichting (mee- of tegenstroom), lengte van het

stroomtraject (75 cm bij horizontaal en 25 cm bij verticaal bedrijf) en van de segmentatie van de elektrode (ongedeeld of gescheiden in drie segmenten). De onderzoeksvraag was:

Wat is het effect van de lengte van de stroomkanalen, verblijftijd, stroomrichting en van elektrode-segmentatie op de vermogensdichtheid en op de efficiëntie van een RED-stack?

In **Hoofdstuk 7** *(The performance of a scaled-up reverse electrodialysis stack)* worden de resultaten van de betreffende experimenten besproken Het bleek dat de verblijftijd een sleutelrol speelt bij de prestaties van de stack. Verder bleek het dat een lang stroomtraject hoge hydrodynamische verliezen veroorzaakt. Meestroom bleek in hogere vermogensdichtheden te resulteren en het effect van de elektroden is marginaal.

De experimenten zoals beschreven in Hoofdstuk 7 hebben veel data opgeleverd en zijn nuttig voor de validatie van een RED model. Daarom waren de volgende onderzoeksvragen:

Hoe kan het RED proces gemodelleerd worden en hoe kan het ontwerp met dit model geoptimaliseerd worden?

In **Hoofdstuk 8** (*Modeling the performance of a reverse electrodialysis stack)* wordt een model van het RED-proces ontwikkeld. Het model is gevalideerd en toegepast op verschillende stacks. Het model bevestigt de resultaten van experimenten zoals beschreven in Hoofdstuk 7. Het belangrijkste is dat lange stromingstrajecten onacceptabel hoge hydrodynamisch verliezen veroorzaken. Met kortere trajecten kunnen er hogere vermogensdichtheden en acceptabele energie-efficiëntie verkregen worden, maar de totale hoeveelheid geproduceerd vermogen is laag in zulke cellen. De conclusie is dat de weg naar opschaling verloopt door de cellen juist kleiner te maken en door een fractaal ontwerp van deze cellen. Er is een patent ingediend voor een fractale oplossing: een integratie van spacers en membranen met een divergerend systeem van voedingskanalen. De vereiste structuren worden in het membraan geperst.

Publications

Scientific Publications

J. Veerman, J. W. Post, S.J. Metz, M. Saakes, G.J. Harmsen,
Reducing power losses caused by ionic shortcut currents in reverse electrodialysis stacks by a validated model.
J. Membr. Sci. 310 (2008) 418-430

J. Veerman, S.J. Metz, M. Saakes, G.J. Harmsen,
Reverse electrodialysis: performance of a stack with 50 cells on the mixing of sea and river water.
J. Membr. Sci. 327 (2009) 136-144

J. Veerman, R.M. de Jong, M. Saakes, S.J. Metz, G.J. Harmsen,
Reverse electrodialysis: Comparison of six commercial membrane pairs on the thermodynamic efficiency and power density.
J. Membr. Sci. 343 (2009) 7–15

J. Veerman, M. Saakes, S.J. Metz, G.J. Harmsen,
Reverse *electrodialysis: evaluation of suitable electrode systems.*
J. Appl. Electrochem. 40 (2010) 1461-1474

J. Veerman, M. Saakes, S.J. Metz, G.J. Harmsen,
Electrical power from sea and river water by reverse electrodialysis: a first step from the laboratory to a real power plant
Submitted to Environmental Science & Technology.

J. Veerman, M. Saakes, S.J. Metz, G.J. Harmsen,
Reverse electrodialysis: a validated process model for design and optimization.
*S*ubmitted to Chemical Engineering Journal.

J.W. Post, J. Veerman, H.V.M. Hamelers, G.J.W. Euverink, S.J. Metz, K. Nymeijer, C.J.N. Buisman,
Salinity-gradient power: Evaluation of pressure-retarded osmosis and reverse electrodialysis.
J. Membr. Sci. 288 (2007) 218–230

M.H. Dirkse, W.P.K. van Loon, J.D. Stigter, J.W. Post, J. Veerman, G.P.A. Bot,
Extending potential flow modelling of flat-sheet geometries as applied in membrane-based systems.
J. Membr. Sci. 325 (2008) 537-545

J.W. Post, C.H. Goeting, J. Valk, S. Goinga, J. Veerman, H.V.M. Hamelers, P.J.F.M. Hack,
Towards implementation of reverse electrodialysis for power generation from salinity gradients.
Desalination and Water Treatment 16 (2010) 182–193

Other publications

J. Veerman,
Rijnwater ontzouten hoeft geen energie te kosten.
Polytechnische Tijdschrift September 1994, 52-55

J. Veerman, J. Krijgsman, J.M. Nederend, G. Oudakker,
Blauwe stroom kansrijk bij Afsluitdijk.
Land en Water 8, September 2004, 28-29

J. Veerman, G.J. Harmsen,
Blauwe elektriciteit, een uitdaging.
NPT Procestechnologie 4, September 2007, 22-23

Patents

J. Veerman,
A fractal spacer for an electrodialysis system and for a reverse electrodialysis system.
Applied 2009

Dankwoord

Ruim vier jaar ben ik betrokken geweest bij het Blue Energy project bij Wetsus. Reden voor een terugblik. Alle hieronder genoemde mensen wil ik bedanken voor de samenwerking, voor de steun, voor de hulp en inzet en voor de leerzame discussies.

Mijn eerste contacten met de membraanwereld was een cursus membraantechnologie in Wageningen in 1992. Reden voor mijn deelname was dat ook bij de NHL Hogeschool, waar ik als docent betrokken was, het vak membraantechnologie geïntroduceerd zou worden. Een van de onderwerpen was het gedrag van ionenwisselende membranen en de Maxwell-Stefan theorie die dat gedrag verklaarde. Dit bracht mij op het idee om brak water te ontzouten met behulp van zout water. Ik legde mijn idee uit aan Hans Wesselingh, een van de docenten. Na enig peinzen zei hij mij dat zoiets wel mogelijk moest zijn, maar raadde mij dringend aan eerst een en ander uit te rekenen alvorens met experimenten te starten. Die les heb ik ter harte genomen. Het proces bleek modelleerbaar met de MS theorie en een publicatie volgde in het PolyTechnisch Tijdschrift. Kortom, het was Hans Wesselingh die in mij het heilig vuur van de wetenschap wist te ontsteken.

De tweede persoon die dit vuur wist aan te wakkeren, was Gerrit Oudakker. Op zeker moment was er een bericht dat zijn aandacht trok: een Russisch onderzoeker, genaamd Victor Kniajev van het Institute of Marine Technoloy Problems in Vladivostok, was er in geslaagd energie uit zoet en zout water op te wekken in een installatie die groot genoeg was om een laptop van stroom te voorzien. Omstreeks het jaar 2000 werd ik opgebeld door Gerrit met de vraag of ik dat ook kon. “Natuurlijk kan ik dat”, zei ik. Omgekeerde elektrodialyse (reverse electrodialysis, RED) bleek echter toch meer haken en ogen te hebben dan ik eerst dacht. Na enig experimenteren bleek de zoutenergie beschikbaar te zijn met een spanningsverschil van anderhalf volt aan de elektroden. Ik was dan ook blij Gerrit te kunnen opbellen met het blijde bericht: “Het werkt, kom zo spoedig mogelijk kijken”. De machine bleek ca. 20 milliwatt te leveren aan een propeller.

Ondertussen was rond 2005 het instituut Wetsus gestart binnen de muren van het Van Hall instituut. Gerrit en ik demonstreerden de RED-generator aan Cees Buisman die direct overtuigd was. Wetsus ging aan de slag met Blue Energy. ‘Daar moet ik ook bij zijn’, was mijn eerste reactie, doch in welke vorm? Jan Steenmeijer, toentertijd directeur Life Sciences, was ook enthousiast en met hulp van Johannes Boonstra van Wetsus wist hij me voor drie dagen per week te detacheren bij Wetsus. Ik schreef een projectvoorstel en hoopte de 20 milliwatt waarmee ik begonnen was, elk jaar met twee nullen te kunnen uitbreiden.

Aan de slag dus bij Wetsus. Projectleider (en later mijn co-promotor) was Sybrand Metz. Typerend waren zijn bemoedigende woorden als ik met praktische problemen bij hem kwam. "O wat leuk, zo'n probleem", zei hij dan, "zoiets vraagt om een adequate oplossing". En het is die visie die ik later in heel Wetsus tegenkwam: wetenschappelijk onderzoek kent alleen uitdagingen. Problemen zijn dingen voor mensen met psychische moeilijkheden of in het beste geval puzzels voor schakers. In een later stadium was het ook Maarten Biesheuvel die met gouden tips kwam om een rebutal kort, krachtig en kordaat te formuleren.

Gelijkertijd met mij begon ook Jan Post. Met aanvankelijk eenvoudige middelen en een elektrodialyse-apparaat gingen we aan de slag. Ondertussen doken we de literatuur in om onze omgekeerde elektrodialysie (RED) te vergelijken met de osmosetechniek die bekend stond als 'pressure retarded osmosis' (PRO). Uiteindelijk bleek het dat voor de combinatie zeewater met rivierwater onze eigen RED technieken de beste perspectieven bood en met hulp van Jan' s begeleider Bert Hamelers, zijn promotor Cees Buisman, Gert-Jan Euvering en Kitty Nijmeijer, mondde dit uit in de eerste Wetsus-publicatie over Blue Energy. Die brede groep van auteurs was ook nuttig want het schiep een onderlinge band in een tijd dat het buiten onze groep nog geen uitgemaakte zaak was welke techniek - PRO of RED - de meeste perspectieven bood.

Ondertussen had ik een promotor bereid gevonden zijn vertrouwen in mij te stellen: Jan Harmsen die toen via de Hoogewerff leerstoel aan de Technische Universiteit Delft verbonden was. Jan had een open oor als het me niet mee zat en wist zijn luisteren zo nu en dan te onderbreken met een kritische vraag. Dan blijkt, dat je door het doen van je verhaal, je zelf ook eigenlijk al de oplossingen formuleert. Later vertrok Jan naar de Rijksuniversiteit Groningen en werd ons overleg meer gestructureerd, zeker in de laatste fase. En vooral wist Jan mijn gedachtestromen zodanig te kanaliseren dat deze – eenmaal op papier gezet – ook voor anderen begrijpelijk werden. Voor een artikel dat we een paar jaar geleden samen schreven voor het tijdschrift NPT procestechnologie, moesten we een foto insturen. Beiden bleken we een jeugdopname gebruikt te hebben.

Na korte tijd bij Wetsus werden onze gelederen versterkt door Piotr Długołęcki. Door Piotr hadden we nu ook de kennis en energie van zijn begeleidster Kitty Nijmeijer en zijn promotor Matthias Wessling verankerd binnen het Blue Energy project van Wetsus. We waren nu met drie promovendi en drie universiteiten klaar voor de grote stap voorwaarts. Piotr's kerntaak lag in het zoeken naar de juiste membranen, Jan had de uitdaging alles wat met vervuiling te maken had naar behoren op te lossen en mijn taak was het ontwerp van de installatie. Later bleek dat onze afgebakende gebieden aan het vervloeien waren.

Zoals al eerder genoemd, had ik ambitieuze plannen wat betreft het te genereren vermogen. De testopstelling moest uitgebreid worden en een energiek stagiair, Sjoerd Zijlstra, diende zich aan. Sjoerd ging voortvarend aan de slag en na enige maanden had hij een complete en grootschalige voeding voor mij en ook een voor Jan Post ontworpen en gebouwd, hierbij geholpen door Wim Borgonje, Harrie Bos en later ook door Harm van der Kooi. Met name Harrie heeft er erg veel tijd in deze apparaten gestopt.

Nieuwe stagiaires verschenen. Met Ynse Haitsma en Mark Hazenberg ben ik begonnen te zoeken naar het meest ideale elektrolyt. We concentreerden ons op het systeem rood en geel bloedloogzout in een bulk van natriumchloride en konden uiteindelijk de optimale concentraties vaststellen. Met Mariët Slagter maakte ik een nieuw ontwerp voor de kleine stack. We kochten een pers en konden zodoende voortaan zelf stacks bouwen. We waren nu in staat een stack te maken bestaande uit 50 cellen, die meer dan 1 Watt bleek te leveren, meer dan 50 maal de 20 milliwatt waar we ooit mee begonnen.

Op zeker moment kwam Michel Saakes in het team. Als echt elektrochemicus, gepokt en gemazeld in de wereld van de lithium-ion batterij, wist hij ons te overtuigen nieuwe meetmethoden te gebruiken en introduceerde hij moderne potentiostaten op het lab. Langzamerhand begon elektrochemie een belangrijk item te worden niet alleen voor ons maar ook voor de mensen van de biobrandstofcel. Dat was aanvankelijk vooral mijn kamergenoot Rene Rozendal, die met zijn enthousiasme en zijn fungeren als voortrekker uiteindelijk in drie thema's van Wetsus zijn sporen wist achter te laten.

Met Martijn Dirkse uit Wageningen en de stagiairs Pieter van Norel en Rade Matic werd de hydrodynamica van het water in de spacerruimte onder de loep genomen. Met de stagiairs werden bij Wetsus experimenten uitgevoerd om de drukval in diverse celconfiguraties te meten. Verder maakten we filmopnames van geïnjecteerde hoeveelheden inkt in een doorzichtige cel.

Al snel in het begin van mijn promotieperiode werd het bedrijf REDstack opgericht, een samenwerking tussen diverse bedrijven die elkaar al kenden als participant van het thema energie. Pieter Hack was daar de bezielende directeur en Jan Post trad er als deeltijdwerknemer in dienst. Het was REDstack die een grote stack financierde die meer mogelijkheden voor wetenschappelijk onderzoek dan de tot dan toe gebruikte kleine stacks. Jan Valk van Landustrie tekende voor het ontwerp. De bedoeling was dat de voeding zowel horizontaal als verticaal doorgeleid kon worden en dat de elektroden ook afzonderlijk belast konden worden.

Het bouwen van de stack werd gedaan door drie stagiairs: Feiko Reinalda, Bertus Nobach en Wytze Kingma. Gedrieën hebben ze de stack gestapeld tot 25 celparen waarna Feiko de eerste experimenten ging uitvoeren met de stack. Reinald Mark de Jong zag kans de stack uit te breiden tot 50 cellen en er een aantal experimenten mee te doen. Verder maakte Reinald ook een start met metingen aan met zoutmengsels waarbij we voor de analyse dankbaar gebruik konden maken van de expertise van de mensen van het lab: Janneke Tempel, Jelmer Dijkstra en Pieter Wartena.

De grote stack had een oppervlak van achttien vierkante meter membraan en zou dus bijna twintig watt kunnen opleveren. Dat was duizend maal meer vermogen dan de twintig milliwatt waar drie jaar geleden mee begonnen werd en leidde tot de "RED-wet" die zegt dat het RED-vermogen zich elk jaar vertienvoudigt. Zo is in ieder geval makkelijk een antwoord te geven op de vraag hoe lang het nog duurt voordat er een installatie van tweehonderd megawatt in de Afsluitdijk komt: nog zeven nullen erbij dus nog zeven jaar opschalen.

De Rijksuniversiteit Groningen begon ook aandacht te krijgen voor het Blue Energy project. Bart Bouter maakte een scriptie over het onderwerp en Gijsbert Haaksman en Jeroen Bokhove gingen aan de slag met het design van een Blue Energy installatie. Simon Grasman begon in die tijd aan zijn afstudeeropdracht bij Wetsus, ongeveer tegelijkertijd met Piet Leijstra uit Twente. Beiden traden later in dienst bij REDstack en aldaar mocht ik weer met ze samenwerken.

Uit het bovenstaand overzicht blijkt dat stagiairs steeds een zeer belangrijke bijdrage hebben geleverde aan het welslagen van het Blue Energy project. In het laatste stadium waren dat Freerk Mellema, Jan Jansen, Daniël Beerlings en Tiara Stoker. Het waren vooral HBO-studenten die participeerden in ons Blue Energy team en het waren lieden van divers pluimage: werktuigbouwers, elektrotechnici, chemisch technologen, chemisch analisten en milieukundigen.

Natuurlijk waren mijn collega's van Van Hall en de NHL ook dicht in de buurt en dat was vaak handig omdat dat een goudmijn is van kennis over de meest uiteenlopende vakgebieden. Met Jan van Delden ben ik doorgedrongen in de (on)mogelijkheden van DEA (Data Envelopment Analysis) en Piet Hofman's willig oor heb ik gebruikt om mijn thermodynamische kennis te toetsen. Verder moet ik mijn beide steunpilaren voor het Engels bedanken: Folkert van Beijma en Yolanda Wijnsma.

Eerdere promovendi konden nog iedereen bij Wetsus persoonlijk noemen in hun dankwoord. Maar Wetsus groeit exponentieel. In dit overzicht heb ik mij beperkt tot die mensen waarin ik direct te maken had met het onderwerp Blue Energy. Alle anderen waarmee ik gezellig een boterham gegeten heb, waar ik mee geboerengolfd heb of op andere wijze mee verpoosd heb wil ik ook bedanken voor de gezelligheid, het vertrouwen en de vriendschap tijdens de jaren bij Wetsus.

Rest mij nog te noemen de viermaandelijkse hoogtepunten: de themateam-bijeenkomsten. Het bijzondere daarvan is dat je ziet dat wetenschap serieus genomen wordt door de industrie. Het blikveld van de participanten is anders dan van de universitaire wereld. Daar waar de wetenschap houdt van diepgraverij, denkt de industrie aan expansie. Het was vooral Maarten van Riet die met zijn enthousiasme de bijeenkomsten een levendig verloop wist te geven. Daarnaast was het Pieter Hack die door zijn kennis van het zakenleven gestalte wist te geven aan de formele kanten van ons themateam en tevens de brug was naar REDstack. En Marcel Geers leerde ik kennen als iemand die onverzadigbaar was wat betreft alles wat we aan wetenschappelijk materiaal produceerden. Gelukkig voor hem is er een nieuw jong en krachtig Blue Energy team, bestaande uit het driemanschap Bruno Bastos, David Vermaas en Enver Guler, dat erg vernieuwend bezig is en in korte tijd op alle fronten forse resultaten heeft geboekt.

Zeer in het bijzonder wil ik de leden van de beoordelingscommissie, de hoogleraren Michèl Boesten, Freek Kapteijn en Matthias Wessling bedanken voor hun energie die ze gestoken hebben in het lezen van dit proefschrift en voor de daaruit voortvloeiende suggesties om de leesbaarheid van dit proefschrift te stroomlijnen. En verder beschouw ik het als een grote eer dat behalve deze genoemde drie ook de hoogleraren Martien Cohen Stuart, Ton Schoot Uiterkamp en Hans Wesselingh bereid zijn de oppositie te voeren. Een dergelijke krachtige oppositie is alleen het hoofd te bieden met tactische en bekwame hulp van geschoolde paranimfen en ik prijs mij gelukkig dat mijn dochteren Vera en Roos zich van deze taak willen kwijten.

Ten tenslotte: waarom doen we dit allemaal? Momenteel verstoken we per jaar een hoeveelheid fossiele brandstof waar de natuur bijna een miljoen jaar over gedaan heeft om die te vormen. Die voorraden zijn vooral in het Carboon aangelegd, een periode die zestig miljoen jaar duurde. De rekensom is dus dat we er nog zestig jaar verder mee kunnen. Daarbij komt dan nog het probleem van de klimaatsverandering door de opwarming van de aarde. Het is duidelijk dat er duurzame oplossingen moeten komen voor onze energievoorziening. Het is onze generatie die het meeste heeft opgesoupeerd van de bodemschatten. Het is dus ook onze generatie die naar alternatieven zal moeten

zoeken. Ik ben blij daar een kleine rol in te hebben mogen spelen. Het geeft een goed gevoel mee hebben mogen werken aan het aanboren van een nieuwe energiebron die in principe schoon en duurzaam is.

Wergea, 20 augustus 2010

Joost Veerman